

Dissertation

submitted to the

Combined Faculty of Natural Sciences and Mathematics

of the Ruperto Carola University Heidelberg, Germany

for the degree of

Doctor of Natural Sciences

Presented by

Benno Zehnder, MSc ETH Biology

born in: Zürich, Switzerland

Oral Examination: 16.09.2021

**Genetic code expansion as a tool for the
visualisation of Hepatitis B and Delta viruses**

Referees: Prof. Dr. Hans-Georg Kräusslich
Prof. Dr. Stephan Urban

I. Abstract

Hepatitis B virus (HBV) and hepatitis delta virus (HDV) are widespread human pathogens that cause acute and chronic infections of the liver associated with inflammation, cirrhosis, and hepatocellular carcinoma. Despite the medical burden caused by HBV and HDV, therapeutic options are limited, and curative therapy is not available yet. The identification of the bile acid transporter sodium taurocholate cotransporting polypeptide (NTCP) as functional receptor for both viruses has provided new opportunities to study virus and host factors involved in virus entry and maintenance of viral persistence *in vitro*. The present study aimed to investigate the contribution of *de novo* synthesised HBV core protein (HBc) to the maintenance of HBV persistence, and to generate fluorescently labelled HBV and HDV for the study of viral entry and trafficking.

We engineered an infectious HBV mutant with a genome encoding a stop codon in the HBc ORF (Δ HBc HBV), which could not initiate nucleocapsid production upon infection. *In vitro* infection with wild-type (WT) and Δ HBc HBV resulted in comparable numbers of covalently closed circular (ccc)DNA, which is the transcriptionally active template for all viral transcripts and is the determinant factor of HBV persistence. During long-term infection in HepG2-NTCP cells, cccDNA levels, transcription of viral RNA, and secretion of viral proteins remained stable in WT and Δ HBc HBV-infected cells. These findings suggested that HBV cccDNA remained stable without requiring reimport of newly synthesised nucleocapsids *in vitro*. Furthermore, lack of *de novo* produced HBc did not affect the transcriptional activity of cccDNA.

The generation of fluorescently labelled HBV and HDV has been hampered by the complex genome organisation of both viruses, structural restriction of these small virions, and the large excess of non-infectious subviral particles. For this study, the amber suppression technology was chosen as labelling strategy. This method expands the genetic code by site-specific incorporation of non-canonical amino acids (ncAA) in response to amber stop codons. Combined with click chemistry fluorophores, this is currently the smallest fluorescent tag that can be genetically encoded into proteins. Amber stop codons were inserted at 11 positions in the HBc ORF, and the incorporation of ncAA in response to these stop codons could rescue the expression of full-length HBc. Secretion of infectious HBV particles was observed after genetic encoding of N-Propargyl-L-lysine in HBc, which enabled copper-catalysed click labelling and visualisation of incoming nucleocapsids during *in vitro* infection.

For the fluorescent labelling of HDV, we capitalised on the naturally present amber stop codon which terminates translation of the small hepatitis delta antigen (S-HDAg). During HDV replication, this amber stop codon is edited to a tryptophan codon, resulting in expression of a large HDAg (L-HDAg). Amber suppression mediated incorporation of ncAA at the amber stop could induce the production of L-HDAg with ncAA instead of tryptophan. Interestingly, the early expression of L-HDAg increased secretion and infectivity of HDV particles. L-HDAg could be labelled with a click chemistry functionalised fluorophore in transfected cells and in purified virions.

This study highlights the persistence of HBV cccDNA in infected cells without requiring continuous replenishment by nucleocapsid reimport, suggesting that therapeutic targeting of capsid reimport is likely not sufficient to eliminate cccDNA. Furthermore, genetic code expansion mediated labelling of HBV and HDV provides a tool to visualise viral entry processes.

II. Zusammenfassung

Hepatitis B Virus (HBV) und Hepatitis Delta Virus (HDV) sind humane Krankheitserreger, die akute und chronische Leberinfektionen auslösen, welche zu Leberentzündung, Zirrhose und Leberzellkarzinom führen können. Trotz der gesundheitlichen Belastungen durch HBV und HDV sind Therapieoptionen limitiert, wobei bisher keine Heilung verfügbar ist. Die Entdeckung des Gallensäuretransporters Natrium Taurocholat Cotransport Polypeptid (NTCP) als Eintrittsrezeptor für beide Viren eröffnete neue Möglichkeiten, um die Rolle von Virus- und Wirtsfaktoren für den viralen Eintritt und für das Persistieren der viralen Genome zu untersuchen. Die vorliegende Studie untersucht die Bedeutsamkeit von *de novo* synthetisiertem HBV Core Protein (HBc) für die Erhaltung der Persistenz von HBV. Zudem war das Ziel dieser Arbeit die Entwicklung von fluoreszenzmarkierten HBV und HDV Partikeln, um den viralen Eintrittsprozess und intrazellulären Transport zu untersuchen.

Wir haben eine infektiöse HBV Mutante entwickelt, die in ihrem Genom ein Stopcodon im HBc Gen enthält (Δ HBc HBV). Diese Mutante konnte nach der Infektion keine Nukleokapside produzieren. Nach *in vitro* Infektion mit Wildtyp (WT) und Δ HBc HBV wurden vergleichbare Mengen kovalent geschlossene zirkuläre (ccc)DNA gemessen. cccDNA ist die Vorlage für sämtliche virale Transkripte und damit zwingend notwendig für die virale Persistenz. cccDNA Werte, die Transkription viraler RNA und die Sekretion viraler Proteine blieben unverändert stabil in einer Langzeitinfektion mit WT und Δ HBc HBV in HepG2-NTCP Zellen. Die Erkenntnisse deuten an, dass HBV cccDNA auch ohne Reimport von neu synthetisierten Nukleokapsiden sehr stabil bleibt *in vitro*. Zudem hatte die Abwesenheit von *de novo* produziertem HBc keinen Einfluss auf die Transkriptionsaktivität von cccDNA.

Die Entwicklung von fluoreszenzmarkiertem HBV und HDV ist erschwert durch die komplexe Organisation beider viralen Genome, durch die strukturellen Einschränkungen dieser kleinen Viren und durch den Überfluss von nicht infektiösen subviralen Partikeln. Um diese Hindernisse zu überwinden, haben wir die Amber Suppression Technologie eingesetzt. Diese Methode erweitert den genetischen Code, indem nicht-kanonische Aminosäuren (ncAA) positionsspezifisch als Antwort auf ein Amber Stopcodon eingebaut werden. Kombiniert mit Click-Chemie Fluorophoren ist das zurzeit die kleinste fluoreszierende Markierung, die genetisch in Proteinen kodiert werden kann. Wir haben 11 Amber Stopcodons in den HBc Leserahmen mutiert und den Einbau von ncAA getestet. Der Einbau von ncAA konnte die Expression von vollständigem HBc wiederherstellen. Nach dem Einbau von N-Propargyl-L-

Lysin wurde die Sekretion von infektiösem HBV beobachtet. Dieses konnte mittels kupferkatalysierter Click-Chemie markiert werden und ermöglichte somit die Visualisierung von eingehenden viralen Partikeln während einer *in vitro* Infektion.

Für die Fluoreszenzmarkierung von HDV haben wir das natürlich vorkommende Amber Stopcodon von HDV ausgenutzt, welches die Translation des kleinen Hepatitis Delta Antigens (S-HDAg) beendet. Dieses Stopcodon wird während der HDV Replikation zu einem Tryptophan Codon editiert, was dann zur Expression des grossen HDAg (L-HDAg) führt. Wenn Amber Suppression an diesem Amber Stopcodon eine ncAA einbaut, führt dies zur Produktion von L-HDAg mit einer ncAA anstelle des Tryptophans. Interessanterweise wird durch die frühe Expression von L-HDAg mehr HDV sekretiert und die Infektiosität dieser Partikel erhöht. Wir konnten L-HDAg sowohl in transfizierten Zellen als auch in aufgereinigten Viren mit einem Click-Chemie Fluorophor markieren.

In dieser Arbeit wird die Persistenz der HBV cccDNA in infizierten Zellen hervorgehoben. Zum Erhalt der cccDNA wird der Reimport von Nukleokapsiden nicht benötigt. Diese Erkenntnis deutet darauf hin, dass Behandlungen, die die Produktion von Nukleokapsiden inhibieren, wahrscheinlich nicht genügen, um cccDNA zu eliminieren. Zudem bildet die Fluoreszenzmarkierung von HBV und HDV mittels Amber Suppression eine neue Grundlage, um virale Eintrittsprozesse zu visualisieren.

III. Table of contents

I.	Abstract	I
II.	Zusammenfassung	III
III.	Table of contents	V
IV.	List of abbreviations	XI
1.	Introduction	1
1.1.	Viral hepatitis	1
1.1.1.	Historical background	2
1.1.2.	Epidemiology and pathology	4
1.1.2.1.	Hepatitis B.....	4
1.1.2.2.	Hepatitis D.....	6
1.1.3.	Antiviral therapies for hepatitis B and D	7
1.1.3.1.	Treatment of Hepatitis B.....	8
1.1.3.2.	Treatment of hepatitis D.....	10
1.2.	Hepatitis B virus.....	12
1.2.1.	Classification.....	12
1.2.2.	Virus structure	12
1.2.3.	Genome organisation.....	13
1.2.4.	Viral transcripts and proteins	14
1.2.5.	HBV life cycle.....	17
1.2.5.1.	Entry into host cells.....	17
1.2.5.2.	Formation and maintenance of HBV cccDNA	19
1.2.5.3.	Replication and spread	20
1.3.	Hepatitis D virus.....	23
1.3.1.	Virus structure and genome.....	23
1.3.2.	HDV life cycle	24
1.4.	Fluorescent labelling of HBV and HDV	27

1.4.1. Labelling techniques for viruses and their application for HBV and HDV	27
1.4.1.1. Chemical labelling of proteins	27
1.4.1.2. Fluorescent proteins	28
1.4.1.3. Self-labelling enzymes	28
1.4.1.4. Stainable peptide tags.....	29
1.4.1.5. Targeting lipids or nucleic acids for labelling.....	29
1.4.2. Challenges for labelling of HBV and HDV	30
1.5. Site-specific protein labelling using amber suppression technology and click chemistry	32
1.5.1. Amber suppression mediated incorporation of non-canonical amino acids	32
1.5.2. Click chemistry labelling	34
1.5.2.1. Copper catalysed azide-alkyne cycloaddition (CuAAC)	34
1.5.2.2. Strain-promoted azide-alkyne cycloaddition (SPAAC).....	35
1.5.2.3. Strain-promoted inverse-electron demand Diels-Alder cycloaddition (SPIEDAC).....	35
1.5.2.4. Click chemistry functionalised silicon rhodamine (SiR) dyes	35
1.5.3. Amber suppression mediated labelling of viral proteins.....	36
1.6. Aims of this study	39
2. Materials & Methods.....	41
2.1. Materials.....	41
2.1.1. Bacterial strains	41
2.1.2. Eukaryotic cell lines	41
2.1.3. Cell culture media	41
2.1.4. Viruses.....	42
2.1.5. Antibodies	42
2.1.6. Chemicals	43
2.1.7. Buffers and solutions.....	44
2.1.8. Enzymes	45

2.1.9. Kits	46
2.1.10. Plasmids	46
2.1.11. Oligonucleotides.....	48
2.1.12. Software	49
2.2. Methods.....	50
2.2.1. Molecular cloning	50
2.2.1.1. Point mutation	50
2.2.1.2. Restriction digestion.....	50
2.2.1.3. Agarose gel electrophoresis	51
2.2.1.4. Ligation and transformation	51
2.2.1.5. Plasmid preparation.....	51
2.2.1.6. Sequencing	52
2.2.2. Cell culture	52
2.2.2.1. Maintenance of eukaryotic cells.....	52
2.2.2.2. Freezing and thawing of cells.....	52
2.2.2.3. Differentiation of HepaRG-NTCP cells.....	52
2.2.2.4. Transfection of Huh7 cells	53
2.2.2.5. Production and purification of Δ HBc HBV from transfected cells.....	53
2.2.2.6. Precipitation with PEG.....	54
2.2.2.7. Infection with HBV and HDV	54
2.2.2.8. Long-term infection of HepG2-NTCP cells.....	54
2.2.2.9. Incorporation of ncAA	55
2.2.2.10. Production and purification of HDV-TCO*.....	55
2.2.3. Detection of DNA and RNA	55
2.2.3.1. Caesium chloride (CsCl) density gradient centrifugation and HBV DNA dot blot.....	55
2.2.3.2. Quantification of cccDNA and total HBV DNA by cccDNA inversion quantitative (cinq)PCR.....	56

2.2.3.3. Detection of integrated HBV DNA by inverse nested PCR.....	57
2.2.3.4. Southern blotting	58
2.2.3.5. Quantitative PCR (qPCR) of HBV RNA	59
2.2.3.6. qPCR of viral HDV RNA.....	60
2.2.4. Detection of proteins	60
2.2.4.1. HBsAg/HBeAg measurement	60
2.2.4.2. SDS-PAGE.....	61
2.2.4.3. Western blotting	61
2.2.4.4. Immunofluorescence	62
2.2.4.5. SPIEDAC click labelling with SiRTet.....	62
2.2.4.6. CuAAC click labelling with SiR-Azide	62
2.2.4.7. Labelling of HDV-TCO* with SiRTet.....	63
3. Results	65
3.1. Maintenance and regulation of cccDNA in the absence of <i>de novo</i> synthesised HBV nucleocapsids	65
3.1.1. Generation and characterisation of HBc-deficient (Δ HBc) HBV	66
3.1.1.1. Trans-complementation of HBc-deficient HBV with WT HBc rescues the secretion of HBV virions.....	66
3.1.1.2. Δ HBc HBV is as infectious as WT HBV	67
3.1.2. Establishment of cccDNA after infection with Δ HBc HBV	70
3.1.3. The role of HBc in long-term maintenance and regulation of cccDNA	72
3.1.3.1. cccDNA is maintained during long-term infection of HepG2-NTCP cells	72
3.1.3.2. <i>De novo</i> expressed HBc does not affect transcription from cccDNA.....	74
3.2. Amber suppression mediated incorporation of ncAA into the HBV core protein for click chemistry labelling	77
3.2.1. Optimisation of amber suppression.....	78
3.2.2. Identification of optimal amino acid sites for the introduction of ncAA into HBc	83

3.2.2.1. HBeAg secretion is rescued by the incorporation of ncAA through amber suppression	84
3.2.2.2. Amber suppression mediated ncAA incorporation rescues full-length HBc expression.....	86
3.2.3. Click chemistry labelling of incorporated amino acids.....	87
3.2.4. Secretion and infectivity of HBV with incorporated ncAA.....	90
3.2.4.1. HBV secretion is impaired by the incorporation of large ring structured ncAA	90
3.2.4.2. HBV remains infectious after incorporation of ncAA in the capsid.....	92
3.2.4.3. The incorporation of PrK allows secretion of HBV without impairing infectivity	96
3.2.5. Visualisation of HBV-T67PrK.....	99
3.2.5.1. Copper-catalysed click chemistry specifically labels HBV-T67PrK.....	99
3.2.5.2. HBV-T67PrK particles are internalised into HepG2-NTCP cells and transported to the nuclear periphery.....	100
3.2.5.3. Heparin treatment inhibits internalisation of HBV-T67PrK.....	102
3.3. Incorporation of TCO* at the HDV amber/W site for click chemistry labelling.....	105
3.3.1. Incorporation of TCO* at the HDV amber/W site.....	106
3.3.1.1. Amber suppression induces the expression of L-HDAg.....	106
3.3.1.2. L-HDAg with incorporated TCO* can be click labelled in live cells.....	107
3.3.2. Incorporation of TCO* into HDV virions.....	109
3.3.2.1. Amber suppression mediated induction of L-HDAg enhances HDV secretion	109
3.3.2.2. HDV remains infectious when every L-HDAg is exclusively induced by amber suppression instead of ADAR1 editing.....	111
3.3.3. Production and infectivity of HDV-TCO*	115
3.3.4. Labelling of HDV virus particles	117
3.3.5. Increased specific infectivity of HDV-TCO*	118
4. Discussion	121

4.1. Newly produced HBc does not contribute to cccDNA maintenance or expression....	121
4.1.1. cccDNA is maintained in the absence of <i>de novo</i> HBc.....	122
4.1.2. <i>De novo</i> expressed HBc does not alter HBV transcription	124
4.1.3. Advances in molecular tools	125
4.1.4. Virological and clinical implications	126
4.1.5. Limitations and future work.....	128
4.2. Amber suppression mediated labelling of HBc.....	129
4.2.1. Investigation of HBV entry using click labelling.....	129
4.2.2. Amber stop codon suppression within the HBc ORF	131
4.2.3. Limitations and future work.....	131
4.3. Labelling of HDV ribonucleoproteins.....	134
4.3.1. Fluorescent labelling of cellular and virion L-HDAg	134
4.3.2. HDV secretion and infectivity are enhanced by amber suppression.....	135
4.3.3. Reversion of ochre stop mutation.....	137
4.3.4. Limitations and future work.....	138
4.4. Application of genetic code expansion in HBV and HDV virology.....	139
4.4.1. Challenges of the amber suppression technology	139
4.4.2. Advancements and future applications of genetic code expansion.....	140
4.5. Final conclusions.....	142
5. References	143
6. Publications	174
6.1. Peer-reviewed publications	174
6.2. Oral presentations.....	174
6.3. Poster presentations.....	175
7. Acknowledgments.....	176

IV. List of abbreviations

aaRS	Aminoacyl-tRNA synthetase
AAV	Adeno-associated virus
ADAR1	Adenosine deaminase acting on RNA 1
ALT	Alanine aminotransferase
APS	Ammonium persulfate
ATP	Adenosine triphosphate
AuAg	Australia antigen

BCN	Bicyclo nonyne-lysine
BOC	N-epsilon-t-butyloxycarbonyl L-lysine
BSA	Bovine serum albumin

cccDNA	Covalently closed circular DNA
cDNA	Complementary DNA
CHB	Chronic hepatitis B
CHD	Chronic hepatitis D
cinqPCR	cccDNA inversion quantitative PCR
CpK	Cyclopropene L-lysine
CsCl	Caesium chloride
C-terminus	Carboxy terminus
CuAAC	Copper catalysed azide-alkyne cycloaddition

Da	Dalton
dCTP	deoxycytidine triphosphate
DDB1	DNA-damage binding protein 1
ddPCR	Droplet digital PCR
Δ HBc HBV	HBc-deficient HBV
DHBV	Duck hepatitis B virus
DMEM	Dulbecco's Modified Eagle Medium
DMSO	Dimethylsulfoxide
DNA	Deoxyribonucleic acid
dpi	Days post infection
DR	Direct repeat
dsDNA	Double-stranded linear DNA
DTT	Dithiothreitol

EASL	European Association for the Study of the Liver
<i>E. coli</i>	<i>Escherichia coli</i>
EdC	Deoxy-5-ethynylcytidine
EDTA	Ethylenediaminetetraacetic acid
EdU	Deoxy-5-ethynyluridine
EEA1	Early endosome antigen 1

EGFR	Epidermal growth factor receptor
ELISA	Enzyme-linked immunosorbent assay
Enh	Enhancer
Env	HIV envelope glycoprotein
ER	Endoplasmic reticulum
eRF	Eukaryotic release factor
ESCRT	Endosomal sorting complexes required for transport
FBS	Fetal bovine serum
FEN1	Flap structure-specific endonuclease 1
FP	Fluorescent protein
FRET	Förster resonance energy transfer
GFP	Green fluorescent protein
h	Hour
HA	Hemagglutinin
HAV	Hepatitis A virus
HBc	Hepatitis B core protein
HBeAg	Hepatitis B e antigen
HBsAg	Hepatitis B surface antigen
HBV	Hepatitis B virus
HBx	Hepatitis B X protein
HCC	Hepatocellular carcinoma
HCV	Hepatitis C virus
HDAg	Hepatitis delta antigen
HDV	Hepatitis delta virus
HEV	Hepatitis E virus
HIV	Human immunodeficiency virus
HSPG	Heparan sulphate proteoglycan
HSV	Herpes simplex virus
IAV	Influenza A virus
IF	Immunofluorescence
IFN- α	Interferon- α
kb	Kilobase
LB	Lysogeny broth
L-HBsAg	Large hepatitis B surface antigen
L-HDAg	Large hepatitis delta antigen
M	Molar
<i>M. barkeri</i>	<i>Methanosarcina barkeri</i>
mge	Multiplicity of genome equivalents
M-HBsAg	Middle hepatitis B surface antigen
min	Minute
<i>M. jannaschii</i>	<i>Methanocaldococcus jannaschii</i>

<i>M. mazei</i>	<i>Methanosarcina mazei</i>
mRNA	Messenger RNA
MVB	Multivesicular body
MyrB	Myrcludex B
NAP	Nucleic acid polymer
ncAA	Non-canonical amino acid
NHS	N-Hydroxysuccinimide
NLS	Nuclear localisation signal
NPC	Nuclear pore complex
nt	Nucleotide
NTCP	Sodium taurocholate cotransporting polypeptide
N-terminus	Amino terminus
NUC	Nucleos(t)ide analogue
ORF	Open reading frame
PAGE	Polyacrylamide gel electrophoresis
PBS	Phosphate buffered saline
PCR	Polymerase chain reaction
PD-1	Programmed death 1
PEG	Polyethylenglycol
PFA	Paraformaldehyde
pgRNA	Pregenomic RNA
PHH	Primary human hepatocytes
PrK	N-Propargyl-L-Lysine
Pyl	Pyrrolysine
PylRS	Pyrrolysine-tRNA synthetase
qPCR	Quantitative PCR
rcDNA	Relaxed circular DNA
RIG-I	Retinoic acid inducible gene I
RNA	Ribonucleic acid
RNP	Ribonucleoprotein
rpm	Revolutions per minute
RT	Room temperature
SCO	Cyclooctyne-lysine
SDS	Sodium dodecyl sulfate
SiR	Silicon rhodamine
SiRTet	SiR-tetrazine
S-HBsAg	Small hepatitis B surface antigen
S-HDAg	Small hepatitis delta antigen
SMC5/6	Structural maintenance of chromosome 5/6
SPAAC	Strain-promoted azide-alkyne cycloaddition
SPIEDAC	Strain-promoted inverse-electron demand Diels-Alder cycloaddition

SSC	Standard saline citrate
SVP	Subviral particle
<hr/>	
TAE	Tris-acetate-EDTA buffer
TBS	Tris buffered saline
TBS-T	Tris buffered saline - tween 20
TC	Tetracysteine
TCO*	Trans-Cyclooct-2-ene L-lysine
TDP2	tyrosyl-DNA phosphodiesterase 2
TDF	Tenofovir disoproxil
TE	Tris-EDTA buffer
TEMED	Tetramethylethylene-diamine
TLR	Toll-like receptor
TN	Tris-NaCl buffer
TP	Terminal protein
Tris	Tris(hydroxymethyl)-aminomethane
tRNA	Transfer RNA
TyrRS	Tyrosyl-tRNA synthetase
<hr/>	
U	Unit
UV	Ultraviolet
<hr/>	
vge	Viral genome equivalent
VSV	Vesicular stomatitis virus
<hr/>	
WB	Western blot
WHO	World health organisation
wpi	Weeks post infection
WT	Wild-type

1. Introduction

1.1. Viral hepatitis

Viral hepatitis describes the inflammation of the liver caused by viral infection. Viral hepatitis is a leading cause of death and disability worldwide, causing more than 1.4 million deaths per year (Stanaway et al. 2016). Five main hepatitis viruses have been described: hepatitis A virus (HAV), hepatitis B virus (HBV), hepatitis C virus (HCV), hepatitis D virus (HDV), and hepatitis E virus (HEV). These five viruses share the tropism for liver cells but are genetically unrelated.

HAV and HEV are positive-sense single-stranded RNA viruses which both cause acute, self-limiting infections and are transmitted by a faecal-oral route. Infections mostly occur through exposure to contaminated food or water, or to infected persons. Both viruses are mostly endemic in developing countries and their infection can be prevented by improvement of hygiene and sanitation measures. A safe and efficient vaccine for immunoprophylaxis of HAV is available since 1992, whereas a vaccine to prevent HEV infection has been licensed in China but not yet elsewhere (WHO 2017; Tahaei et al. 2012).

HCV, another positive-sense single-stranded RNA virus, is transmitted parenterally mainly by injection drug use, sexual transmission, or especially in the past with a lack of testing by contaminated blood products. HCV infections establish chronicity in 75-80% of patients which leads to liver complications like cirrhosis and hepatocellular carcinoma in 10-20% of chronically infected patients (HCC). Currently, 71 million individuals are estimated to be chronically infected with HCV. A vaccine to prevent HCV infection is not available, but therapy using direct-acting antivirals can achieve cure in more than 90% of infected patients (Spearman et al. 2019).

HBV can be transmitted by parenteral contact with infected body fluids but is most often vertically transmitted from mother to child. HBV infections in adults are mostly acute and self-limiting but 80-90% of perinatally infected newborns develop chronicity. Chronic hepatitis B (CHB) is defined by viral persistence for more than 6 months but often lasts for decades or lifelong. It is associated with chronic inflammation of the liver and a highly elevated risk of developing cirrhosis and HCC. It is estimated to affect 257-291 million infected individuals worldwide (WHO 2017; Polaris Observatory 2018).

HDV can only propagate in the presence of HBV and therefore productive HDV infection requires co-infection or a pre-existing infection with HBV. Estimations on HDV prevalence range from 12 to 72 million patients globally (Stockdale et al. 2020; Miao et al. 2020; Chen et al. 2019). Chronic hepatitis D (CHD) infection is associated with an elevated risk of developing liver cirrhosis and HCC compared to CHB. While a vaccine is available against HBV, which also prevents HDV infections, curative treatment has not yet been achieved for HBV or HDV. Current therapies can reduce the viral load but rarely result in sustained clearance of chronic infection.

1.1.1. Historical background

The identification of hepatitis viruses has been particularly difficult due to the lengthy incubation time and the lack of animal and cell culture models. Epidemic jaundice was already described by Hippocrates around 400 years B.C. and in the 8th century, pope Zackary wrote a letter to the bishop in Mainz mentioning the contagious nature of jaundice (Trepo 2014). Transmission of serum hepatitis was first described in 1885, when outbreaks of jaundice were observed following vaccinations against smallpox in the German cities Bremen and Merzig (Lurmann 1885; Jehn 1885). At that time, smallpox vaccines were obtained from lesions induced by previous vaccinations of other people, and yellow fever vaccines were supplemented with human serum as stabiliser (Gerlich 2013). Further transmission of serum hepatitis was promoted by re-using of needles with the introduction of medications like insulin for diabetes treatment (Flaum et al. 1926). Yellow fever vaccinations lead to several outbreaks of hepatitis in the 1930s-40s, for example the US Army experienced a massive outbreak with more than 50,000 cases (Turner et al. 1944). A retrospective analysis, performed more than 40 years later with surviving veterans, confirmed that this outbreak had indeed been caused by HBV (Seeff et al. 1987). Strikingly, CHB was only found in one subject. Even earlier, jaundice was connected to certain lots of the vaccine and no more cases of jaundice occurred with the omission of human serum, unfortunately this was not applied in the mass vaccinations in the US (Fox et al. 1942). In a series of ethically questionable experiments conducted on human volunteers, transmission routes, incubation time, and symptoms of infectious hepatitis (later named hepatitis A) and serum hepatitis (hepatitis B) were characterised (Findlay and Willcox 1945; Neefe et al. 1944). These findings were confirmed by long term infection studies performed at the New York Willowbrook State School on handicapped children and adults, unimaginable by today's ethical standards (Krugman et al. 1967). Although these experiments

did not lead to a breakthrough in the discovery of the etiologic agents, at least they contributed to the discussion on research ethics (Rothman 1982).

The key discovery in the identification of HBV was made when Blumberg and Alter used immunodiffusion assays to analyse reactivity of sera from haemophilia patients with Blumberg's collection of sera from populations around the world. The haemophilia patients had been at high risk for contracting hepatitis B because they had received multiple blood transfusions and on the other hand, some of the samples collected by Blumberg originated from geographic regions with high hepatitis B prevalence. The sera of two haemophilia patients were found to immunoprecipitate with a sample collected from an indigenous Australian. Without knowing that this was the first direct detection of the HBV surface antigen (HBsAg), the authors named it the Australia antigen (AuAg) (Blumberg et al. 1965). The connection between AuAg and hepatitis B was made a few years later following a series of observations. A technician in Blumberg's lab, whose serum had previously served as negative control, became ill and her serum had become AuAg-positive (Blumberg et al. 1968). Using similar immunodiffusion assays, Prince tested a number of patients with serum hepatitis, including samples from the Willowbrook State School, and thereby connected the immunoprecipitation band to serum hepatitis and to AuAg (Prince 1968a, 1968b). Confirming the infectious nature of AuAg, patients who received AuAg-positive transfusions developed abnormal liver functions and became positive for AuAg (Okochi and Murakami 1968). Following the first evidence that linked HBsAg to serum hepatitis, blood banks were routinely screened for HBsAg which helped to prevent further transmission of hepatitis B.

HBV virions were finally detected by Dane et al. using immunoelectron microscopy and are still referred to as Dane particles (Dane et al. 1970). DNA polymerase activity was found within HBV particles in 1973 and the HBV genome was cloned and sequenced in 1979 (Kaplan et al. 1973; Pasek et al. 1979). Cloned HBV DNA was experimentally injected into chimpanzees and resulted in replication of HBV within the liver accompanied by acute hepatitis, providing final proof that the Dane particle with the enclosed DNA is the causative agent of hepatitis B (Will et al. 1982). The first vaccine against HBV was based on purified and inactivated HBsAg derived from CHB patients (Blumberg and Millman 1972). Genetic engineering enabled expression of HBsAg in yeast cells which became the standard vaccine against HBV (Valenzuela et al. 1982; McAleer et al. 1984).

HAV was identified in 1973 as spherical 27 nm particles by immunoelectron microscopy in stool samples of HAV infected patients (Feinstone et al. 1973). An inactivated HAV vaccine

has been licensed in the 1990s. Even after screening for HBsAg in blood transfusions, cases of serum hepatitis following transfusions still occurred, leading to the presumption of a “Non-A Non-B” hepatitis virus (later named HCV) (Alter et al. 1975). HCV was the first virus to be identified by a direct molecular approach when cDNA from an infected chimpanzee was recombinantly expressed and screened against the serum of an infected patient (Choo et al. 1989). Potent direct-acting antivirals with curative effect are now available to treat chronic hepatitis C.

The discovery of HDV began in 1977 when Rizzetto et al. described a new antigen in HBsAg-positive liver biopsies (Rizzetto et al. 1977). This novel antigen was named “delta” and was only found in HBV patients, so it was initially considered to be an additional marker for HBV infections. Subsequent infection experiments in chimpanzees found that the delta antigen was part of a defective virus that required HBV as a helper virus (Rizzetto et al. 1980a). During the acute phase of infection, the delta antigen was associated with HBsAg and a small RNA molecule in the serum of infected chimpanzees (Rizzetto et al. 1980b). The delta antigen associated particles with a size of 35-37 nm were consequently named HDV. The structure and sequence of HDV RNA were subsequently analysed and published (Wang et al. 1986).

Finally, HEV was discovered after outbreaks of infectious hepatitis with no evidence of HAV. The Russian virologist Balayan acquired the disease himself by swallowing faecal extracts of patients, developed hepatitis A like symptoms, and identified viral particles in his stool by immunoelectron microscopy (Balayan et al. 1983).

1.1.2. Epidemiology and pathology

1.1.2.1. Hepatitis B

Around 29 million people have been diagnosed with chronic HBV infection, but it is estimated that this only represents ~10% of the >250 million people currently living with CHB worldwide (WHO 2017; Polaris Observatory 2018). The transmission rates are decreasing following vaccination programs and prevention of mother-to-child transmission using antiviral treatments. High prevalence of HBsAg is found in Sub-Saharan Africa, Oceania, and large parts of Asia (Figure 1.1). North Africa, the Middle East, and parts of Eastern Europe have a moderate incidence of hepatitis B. High income countries in North America, Western Europe, Australia, and Japan generally display low HBsAg prevalence (Polaris Observatory 2018).

HBV related deaths caused by liver cirrhosis or liver cancer are still increasing and CHB accounted for around 800,000 deaths worldwide in 2015 (WHO 2016). Furthermore, people living with CHB suffer from stigma and discrimination (Tu et al. 2020a).

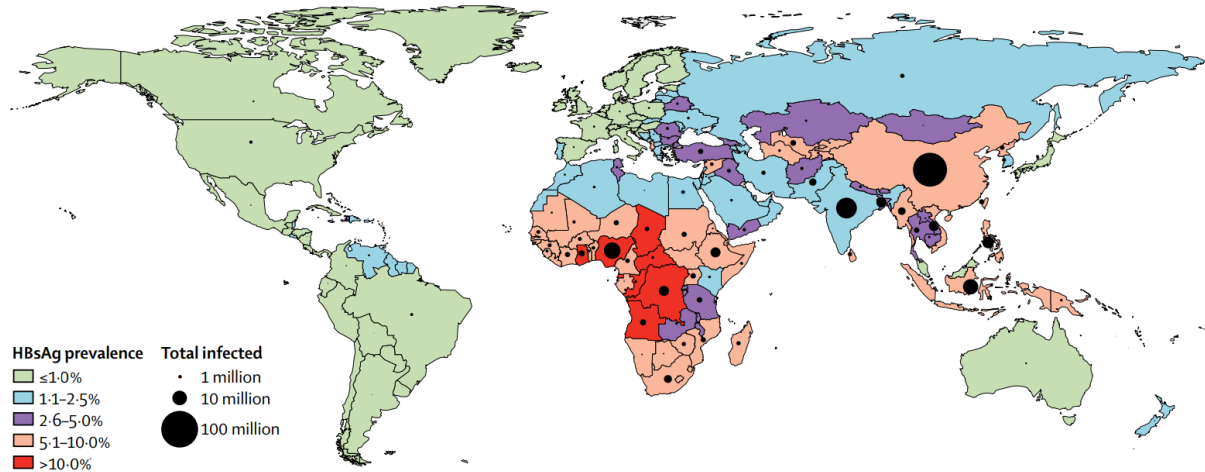


Figure 1.1. Estimates of HBV prevalence in 2016. The estimation of HBsAg prevalence for countries is based on data and modelling. Data was extrapolated from countries with the same or similar burden of diseases if data for a country was not available. From (Polaris Observatory 2018) with permission.

The probability of developing chronicity decreases with age and ~95% of adults can clear newly acquired HBV infections, often without any symptoms. Upon HBV infection, virus replication does not induce cytopathic effects but hepatocyte damage during acute infections is mainly mediated by infiltrating CD8⁺ T cells (Thimme et al. 2003). Acutely resolving infections are cleared by an efficient immune response against HBV. Robust adaptive T cells, antiviral effect by expression of cytokines, and induction of B cells which produce neutralising antibodies against HBsAg terminate acute infections.

Perinatal exposure of neonates to HBV from a HBV-positive mother leads to a chronic infection in 80-90% of cases (Edmunds et al. 1993). Chronically infected patients have weaker T cell responses, and their T cells show an exhausted phenotype probably caused by the constant high concentration of viral antigens (Boni et al. 2007). Chronic infection, which can last lifelong, is a dynamic process depending on the interaction between HBV replication and the host immune system. The European Association for the Study of the Liver (EASL) classifies chronic hepatitis B infection in five phases, taking into account markers of liver inflammation and viral markers like HBV e antigen (HBeAg), HBV DNA, and HBsAg (EASL 2017). These phases may be but are not necessarily strictly consecutive. The first phase is the HBeAg-positive chronic HBV infection or immune tolerant phase. This phase is characterised by high levels of HBeAg and high viremia, but minimal liver inflammation. During this phase, patients are highly infectious. In the second phase, HBeAg-positive CHB, HBeAg and HBV DNA levels remain high and

additionally, alanine aminotransferase (ALT) levels are elevated. Liver inflammation and progression to fibrosis are detectable. These two phases can both last for years before a patient may achieve HBeAg seroconversion and move to the HBeAg-negative chronic infection phase. If patients fail to control HBV, they may progress to HBeAg-negative CHB (EASL 2017).

The HBeAg-negative chronic HBV infection or inactive carrier phase is characterised by the presence of anti-HBeAg antibodies, low HBV DNA, and normal ALT levels indicating that there is no detectable liver inflammation. These patients generally have a low risk of developing cirrhosis or HCC, but progression to HBeAg-negative CHB may occur. Compared to the chronic HBV infection phase, HBeAg-negative CHB is characterised by persistent or fluctuating levels of serum HBV DNA and ALT levels. Advanced liver damage can be observed during this phase.

Finally, the HBsAg-negative phase is characterised by lack of detectable serum HBsAg and may include the presence of anti-HBsAg antibodies. This phase is also referred to as occult HBV infection. Patients with occult HBV infection have a minimal risk of developing liver cirrhosis and HCC, but often HBV DNA can still be detected in the liver and immunosuppression can lead to HBV reactivation. The loss of HBsAg is currently regarded as functional cure and optimal treatment endpoint. Functional cure is associated with an improved clinical outcome and a decrease in the risk of developing cirrhosis or HCC. A complete cure from CHB is additionally constituted by eradication of intrahepatic HBV DNA (Lok et al. 2017). However, elimination of the persistent nuclear forms of HBV DNA, covalently closed circular DNA (cccDNA) and integrated DNA, cannot be achieved with current treatment options.

1.1.2.2. Hepatitis D

The estimation of HDV prevalence is difficult because HDV infections are not routinely tested for in most settings and the prevalence vastly differs depending on geographic regions. Recent meta-analyses estimated the total number of HDV patients to be between 12-72 million worldwide (Stockdale et al. 2020; Miao et al. 2020; Chen et al. 2019). Highly endemic regions are found in Mongolia, Central Asia, West and Central Africa, the Amazon basin in South America, and some areas of Eastern Europe (Figure 1.2). Like HBV, HDV is transmitted by parenteral routes. Injection drug users and people with high-risk sexual behaviour are at high risk of HDV infection (Stockdale et al. 2020). In regions of high endemicity, transmission within household contacts has been reported (Sagnelli et al. 1992; Francois-Souquiere et al. 2016). In contrast to HBV, perinatal transmission from mother to child is uncommon (Ramia

and Bahakim 1988). Vaccination against HBV protects from HDV infection, therefore the implementation of vaccination programs against HBV has led to a reduction of HDV prevalence (Rizzetto et al. 2021).

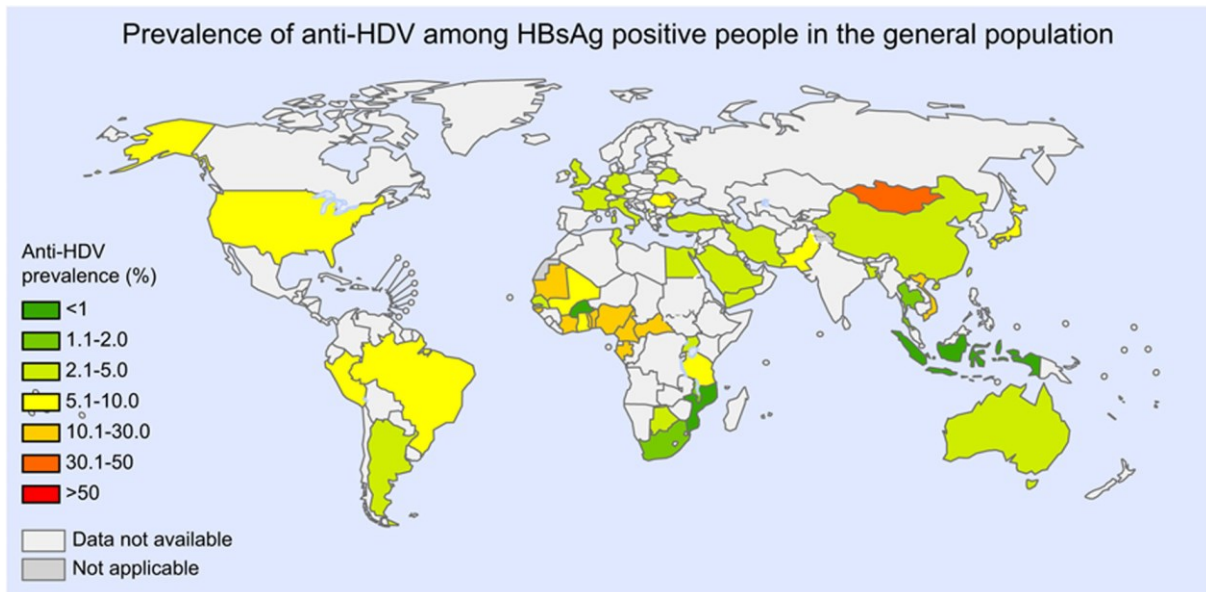


Figure 1.2. Estimates of HDV prevalence. HDV prevalence is shown as number of people who have antibodies against HDV among HBsAg-positive individuals and was estimated based on globally available epidemiological data from 1998 to 2019. From (Stockdale et al. 2020).

Newly acquired co-infection with HBV and HDV can cause severe hepatitis, but it is generally self-limiting, similar to HBV mono-infection in adults (Smedile et al. 1982; Caredda et al. 1985). Co- or super-infection with HDV induces severe liver damage, demonstrated by the highest ALT peak ever documented in chimpanzee studies (Engle et al. 2020). In contrast to co-infection, super-infection of CHB patients with HDV leads to progressive CHD in more than 90% of cases (Farci and Niro 2012). Chronic infection with HBV and HDV is more severe than CHB without HDV. CHD patients progress faster to cirrhosis, have a 3-fold higher risk of developing HCC, and a 2-fold increased mortality when compared with CHB alone (Fattovich et al. 2000).

1.1.3. Antiviral therapies for hepatitis B and D

Vaccination programs to prevent HBV infections have been enormously successful. For example, the nationwide vaccination program in Taiwan, launched in 1984, has steadily decreased HBsAg prevalence and HCC incidence (Chien et al. 2006). In addition, hepatitis B immunoglobulins (HBIG), human plasma derived polyclonal antibodies against HBsAg, are used as postexposure prophylaxis and to prevent vertical transmission during childbirth of

infants born to mothers with CHB (Habib and Shaikh 2007). Nevertheless, millions of people live with CHB or CHD and are in need for antiviral treatment.

1.1.3.1. Treatment of Hepatitis B

The main goal for treatment of patients with CHB is to improve survival and quality of life by preventing disease progression and development of liver cirrhosis and HCC. Currently, eight drugs are approved for the treatment of chronic HBV infection: conventional and pegylated interferon- α (IFN- α) and the six nucleos(t)ide analogues (NUCs) lamivudine, adefovir, telbivudine, entecavir, tenofovir, and its prodrug tenofovir alafenamide.

IFN- α is administered by subcutaneous injection and has both immunostimulatory and direct antiviral effects. IFN- α was shown to activate the nuclear deaminase APOBEC3A which in turn utilises the HBV core protein (HBc) to target and deaminate cccDNA suggesting a non-cytolytic clearance of infection (Lucifora et al. 2014). Furthermore, interferon stimulated genes are reported to be involved in epigenetic and transcriptional control of cccDNA (Belloni et al. 2012; Uprichard et al. 2003). On the immunological side, IFN- α induces expansion of natural killer cells that can target HBV infected cells (Gill et al. 2016). In contrast to mono-treatment with NUCs, IFN- α treatment reduces HBsAg levels in patients (Brunetto et al. 2009). However, while IFN- α treatment may be more effective than NUC treatment with respect to HBsAg loss and thus functional cure, still only a minority of patients treated with IFN- α achieve functional cure (EASL 2017). IFN- α treatment often causes considerable side effects and not all patients are eligible to IFN- α treatment.

NUCs can be taken orally, and they directly inhibit reverse transcription of HBV pregenomic RNA (pgRNA) to the viral relaxed circular DNA (rcDNA). Lamivudine, the first NUC approved for treatment of hepatitis B, was previously licensed as human immunodeficiency virus (HIV) drug (Dienstag et al. 1995). NUC treatment results in a decline of serum HBV DNA in virtually all patients and HBeAg seroconversion in many cases, but it does not significantly affect cccDNA or HBsAg levels (Werle-Lapostolle et al. 2004). Therefore, NUC treatment is often maintained indefinitely to prevent viral relapse. Emergence of viral resistance to NUCs is a major problem for some drugs of this class. Drug resistance has mostly been described for the early NUCs lamivudine (80% resistance after 5 years), adefovir (29% after 5 years), and telbivudine (21% after 2 years) (Zoulim and Locarnini 2009). Entecavir and tenofovir are associated with a much higher barrier to resistance. However, pre-existing resistance to lamivudine increases the risk of additional resistance mutations to adefovir and entecavir (Lee et al. 2006; Tenney et al. 2009). After ten years of treatment with tenofovir, almost all patients

achieved sustained reduction in serum HBV DNA and HBeAg levels with no detectable resistance (Marcellin et al. 2019). Current treatment with NUCs improves the quality of life and survival of patients by improving liver functions and reducing the risk of HCC (Liaw et al. 2004), but the therapy with NUCs is not curative.

Other direct-acting antivirals and immunomodulatory drug are being investigated. Several capsid inhibitors are currently in clinical trials for treatment of CHB. Two different categories of capsid inhibitors are of interest: core protein allosteric modulators cause misassembly of capsids, whereas capsid assembly modulators lead to formation of empty capsids devoid of nucleic acids (Fanning et al. 2019). Capsid inhibitors not only block the formation of nucleocapsids and subsequent replication but can also prevent infection from incoming virions (Guo et al. 2017; Berke et al. 2017). Furthermore, capsid inhibitors might interfere with HBc mediated cccDNA transcription and stability (Lahlali et al. 2018; Chong et al. 2017; Belloni et al. 2015). Treatment with capsid inhibitors in clinical studies has shown decline in serum HBV DNA and RNA but not HBsAg (Yuen et al. 2019a; Fanning et al. 2019).

Targeting viral transcripts and proteins is a promising approach because the reduction of viral antigens might help to recover an HBV-specific immune response. siRNAs that target HBV RNAs have shown significant and sustained reduction of HBsAg levels in clinical trials (Yuen et al. 2020; Yuen et al. 2019b). Another group of antiviral drugs that decrease HBsAg levels are nucleic acid polymers (NAPs). NAPs impair the secretion of HBsAg without accumulating intracellular HBsAg or affecting other viral markers, however the exact mechanism remains unknown (Boulon et al. 2020). In clinical trials, NAP treatment (in addition to a backbone therapy with tenofovir and IFN- α) resulted in reduction of HBsAg and most strikingly, 14 of 36 patients reached functional cure with persistent HBsAg seroconversion (Bazinet et al. 2020).

The activation of HBV specific T cells and neutralising antibodies against HBsAg is important for achieving functional cure. Thus, several strategies targeting the innate and adaptive immune systems are being pursued. Agonists of Toll-like receptors (TLR) and retinoic acid inducible gene I (RIG-I) are used to activate innate immunity but have so far only been shown to achieve moderate decline of HBsAg (Janssen et al. 2018; Gane et al. 2021; Yuen et al. 2019c). Exhausted T cells in CHB patients overexpress programmed death 1 (PD-1) which negatively regulates T cell activation (Boni et al. 2007). A pilot study investigating an inhibitor against PD-1 suggests a decline of HBsAg levels in most patients (Gane et al. 2019). However, anti-PD-1 drugs are not able to restore an immune response in all patients, likely due to immune factors beyond PD-1 expression (Bensch et al. 2014; Wykes and Lewin 2018). Several

therapeutic vaccines have been tested but have unfortunately failed to induce HBV specific immunity. The low efficacy of therapeutic vaccines might be explained by the exhausted phenotype of T cells and the immunotolerance caused by the high levels of HBeAg and HBsAg in CHB patients (Fanning et al. 2019).

A complete cure from HBV DNA is unlikely to be feasible as it requires eradication of all viral markers, including the highly persistent cccDNA and integrated HBV. Therefore, functional cure, which is characterised by elimination of HBsAg and associated with improved clinical outcomes, is regarded as optimal treatment endpoint in most clinical studies. To achieve HBV functional cure, combinations of antiviral therapy that suppresses HBV replication (and ideally reduces HBsAg levels) together with an activation of the immune response are likely needed.

1.1.3.2. Treatment of hepatitis D

Until recently, off-label use of IFN- α was the only treatment option for HDV infection. Treatment of CHD patients with IFN- α for 48 weeks resulted in HDV RNA negativity in about 24% of cases, however viral relapse was observed in many patients in a long-term follow-up study (Wedemeyer et al. 2011; Heidrich et al. 2014). Another study extended the IFN- α treatment to 96 weeks but could not improve the virological response rates and HDV relapse still occurred in patients with residual low HDV RNA levels (Wedemeyer et al. 2019b; Bremer et al. 2021). Taking into account the side effects caused by IFN- α treatment, these results highlighted the need for better treatment options against CHD.

Myrcludex B (MyrB, Bulevirtide, Hepcludex), a first-in-class entry inhibitor, was recently the first drug to be approved for CHD treatment in Europe (Kang and Syed 2020). MyrB is a synthetic peptide comprising amino acids 2-48 of the preS1 region of the large HBV surface protein (L-HBsAg) with N-terminal myristoylation. MyrB can efficiently bind to the HBV receptor sodium taurocholate cotransporting polypeptide (NTCP) and block entry of HBV and HDV at low concentrations (Gripon et al. 2005; Glebe et al. 2005; Yan et al. 2012). Daily subcutaneous administration of MyrB showed a strong effect on serum HDV RNA levels in a dose-dependent manner and liver biopsies showed an elimination of HDV-positive hepatocytes (Bogomolov et al. 2016; Wedemeyer et al. 2018; Allweiss et al. 2018a). Unfortunately, viral relapse occurred in most patients after 24 weeks of treatment. However, HDV RNA continuously decreased over time indicating that longer therapies may be needed to eliminate HDV. Combination therapy with MyrB and IFN- α demonstrated high rates of sustained HDV RNA loss 24 weeks after cessation of treatment (Wedemeyer et al. 2019a). Remarkably, the most recently presented data showed a synergistic effect on HBsAg by low concentration

dosing of MyrB and IFN- α treatment, suggesting a benefit in the application of combination treatment for CHB patients (Wedemeyer et al. 2020). Monotherapy with MyrB did not significantly decrease HBV DNA levels (Bogomolov et al. 2016), indicating that HBV does not require continuous reinfection to maintain persistence.

Lonafarnib is an inhibitor of human farnesyl transferase, thus it inhibits the prenylation of the large hepatitis delta antigen (L-HDAg) which is required for assembly of virions. Lonafarnib treatment could substantially reduce HDV RNA levels in patients, but adverse effects were frequently observed (Koh et al. 2015). Co-administration with ritonavir (a cytochrome P450 3A4 inhibitor) allowed to reduce the lonafarnib dosage, resulting in enhanced virological response and better tolerability (Yurdaydin et al. 2018).

The HBsAg assembly/secretion inhibiting NAPs are also investigated in CHD patients. Combination with IFN- α demonstrated sustained control of HBV and HDV up to 3.5 years after cessation of therapy (Bazinet et al. 2021). Even though the exact mode of action of NAPs remains unclear, the reported rates of HBsAg loss are promising for achieving cure from hepatitis B and D.

1.2. Hepatitis B virus

1.2.1. Classification

HBV is classified in the genus *Orthohepadnavirus* within the family *Hepadnaviridae*, a family comprising small enveloped viruses with a partially double-stranded DNA genome that infect the liver. As double-stranded DNA viruses that have an RNA intermediate and a reverse transcription step during their replication, *Hepadnaviridae* are classified in the seventh group in the Baltimore classification. A sister family of non-enveloped fish viruses related to *Hepadnaviridae*, designated nakednaviruses, was recently reported (Lauber et al. 2017). Within the family of *Hepadnaviridae*, five genera are described: *Parahepadnavirus*, *Metahepadnavirus*, *Herpetohepadnavirus*, *Avihepadnavirus*, and *Orthohepadnavirus* (Magnius et al. 2020). *Meta-* and *Parahepadnaviruses* were discovered in fish, *herpetohepadnavirus* was found to infect reptiles and frogs, members of *Avihepadnavirus* infect birds, and finally *Orthohepadnavirus* is found in mammals. The prototype member of the genus *Orthohepadnavirus* HBV has a narrow host range and tissue tropism, infecting only liver cells of humans and chimpanzees.

1.2.2. Virus structure

The infectious HBV virion, known as Dane particle, is 42 nm in diameter and consists of a DNA containing nucleocapsid and a membrane envelope (Figure 1.3). The viral genome is a partially double-stranded rcDNA molecule with a covalently attached viral polymerase (Gerlich and Robinson 1980; Bartenschlager et al. 1990). The genome is inside an icosahedral capsid (T = 4 symmetry) composed of 120 dimers of HBc (Wynne et al. 1999). The nucleocapsid is wrapped in an endoplasmic reticulum (ER) derived lipid envelope with the three HBV envelope proteins small (S-HBsAg), middle (M-HBsAg), and large (L-HBsAg) HBV surface antigens (Heermann et al. 1984).

Additionally, non-infectious, nucleocapsid-deficient subviral particles (SVPs) in spherical or filamentous form are generally present in sera of HBV infected patients (Figure 1.3) (Dane et al. 1970). Spheres have a diameter of 22 nm and contain S- and M-HBsAg but only trace amounts of L-HBsAg (Heermann et al. 1987; Short et al. 2009). Filaments, on the other hand, have a tubular structure with variable length and are composed of all three envelope proteins in a similar ratio compared to Dane particles. SVPs are highly abundant in patients with an

approximately 3000-fold excess over infectious virions (Gerlich 2013). The large number of non-infectious particles is hypothesised to act as a decoy to the immune system and neutralise anti-HBsAg antibodies (Rydell et al. 2017).

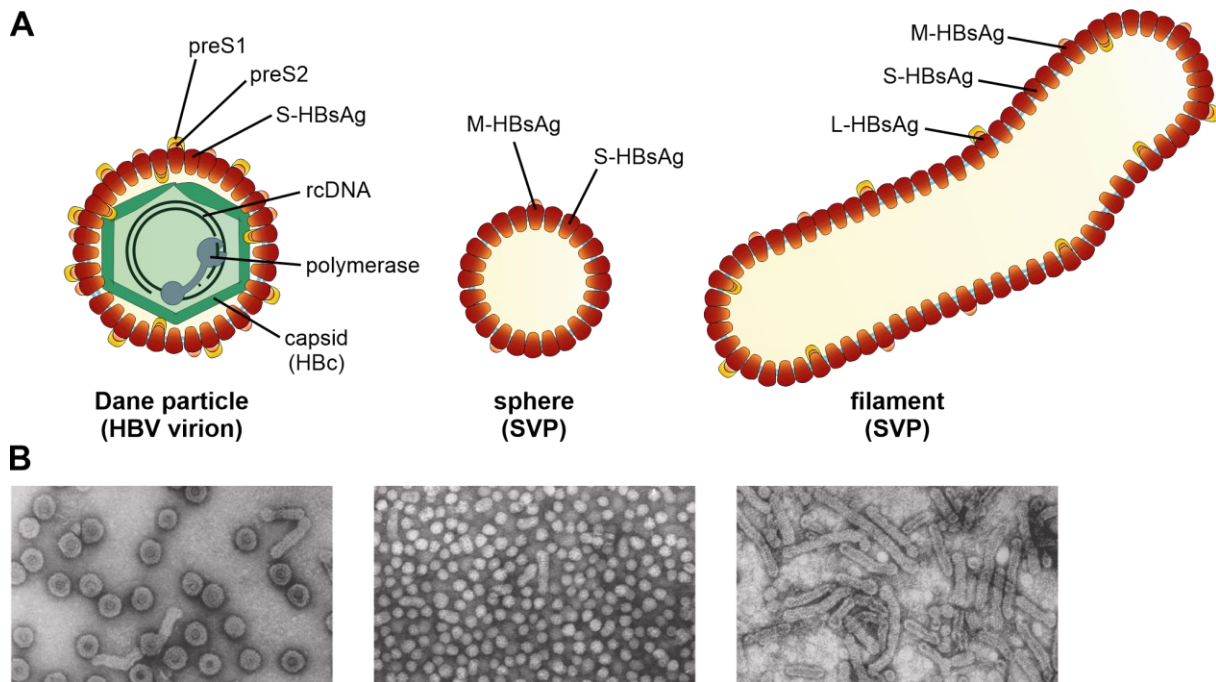


Figure 1.3. Structure of HBV virions and SVPs. (A) The infectious Dane particle is a polymerase-bound, encapsidated, and enveloped rcDNA molecule. The envelopes of virions and filamentous SVPs contain S-, M-, and L-HBsAg, the latter is mostly absent in spherical SVPs. SVPs do not contain a nucleocapsid and are therefore not infectious. (B) Electron microscopy images (negative staining) of HBV virions, spherical SVPs, and filaments. Modified from (Gerlich 2013).

1.2.3. Genome organisation

The HBV genome is only ~3.2 kb in size but characterised by very compact organisation (Figure 1.4). Every nucleotide encodes for a protein, about half of them are part of two open reading frames (ORFs). Additionally, cis-acting elements such as two enhancers (Enh1 and Enh2), four promoters (core, preS1, preS2/S, X), polyadenylation, encapsidation (epsilon), and replication (direct repeat 1 and 2) signals are part of the genetic information. Thus, the HBV genome is arguably considered the most highly evolved genome on earth (Seitz et al. 2020).

The viral rcDNA genome has a complete minus strand with a short redundancy, whereas the incomplete plus strand starts at the direct repeat 2 (DR2) and has a variable 3'-end comprising 50-80% of the genome (Lutwick and Robinson 1977). Upon infection, rcDNA is converted by cellular enzymes inside the nucleus to cccDNA. cccDNA is the transcriptionally active form of HBV DNA and serves as template for all viral transcripts.

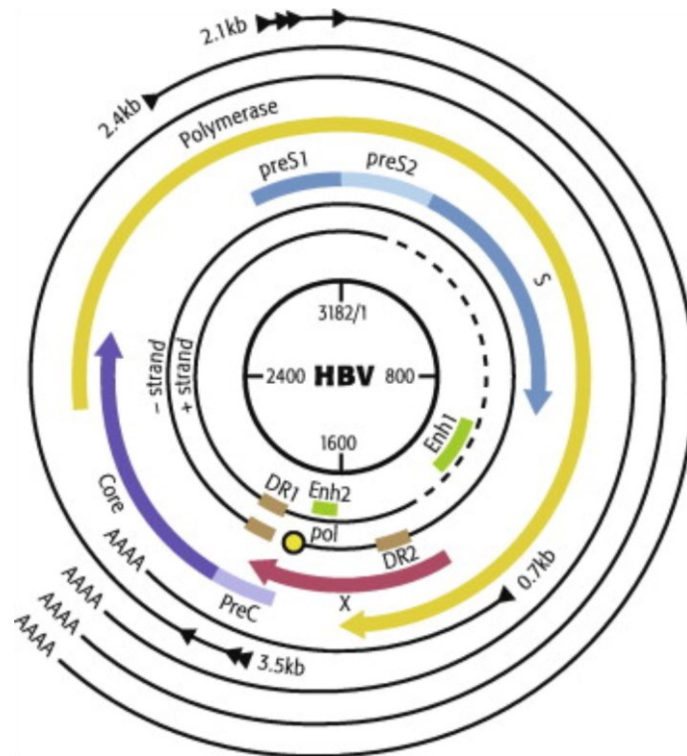


Figure 1.4. Genome organisation of HBV. A genome of HBV genotype D is shown here. From inside to outside, the following features of the HBV genome are depicted: the genomic scale with start and end at an EcoRI restriction site; plus and minus strands of the rcDNA with enhancer regions (Enh1 and Enh2), direct repeats (DR1 and DR2), and attached polymerase (pol); four overlapping ORFs that encode for seven proteins; four overlapping viral transcripts that all use the same polyadenylation (AAAA) signal at the 3'-end. From (Gish et al. 2015) with permission.

1.2.4. Viral transcripts and proteins

HBV transcription is regulated by four promoters and two enhancers through recruitment of transcription factors, many thereof are specifically enriched in hepatocytes (Quasdorff and Protzer 2010). Five different RNAs are transcribed from the minus strand of cccDNA, and they all share the same 3'-end because there is only one polyadenylation signal present. HBV transcripts are all capped and polyadenylated. The five different RNA forms expressed by HBV are: three subgenomic mRNAs (preS1, preS2/S, and X) with sizes 2.4 kb, 2.1 kb, and 0.7 kb, respectively; a greater-than-genome length precore mRNA (3.5 kb); and a just a little shorter pgRNA (Figure 1.5).

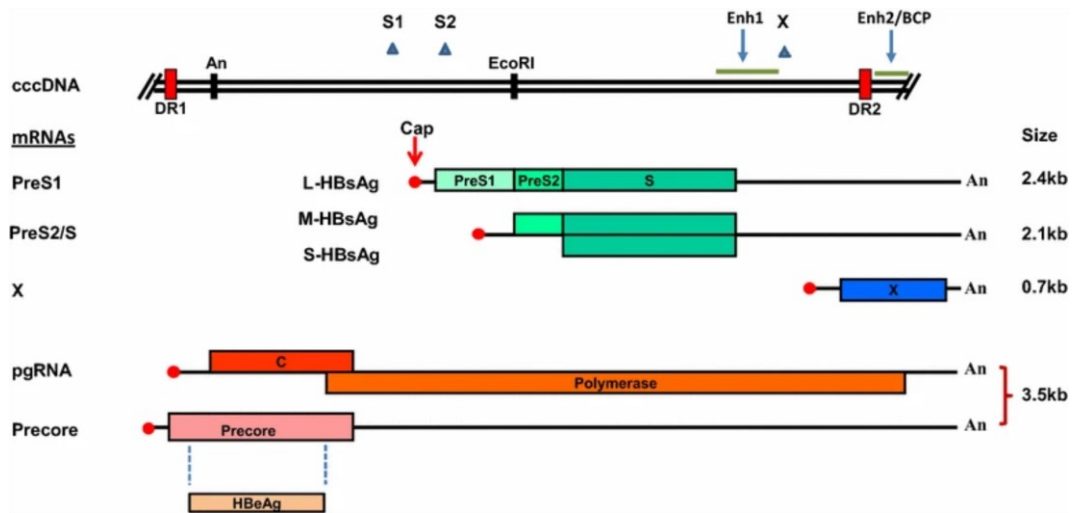


Figure 1.5. HBV transcripts. cccDNA is depicted in linear outline. DR1, DR2, Enh1, Enh2, polyadenylation signal (An), EcoRI restriction site, preS1, preS2/S, X and core promoters are indicated. The five viral transcripts with encoded ORFs are shown. BCP, basal core promoter. From (Karayiannis 2017) with permission.

The core promoter drives the transcription of two greater-than-genome length RNAs with a size of 3.5 kb and different 5'-ends. pgRNA is shorter by a few nucleotides and encodes HbC and polymerase proteins. Additionally, pgRNA is packaged into capsids where it serves as the template for reverse transcription to rcDNA. HBV polymerase has a molecular weight of 90 kDa and is expressed from the largest ORF which covers nearly 80% of the genome. The polymerase is composed of three domains: the terminal protein domain (TP) at the N-terminus is exclusively found in hepadnaviruses and acts as protein primer for minus strand synthesis; the RNA- and DNA-dependent reverse transcriptase/polymerase domain; and the C-terminal RNase H domain responsible for degradation of pgRNA concurrent with minus strand synthesis.

HbC comprises 183 amino acids and has a molecular weight of 21 kDa. The N-terminal domain (amino acids 1-140) mediates the formation of dimers and assembly of capsids. HbC dimers have a distinctive spike structure which is formed by a four helix bundle with two helices from each monomer (Bottcher et al. 1997). Most capsids are composed of 120 HbC dimers and form an icosahedral shape with T=4 symmetry. A minor fraction of capsids is formed from 90 dimers with a T=3 symmetry (Dryden et al. 2006). The arginine-rich C-terminal domain (149-183) is crucial for specific packaging of pgRNA but dispensable for capsid assembly.

HBeAg is the final product of translation from the second greater-than-genome length RNA, the precore mRNA. The precore protein is translated in-frame with the HbC ORF but translation initiates at an upstream start codon resulting in an N-terminal extension of 29 amino acids. The N-terminus contains a signal peptide that directs translation to the ER lumen. The precore

protein undergoes N- and C-terminal cleavage, removing 19 amino acids at the N-terminus and 29 amino acids at the C-terminus (Garcia et al. 1988; Messageot et al. 2003). The final 17 kDa HBeAg is secreted. While it is dispensable for HBV replication, it might induce immunologic tolerance during infection of newborns (Milich et al. 1990).

The three HBV envelope proteins are encoded by the preS/S ORF and are translated from the preS1 and preS2/S mRNAs. The 226 amino acid sequence of S-HBsAg is shared by all three envelope proteins. Expression of L- and M-HBsAg starts from alternative in-frame start codons upstream of the S sequence. M-HBsAg is extended by the preS2 sequence (55 amino acids), and L-HBsAg is additionally extended by the preS1 sequence (108 or 119 amino acids depending on the genotype) (Seitz et al. 2020). The S-HBsAg domain contains four helical transmembrane domains which anchor the envelope proteins into membranes with both the N- and C-terminus oriented towards the ER lumen (Eble et al. 1987; Bruss 2007). The glycosylated “a”-determinant, situated between transmembrane domains 2 and 3, is exposed at the outside of (sub)viral particles and elicits the most effective neutralising antibody response (Zanetti et al. 2008). L-HBsAg is modified by myristic acid at the preS1 N-terminus (glycine 2) which is crucial for infectivity (Persing et al. 1987; Gripon et al. 1995). The preS region (preS1 + preS2) of L-HBsAg has a dual topology (Ostapchuk et al. 1994; Bruss et al. 1994). Initially after translation, the preS domain is located at the cytosolic side of the ER membrane, where the amino acid residues 92-113 are important for nucleocapsid binding and envelopment (Bruss 1997). A maturation process translocates the preS1 domain across the viral membrane to be exposed at the outside of the virion. The exposed preS is prerequisite for infectivity, as the N-terminal 77 amino acid residues and the myristoylation are essential for the interaction with cellular attachment and uptake receptors (Le Seyec et al. 1999; Bruss et al. 1996; Seitz et al. 2016).

The 154 amino acid hepatitis B X (HBx) protein is translated from the X mRNA. Using HBx overexpression systems, HBx was described to interact with a large number of cellular factors involved in signalling pathways, apoptosis, and cell cycle regulation (Geng et al. 2015; Slagle and Bouchard 2016). Through interaction with DNA-damage binding protein 1 (DDB1), HBx can recruit the host ubiquitin machinery and promote the degradation of the structural maintenance of chromosome 5/6 (SMC5/6) complex, an important function of HBx evidenced in an authentic infection system (Decorsiere et al. 2016). The SMC5/6 complex can suppress transcription from cccDNA in the absence of HBx *in vivo* (Allweiss et al. 2021).

1.2.5. HBV life cycle

1.2.5.1. Entry into host cells

HBV entry starts with attachment at the plasma membrane of hepatocytes and ends with the release of the viral rcDNA genome into the nucleus (Figure 1.6). Entry of HBV requires attachment with low specificity to heparan sulphate proteoglycans (HSPGs) (Schulze et al. 2007). HSPGs are ubiquitously expressed on the surface of many cell types and are therefore not solely responsible for the strict hepatotropic nature of HBV. Infection experiments in chimpanzees have shown that extremely low amounts of virus (possibly a single infectious virion) are sufficient to productively infect the entire liver (Asabe et al. 2009), suggesting that HBV developed a mechanism to avoid attachment to extrahepatic cells. Seitz and colleagues have proposed a mechanism that HBV has developed to avoid attachment to cells before reaching the liver (Seitz et al. 2016). Virions contain a mixture of two topological variants of L-HBsAg: the preS1 is oriented inside of the viral membrane, where it plays an important role for the envelopment of nucleocapsids, and after secretion it undergoes a topological switch to the outside of the envelope, where it mediates attachment to host cells (Bruss et al. 1994; Seitz et al. 2016). As long as the preS domain remains at the interior of the envelope, virions do not adhere to HSPG. This allows them to circulate freely from the site of transmission to the liver. It remains unclear how the conversion of the preS domain is promoted specifically in the liver. Virions might be mechanically trapped in fenestrated hepatic sinusoidal endothelium until their preS domain translocates to the outside.

Once the preS domain is exposed, high-affinity binding to its receptor NTCP is triggered (Yan et al. 2012; Ni et al. 2014). NTCP is selectively expressed at the basolateral membrane of hepatocytes (Stieger et al. 1994), consistent with the putative transport of HBV to the perisinusoidal space. Infection experiments in differentiated HepaRG cells, which form islands of polarised hepatic cells, showed that HBV preferentially infects hepatocytes from the basolateral (in contrast to the apical) membrane (Schulze et al. 2012). Binding of HBV to NTCP is mediated by the preS1 domain of L-HBsAg (Le Seyec et al. 1999), of which the N-terminal 75 amino acid residues and myristoylation at glycine 2 are crucial for infectivity (Bruss et al. 1996; Blanchet and Sureau 2007). Synthetic myristoylated peptides containing the N-terminal sequence of the preS1 domain efficiently bind to NTCP and are potent inhibitors of HBV infection (Gripon et al. 2005). In addition, preS1 derived peptides inhibit NTCP-mediated uptake of taurocholate and other inhibitors of NTCP, vice versa, interfere with HBV entry (Donkers et al. 2017). Epidermal growth factor receptor (EGFR) interacts with NTCP and might

mediate the translocation from the plasma membrane to endocytic vesicles (Iwamoto et al. 2019).

To pass the cellular membrane, HBV probably depends on endocytic processes. Previous studies found caveolin-dependent entry of HBV in HepaRG cells (Macovei et al. 2010) and clathrin-mediated endocytosis in immortalised primary human hepatocytes (Huang et al. 2012). A recent publication used NTCP expressing HepG2 cells and reinforced a clathrin-dependent infection pathway of HBV (Herrscher et al. 2020).

HBV infection depends on the GTPases Rab5 and Rab7 (Macovei et al. 2013), which regulate the transport of endocytic vesicles from the plasma membrane to early endosomes (Rab5) and from early to late endosomes and lysosomes (Rab7) (Mercer et al. 2010). Vesicular transport to the *trans*-Golgi network (Rab9) or recycling endosomes (Rab11) are not critical for HBV infection (Macovei et al. 2013), suggesting that HBV is transported from early to mature endosomes. The molecular mechanism and cellular location of membrane fusion remain unclear. Acidification of endosomal vesicles is not essential for infection of duck hepatitis B virus (DHBV) (Rigg and Schaller 1992; Funk et al. 2006), while endosomal maturation is crucial for DHBV (Funk et al. 2006) and HBV (Macovei et al. 2013). Co-trafficking with NTCP and EGFR to late endosomes seems to be essential for productive infection (Iwamoto et al. 2020), suggesting release of nucleocapsids to occur there.

As most DNA viruses, HBV depends on the nuclear replication machinery and therefore HBV nucleocapsids are transported towards the nucleus after membrane fusion. HBV nucleocapsids bind to microtubules and the chaperone dynein LL1 *in vitro*, which might act as a linker to the dynein motor complex and thereby mediate retrograde transport towards the nuclear pore complex (NPC) (Osseman et al. 2018). HBc contains a nuclear localisation signal (NLS) in the C-terminus (Eckhardt et al. 1991) that becomes exposed on the capsid surface after phosphorylation (Kann et al. 1999). With a diameter of 36 nm, the HBV capsid is at the upper limit of potential cargo through the NPC. Recombinant capsids seem to accumulate at the nuclear envelope and only phosphorylated capsids are found at the nuclear side of NPCs but not in the free karyoplasm (Pante and Kann 2002; Paci et al. 2020). It remains unclear if disassembly of the capsid and release of rcDNA takes place within the nuclear basket or in the free karyoplasm. A recent study however suggests that not the nuclear transport of capsids, but the conversion of rcDNA to cccDNA is the rate-limiting step of HBV infection in cell culture (Chakraborty et al. 2020).

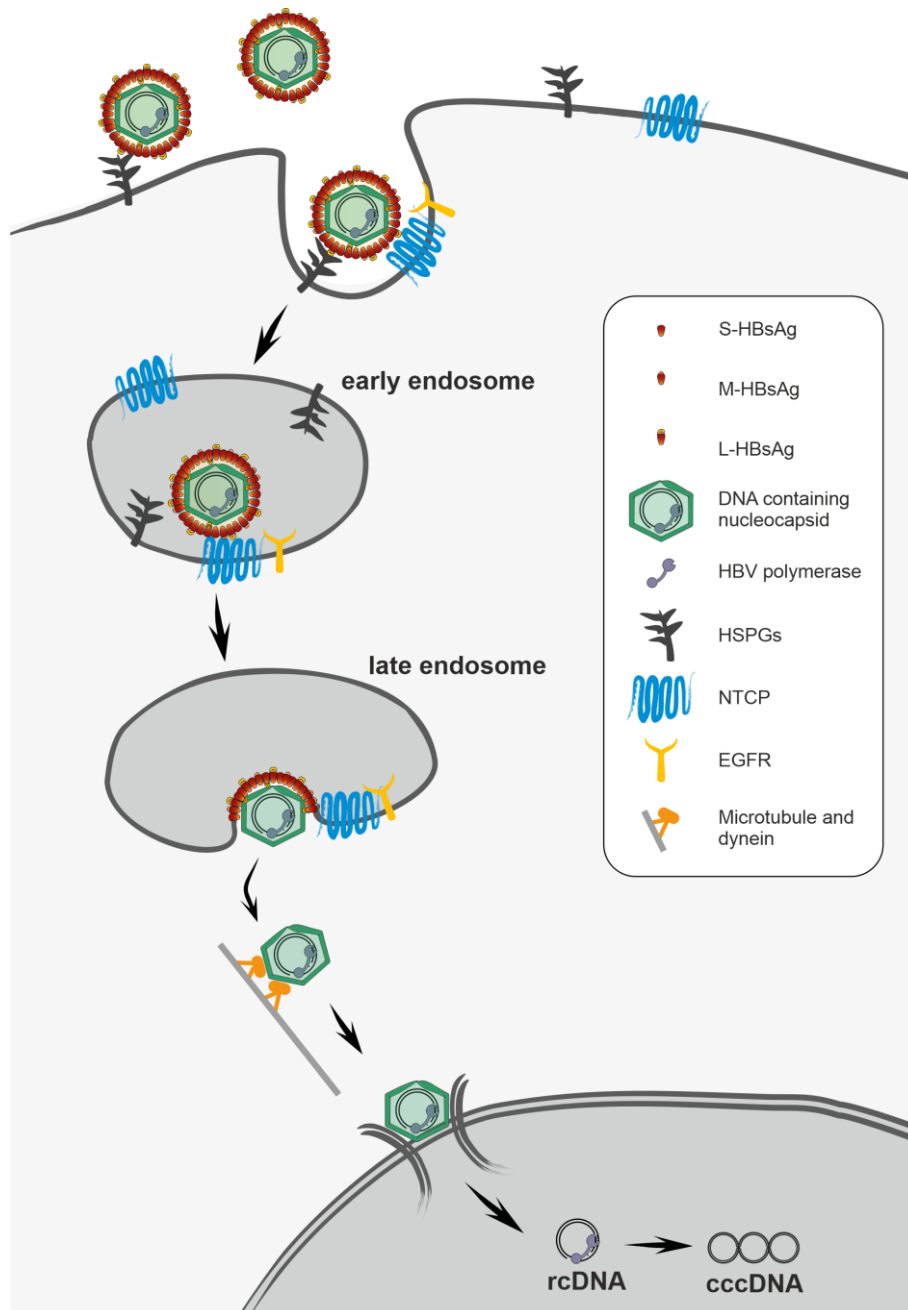


Figure 1.6. Overview of HBV entry. HBV entry begins with attachment to HSPGs followed by specific binding of preS1 to the receptor NTCP. Uptake is mediated by coated vesicles and the virus is internalised along the endocytic route to late endosomes. The mechanism and location of viral and cellular membrane fusion presently remain unclear. Released nucleocapsids are transported along microtubules to the NPC. The rcDNA is released into the nucleoplasm where it is converted to cccDNA by cellular enzymes.

1.2.5.2. Formation and maintenance of HBV cccDNA

Once inside the nucleus, rcDNA is converted to cccDNA. This process involves removal of the covalently bound viral polymerase from the minus strand and removal of the RNA primer from the plus strand of rcDNA. The terminal redundancy is cleaved from the minus strand, the plus strand is completed, and both DNA strands are ligated to form cccDNA. Several cellular

enzymes have been described to be involved in this process. Cleavage of the viral polymerase from rcDNA is performed by tyrosyl-DNA phosphodiesterase 2 (TDP2) (Koniger et al. 2014) and the 5' redundant sequence of the minus strand is removed by flap structure-specific endonuclease 1 (FEN1) (Kitamura et al. 2018). Cellular DNA polymerases are required to complete the plus strand. Polymerases κ , λ , and η are involved in filling the gap during the initial infection (Qi et al. 2016), while polymerases α , δ , and ϵ were described to mediate cccDNA formation during intracellular amplification with polymerase α repairing the nick in the minus strand (Tang et al. 2019). Additionally, DNA ligase 1 and 3 were reported to be required for ligation of both strands of rcDNA (Long et al. 2017).

After formation, cccDNA stays as highly stable episome in the nucleus and serves as template for all viral transcripts. cccDNA resembles a mini-chromosome that is complexed with histones and HBc (Bock et al. 1994; Bock et al. 2001) and it is the determinant factor for HBV persistence. The initial infection is the main contributor to intracellular cccDNA levels, however during replication nucleocapsids are synthesised in the cytoplasm. Instead of being enveloped and secreted, these newly synthesised nucleocapsids may enter the nucleus and thereby replenish the cccDNA pool. This amplification through intracellular reimport has been described in the related DHBV (Wu et al. 1990). Treatment with inhibitors of reverse transcription of pgRNA to rcDNA, such as NUCs, are used as therapy for CHB but is usually not sufficient to achieve (functional) cure. These inhibitors can only affect cccDNA indirectly through inhibition of *de novo* produced nucleocapsid and subsequent intracellular or extracellular amplification of cccDNA. Only partial reductions in cccDNA levels were observed in treated patients (Werle-Lapostolle et al. 2004), suggesting that the inhibition of reverse transcription is incomplete or that cccDNA levels are highly stable without the need for replenishment.

1.2.5.3. Replication and spread

RNAs transcribed from cccDNA are exported from the nucleus and translated to synthesise the seven HBV proteins. pgRNA is sufficient to produce new nucleocapsids, providing the template for translation of HBc and polymerase and acting as template for reverse transcription to rcDNA (Yu et al. 2019). The viral polymerase binds the epsilon stem-loop structure of pgRNA, which is a prerequisite for packaging of pgRNA and polymerase into capsids (Bartenschlager and Schaller 1992). A tyrosine residue of the polymerase TP domain serves as protein primer for the synthesis of a short DNA oligo which is then transferred to a matching sequence in DR1 close to the 3' end of pgRNA. From there, the minus strand is synthesised including a redundant

sequence. Meanwhile, pgRNA is degraded by RNase H activity except for the capped 5'-end, which is translocated to DR2 of the previously synthesised minus strand. The incomplete plus strand is elongated from the RNA primer to the 5'-end of the minus strand where exchange of the redundant sequences allow elongation to proceed (Nassal 2015). In a minority of replication events, the RNA primer is not transferred to DR2, but elongation of the plus strand is primed from DR1, resulting in the formation of double-stranded linear DNA (dslDNA) (Tu et al. 2017). Infection with dslDNA containing HBV can result in integration of dslDNA into the host genome (Yang and Summers 1999). Although integrated HBV DNA is not replication-competent, it is thought to contribute to the carcinogenic potential of chronic hepatitis B (Tu et al. 2017).

Mature nucleocapsids are enveloped at the ER. Envelopment strictly depends on S- and L-HBsAg but not M-HBsAg, and interactions with the preS domain of L-HBsAg and a cytosolic domain of S-HBsAg have been reported (Bruss and Ganem 1991; Ni et al. 2010; Bruss 1997; Loffler-Mary et al. 2000). The mature HBV virion is densely packed with capsid and envelope proteins with multiple interactions (Seitz et al. 2007). Virions utilise the endosomal sorting complexes required for transport (ESCRT) and secretion proceeds through multivesicular bodies (MVBs) (Figure 1.7) (Watanabe et al. 2007). While filamentous SVPs are also secreted via MVBs, spherical SVPs are released through the constitutive secretion pathway (Jiang et al. 2015; Patient et al. 2007).

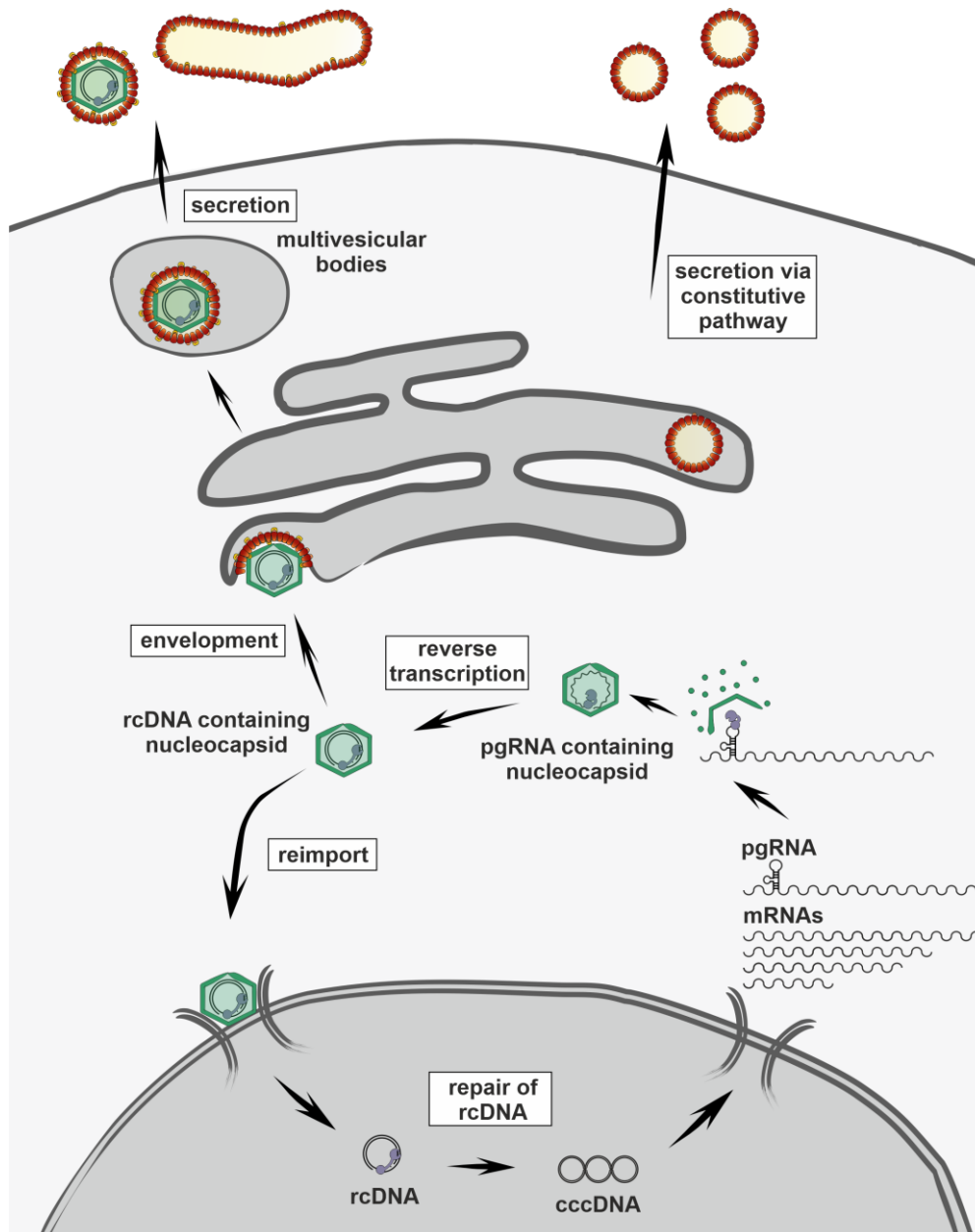


Figure 1.7. Replication of HBV. Transcription from cccDNA leads to subgenomic and greater-than-genome length RNAs which are translated to viral proteins. HBV polymerase binds to the epsilon region of pgRNA and is packaged into nucleocapsids assembled by HBe dimers. Reverse transcription to rcDNA occurs within the nucleocapsid which may then be reimported to the nucleus to amplify the cccDNA levels or be enveloped by S-, M-, and L-HBsAg. Envelopment occurs at the ER followed by secretion of virions and filamentous SVPs via MVBs, whereas spherical SVPs are secreted by the constitutive pathway.

1.3. Hepatitis D virus

HDV is an RNA virus classified within the genus *Deltavirus* with a genome replication mechanism that resembles that of plant viroids. Depending on the envelopment by HBV envelope proteins for dissemination and infection, HDV is a satellite virus of HBV. HDV infection is, in general, only observed with HBV co-infection or as superinfection of HBV-infected individuals.

Recently, deltavirus-like agents were discovered in snakes, birds, rodents, bats, deer, and various vertebrates and invertebrates in the absence of hepadnaviruses (Hetzel et al. 2019; Wille et al. 2018; Paraskevopoulou et al. 2020; Bergner et al. 2021; Chang et al. 2019). These findings indicate transmission of deltavirus-like agents using other helper viruses or even independent of helper viruses. Supporting the theory of non-hepadnaviral helper viruses, human HDV was observed to be productively secreted using envelopes of HCV, vesicular stomatitis virus (VSV), and flaviviruses (Perez-Vargas et al. 2019).

1.3.1. Virus structure and genome

The HDV genome is composed of a circular single-stranded RNA with negative polarity and extensive intramolecular base-pairing (Figure 1.8A) (Kos et al. 1986). With a length of ~1700 nucleotides, it constitutes the smallest known genome of mammalian viruses (Wang et al. 1986; Kuo et al. 1988a; Lempp et al. 2016). The unbranched rod-shaped RNA structure encodes one ORF for the expression of hepatitis delta antigen (HDAg). HDAg is expressed in two forms: small HDAg (S-HDAg, 195 amino acids) and the C-terminally extended L-HDAg (214 amino acids).

The C-terminal domain of L-HDAg includes a prenylation motif at cysteine 211, where a farnesyl moiety is covalently linked (Glenn et al. 1992; Otto and Casey 1996). One HDV RNA genome assembles with ~200 molecules of S- and L-HDAg to form a ribonucleoprotein (RNP) complex which is enveloped by the HBV envelope proteins (Figure 1.8B) (Gudima et al. 2002). The secreted HDV virion has a size of 35-37 nm (Rizzetto et al. 1980b).

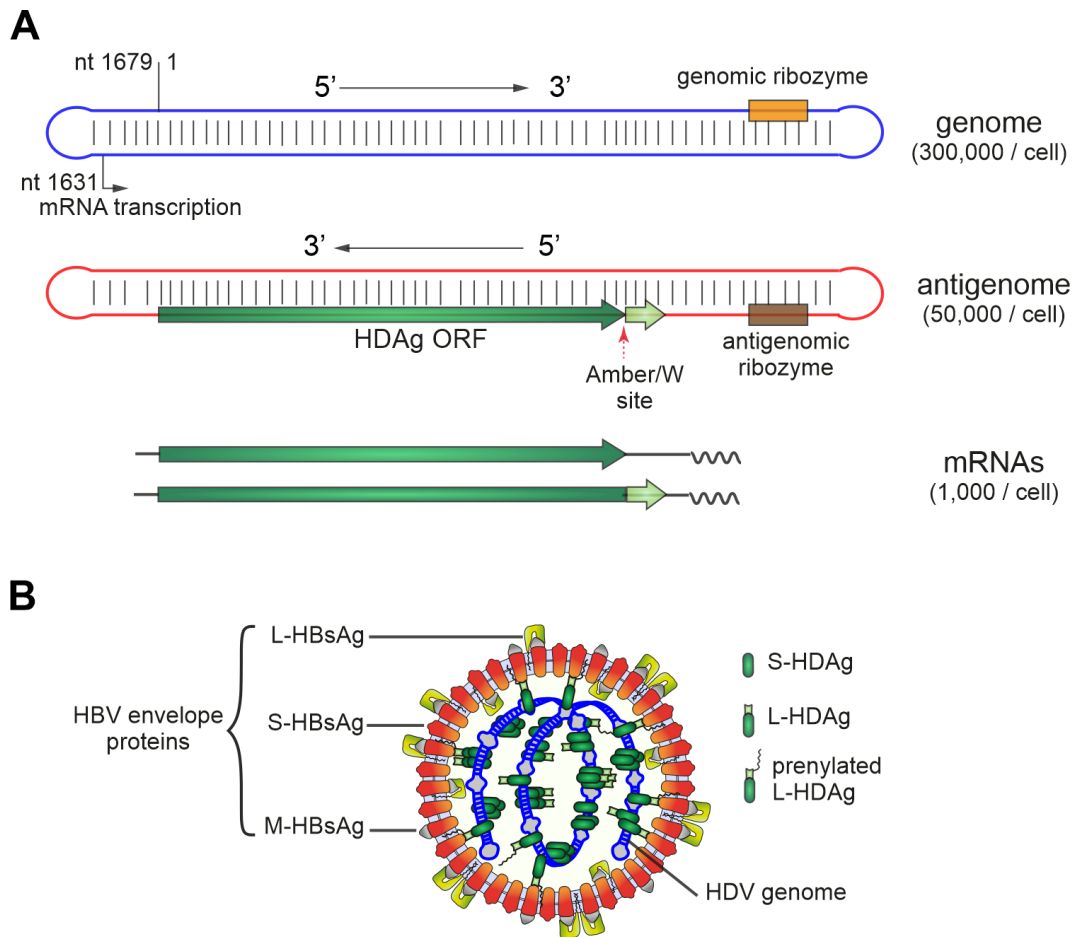


Figure 1.8. Genome and structure of HDV. (A) HDV genome (blue) is circular, has a rod-like structure, and is highly self-pairing. The antigenome (red) is complementary to the genome and has a similar structure. HDV mRNA is transcribed from the genome and encodes S- and L-HDAg. Ribozymes, the amber/W site, mRNA transcription start site, and HDAg ORF are indicated. (B) HDV RNA genome forms an RNP together with S- and L-HDAg and is enveloped by HBV envelope proteins. L-HDAg is prenylated at the C-terminal domain which is essential for interaction with HBsAg. Modified from (Zhang and Urban 2020).

1.3.2. HDV life cycle

Due to use of the HBV envelope, HDV is strictly hepatotropic. Consequently, early phases of virus entry are proposed to be the same: HDV initially attaches to HSPGs followed by specific binding of the preS1 domain to NTCP (Figure 1.9) (Lamas Longarela et al. 2013; Yan et al. 2012; Ni et al. 2014). Virus entry steps from the interaction with NTCP until transport to the nucleus are poorly characterised. It is unclear how HDV is taken up into the cell, where and how membrane fusion is triggered, and how the RNP is transported towards the nucleus.

Guided by HDAg, which contains a NLS, the incoming HDV RNP is imported into the nucleus (Chou et al. 1998). HDV RNA replication occurs exclusively in the nucleus and depends on cellular enzymes because unlike other RNA viruses, HDV does not encode an RNA-dependent

RNA polymerase. The host RNA polymerases I and II have been reported to be responsible for HDV replication and transcription of HDAg mRNA (Macnaughton et al. 2002; Chang et al. 2008; Greco-Stewart et al. 2007). The HDV genome is replicated by a double rolling circle mechanism resulting in multiple copies of antigenomic and genomic RNA (Macnaughton et al. 2002; Chen et al. 1986). These concatemers are cleaved to unit length monomers by ribozyme activity present on both genome and antigenome (Figure 1.8A) (Kuo et al. 1988b). Whether ligation of the monomeric genomes and antigenomes to circular RNAs is mediated by intramolecular ribozyme activity or by cellular ligases remains unclear.

The S-HDAg is translated from an ~800 nt mRNA transcribed from genomic HDV RNA (Hsieh et al. 1990). S-HDAg is essential for HDV replication (Kuo et al. 1989), and possibly recruits chromatin remodelers and cellular RNA polymerase II via mimicry of histone acetylation (Abeywickrama-Samarakoon et al. 2020). During the course of replication, the HDV antigenome is subjected to RNA editing at the amber/W site, changing the amber stop codon (UAG) to a tryptophan codon (UGG). This editing process is mediated by the host enzyme adenosine deaminase acting on RNA 1 (ADAR1) (Polson et al. 1996; Wong and Lazinski 2002). Editing at this amber/W gives rise to an mRNA that encodes the L-HDAg, which is similar to S-HDAg, but C-terminally extended by 19 amino acids. L-HDAg is known to repress replication of HDV, but is essential for virus assembly and secretion (Chao et al. 1990). The C-terminal extension of L-HDAg contains a prenylation site on which a farnesyl-moiety is attached post-translationally (Glenn et al. 1992; Otto and Casey 1996). Upon farnesylation of L-HDAg, HDV replication is down-regulated and assembly of RNPs is initiated (Hwang and Lai 1994; Chang et al. 1991; Hwang and Lai 1993).

HDV genomes are packaged with S- and L-HDAg and exported from the nucleus into the cytoplasm. The RNP is enveloped by a lipid bilayer, which carries the HBV envelope proteins, through an interaction of the farnesylated L-HDAg with the cytoplasmic domain of HBsAg. The HBV envelope proteins may originate from cccDNA or from integrated forms of HBV DNA in the co-infected cell (Freitas et al. 2014). It is presently unclear whether HDV is secreted like HBV via MVB or like SVPs using the constitutive secretory pathway.

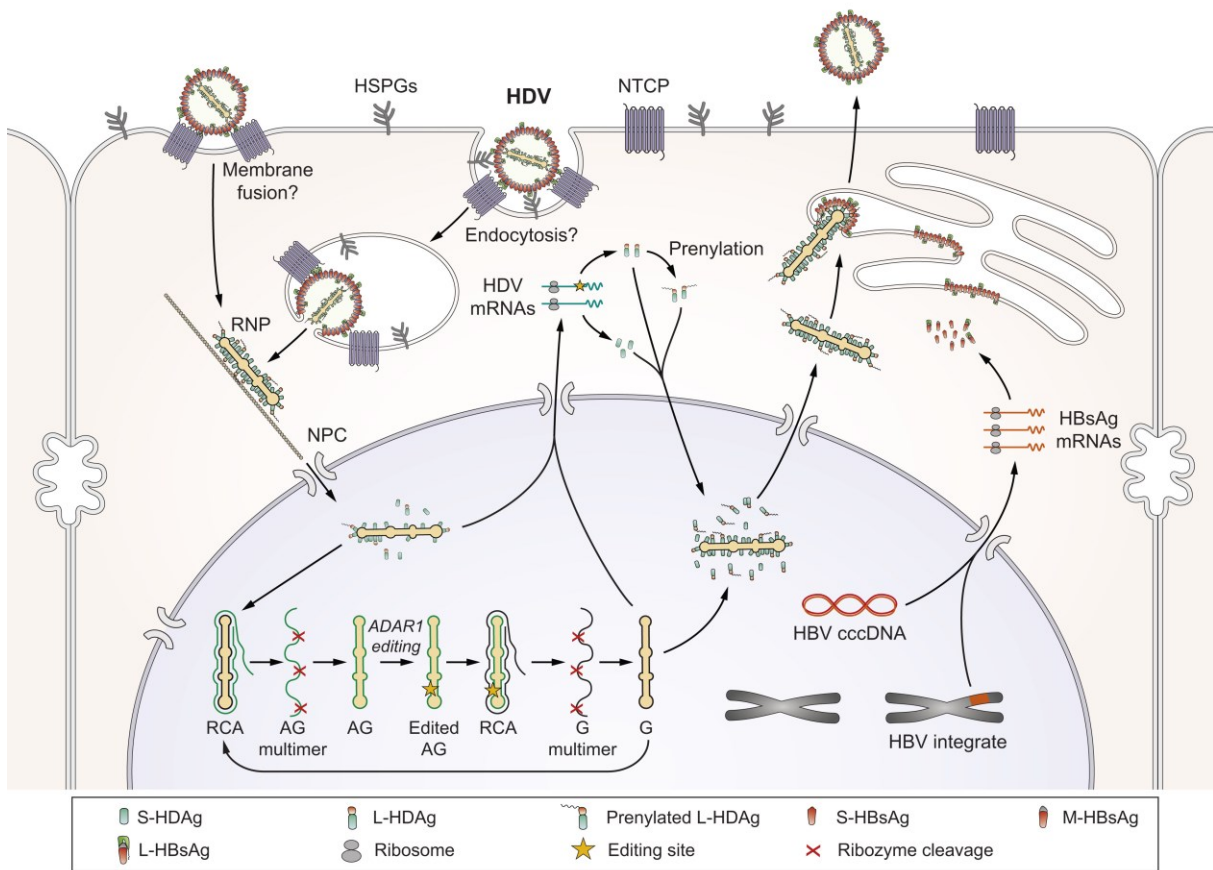


Figure 1.9. The replication cycle of HDV. As for HBV, attachment to HSPGs and binding to the receptor NTCP are required for HDV to enter hepatocytes. How HDV is transported to the nucleus is currently unknown. Inside the nucleus, HDV replicates via double rolling circle amplification, generating linear multimers of antigenome and genome. These concatemers are cleaved to monomers by intramolecular ribozyme activity. HDV mRNA is transcribed from HDV genomes and initially codes for S-HDAg which is required for replication. With ongoing replication, ADAR1 mediated editing at the amber/W site of the antigenome results in the production of L-HDAg. Farnesylation of a prenylation motif at the C-terminus of L-HDAg mediates suppression of replication and induces RNP assembly and secretion. HBV envelope proteins can be provided by expression from cccDNA or integrated HBV DNA. AG, antigenome; G, genome; RCA, rolling circle amplification. From (Zhang and Urban 2021).

1.4. Fluorescent labelling of HBV and HDV

Advances in fluorescent labelling techniques in combination with fluorescence and high resolution microscopy provide possibilities to visualise viruses and investigate viral entry and intracellular trafficking processes (Sun et al. 2013). This not only helps to understand the virus entry pathways but can also provide insights to cellular processes involved in uptake of ligands and endosomal trafficking (Marsh and Helenius 2006). As convenient cell culture systems for HBV and HDV are available now, direct visualisation using fluorescently labelled viral particles may elucidate unknown mechanisms of HBV and HDV entry processes. During the course of this work, we published a review focusing on visualisation approaches of HBV (Zhang et al. 2016). This chapter includes modified parts of this review article.

1.4.1. Labelling techniques for viruses and their application for HBV and HDV

There is a vast number of published methods used for virus labelling, ranging from conventional chemical labelling techniques to more recently developed stainable peptide tags. Virus labelling approaches should ideally result in functional virus particles with strong, specific, and photostable fluorescence.

1.4.1.1. Chemical labelling of proteins

Chemical fluorophores have the advantage of being smaller and more photostable than protein tags. They have previously been used to label proteins of VSV (Cureton et al. 2009), influenza A virus (IAV) (Lakadamyali et al. 2003), or poliovirus (Brandenburg et al. 2007).

In an early attempt to visualise HBV attachment to cells, SVPs were conjugated to polystyrene beads through glutaraldehyde and amine group coupling (Paran et al. 2001). Using this non-fluorescent visualisation method, attachment of bead-conjugated SVPs to HepG2 cells was observed. The attachment of HBV envelope proteins could be detected at single cell resolution and confirmed the contribution of regions within both S-HBsAg and preS1 to the binding to host cells. Fluorescent labelling of SVPs has been reported with N-Hydroxysuccinimide (NHS) esters of fluorescent dyes which target lysines and primary amines at the N-terminus by ester crosslinking. After labelling S-HBsAg with a Cy5-coupled NHS ester, SVPs were taken up by COS-7 cells. Uptake of labelled SVPs was regulated by caveolin mediated endocytosis and intracellular transport depended on actin filaments (Hao et al. 2011).

To study the nuclear import of cargo, Paci and colleagues used maleimide chemistry to couple fluorescent dyes to recombinant HBV capsids (Paci et al. 2020). Labelled capsids were added to permeabilised HeLa cells where they accumulated at the nuclear envelope but were not efficiently imported into the nucleoplasm.

1.4.1.2. Fluorescent proteins

Genetically encoded fluorescent proteins (FPs) such as green fluorescent protein (GFP) can be used to directly label viral proteins. A broad range of FPs with different excitation and emission wavelengths, photostability, and brightness is available. FPs are ~25 kDa in size which is large compared to chemical fluorophores. Thus, genetical encoding of FPs can interfere with the genomic structure of viruses and fusion of FPs to viral proteins might abrogate virus functions. Fusion with FPs has for example been applied to herpes simplex virus (HSV) (Desai and Person 1998) or HIV (Koch et al. 2009; Muller et al. 2004) and was even applied to study viral architecture using super resolution microscopy in vaccinia virus, which is considerably larger than HBV (Gray et al. 2016).

For HBV, labelling of envelope and capsid proteins with FPs has been reported. Due to their large size, insertion of FPs into the HBV genome abrogates viral replication. Therefore, fluorescent fusion proteins have to be trans-complemented with wild-type (WT) HBV genome. In previous studies, GFP has been N-terminally fused to S-HBsAg (Lambert et al. 2004) or M-HBsAg (Florian et al. 2014). Both fluorescent fusion proteins could be incorporated into secreted HBV virions or SVPs after trans-complementation with the HBV genome. However, both studies could not show productive infection of these fluorescent particles. Furthermore, separation of fluorescent virions from SVPs has not been reported. To avoid an excess of fluorescently labelled SVPs, an alternative could be labelling of HBV capsids. Replacement of amino acids P79 and A80 at the tip of the spike of HBc with GFP results in fluorescent capsid-like particles (Kratz et al. 1999). The spike of HBV capsids forms multiple interactions with the envelope proteins (Seitz et al. 2007). Therefore, capsids with such large structures exposed at the surface would not be enveloped due to steric hindrance.

1.4.1.3. Self-labelling enzymes

Self-labelling proteins can be specifically and covalently tagged with fluorophore-linked substrates. They provide several advantages over FPs: fluorescence can be initiated at a given time by addition of the substrate for pulse-chase analysis, higher variability regarding fluorophores that can be used to label the same fusion protein, and more photostable

fluorophores. However, self-labelling proteins have a similar size as FPs. Successful virus labelling was shown for SNAP- and Halo-tag, which have been applied to HIV (Eckhardt et al. 2011) and pseudorabies virus (Liu et al. 2016), respectively.

Attempts to label HBV or HDV with self-labelling proteins have not been reported yet. Due to the size of these proteins, most likely such attempts would run into the same problems as fusion with FPs, interfering with the HBV genome size restriction, capsid formation, and/or envelopment.

1.4.1.4. Stainable peptide tags

Incorporation of small peptide tags into target proteins allow a more specific labelling with chemical fluorophores. Different labelling strategies exist for peptide tags. Some peptide tags require specific enzymes for the covalent attachment of fluorescent dyes (e.g., sortase tag, A1 tag, Q3 tag, LAP tag). Other short peptide tags (e.g. BC2 tag, ALFA tag, etc.) can be targeted by fluorescently labelled nanobodies for high resolution microscopy. One well characterised small tag is the tetracysteine (TC) tag which is 6-12 amino acids in size and can be labelled with biarsenical dyes. Successful visualisation using TC tag has been reported for HIV (Rudner et al. 2005) and HCV (Coller et al. 2012).

For HBV, the TC tag has been incorporated into HBc and labelled with a biarsenical dye (Sun et al. 2014). Secretion of fluorescent particles was observed, and labelled particles could be internalised into HepG2 cells. However, the authors have not provided evidence that these labelled particles were indeed infectious HBV virions.

1.4.1.5. Targeting lipids or nucleic acids for labelling

As alternatives to protein labelling, lipids of viral membranes or the viral genome serve as additional labelling targets. Lipophilic dyes have been used to fluorescently label several viruses, such as HIV (Miyachi et al. 2009), HCV (Coller et al. 2009), and HBV SVPs (Hao et al. 2011). Nucleic acid binding dyes have been used to label poliovirus (Brandenburg et al. 2007) or IAV (Liu et al. 2012) but neither has been reported for HBV or HDV.

Ethynyl-modified nucleosides can be incorporated into virus genomes during replication and labelled with azide-coupled dyes in click chemistry reactions. This has been successfully applied to adenovirus, HSV, vaccinia virus (Wang et al. 2013a), and HIV (Peng et al. 2014). For HBV, deoxy-5-ethynylcytidine (EdC) has been incorporated into HBV virions without affecting infectivity in HepG2-NTCP cells (Winer et al. 2018). EdC containing HBV was used

to inoculate human NTCP transgenic mice and labelled after 18 hours. Only in the presence of human NTCP, entry of HBV was observed suggesting specific labelling of incoming HBV genomes. Unfortunately, the copper-catalysed click chemistry reaction is not compatible with live cell imaging and has to be performed in fixed cells.

The ANCHOR technology would enable live cell labelling of DNA after release of the viral genome and possibly during genome replication. This system involves a target DNA sequence which is specifically recognised by a protein fused to an FP and it has been applied to visualise DNA of adenovirus (Komatsu et al. 2018) and HIV (Blanco-Rodriguez et al. 2020; Müller et al. 2020). Because the ANCHOR system only binds to double-stranded DNA, it could enable specific visualisation of cccDNA, and early work has been presented by Kann et al. at the international HBV meeting 2019. However, the integration of the target DNA sequence into the HBV genome requires trans-complementation with viral proteins and possibly impairs viral infectivity and replication.

1.4.2. Challenges for labelling of HBV and HDV

Fluorescent labelling of HBV is difficult to achieve for several reasons. One of the hallmarks of HBV replication is the massive excess of non-infectious SVPs. The abundance of SVPs complicates chemical labelling techniques which are generally unspecific. Thus, virions have to be carefully purified and separated from non-infectious particles. Heparin affinity chromatography has been used to separate infectious virions from spherical SVPs, as the binding to heparin depends on preS1 of L-HBsAg (Zahn and Allain 2005; Schulze et al. 2007). A combination of size-exclusion chromatography and isopycnic sucrose density gradient centrifugation can further purify viral particles (Seitz et al. 2007), but a complete separation of virions from spherical and filamentous SVPs is very difficult to obtain. Furthermore, chemical labelling methods modify many exposed amino acids (usually lysine or cysteine residues), which might interfere with protein function.

In addition, the HBV genome has a size limitation and a tight organisation with overlapping ORFs, making introduction of a complete reporter gene coding for a FP while maintaining replication competence very unlikely (Protzer et al. 1999; Wang et al. 2013b; Nassal 2015). Therefore, fusion of viral proteins with FPs or protein tags generally requires trans-complementation with a WT genome for packaging. In the densely packed HBV virion, capsid and envelope are in close contact and form multiple interactions (Seitz et al. 2007). Insertion of a large tag into HBV capsid would probably interfere with protein-protein

interactions which are crucial for capsid assembly and envelopment. Mutational analysis of HBc has revealed that already single amino acid changes to alanine affected both capsid formation and particle envelopment (Ponsel and Bruss 2003). Therefore, HBV that encodes a directly detectable tag and maintains its infection competence is not available up to date.

For similar reasons, fluorescent labelling of HDV has not been achieved yet. HDV has a very small genome with a single-stranded RNA in circular conformation (Lempp et al. 2016). Alterations of the highly self-complementary genome can easily disrupt the genome structure and require adaptations at the complementary side to maintain replication competence. S- and L-HDAg are both present in HDV virions (Gudima et al. 2002) and could be used for direct fluorescent tagging, provided protein functions and ADAR1 mediated editing at the amber/W site are not compromised. Because of the need for HBV envelope proteins, production of HDV is also accompanied by an excess of SVPs. Therefore, purification protocols have to be applied to HDV as well in order to obtain specifically labelled virions.

1.5. Site-specific protein labelling using amber suppression technology and click chemistry

The amber suppression technology employs the site-specific incorporation of single non-canonical amino acids (ncAA) into target proteins and thereby expands the genetic code which in natural translation only includes 20 canonical amino acids. The incorporation of specific ncAA allows subsequent fluorescent labelling with click chemistry (Nikic et al. 2015). We chose this technology to label HBV Hbc and HDV L-HDAg, as other protein labelling strategies may impair genome structure, protein function, and virus assembly, as described above. Moreover, labelling of capsid and RNP eliminates the need to use laborious purification methods to separate virions from fluorescent SVPs.

1.5.1. Amber suppression mediated incorporation of non-canonical amino acids

Translation from genetic information to amino acid sequence in proteins is mediated by the genetic code. Two types of adaptor molecules are essential for correct incorporation of amino acids. Aminoacyl-tRNA synthetases (aaRS) are enzymes that recognise the correct amino acid and the corresponding tRNA and attach the first to the latter. tRNAs then deliver amino acids to ribosomes, bind to the correct codon of the mRNA, and mediate the incorporation of the amino acid into the nascent polypeptide chain. The genetic code of eukaryotes is made up of 20 amino acids with one aaRS for each amino acid.

Ribosomal translation is terminated at one of the three stop codons: amber (UAG), ochre (UAA), and opal (UGA). Stop codons do not have a corresponding tRNA but are recognised by proteins called release factors which in turn mediate termination of translation and release of the newly synthesised protein from the ribosome.

By decoding one of the stop codons (usually the amber stop codon) with a tRNA directed against this codon, ncAA can be inserted into the protein and thereby the genetic code is expanded. As incorporation of ncAA results in readthrough of the amber stop codon, this is also referred to as amber suppression technology. Chemically aminoacylated tRNAs with an anticodon complementary to the amber stop have been used to incorporate ncAA into proteins *in vitro* (Noren et al. 1989). Wang et al. took advantage of a tyrosyl-tRNA/tRNA synthetase pair (TyrRS/tRNA^{Tyr}) from *Methanocaldococcus jannaschii* to genetically encode ncAA in

E. coli (Wang et al. 2001). The *M. jannaschii* TyrRS/tRNA^{Tyr} pair system is orthogonal to the bacterial translation machinery, meaning it does not interact with *E. coli* endogenous tRNAs, aaRS, or canonical amino acids. Unfortunately, the *M. jannaschii* TyrRS/tRNA^{Tyr} pair is not orthogonal to eukaryotic tRNAs and synthetases and cannot be applied for genetic code expansion in mammalian cells (Davis and Chin 2012).

The pyrrolysine-tRNA synthetase (PylRS) and its cognate tRNA (tRNA^{Pyl}) which are present in a small number of archaea and bacteria are probably the most useful and most often used tRNA/synthetase pair for genetic code expansion. Readthrough of an in-frame amber stop codon was first observed in the archaeon *Methanosarcina barkeri* (Burke et al. 1998). The tRNA^{Pyl} and the corresponding PylRS were then discovered to incorporate the ncAA pyrrolysine in response to the amber stop codon (Srinivasan et al. 2002; Hao et al. 2002; Polycarpo et al. 2004). When the PylRS/tRNA^{Pyl} pair is exogenously expressed in *E. coli*, in-frame amber stop codons can be efficiently suppressed in the presence of a pyrrolysine analogue (Polycarpo et al. 2006). Importantly, the PylRS/tRNA^{Pyl} pair is orthogonal to bacterial (Neumann et al. 2008) and eukaryotic (Mukai et al. 2008) translation machineries, meaning it does not interact with endogenous tRNAs, aaRS, or canonical amino acids nor are pyrrolysine analogues used as substrates by cellular aaRS.

Currently, PylRS/tRNA^{Pyl} from *Methanosarcina mazei* is most frequently used in genetic code expansion experiments and is also applied in this study. The amino acid substrate binding pocket of PylRS from *M. mazei* is partially exposed and offers space for bulky hydrophobic side chains (Kavran et al. 2007). The introduction of two mutations into the PylRS (Y306A and Y384F, PylRS^{AF}) can expand the substrate binding pocket and allows the incorporation of bulky ncAA which can be used in copper-free click chemistry reactions (Figure 1.10) (Yanagisawa et al. 2008; Plass et al. 2011). The *M. mazei* PylRS/tRNA^{Pyl} pair has been shown to be orthogonal and functional in mammalian cells (Mukai et al. 2008; Chen et al. 2009) and animals (Ernst et al. 2016), allowing the application of genetic code expansion in our cell culture systems.

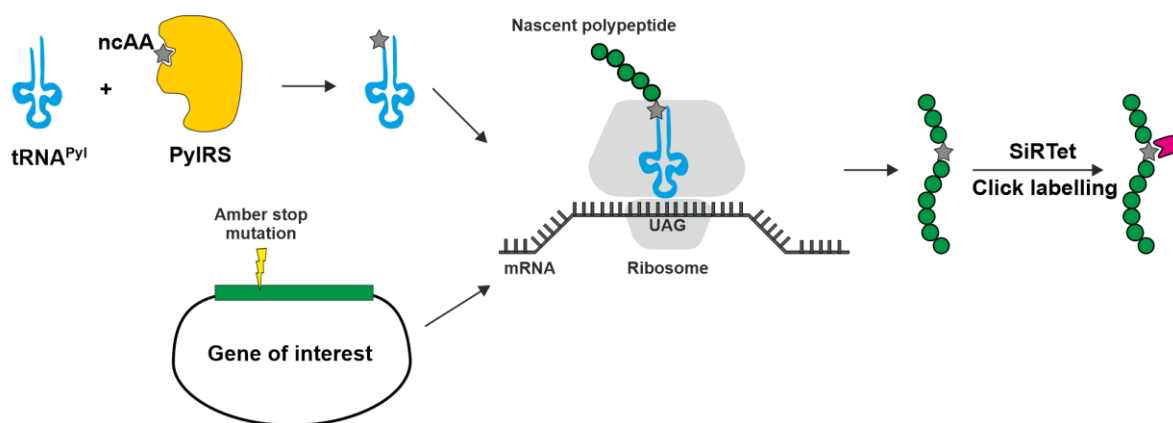


Figure 1.10. Site specific incorporation of clickable ncAA. PylRS (yellow) recognises its cognate tRNA^{Pyl} (blue) and ncAA (star) and charges the former with the latter. The protein of interest is generally expressed exogenously with an introduced in-frame amber stop codon (UAG). The tRNA^{Pyl} is decoded during translation in response to the amber stop codon. Thereby the ncAA is incorporated into the nascent polypeptide and the stop codon is read through. If clickable ncAAs are used, click labelling can be performed in a minimally invasive and site-specific manner.

1.5.2. Click chemistry labelling

The concept of click chemistry was established in 2001 and describes a set of selective “spring-loaded” reactions (Kolb et al. 2001). Click chemistry reactions should only create by-products that can be easily removed, are simple to perform, and are composed of modular components. The components of click chemistry are bioorthogonal, allowing application in cells without interfering or reacting with cell intrinsic molecules (McKay and Finn 2014). Amber suppression mediated incorporation of clickable ncAA in combination with a corresponding click chemistry functionalised fluorescent dye can thus enable site-specific labelling of a protein of interest.

1.5.2.1. Copper catalysed azide-alkyne cycloaddition (CuAAC)

The copper catalysed azide-alkyne cycloaddition (CuAAC) is a reaction between azide and alkyne groups linking them together to a triazole ring catalysed by copper (Tornøe et al. 2002) (Figure 1.11A). Both azide and alkyne groups are generally absent from biological systems and are unreactive to proteins or other cellular molecules (Li and Zhang 2016). Incorporation of alkyne bearing amino acids into proteins in *E. coli* using a PylRS/tRNA^{Pyl} pair enabled site specific CuAAC labelling with an azide coupled fluorescent dye (Milles et al. 2012). However, the required copper catalyst is highly cytotoxic due to the induction of reactive oxygen species (Hong et al. 2010; Kennedy et al. 2011). This strongly reduces biocompatibility and limits the application of CuAAC to fixed cells.

1.5.2.2. Strain-promoted azide-alkyne cycloaddition (SPAAC)

Strain-promoted azide-alkyne cycloaddition (SPAAC) is copper-independent and utilises ring strained alkynes instead of linear alkyne groups (Figure 1.11B) (Agard et al. 2004). Plass et al. synthesised lysine derivatives with cyclooctyne groups and used the *M. mazei* PylRS^{AF}/tRNA^{Pyl} pair to incorporate them into an amber stop mutated GFP and mCherry in *E. coli* (Plass et al. 2011). The incorporated ncAA were click labelled with azide-coupled dyes in living cells, providing evidence for site-specific and minimally invasive protein labelling in live bacteria. Successful SPAAC labelling was subsequently also shown in mammalian cells by the same research group (Borrmann et al. 2012). The main drawback of SPAAC labelling is the much slower reaction rate compared to CuAAC (Prescher and Bertozzi 2005).

1.5.2.3. Strain-promoted inverse-electron demand Diels-Alder cycloaddition (SPIEDAC)

The strain-promoted inverse-electron demand Diels-Alder cycloaddition (SPIEDAC) describes a reaction between a tetrazine and a ring strained alkyne or alkene (Figure 1.11C). Similar to SPAAC, SPIEDAC reactions are bioorthogonal and do not require a catalyst, but they have unusually fast reaction rates making them favourable for labelling of genetically encoded ncAA (Blackman et al. 2008). Efficient and specific labelling of genetically encoded ncAA with ring strained alkyne or alkene groups was achieved in bacterial and mammalian cells (Borrmann et al. 2012; Plass et al. 2012; Nikic et al. 2014).

1.5.2.4. Click chemistry functionalised silicon rhodamine (SiR) dyes

The silicon rhodamine (SiR) dye is a near-infrared fluorophore that is membrane permeable as well as biocompatible (Lukinavicius et al. 2013). Membrane permeability is crucial for our labelling purposes, as the dye has to cross the viral membrane or the cellular membrane to label the viral capsid and ribonucleoprotein inside the enveloped virus or virus replicating cells. To be membrane permeable, a dye must be hydrophobic. Unfortunately, hydrophobic dyes also tend to stick inside the cells and are not easily removed by washing (Nikic et al. 2015). SiR derivatives were shown to be fluorogenic dyes, that is SiR derivatives are mostly non-fluorescent in hydrophobic environments but coupling of SiR derivatives to their target protein tags induces the formation of a fluorescent zwitterion (Lukinavicius et al. 2013).

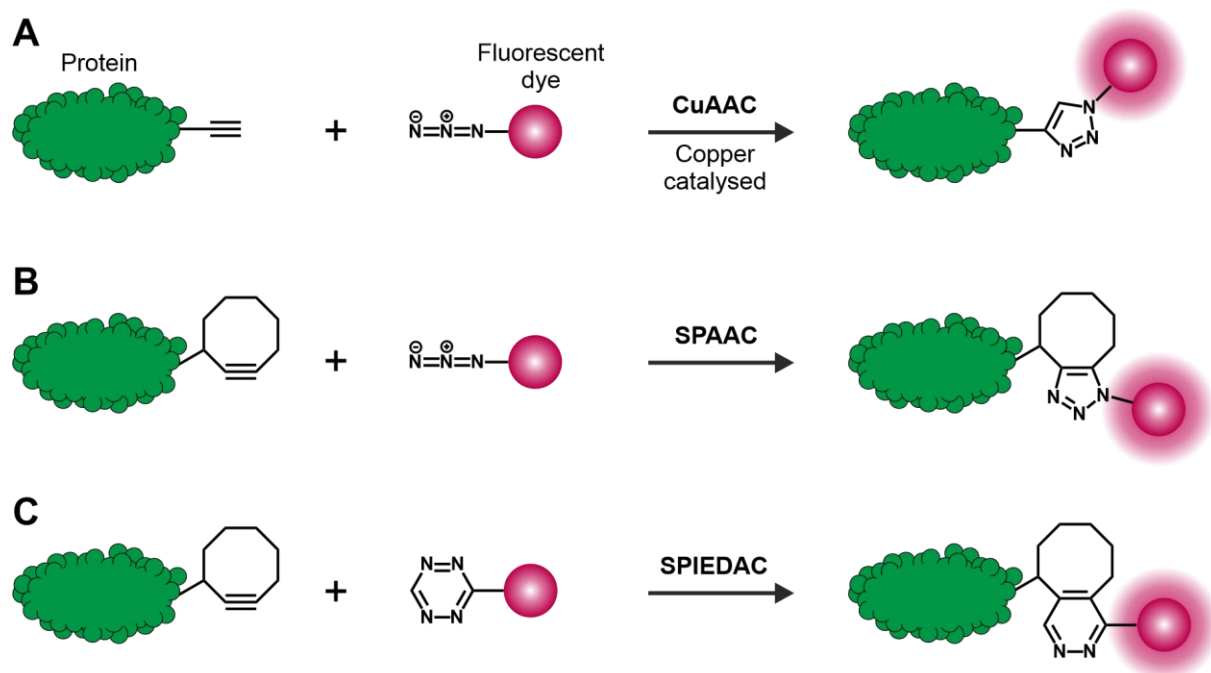


Figure 1.11. Click chemistry reactions. Incorporation of ncAA into proteins (green) enables the direct labelling with fluorescent dyes (magenta) that are coupled to azide or tetrazine. **(A)** In CuAAC, a linear alkyne and an azide react to a triazole catalysed by copper. **(B)** Similarly, an alkyne and azide react in SPAAC to form a triazole ring. However, SPAAC does not need a catalyst but the driving force originates from the ring strained alkyne. **(C)** SPIEDAC describes a cycloaddition between a ring strained alkyne or alkene with a tetrazine resulting in pyridazine and releasing nitrogen.

Tetrazine coupled SiR (SiRTet) was shown to specifically label proteins with incorporated ring strained alkenes in living *E. coli* without the need for fixation or permeabilization (Lukinavicius et al. 2013). Intracellular fluorescent labelling of cytoskeleton proteins was also observed in mammalian cells after genetic encoding of ring strained alkynes (Uttamapinant et al. 2015). SiR fluorophores have far-red emission and excitation wavelengths which make them suitable for live cell imaging as irradiation at longer wavelengths induces less phototoxic effects on cells (Waldchen et al. 2015). Furthermore, they are well suited for super resolution microscopy (Lukinavicius et al. 2013; Uttamapinant et al. 2015).

1.5.3. Amber suppression mediated labelling of viral proteins

Combination of amber suppression mediated incorporation of ncAA and subsequent coupling to synthetic dyes using click chemistry constitutes the smallest fluorescent tag that can be genetically encoded in living cells (Sakin et al. 2016). This property makes it very promising for visualisation approaches of viruses which are intrinsically difficult to label due to their small size. Azide functionalised ncAA have been successfully incorporated into capsid proteins of adeno-associated virus (AAV) and subsequently labelled by SPAAC using a strained alkyne fluorophore (Kelemen et al. 2016). Using a similar labelling approach, fluorescent AAV was

used to study virus entry and intracellular trafficking in imaging experiments (Zhang et al. 2018).

Incorporation of azide bearing ncAA has been assessed at different positions of the VSV envelope glycoprotein and shown a high variation regarding protein expression and viral infectivity (Zheng et al. 2015). SPAAC-mediated site-specific labelling using an alkyne coupled dye enabled tracking of single pseudotyped lentiviral vectors.

The PylRS^{AF}/tRNA^{Pyl} pair was used to incorporate ring strained alkene and alkyne ncAA into the viral envelope and fusion protein hemagglutinin (HA) in virus-like particles of IAV (Nikic et al. 2014). After labelling with two different (non-permeable) click chemistry dyes, dual-labelled filamentous protrusions were observed on the surface of cells. Super resolution microscopy allowed to visualise individual filaments. Das et al. took it one step further, they mutated two positions of HA to amber stop codons and incorporated ring strained alkenes for SPIEDAC labelling (Das et al. 2018). Pseudoviruses were produced by co-expression with HIV core and the incorporated ncAA were subsequently labelled with two tetrazine coupled dyes. Single-molecule Förster resonance energy transfer (FRET) imaging was performed on dual labelled HA and was able to distinguish pre- from post-fusion conformations and an intermediate conformation of HA. The authors used acidification and exposure to the IAV receptor sialic acid to shift the conformation equilibrium to the post-fusion state (Das et al. 2018). The amber suppression technology was certainly pushed to its current limits in this approach, but it enabled real-time single molecule imaging to obtain biological information on HA conformational dynamics.

Similar experiments have been performed on the HIV envelope glycoprotein (Env). Sakin and co-workers have incorporated ncAA into Env in mammalian cells (Sakin et al. 2017). Incorporation of ring strained alkynes did not impair the infectivity of HIV but click labelled Env could not be detected on viral particles, possibly caused by insufficient readthrough efficiency of the inserted stop codon and subsequent low abundance of Env proteins on virions. However, fluorescently labelled Env was observed on the plasma membrane and studied using fluorescence recovery after photo bleaching and super resolution microscopy. The combination of single molecule FRET with genetically encoded ncAA was also performed for HIV Env (Lu et al. 2019). Here, the dual labelling of a single protein was achieved with a combination of tags that require enzymatic labelling and amber suppression mediated incorporation of ncAA. FRET imaging revealed that a structurally uncharacterised conformation of Env might be the predominant form found on virions.

Interestingly, the earliest report that applied amber suppression combined with click chemistry on a mammalian virus investigated HBV envelope proteins. Lin and colleagues have reported the incorporation of ncAA into HBV envelope proteins and used this system to label HDV (Lin et al. 2013). They were able to produce fluorescently labelled S-HBsAg in SVPs. HDV secretion was strongly reduced when ncAA were incorporated into S-HBsAg, but incorporation of ncAA into the preS sequence of L-HBsAg could rescue the production of infectious HDV. Unfortunately, the authors did not show fluorescent labelling of HDV particles, but their experiments hint to a promising approach for labelling HBV and HDV proteins.

1.6. Aims of this study

This work focuses on elucidating processes of HBV and HDV entry, and how HBV cccDNA is maintained in infected cells. To achieve a complete cure from CHB, elimination of the highly persistent cccDNA is required. cccDNA maintenance is hypothesised to be achieved via an extracellular route involving secretion of virions and infection of naïve cells and an intracellular amplification mediated by reimport of newly synthesised nucleocapsids. The contribution of the intracellular pathway to cccDNA levels in long-term infections is however poorly understood.

To investigate viral entry dynamics and mechanisms, the generation of fluorescently labelled HBV and HDV is desirable. Successful fluorescent labelling has neither been reported for HBV nor HDV. Engineering of proteins with ncAA through amber suppression combined with click chemistry labelling denotes the smallest site-specific fluorescent protein labelling method currently available. Hence, this method is a promising tool to fluorescently label HBV and HDV.

The following aims were defined for this thesis:

- (1) Characterisation of the role of newly synthesised HBc for the maintenance of cccDNA during viral replication in long-term *in vitro* HBV infection. Production of an infectious HBV mutant that is incapable of producing HBc after infection allows to investigate the role of *de novo* nucleocapsid formation on cccDNA levels.
- (2) Amber suppression mediated fluorescent labelling of HBV. The aim is to site-specifically engineer the HBc protein using the amber suppression system followed by click chemistry mediated fluorescent labelling of the incorporated ncAA.
- (3) Amber suppression mediated fluorescent labelling of HDV. During HDV replication, the amber stop codon at the amber/W site is edited to produce the L-HDAg. The aim of this project is to take advantage of his convenient amber codon and to incorporate a ncAA instead of the tryptophan into L-HDAg. Fluorescent labelling of HDV RNPs and HBV nucleocapsids could be used to study virus entry and intracellular trafficking.

2. Materials & Methods

2.1. Materials

2.1.1. Bacterial strains

DH5 α and Top10 *E. coli* bacterial strains were used for molecular cloning. These competent cells were home-made by Yi Ni using the rubidium chloride chemical sensitisation protocol from Promega.

2.1.2. Eukaryotic cell lines

Name	Specifications
Huh7	Human hepatoma cell line isolated from a 57-year old patient with HCC (Nakabayashi et al. 1982)
Huh7-NTCP	Huh7 cells with stable expression of NTCP (Ni et al. 2014)
HepaRG-NTCP	Human hepatoma cell line isolated from an HCV-infected patient with HCC, with stable expression of NTCP (Gripon et al. 2002; Ni et al. 2014)
HepG2-NTCP	Human liver carcinoma derived cell line isolated from a 15-year-old patient with HCC, with stable expression of NTCP (Aden et al. 1979; Ni et al. 2014)
PHH	Primary human hepatocytes were obtained by perfusion of liver sections after partial hepatectomy provided by Florian Vondran (University Hospital Hannover). All tissue donors gave written informed consent for the experimental use of liver specimens and the protocol was approved by the ethics review committee of Hannover Medical School (#252-2008).

2.1.3. Cell culture media

	Huh7	Huh7-NTCP, HepG2-NTCP	Huh7-NTCP	HepG2-NTCP	HepaRG- NTCP, PHH
	Growth medium	Growth medium	Infection medium	Infection medium	Infection medium
Medium	DMEM	DMEM	DMEM	DMEM	William's E
FBS	10%	10%	10%	10%	10%
Streptomycin	50 μ g/ml	50 μ g/ml	50 μ g/ml	50 μ g/ml	50 μ g/ml
Penicillin	50 U/ml	50 U/ml	50 U/ml	50 U/ml	50 U/ml
L-glutamine	2 mM	2 mM	2 mM	2 mM	2 mM
Puromycin		5 μ g/ml			
Insulin					5 μ g/ml
Hydrocortisone					50 μ M
DMSO			2%	2.5%	1.5%

2.1.4. Viruses

Virus	Description	Source
HBV	WT HBV was produced by transfection of Huh7 cells with pHBV1.1-WT and purified by heparin affinity chromatography.	This thesis
	Δ HBc HBV was produced by co-transfection with pHBV1.1-T67* and pHBc.	This thesis
	HBV with incorporated ncAA was produced by co-transfection with amber stop mutated pHBV1.1 and an amber suppression plasmid.	This thesis
HDV	WT HDV was produced by co-transfection of Huh7 cells with pJC126 and pHB2.7-gtB.	This thesis
	HDV with incorporated ncAA was produced by co-transfection with pJC126, pHB2.7-gtB, and an amber suppression plasmid.	This thesis
	The virus stock HDV2103 was produced in Huh7 cells by co-transfection with pJC126 and pT7HB2.7 and purified via heparin affinity chromatography.	Zhenfeng Zhang

2.1.5. Antibodies

Primary antibodies/antisera			
Name	Description	Application and dilution	Source
Anti- β -actin	Mouse monoclonal	WB: 1:5000	Sigma Aldrich
Anti-EEA1	Mouse monoclonal	IF: 1:200	BD Biosciences
Anti-HBc Dako	Rabbit polyclonal	IF: 1:3000	Dako
Anti-HBc H746	Rabbit polyclonal	WB: 1:2000	Christa Kuhn
Anti-HBsAg HBC34	Human monoclonal	IF: 1:3000	Davide Corti
Anti HBsAg HBD87	Human monoclonal	IF/WB: 1:3000	Davide Corti
Anti-HDAg VUDA	Serum of HBV/HDV co-infected patient	IF/WB: 1:3000	Heiner Wedemeyer
Anti-HDAg FD3A7	Rabbit monoclonal	IF/WB: 1:3000	Florian Lempp

Secondary antibodies		
Name	Application and dilution	Source
goat anti-human AlexaFluor488	IF: 1:1000	Thermo Fisher Scientific
goat anti-human AlexaFluor555	IF: 1:1000	Thermo Fisher Scientific
goat anti-mouse AlexaFluor488	IF: 1:1000	Thermo Fisher Scientific
goat anti-mouse AlexaFluor546	IF: 1:1000	Thermo Fisher Scientific
goat anti-rabbit AlexaFluor488	IF: 1:500	Thermo Fisher Scientific
goat anti-rabbit AlexaFluor546	IF: 1:500	Thermo Fisher Scientific
goat anti-human IRDye 800CW	WB: 1:20'000	Licor
goati anti-rabbit IRDye 800CW	WB: 1:20'000	Licor
goat anti-mouse IRDye 680RD	WB: 1:20'000	Licor
goat anti-rabbit peroxidase	WB: 1:10'000	Jackson ImmunoResearch

2.1.6. Chemicals

Chemical	Company/Supplier	Cat. No.
[α -P32]deoxycytidine 5'-triphosphate (dCTP)	Hartmann Analytic	SRP-205
Acetic acid	Sigma-Aldrich	33209
Acrylamide/Bisacrylamide(30% w/v)	SERVA electrophoresis	10687
Adenosine 5'-Triphosphate (ATP)	New England Biolabs	P0756
Agarose	Biozym Scientific	840004
Ammonium persulfate (APS)	Thermo Fisher Scientific	10744171
Ampicillin	Carl Roth	K029
Ascorbic acid, L-	Sigma-Aldrich	A4544
B. Braun, Aqua ad iniectabilia (H ₂ O)	University Hospital Heidelberg	
Bicyclo [6.1.0] nonyne-lysine (BCN)	SiChem	SC-8014
β -Mercaptoethanol	Sigma-Aldrich	M6250
Bovine serum albumin (BSA)	Carl Roth	3737.2
Bromophenol blue	Waldeck	4F-057
Calf thymus DNA	Life technologies, Invitrogen	15633-019
Caesium chloride (CsCl)	Invitrogen	15507023
Carrier RNA	Qiagen	52906
Cutsmart buffer	New England Biolabs	B7204S
Cyclooctyne-lysine (SCO)	SiChem	SC-8001
Cyclopropene L-lysine (CpK)	SiChem	SC-8017
Dextran	Sigma-Aldrich	D1662
Dimethylsulfoxide (DMSO)	Merck	102950
Dithiothreitol (DTT)	Sigma-Aldrich	D0632
Dulbecco's Modified Eagle Medium (DMEM)	Life technologies, Invitrogen	41965039
Dulbecco's Phosphate Buffered Saline (PBS)	Sigma-Aldrich	D8537
Ethanol (EtOH)	Sigma-Aldrich	32205
Ethidium bromide	Sigma-Aldrich	E7637
Ethylenediaminetetraacetic acid (EDTA)	SERVA electrophoresis	39760.01
Fetal bovine serum (FBS)	Sigma-Aldrich	S0615
Ficoll PM70	Sigma-Aldrich	F2878
Fluoromount G	Life technologies, Invitrogen	4958-02
GeneRuler DNA Ladder Mix	Thermo Fisher Scientific	SM0331
Glutamine, L-	Life technologies, Invitrogen	25030024
Glycerol	Thermo Fisher Scientific	G/0650/15
Glycine	Sigma-Aldrich	G8898
GlycoBlue Coprecipitant	Thermo Fisher Scientific	AM9516
Heparin sodium salt	Sigma-Aldrich	H3149
HEPES 1M	Thermo Fisher Scientific	12509079
Hoechst 33342	Life technologies, Invitrogen	H3570
Hydrochloric acid (HCl)	Sigma-Aldrich	30721
Hydrocortisone hemisuccinate	Sigma-Aldrich	H4881
Insulin	Sigma-Aldrich	91077C
Isopropanol	Sigma-Aldrich	33539
Lamivudine (3TC)	Sigma-Aldrich	L1295
LB broth (Lennox)	Sigma-Aldrich	L3022
LB broth with agar (Lennox)	Sigma-Aldrich	L2897

Materials & Methods

Lonafarnib	Selleckchem	S2797
Methanol	Sigma-Aldrich	34860
Midori Green Advance	Biozym Scientific	617004
Milk powder	Carl Roth	T145.2
N-epsilon-t-butyloxycarbonyl-L-lysine (BOC)	Iris Biotech	HAA1096
N-Propargyl-L-lysine (PrK)	SiChem	SC-8002
Opti-MEM	Thermo Fisher Scientific	31985047
PageRuler Plus prestained protein ladder	Thermo Fisher Scientific	26619
Paraformaldehyde (PFA)	Sigma-Aldrich	P6148
Penicillin/Streptomycin	Life technologies, Invitrogen	15140-122
Polyethylenglycol (PEG 8000)	Sigma-Aldrich	89510
Polyvinylpyrrolidone	Sigma-Aldrich	PVP40
Puromycin	Invivogen	ant-pr-1
RNase inhibitor	Thermo Fisher Scientific	N8080119
RNAzol RT	Sigma-Aldrich	R4533
Silicon rhodamine azide (SiR-Azide)	Spirochrome	SC009
Silicon rhodamine tetrazine (SiRTet)	Spirochrome	SC008
Sodium azide (NaN ₃)	Sigma-Aldrich	8591
Sodium chloride (NaCl)	Sigma-Aldrich	S7653
Sodium citrate	AppliChem	131655.121
Sodium dodecyl sulfate (SDS)	SERVA electrophoresis	20765
Sodium hydroxide (NaOH)	Sigma-Aldrich	30620
Sucrose	Carl Roth	4621.1
Tenofovir disoproxil (TDF)	Sigma-Aldrich	SML1794
Tetramethylethylene-diamine (TEMED)	Carl Roth	2367.3
trans-Cyclooct-2-en L-lysine (TCO*)	SiChem	SC-8008
TransIT-LT1	Mirus Bio	MIR2300
Tris	Carl Roth	4855.2
Triton X-100	Merck	108603
Tween-20	Carl Roth	9127.1
VIC labelled human RNaseP probe	Bio-Rad	4403328
Western lightning Plus-ECL	PerkinElmer	NEL103001EA
William's E	Life technologies, Invitrogen	22551-022

2.1.7. Buffers and solutions

Buffer	Composition
Media for bacteria cultivation	
LB medium	20 g LB broth in 1000 ml H ₂ O, autoclaved, with or without 100 µg/ml Ampicillin
LB agar plate	35 g LB broth with agar in 1000 ml H ₂ O, autoclaved, 100 µg/ml Ampicillin
Agarose gel electrophoresis	
TAE buffer (50X)	2 M Tris, 1 M glacial acetic acid, 500 mM EDTA (pH 8.0)
Heparin affinity chromatography	
TN buffer	20 mM Tris, 140 mM NaCl (pH 7.4)
TN400 buffer	20 mM Tris, 400 mM NaCl (pH 7.4)

Materials & Methods

TN600 buffer	20 mM Tris, 600 mM NaCl (pH 7.4)
TN2140 buffer	20 mM Tris, 2.14 M NaCl (pH 7.4)

CsCl density gradients	
CsCl solutions	1.2 g/ml (28.9 g CsCl and 100 g H ₂ O), 1.3 g/ml (40.3 g CsCl and 100 g H ₂ O), 1.4 g/ml (54.5 g CsCl and 100 g H ₂ O)
20% sucrose	2 g sucrose and 8 g PBS

DNA dot blot	
Soak I	1.5 M NaCl, 500 mM NaOH
Soak II	3 M NaCl, 500 mM Tris (pH7.4)
SSC buffer (20X)	3 M NaCl, 300 mM sodium citrate (pH 7.0)
Denhardt's buffer (50X)	1% BSA, 1% Ficoll PM70, 1% Polyvinylpyrrolidone
Hybridisation buffer	10 µg/ml calf thymus DNA, 5X Denhardt's, 6X SSC, 0.5% SDS
Wash buffer	1X SSC, 0.5% SDS

Southern blot	
TE buffer	10 mM Tris, 1 mM EDTA (pH 7.5)
Depurination buffer	200 mM HCl
Denaturing buffer	500 mM NaOH, 1.5 M NaCl
Neutralisation buffer	1.5 M NaCl, 1 M Tris (pH 7.4)
Hybridisation buffer	QuikHyb Hybridization solution (Agilent)
Wash buffer	1X SSC, 0.1 % SDS

SDS PAGE	
SDS sample buffer (2X)	0.1 mg/ml bromophenol blue, 10% DTT, 20% glycerol, 6% SDS, 200 mM Tris (pH 6.8)
Resolving gel buffer (4X)	1.5 M Tris, 0.4% SDS, 0.01% NaN ₃ (pH 8.8)
Stacking gel buffer (4X)	500 mM Tris, 0.4% SDS, 0.01% NaN ₃ (pH 6.8)
SDS running buffer (10X)	250 mM Tris, 1.92 M glycine, 1% SDS (pH 8.3)

Western blot	
Blotting buffer	48 mM Tris, 39 mM glycine, 0.04 % SDS, 10% methanol
TBS (10X)	200 mM Tris, 1.37 M NaCl (pH 8.0)
TBS-T	1X TBS, 0.05% Tween-20

Amber suppression	
ncAA stock	100 mM ncAA, 15% DMSO, 200 mM NaOH

2.1.8. Enzymes

Enzyme	Provider	Cat. No.
AmpliTaq Gold DNA polymerase	Thermo Fisher Scientific	4311816
BsiHKAI	New England Biolabs	R0570
ddPCR Supermix for Probes	Bio-Rad	1863024
Fast Digest restriction nucleases	Thermo Fisher Scientific	
GoTaq Flexi DNA polymerase	Promega	M8296
HhaI	New England Biolabs	R0139

Materials & Methods

iTaq Universal SYBR Green Mix	Bio-Rad	1725125
Luna Universal Probe qPCR Master Mix	New England Biolabs	M3004
NcoI	New England Biolabs	R3193
Phusion polymerase	New England Biolabs	M0530
Protease III	ACD	322340
RecJ _f	New England Biolabs	M0264
RQ1 RNase-Free DNase	Promega	M6101
SphI	New England Biolabs	R3182
T4 DNA ligase	New England Biolabs	M0202
Trypsin EDTA	Biochrom	L2143
XbaI	New England Biolabs	R0145

2.1.9. Kits

Kit	Provider	Cat. No.
Click-iT EdU imaging	Thermo Fisher Scientific	C10340
CuAAC cell reaction buffer (BTAA based)	Jena Bioscience	CLK-073
GeneJET PCR purification	Thermo Fisher Scientific	K0702
GeneJET gel extraction	Thermo Fisher Scientific	K0692
GeneJET plasmid miniprep	Thermo Fisher Scientific	K0503
High-capacity cDNA reverse transcription	Thermo Fisher Scientific	4368814
MasterPure Complete DNA and RNA purification	Lucigen	MC85200
Megaprime DNA labelling system	Sigma-Aldrich	RPN1604
NucleoSpin RNA	Macherey-Nagel	740955
NucleoSpin tissue	Macherey-Nagel	740952
Plasmid Plus Midi	Qiagen	12945
QIAEX II gel extraction	Qiagen	20021

2.1.10. Plasmids

Name	Description	Source
pHBV1.1-WT	Eukaryotic expression vector encoding 1.1mer overlength HBV genome driven from a CMV promoter	Christine Bekker
pHBV1.1-S26*	pHBV1.1 with amber stop mutation at position S26 of the HBc ORF	This thesis
pHBV1.1-D32*	pHBV1.1 with amber stop mutation at position D32 of the HBc ORF	This thesis
pHBV1.1-W62*	pHBV1.1 with amber stop mutation at position W62 of the HBc ORF	This thesis
pHBV1.1-T67*	pHBV1.1 with amber stop mutation at position T67 of the HBc ORF	This thesis
pHBV1.1-V74*	pHBV1.1 with amber stop mutation at position V74 of the HBc ORF	This thesis

Materials & Methods

pHBV1.1-N75*	pHBV1.1 with amber stop mutation at position N75 of the HBc ORF	This thesis
pHBV1.1-L76*	pHBV1.1 with amber stop mutation at position L76 of the HBc ORF	This thesis
pHBV1.1-E77*	pHBV1.1 with amber stop mutation at position E77 of the HBc ORF	This thesis
pHBV1.1-L84*	pHBV1.1 with amber stop mutation at position L84 of the HBc ORF	This thesis
pHBV1.1-S87*	pHBV1.1 with amber stop mutation at position S87 of the HBc ORF	This thesis
pHBV1.1-A131*	pHBV1.1 with amber stop mutation at position A131 of the HBc ORF	This thesis
pHBc	pcDNA3.1 eukaryotic expression vector encoding the HBc protein under a CMV promoter	Christine Bekker
pPylRS ^{AF} /tRNA ^{Pyl}	Eukaryotic expression vector encoding the amber suppression pyrrolysine RS(with AF mutation)/tRNA pair from <i>M.mazei</i> under a CMV and an U6 promoter	(Plass et al. 2012)
pmCherry-GFP(TAG)	Eukaryotic expression vector encoding an mCherry-GFP fusion construct with amber stop mutation in the GFP ORF under a CMV promoter	(Plass et al. 2012)
peRF1-E55D	Eukaryotic expression vector encoding the dominant negative E55D mutant of eRF1 under a CMV promoter	(Schmied et al. 2014)
pPylRS/4×tRNA ^{Pyl}	Eukaryotic expression vector encoding the amber suppression pyrrolysine RS under a EF1α promoter and 4 copies of tRNA ^{Pyl} under U6 promoters	(Schmied et al. 2014)
pNESPylRS ^{AF} /tRNA ^{Pyl}	Eukaryotic expression vector encoding the pyrrolysine RS(AF mutation)/tRNA pair with a NES at the N-terminus of the PylRS under a CMV and an U6 promoter	(Nikic et al. 2016)
pNESPylRS ^{AF} /4×tRNA ^{Pyl}	pPylRS/4×tRNA ^{Pyl} with the PylRS replaced by the NESPylRS(AF)	This thesis
pHDAg	Eukaryotic expression vector encoding the HDAG under a CMV promoter	Florian Lempp
pL-HDAg	Eukaryotic expression vector encoding the large HDAG with edited stop codon under a CMV promoter	Florian Lempp
pS-HDAg	Eukaryotic expression vector encoding the small HDAG lacking the C-terminal extension of L-HDAg under a CMV promoter	Florian Lempp
pJC126	Eukaryotic expression vector encoding an 1.1mer overlength antigenome of HDV genotype 1 under a CMV promoter	(Gudima et al. 2002)
pJC126-ochre	pJC126 with TAG stop mutated to TAA	This thesis
pJC126-2×ochre	pJC126 with two TAA stop mutations	This thesis
pHB2.7-gtB	Lentiviral vector encoding a 2700 bp subgenomic fragment of HBV genotype B including the L, M, S, and X ORFs under control of the authentic promoter	(Lempp et al. 2019)
pT7HB2.7	Plasmid encoding a 2700 bp subgenomic fragment of HBV genotype D including the L, M, S, and X ORFs under control of the authentic promoter	(Sureau et al. 2003)
pSHH2.1	Head-to-tail HBV dimer in a pSV08 plasmid under a SV40 promoter	(Cattaneo et al. 1983)
pCHT-9/3091	1.1mer overlength HBV genome under a CMV promoter	(Nassal 1992)

2.1.11. Oligonucleotides

Oligonucleotides for molecular cloning	
Name	Sequence (5' to 3')
HBV1.1 MluI FW	AGATATACGCGTTGACATTGATTATTGACTAG
HBV1.1 EcoRI RV	GTTGTGGAATTCCACTGCATGG
HBc S26Amber FW	GACTTCTTTCCTTAGGTACGAGATCTTC
HBc S26Amber RV	GAAGATCTCGTACCTAAGGAAAGAAGTC
HBc D32Amber FW	CGAGATCTTCTATAGACCGCCTCAGCTC
HBc D32Amber RV	GAGCTGAGGCGGTCTATAGAAGATCTCG
HBc W62Amber FW	GCAATTCTTTGCTAGGGGGA ACTAATG
HBc W62Amber RV	CATTAGTTCCCCCTAGCAAAGAATTGC
HBc T67Amber FW	GGGGA ACTAATGTAGCTAGCTACCTGGG
HBc T67Amber RV	CCCAGGTAGCTAGCTACATTAGTTCCCC
HBc V74Amber FW	CTACCTGGGTGGGTTAGAATTTGGAAGATC
HBc V74Amber RV	GATCTTCCAAATTCTAACCCACCCAGGTAG
HBc N75Amber FW	CTGGGTGGGTGTTTAGTTGGAAGATCCAG
HBc N75Amber RV	CTGGATCTTCCA ACTAACACCCACCCAG
HBc L76Amber FW	GTGGGTGTTAATTAGGAAGATCCAGC
HBc L76Amber RV	GCTGGATCTTCCCTAATTAACACCCAC
HBc E77Amber FW	GGGTGTTAATTTGTAGGATCCAGCGTCTAG
HBc E77Amber RV	CTAGACGCTGGATCCTACAAATTAACACCC
HBc L84Amber FW	CAGCGTCTAGAGACTAGGTAGTCAGTTATGTC
HBc L84Amber RV	GACATAACTGACTACCTAGTCTCTAGACGCTG
HBc S87Amber FW	GACCTAGTAGTCTAGTATGTCAACAC
HBc S87Amber RV	GTGTTGACATACTAGACTACTAGGTC
HBc A131Amber FW	GATTCGCACTCCTCCATAGTATAGACCACCAAATG
HBc A131Amber RV	CATTTGGTGGTCTATACTATGGAGGAGTGCGAATC
pJC126 NheI FW	CACCGGCTAGCCCCGTTGCTTTCTT
pJC126 NotI RV	CGAGCGGCCGCCAGTGTGATGGATATC
pJC126 TAG-TAA FW	CCAGGGATTTCCATAAGATATACTCTTCCCAG
pJC126 TAG-TAA RV	CTGGGAAGAGTATATCTTATGGAAATCCCTGG
pJC126 2xTAA FW	CAGGGATTTCCATAAGATTA ACTCTTCCCAGCCG
pJC126 2xTAA RV	CGGCTGGGAAGAGTTAATCTTATGGAAATCCCTG

Oligonucleotides for detection assays			
Assay	Name	Sequence (5' to 3')	Source
Inverse nested PCR	outer FW	TTCGCTTACCTCTGCACG	(Tu and Jilbert 2017)
	outer RV	AAAGGACGTCCC GCGCAG	
	inner FW	CGCATGGAGACCACCGTGA	

	inner RV	CACAGCCTAGCAGCCATGG	
cinqPCR	cccDNA FW	CACTCTATGGAAGGCGGGTA	
	cccDNA RV	ATAAGGGTTCGATGTCCATGC	
	cccDNA probe	FAM-AACACATAGCGCACCAGCA-BHQ1	(Tu et al. 2020b)
	total HBV DNA FW	GTGTCTGCGGCGTTTTATCA	
	total HBV DNA RV	GACAAACGGGCAACATACCTT	
	total HBV DNA probe	FAM-TGAGGCATAGCAGCAGGATG-BHQ1	
qPCR	GAPDH FW	GAAGGTGAAGGTCGGAGTC	Bingqian Qu
	GAPDH RV	GAAGATGGTGATGGGATTTC	
	HDV FW	GCGCCGGCYGGGCAAC	
	HDV RV	TTCCTCTTCGGGTCGGCATG	(Ferns et al. 2012)
	HDV probe	FAM-CGCGGTCCGACCTGGGCATCCG-BHQ1	
	pgRNA/precure mRNA FW	CTCCTCCAGCTTATAGACC	
	pgRNA/precure mRNA RV	GTGAGTGGGCCTACAAA	(Lucifora et al. 2014)
	total HBV RNA FW	TCAGCAATGTCAACGACCGA	
	total HBV RNA RV	TGCGCAGACCAATTTATGCC	

2.1.12. Software

Name	Application	Provider
CFX Manager	Real-time qPCR analysis	Bio-Rad
ChemDraw	Molecule editor	PerkinElmer
CorelDRAW	Figure preparation	Corel Cooperations
Endnote	Reference management	Clarivate Analytics
Fiji (ImageJ)	Image processing	Open source
GraphPad PRISM	Statistical analysis and figure preparation	GraphPad Software
HoKaWo	Microscopy	Hamamatsu Photonics
ilastik	Image analysis	Open source
Image Studio	Western blot analysis	LI-COR
Leica Application Suite	Confocal microscopy	Leica Microsystems
Microsoft Excel	Statistical analysis	Microsoft
Microsoft Word	Thesis writing	Microsoft
Nanodrop 2000	Analysis of nucleic acid concentrations	Thermo Scientific
NIS-Elements	Microscopy	Nikon Instruments
PyMOL	Protein structure visualisation	Schrödinger
QuantaSoft	ddPCR analysis	Bio-Rad
Quantity One	Dot-blot and Southern blot analysis	Bio-Rad
Vector NTI	Sequence bioinformatics	Life Technologies

2.2. Methods

2.2.1. Molecular cloning

2.2.1.1. Point mutation

The HBc amber mutants were cloned by overlapping PCR. In a first round of PCR, two overlapping fragments from the plasmid pHBV1.1-WT were amplified (first fragment: forward primer HBV1.1 MluI FW and separate reverse primer for each point mutation; second fragment: separate forward primer for each point mutation and reverse primer HBV1.1 EcoRI RV). PCR was performed using Phusion DNA polymerase and PCR conditions were initial denaturing at 98 °C for 30 s; denaturing at 98 °C for 7 s followed by annealing at 58 °C for 20 s and elongation at 72 °C for 60 s (30 cycles); at last elongation at 72 °C for 7 min. The overlapping sequences of both fragments contained the desired mutation introduced by the primer design. The PCR products were analysed by agarose gel electrophoresis and purified with the GeneJET gel extraction kit. The two fragments were then annealed and amplified in a second PCR round (primers HBV1.1 MluI FW and HBV1.1 EcoRI RV) with the same PCR program. The PCR product and the original plasmid were digested with MluI and EcoRI. Agarose gel electrophoresis was used to isolate and purify the empty vector and the PCR product with the inserted point mutation. The PCR product was finally ligated back into the pHBV1.1 vector using T4 DNA ligase.

HDV ochre stop mutants were also generated by overlapping PCR. Fragments containing the desired mutation were amplified from plasmid pJC126, digested with NheI and NotI, and ligated back into pJC126.

2.2.1.2. Restriction digestion

Restriction digestions were performed using Fast Digest restriction nucleases. 1-5 µg of DNA were incubated with 1 µl of the respective restriction enzyme(s) in 1X Fast Digest Green buffer in a total volume of 30 µl for 1 h at 37 °C. The digested products were analysed by agarose gel electrophoresis and extracted using the GeneJET gel extraction kit.

For the generation of the plasmid pNESPyIRS^{AF}/4×tRNA^{PyI}, the NESPyIRS sequence was excised from plasmid pNESPyIRS^{AF}/tRNA^{PyI} using the restriction enzymes PmeI and NotI. Similarly, the plasmid pPyIRS^{AF}/4×tRNA^{PyI} was digested with PmeI and NotI. The

NESPyIRS^{AF} sequence was then ligated into the backbone containing 4 copies of the tRNA^{Pyl} using T4 DNA ligase.

2.2.1.3. Agarose gel electrophoresis

1-2 % agarose was dissolved in 1X TAE buffer by microwaving. 0.5 µg/ml ethidium bromide or a 1:20'000 dilution of Midori Green Advance was added before pouring into a gel chamber. The gel was run at 120 V for 20-40 min. 6 µl GeneRuler DNA ladder mix were loaded as marker. Gels were analysed on a UV table (ethidium bromide) or a blue/green light transilluminator (Midori Green). The desired DNA fragments were excised with a scalpel and extracted using the GeneJET gel extraction kit.

2.2.1.4. Ligation and transformation

Digested plasmid backbone and insert were mixed at a molar ratio of ~1:5 and ligation was performed using 0.25 µl T4 DNA ligase in a total volume of 5 µl 1X T4 DNA ligase reaction buffer for 30 min at room temperature (RT).

For transformation, the ligation mix was incubated with 50 µl competent bacteria on ice for 30 min. The heat shock was performed in a water bath at 42 °C for 90 s and the bacteria were moved back on ice for 2 min. 950 µl LB without antibiotics were added and the bacteria were allowed to grow for 1 h at 37 °C while shaking. The bacteria were pelleted by centrifugation at 900 g for 3 min and the supernatant was poured off. After resuspension of the bacterial pellet in the remaining liquid LB, the bacteria were distributed on an LB agar plate containing 100 µg/ml ampicillin and allowed to grow overnight at 37 °C.

2.2.1.5. Plasmid preparation

For miniprep, bacteria colonies were picked from LB agar plates and grown in 3 ml LB with 100 µg/ml ampicillin overnight at 37 °C while shaking at 180 rpm. 2 ml of the bacterial culture were used for plasmid extraction, which was performed using the GeneJET plasmid miniprep kit according to the manufacturer's protocol. The purified plasmid was eluted in 50 µl H₂O.

For midiprep, 50 ml LB (100 µg/ml ampicillin) were inoculated with 50 µl bacteria culture. After overnight incubation at 37 °C and shaking at 180 rpm, plasmid extraction was performed using the Plasmid Plus Midi kit according to the manufacturer's protocol. The DNA concentration was determined using a NanoDrop spectrophotometer and diluted to a final concentration of 1 µg/µl in H₂O.

2.2.1.6. Sequencing

Point mutations were confirmed by Sanger sequencing using the Eurofins GATC sequencing service according to the instructions of Eurofins GATC.

2.2.2. Cell culture

2.2.2.1. Maintenance of eukaryotic cells

All eukaryotic cells were maintained in an incubator at 37 °C, 5% CO₂ supply, and 95% humidity. All work with cells was performed in a sterile cell culture hood with laminar flow. Cells were generally split every 2-3 days to avoid overgrowing. Briefly, the cells were rinsed once with sterile PBS and incubated with trypsin-EDTA at 37 °C until detachment of the cells could be observed. When detached, trypsin was inactivated by addition of complete cell culture medium and the cells were resuspended by pipetting up and down. Before seeding, the cell number was determined using a BioRad TC20 automated cell counter. For passaging, the cells were split in ratios ranging from 1:4 to 1:10.

2.2.2.2. Freezing and thawing of cells

To freeze cells, they were trypsinised in the proliferating phase (~80% confluency) and resuspended in complete medium. The cell suspension was centrifuged at 500 g for 5 min and the supernatant was discarded. The cell pellet was resuspended in complete medium (1.4 ml for one T75 flask of cells) and the same volume of freezing medium (20% DMSO in FBS) was added, resulting in a 10% DMSO concentration. The cell suspension was aliquoted into cryotubes. The aliquots were frozen in a freezing box containing isopropanol at -80 °C overnight and finally transferred to a liquid nitrogen tank for long-term storage.

2.2.2.3. Differentiation of HepaRG-NTCP cells

HepaRG-NTCP cells were cultivated in T75 flasks and seeded and split once per week using HepaRG growth medium. Differentiation of HepaRG-NTCP cells was performed using a 4-week protocol, as described previously (Gripon et al. 2002). After trypsinisation and cell counting, cells were seeded in a density of 2×10^5 cells/ml into 12 or 24 well plates. The growth medium was changed one week after seeding. Another week later, the growth medium was replaced with differentiation medium containing 1.5% DMSO to induce differentiation of the cells. Over the following two weeks, the medium was changed three times per week. At the end

of this four-week differentiation protocol, differentiation of the cells to hepatocyte-like islands and biliary-like cells could be observed by light microscopy.

2.2.2.4. Transfection of Huh7 cells

Huh7 cells were seeded one day before transfection. Concentration of the cell suspension after trypsinisation was determined and diluted to 3×10^5 cells/ml. 500 μ l, 1 ml, or 2 ml of the cell suspension were added to each well of a 24-, 12-, or 6-well plate, respectively. For plasmid transfection, TransIT-LT1 reagent was used according to the manufacturer's instructions. For a 24 well, 50 μ l of Opti-MEM was mixed with 500 ng plasmid DNA and 1.5 μ l TransIT-LT1. The mixture was incubated at RT for 15-30 min before it was added dropwise to the cells.

2.2.2.5. Production and purification of Δ HBc HBV from transfected cells

For medium to large scale production of HBV, Huh7 cells were seeded into 10 cm dishes one day before transfection. 10 ml cell suspension with a concentration of 5×10^5 cells/ml were seeded into every dish. Per dish, 500 μ l Opti-MEM were mixed with 5 μ g plasmid DNA (2.5 μ g pHBV1.1-T67* + 2.5 μ g pHBc) and 15 μ l TransIT-LT1. As control, cells were transfected with 5 μ g of pHBV1.1-WT. The transfection mixture was incubated 15-30 min at RT and then dropwise added to the cells. One day after transfection, the cells were washed once in PBS and further maintained in complete growth medium. Supernatants were collected on day 3, 5, 7, and 9 after transfection. The collected supernatants were immediately centrifuged at 500 g for 5 min to remove cell debris and subsequently transferred to fresh tubes and stored at 4 °C. At day 9 post transfection the supernatants were pooled and filtered using a stericup with a 0.45 μ m PVDF membrane.

For virus purification, the supernatants were applied to heparin affinity chromatography using a 5 ml heparin-sepharose column at a flow rate of 1 ml/min. The column was washed with TN buffer and virions were eluted by gradual increase to TN2140 buffer over 10 column volumes. Three virus containing fractions were determined by absorbance at 280 nm UV, pooled (7.5 ml), and diluted with sterile H₂O to a final NaCl concentration of 140 mM. The virus was further concentrated on an Amicon Ultra-15 centrifugal filter unit with 100 kDa cutoff at 4 °C and 3000 g until it was reduced to ~5-6 ml. FBS (10% of the final volume) was added as stabiliser, the virus stock was aliquoted, and stored at -80 °C. The concentration of HBV genome equivalents per ml were quantified using the COBAS AmpliPrep/COBAS TaqMan HBV Test (Roche) by the Heidelberg University Hospital Virology Diagnostics Department.

2.2.2.6. Precipitation with PEG

Cell culture supernatant from transfected cells was mixed with PEG 8000 (6% of final volume) and precipitated overnight at 4 °C. After centrifugation at 12,000 g at 4 °C for 60 min, the supernatant was discarded, and the pellet was resuspended in PBS containing 10% FBS (~1/100 of the original volume). The resuspended pellet was incubated at 4 °C overnight while constantly rotating. Finally, the virus preparation was centrifuged (6,200 g, 5 min, 4 °C) and the supernatant was transferred to a fresh tube and stored at -80 °C.

2.2.2.7. Infection with HBV and HDV

HepaRG-NTCP cells were differentiated as described above before infection. HepG2-NTCP and Huh7-NTCP cells were seeded one day before infection at 5×10^5 cells/ml and 3×10^5 cells/ml, respectively. Upon receipt of PHH, the cells were examined on a light microscope and medium was exchanged. PHH were usually used for infection of the day of receipt.

Infection was performed with half the media volume of what was commonly used during cell culture, for example cells in a 24 well format were infected with 250 μ l of inoculum. 225 μ l of infection medium (containing DMSO) were mixed with 25 μ l PEG 8000 (40%) and virus preparation. If large volumes of virus stock were used, the amount of infection medium was reduced accordingly. The inoculation mix was added to the cells and infection was performed overnight at 37 °C. Cells were washed three times with PBS to remove leftover input virus and fresh infection medium was added. For entry inhibition and viral input control, the cells were pre-treated for 30 min and co-treated during infection with 500 nM MyrB.

2.2.2.8. Long-term infection of HepG2-NTCP cells

HepG2-NTCP cells in 24 well plates were infected with 40 mge (multiplicity of genome equivalents). One day post infection (dpi), the cells were washed 3 times with PBS and 1 ml of infection medium was added to each well. Starting 8 dpi, the cells were washed with PBS and the medium was replaced. Supernatant from the wells which were maintained for 9 weeks was collected for analysis of secreted viral antigens. One well for each condition was trypsinised and the cells were resuspended in infection medium. The cell suspension was centrifuged at 500 g for 5 min and the supernatant was discarded. The cell pellet was frozen at -80 °C. At the end of the long-term infection, the cell pellets were thawed, and DNA or RNA was extracted for further analysis.

2.2.2.9. Incorporation of ncAA

Huh7 cells were co-transfected with the plasmid expressing the protein of interest containing an amber stop codon and with one of the amber suppression constructs. One day after transfection, the cells were washed once with PBS and fresh medium was added. The ncAA were typically added two days after transfection. In the 24 well format, 1.25 μ l ncAA stock solution was mixed with 3.75 μ l 1 M HEPES and added to the cell culture supernatant. This resulted in a final ncAA concentration of 250 μ M. HEPES was used to buffer the NaOH in the ncAA stock solution. For testing of amber suppression efficiency, the inexpensive ncAA BOC was used.

2.2.2.10. Production and purification of HDV-TCO*

Huh7 cells were seeded into 10 cm dishes one day before transfection. 10 ml cell suspension with a concentration of 5×10^5 cells/ml were seeded into every dish. Per dish, 500 μ l Opti-MEM were mixed with 5 μ g plasmid DNA (1.67 μ g pJC126 + 1.67 μ g pNESPyIRS^{AF}/4 \times tRNA^{Pyl} + 1.67 μ g pHB2.7-gtB) and 15 μ l TransIT-LT1. The transfection mixture was incubated 15-30 min at RT and then dropwise added to the cells. One day after transfection, the cells were washed once in PBS and further maintained in complete growth medium. 4 days post transfection, 25 μ l TCO* stock solution was mixed with 75 μ l 1 M HEPES and added to each dish. The supernatant was collected 7 days post transfection and filtered using a stericup with a 0.45 μ m PVDF membrane.

For virus purification, the supernatant was applied to heparin affinity chromatography using a 1 ml heparin-sepharose column and a peristaltic pump. The column was washed with 10 ml TN buffer. The column was detached from the pump and a syringe was used to apply elution buffers. Elution was performed with 1 ml TN400 followed by 2 ml TN600. 500 μ l fractions were collected during elution. 166 μ l H₂O were added to fractions 2, 3, and 4 and 500 μ l H₂O were added to fractions 5 and 6 to reduce NaCl concentrations.

2.2.3. Detection of DNA and RNA

2.2.3.1. Caesium chloride (CsCl) density gradient centrifugation and HBV DNA dot blot

The CsCl density gradient was prepared in 4 ml ultracentrifuge tubes. From bottom to top, 500 μ l CsCl solutions with densities 1.4 g/ml, 1.3 g/ml, 1.2 g/ml, and a 20% sucrose solution were carefully layered. The samples (raw supernatant or PEG precipitate) were carefully added on top of the gradient. The tubes were filled up and balanced by adding PBS if necessary. The

gradients were centrifuged with a SW60 rotor in a Beckman Optima XE-90 ultracentrifuge at 58,000 rpm (453,300 g) for 3.5 h at 20 °C. After the centrifugation, a fractionator (Beckman fraction recovery system) was used to take 6 drops per fraction into a round bottom 96 well plate.

Dot blotting was performed using a minifold microfiltration system. The minifold was assembled with a positively charged nylon membrane and two layers of Whatman 3MM paper inside. Membrane and filter papers were soaked in PBS before assembly. After application of vacuum, all wells of the system were washed twice with PBS. Then the fractions from the CsCl density gradient were loaded and the system was washed again twice with PBS. As standard, HBV genome was excised with SacI from the plasmid pHBV1.1-WT, purified, and extracted from an agarose gel. The nylon membrane was laid on a Whatman 3MM paper soaked in Soak I twice for 90 s and twice for 60 s on a Whatman 3MM paper soaked in Soak II. The membrane was crosslinked by using the autocrosslink mode twice in a UV Stratalinker 1800.

The HBV DNA specific hybridisation probe was produced using the Megaprime DNA labelling kit. 5 µl template DNA (5 µl of SacI linearized pCHT-9/3091 plasmid, 5 ng/µl) was mixed with 5 µl random primer and 16 µl H₂O. This DNA and primer mixture was denatured at 95 °C for 5 min and immediately put on ice. 4 µl dGTP, 4 µl dATP, 4 µl dTTP, and 5 µl reaction buffer were added. 2 µl Klenow fragment (1 U/µl) and 4 µl ³²P-labelled dCTP were added to the tube and it was incubated for 30 min at 37 °C. The probe was loaded on an illustra microspin column and centrifuged 1 min at 750 g. The radioactive probe in the flow-through was denatured at 95 °C for 30 min. In the meantime, the membrane was blocked in hybridisation buffer at 68 °C. The radioactive probe was then added to the hybridisation buffer and incubated overnight at 68 °C. The membrane was washed three times with dot blot wash buffer for 15 min at 68 °C. A ³²P-sensitive film (Fuji) was exposed to the membrane overnight and imaged using a Bio-Rad Phospho PharosFX imager. A linear HBV fragment, excised from pHBV1.1-WT, was used as DNA standard for quantification.

2.2.3.2. Quantification of cccDNA and total HBV DNA by cccDNA inversion quantitative (cinq)PCR

cccDNA was quantified by a novel assay called cccDNA inversion quantitative (cinq)PCR (Tu et al. 2020b). DNA samples of HBV-infected cells were prepared using the NucleoSpin tissue kit. The samples were eluted in 50 µl elution buffer (pre-warmed to 70 °C). In a 96 well format, 10 µl of the DNA extract were mixed with 7.25 µl H₂O, 2 µl CutSmart buffer, 0.5 µl HhaI, and 0.25 µl RecJ_f. This digestion reaction was cycled three times between 37 and 42 °C (15 min

each step) and stopped by incubation at 80 °C for 20 min. A ligation mix containing 5.5 µl H₂O, 1 µl CutSmart buffer, 3 µl ATP, and 0.5 µl T4 ligase was added to the reaction mix and ligation was performed for 2 h at 16 °C. The ligation was stopped by incubation at 80 °C for 20 min. A linearization mix consisting of 4 µl H₂O, 0.5 µl CutSmart buffer, and 0.5 µl XbaI was added to the reaction mix. Linearization was performed at 37 °C for 60 min and stopped at 80 °C for 20 min.

For droplet digital PCR (ddPCR) analysis, 2 µl of the sample were added to a ddPCR reaction composed of 7.8 µl H₂O, 10 µl ddPCR supermix, 1 µl VIC-labelled RNaseP probe, forward primer, reverse primer, and FAM-labelled probe (0.03 µl each; 100 µM). Two reactions were prepared for every sample containing primers and probe for either total HBV DNA or cccDNA. Droplets were generated using a BioRad QX200 Droplet Generator according to the manufacturer's protocol. Briefly, a DG8 cartridge was loaded with 20 µl of the ddPCR mix and 70 µl of droplet generation oil and sealed with a DG8 gasket. After droplet generation, the emulsion was transferred to a 96 well plate, which was sealed with an aluminium foil using a PX1 PCR plate sealer. The intra-droplet PCR was run with the following program: 10 min at 95 °C; 40 cycles of 10 s at 95 °C, 15 s at 54 °C, and 20 s at 68 °C; finished with 10 min at 95 °C. Droplet reading was performed using the FAM and VIC channels of a BioRad QX200 Droplet Reader and data analysis was performed using the QuantaSoft software.

2.2.3.3. Detection of integrated HBV DNA by inverse nested PCR

Integrated HBV DNA was detected as reported previously (Tu and Urban 2018). For this purpose, Huh7-NTCP cells in a 12 well were infected with HBV, treated with 5 µM tenofovir disoproxil and 10 µM lamivudine from 3 dpi, transferred to a 6 well 5 dpi, and harvested 7 dpi for DNA extraction. DNA extraction was performed using the NucleoSpin tissue kit according to the manufacturer's instructions.

For the DNA inversion, ~2 µg of the total DNA extract was incubated in a restriction digestion mix (10 U NcoI, 1X CutSmart buffer) at 37 °C for 1 h, followed by 20 min at 80 °C for inactivation of the restriction enzyme. 400 µl of 1X T4 DNA ligase buffer and 500 U of T4 DNA ligase were added to the sample and ligation was performed at RT for 2 h, followed by inactivation at 70 °C for 20 min. 10 µl 10% w/v SDS were added to ensure inactivation. NaCl to a final concentration of 100 mM, dextran (35-45 kDa) to a final concentration of 90 µg/ml, and 900 µl 100% EtOH were added. The DNA was precipitated at -20 °C overnight. The precipitated DNA was pelleted by centrifugation at 14,000 g for 15 min, the supernatant was removed, the DNA pellet washed with 500 µl of 70% EtOH and centrifuged again at 14,000 g

for 15 min. After removal of the supernatant, the DNA pellet was air-dried at RT for 20 min. The pellet was dissolved in 20 μ l H₂O and 20 μ l of a restriction enzyme mix was added resulting in a 40 μ l reaction volume containing 1X CutSmart buffer, 5 U of BsiHKAI, and 5 U of SphI. This restriction enzyme reaction was incubated first at 37 °C for 1 h and then at 65 °C for 1 h.

For the nested PCR, 10 μ l DNA was added to 170 μ l 1X AmpliTaq Gold PCR mix (containing 0.5 μ M outer forward and 0.5 μ M outer reverse invPCR primers). Three serial dilutions at a ratio of 1:3 were performed by transferring 60 μ l into 120 μ l of PCR mix. 10 μ l of reaction mixture were added to separate wells of a 96 well plate. The PCR was run with the following conditions: 10 min at 95 °C; 35 cycles of 15 s at 95 °C, 15 s at 54 °C, and 3 min at 72 °C; finished with 7 min at 72 °C. A 96 pin replicator was used to transfer the PCR products to a second PCR plate containing 10 μ l of 1X GoTaq Flexi Green PCR mix (containing 0.5 μ M inner forward and 0.5 μ M inner reverse invPCR primers) in each well. The second PCR was carried out with the same conditions except for reducing the initial denaturation step at 95 °C to 2 min.

For the analysis of the PCR products, they were run on an agarose gel. DNA bands were excised from the dilutions of which single PCR products could be resolved. DNA was extracted using the QIAEX II gel extraction kit and sequenced by Eurofins GATC using the inner forward invPCR primer. Virus-cell junctions were confirmed by nucleotide BLAST analysis. The integration frequency was calculated by multiplying the dilution factor of inverted DNA templates with the number of virus-cell junctions detected at that dilution and normalisation to the amount of total DNA input into the inversion reaction.

2.2.3.4. Southern blotting

HepG2-NTCP cells were infected with HBV in 6 well plates and cccDNA was extracted and enriched using the MasterPure Complete DNA and RNA purification kit as per the manufacturer's protocol with minor modifications (doubling of buffer volumes to ensure complete lysis). Cells were washed with PBS twice, incubated with 1.2 ml Tissue and Cell Lysis solution, and cell lysates were transferred to a 2 ml tube. Treatment with Proteinase K was omitted to enrich for protein free DNA. The cell lysates were placed on ice for 5 min and hydrolysed with 15 μ g/ml RNase A at 37 °C for 30 min. 0.6 ml MPC buffer was added, and the samples were incubated on ice for 5 min. The samples were centrifuged at 13,800 g at 4 °C for 10 min and the supernatants were transferred to a new tube. The samples were centrifuged at 13,800 g again for 5 min, the supernatants were transferred to a new tube, and an equal volume of isopropanol was added to precipitate cccDNA-enriched DNA. The DNA was pelleted by

centrifugation at 13,800 g at 4 °C for 10 min. The pellet was washed with an equal volume of 70% v/v ethanol, air-dried and dissolved with 50 µl TE buffer.

DNA samples were loaded on a 1.2% agarose gel and gel electrophoresis was performed at 125 V for 3 h. The gel was then soaked in depurination buffer for 10 min at RT. The gel was washed three times in H₂O, incubated in denaturing buffer for 1 h at RT, washed again three times in H₂O, and soaked in neutralisation buffer for 1 h at RT. The gel was washed once in H₂O and incubated in 20X SSC buffer for 15 min. For blotting the DNA onto a nylon membrane, a transfer apparatus was assembled: Two Whatman 3MM papers were laid on a scaffold chamber with the edges of the papers soaking in 20X SSC buffer. From bottom to top, the gel, a positive-charged nylon membrane, and two Whatman papers were laid on the apparatus. The boundaries of the gel were sealed with parafilm. A stack of dry paper towels and a weight (1000 g) were laid on top of the Whatman papers. The capillary transfer was allowed to run overnight. The next day, the membrane was crosslinked twice using the autocrosslink mode in a UV Stratalinker 1800. Hybridisation with a ³²P-labelled HBV specific probe was performed as described for the HBV DNA dot blot.

2.2.3.5. Quantitative PCR (qPCR) of HBV RNA

RNA was extracted from infected cells using the NucleoSpin RNA extraction kit according to the manufacturer's protocol. RNA concentrations were determined using a NanoDrop spectrophotometer and 500 ng of the cellular RNA was used in a reverse transcription reaction to generate cDNA. Reverse transcription was performed with the High-capacity cDNA reverse transcription kit in a total volume of 20 µl (containing 500 ng RNA, 1X reverse transcription buffer, 1X reverse transcription random primers, 4 mM dNTP mix, 20 U RNase inhibitor, and 50 U MultiScribe reverse transcriptase). The reaction was performed with the following protocol: 10 min at 25 °C, 2 h at 37°C, 5 min at 85 °C, and hold at 4 °C. The cDNA was then diluted fivefold with H₂O.

Expression levels of pgRNA/pre-core mRNA and total HBV RNA were quantified using specific primers. The qPCR was performed in a total volume of 15 µl reaction (1X iTaq SYBR Green Mix, 400 nM forward primer, 400 nM reverse primer, and 3 µl of the diluted cDNA) with the following protocol: initial denaturation at 95 °C for 10 min; 40 cycles of 95 °C for 10 s and 60 °C for 30 s with fluorescence reading at the end of each cycle; then 65 °C to 95 °C in 0.5 °C increments for melt curve analysis. Absolute copy numbers of transcripts were calculated using a pSHH2.1 plasmid standard, previously quantified using the COBAS AmpliPrep/COBAS TaqMan HBV Test.

2.2.3.6. qPCR of viral HDV RNA

For RNA extraction, 10 µl of heparin affinity purified HDV were mixed with 190 µl H₂O, 2 µg carrier RNA, and 500 µl RNAzol. After vortexing for 15 s, samples were incubated at RT for 15 min. The samples were centrifuged at 12,000 g for 15 min and 600 µl from the top of the samples were transferred to new tubes. 2 µl GlycoBlue Coprecipitant and 600 µl isopropanol were added to each sample. After 10 min incubation at RT, the samples were centrifuged at 12,000 g for 10 min and the supernatant carefully discarded. The blue RNA pellet was washed twice with 500 µl 75% EtOH and centrifuged at 8000 g for 2 min after each wash. Residual EtOH was completely removed, and the RNA was resuspended in 40 µl H₂O.

The extracted RNA was treated with RQ1 RNase-Free DNase at 37 °C for 10 min, followed by a heat-shock at 95 °C for 5 min, and immediately transferred to -80 °C. Reverse transcription was performed with the High-capacity cDNA reverse transcription kit in a total volume of 20 µl (containing 10 µl RNA, 1X reverse transcription buffer, 1X reverse transcription random primers, 4 mM dNTP mix, 20 U RNase inhibitor, and 50 U MultiScribe reverse transcriptase). The reaction was performed with the following protocol: 10 min at 25 °C, 2 h at 37°C, 5 min at 85 °C, and hold at 4 °C. The cDNA was then diluted 2.5-fold with H₂O.

HDV RNA was quantified using specific primers. The qPCR was performed in a total volume of 15 µl reaction (1X Luna universal probe mix, 400 nM forward primer, 400 nM reverse primer, 200 nM probe, and 3 µl of the diluted cDNA) with the following protocol: initial denaturation at 95 °C for 60 s; 40 cycles of 95 °C for 15 s and 60 °C for 30 s with fluorescence reading at the end of each cycle. Cycle threshold values were used to determine HDV RNA levels relative to the virus stock HDV2103.

2.2.4. Detection of proteins

2.2.4.1. HBsAg/HBeAg measurement

HBsAg and HBeAg in the supernatant of infected or transfected cells were measured by enzyme-linked immunosorbent assay (ELISA). Cell culture supernatants were collected at the indicated days and centrifuged at 2,300 g for 5 min to remove cell debris. If necessary due to expected high analyte concentrations, the supernatants were diluted in PBS. HBsAg levels were quantified by an Architect HBsAg ELISA (Abbott) and HBeAg was quantified by an ADVIA Centaur HBeAg ELISA (Siemens Diagnostic). The measurements were performed by the analytical centre of the University Hospital Heidelberg.

2.2.4.2. SDS-PAGE

Sodium dodecyl sulphate (SDS) polyacrylamide gel electrophoresis (PAGE) was used to separate proteins (Laemmli 1970). Cells were lysed in 2X SDS sample buffer and denatured at 95 °C for 10 min. The samples were centrifuged at 16,000 g for 10 min, loaded onto SDS polyacrylamide gels, and run at 80-140 V until the desired separation was achieved. PageRuler Plus prestained protein ladder was used as marker for protein size. 12% SDS gels were used for detection of HBc and 15% SDS gels were used for the separation of S- and L-HDAg.

The compositions of the SDS polyacrylamide gels (for 4 gels) were the following:

Stacking gel: 2 ml 30 % acrylamide; 2.5 ml 4X stacking gel buffer; 5.5 ml H₂O; 10 µl TEMED; spatula tip APS

Separating gel (12%): 8 ml 30% acrylamide; 5 ml 4X separating gel buffer; 7ml H₂O; 20 µl TEMED; spatula tip APS

Separating gel (15%): 10 ml 30% acrylamide; 5 ml 4X separating gel buffer; 5 ml H₂O; 20 µl TEMED; spatula tip APS

In-gel fluorescence was used for detection of SiRTet labelled proteins. SiRTet covalently binds to incorporated BCN and TCO* and its maximum emission wavelength is at 674 nm. Scanning protein gels in the 700 nm channel of an Odyssey imaging system (LI-COR) allowed for detection of SiRTet labelled proteins. Scanned gels were analysed using the ImageStudio software.

2.2.4.3. Western blotting

After SDS-PAGE, proteins were transferred onto a nitrocellulose or a methanol-activated PVDF membrane by semi-dry blotting. From bottom to top, a thick blot filter paper, the membrane, the protein gel, and another filter paper were soaked in transfer buffer and layered. Protein transfer was performed at 25 V for 30 min. The membrane was blocked in 5% milk powder in TBS for 1 h at RT. Primary antibodies were diluted in 5% milk powder in TBS-T and incubated with the membrane overnight at 4 °C while shaking. The membrane was washed four times with TBS-T and then incubated with the secondary antibodies (diluted in 5% milk powder in TBS-T) for 1 h at RT. The blot was washed twice in TBS-T and twice in TBS, scanned using an Odyssey imaging system (LI-COR), and analysed using the Image Studio software. For peroxidase-conjugated secondary antibodies, membranes were incubated with ECL substrate and the chemical signal was developed by an ECL chemocam imager (Intas).

2.2.4.4. Immunofluorescence

Cells were washed once with PBS, followed by fixation in 4% PFA (250 μ l per 24 well) for 20 min at RT, three washes with PBS, and permeabilization in 0.25% Triton X-100 in PBS for 30 min at RT. The cells were then incubated with the primary antibodies at the indicated dilutions in 2% BSA in PBS or 5% milk in PBS at 4 °C overnight. The next day the cells were washed three times in PBS, incubated with the secondary antibodies at the indicated dilutions together with 1 μ g/ml Hoechst in the same buffer as the primary antibodies for 1 h at RT in the dark. The cells were washed three times with PBS and imaged on an inverted fluorescence microscope (Leica). If the cells were grown on coverslips, the coverslips were washed once in H₂O and mounted onto glass slides using 6 μ l Fluoromount G.

2.2.4.5. SPIEDAC click labelling with SiRTet

Click labelling with SiRTet was performed in live cells. After the incorporation of ncAA, the cells were washed extensively to remove excessive ncAA (Schvartz et al. 2017). The cells were washed quickly three times with medium and then another three times for ~30 min at 37 °C. The SiRTet stock solution (500 μ M) was diluted 1:500 in serum free medium (Opti-MEM) and 250 μ l were added to a 24 well. Labelling was performed at 37 °C for 20 min. The cells were then washed again with medium 3 times quickly and 3 times for 30 min.

2.2.4.6. CuAAC click labelling with SiR-Azide

Incorporated N-Propargyl-L-lysine (PrK) was labelled in fixed cells or virus on coverslips using the CuAAC cell reaction buffer kit (Jena Bioscience). Coverslips were washed once with PBS, followed by fixation in 4% PFA (250 μ l per 24 well) for 20 min (cells) or 5 min (virus) at RT, three washes with 3% BSA in PBS, permeabilization in 0.5% Triton X-100 in PBS for 20 min, and two more washes with 3% BSA in PBS. The CuAAC reaction was performed according to the manufacturer's instructions using a volume of 250 μ l per coverslip. First, CuSO₄ and the Cu(I) stabilizing ligand BTTAA were mixed to a final concentration of 33.33 mM and 45.45 mM, respectively. SiR-Azide (final concentration 20 μ M), CuSO₄/BTTAA premix (2 mM/10 mM), and Na-Ascorbate (100 mM) were added to Na-Phosphate reaction buffer and incubated on the samples for 30 min protected from light. Cells were washed twice with 3% BSA in PBS and immunofluorescence was performed as described above.

2.2.4.7. Labelling of HDV-TCO* with SiRTet

HDV-TCO* elution fractions 2 and 3 after heparin column purification were pooled together and concentrated on an Amicon Ultra-0.5 centrifugal filter unit with 100 kDa cutoff at 4 °C and 5000 g until it was reduced to ~200 μ l. Concentrated HDV-TCO* was recovered by spinning the filter upside-down in a new tube for 2 min at 1000 g and 4 °C. 2 μ l SiRTet stock solution (500 μ M) was diluted in 800 μ l serum free medium (Opti-MEM) and added to concentrated HDV-TCO* for 30 min on a shaker. After labelling, the sample was applied to a centrifugal filter unit again and washed twice with 500 μ l TN buffer and finally concentrated to ~200 μ l.

3. Results

3.1. Maintenance and regulation of cccDNA in the absence of *de novo* synthesised HBV nucleocapsids

The data presented in this chapter has been published (Tu et al. 2021).

cccDNA is formed during the initial infection of a hepatocyte with HBV when the incoming rcDNA is repaired to a complete circular DNA. The subsequent transcription from cccDNA leads to *de novo* production of nucleocapsids containing rcDNA. These mature nucleocapsids are thought to be reimported into the nucleus where they can replenish the cccDNA levels. In this project, we capitalise on the HBc stop mutants, originally created for the incorporation of ncAA, to generate HBV virions with a genome defective in producing HBc after infection (Δ HBc HBV). Previously, it has been shown that *de novo* produced HBc is not necessary for the establishment of cccDNA (Qi et al. 2016). We aimed to further characterise infection with Δ HBc HBV and to determine the contribution of *de novo* produced nucleocapsids to cccDNA levels in long-term *in vitro* infection systems. After the initial formation of cccDNA, the cccDNA levels remain stable for a long duration. This long-term maintenance can be explained by two models (Figure 3.1). In the dynamic model, *de novo* synthesised nucleocapsids circulate back into the nucleus and contribute to the cccDNA pool. At the same time, the existent cccDNA is degraded and therefore undergoes a continuous turnover. In this model, cells infected with Δ HBc HBV would be expected to slowly lose intracellular cccDNA while cells infected with WT HBV maintain the cccDNA levels. Alternatively, the static model comprises a very stable cccDNA with neglectable reimport of newly formed nucleocapsids. In the static model, cccDNA levels should persist independent of the presence of *de novo* synthesised HBc.

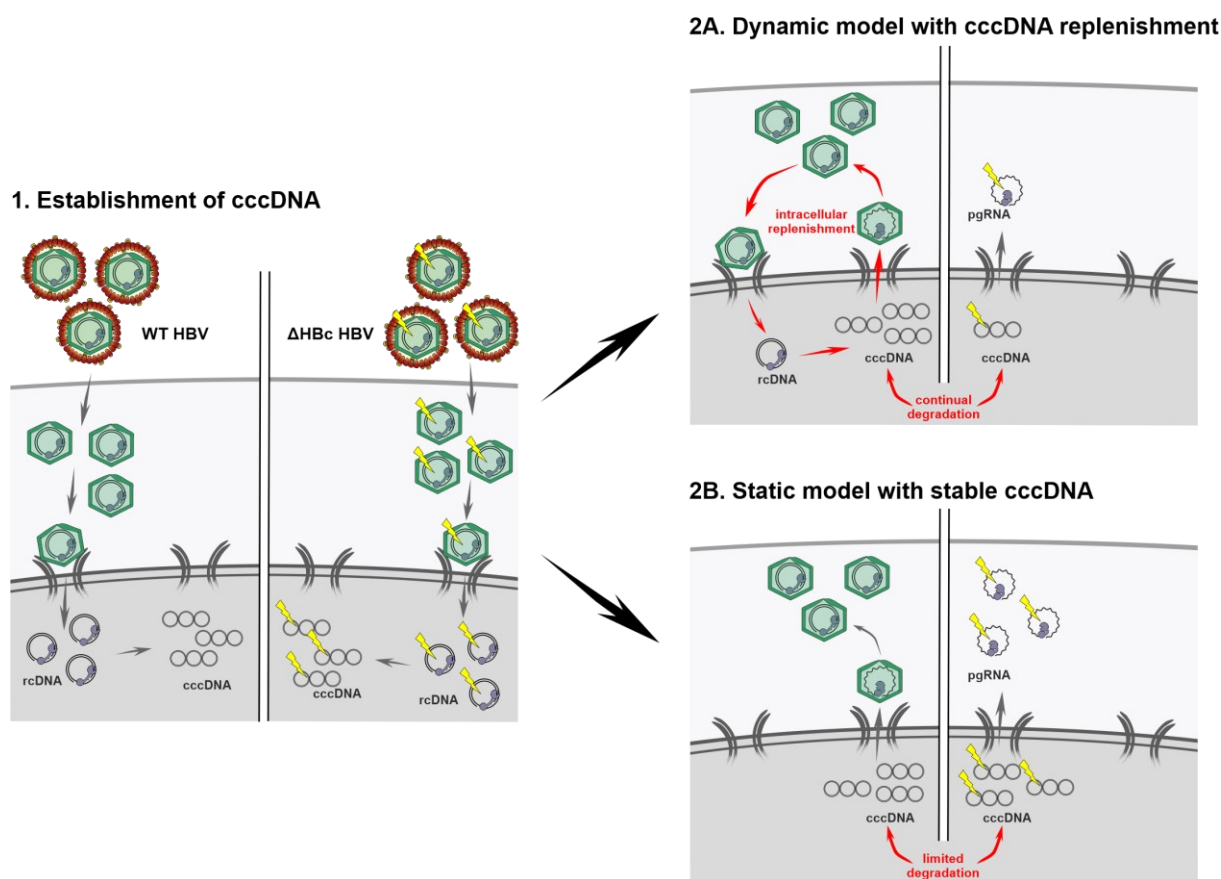


Figure 3.1. Two potential models of cccDNA maintenance in chronic HBV infection. After initial infection and cccDNA formation (1), cccDNA levels remain stable over long durations. In the dynamic model of cccDNA maintenance (2A), cccDNA undergoes a continuous turnover due to constant degradation and renewal via reimport of newly synthesised nucleocapsids. In the static model (2B), cccDNA is considered to be very stable and the contribution of nucleocapsid recycling is neglectable.

3.1.1. Generation and characterisation of HBc-deficient (Δ HBc) HBV

3.1.1.1. Trans-complementation of HBc-deficient HBV with WT HBc rescues the secretion of HBV virions

Δ HBc HBV was generated by co-transfecting Huh7 producer cells with an overlength HBV genome containing a stop codon introduced at site T67 of HBc (pHBV1.1-T67*) and a plasmid expressing only WT HBc (pHBc) (Figure 3.2A). WT HBV stocks were generated by transfection with pHBV1.1-WT. Supernatants from the transfected Huh7 cells were collected, precipitated with PEG, and analysed for HBV DNA by an analytical CsCl density gradient and DNA dot blot. pgRNA derived from pHBV1.1-T67* contains a stop codon at position T67 of the HBc ORF. As expected, transfection with pHBV1.1-T67* did therefore not result in the secretion of HBV DNA containing particles (Figure 3.2B). Trans-complementation with WT HBc could rescue the generation of naked capsids (NC) and enveloped virus particles (VP). Quantification by densitometry of the three VP containing fractions resulted in comparable

levels of WT (1.2×10^8 vge/ μ l) and Δ HBc HBV (1.5×10^8 vge/ μ l) indicating that trans-complementation with WT HBc can efficiently rescue the assembly and secretion defect of an HBc deficient genome. Furthermore, the overexpression of HBc did not affect the ratio between NC and VP. The supernatants of transfected cells containing either WT or Δ HBc HBV were pooled, purified by heparin affinity chromatography, concentrated, and analysed for number of viral genomes by qPCR before they were used as inocula for infection experiments.

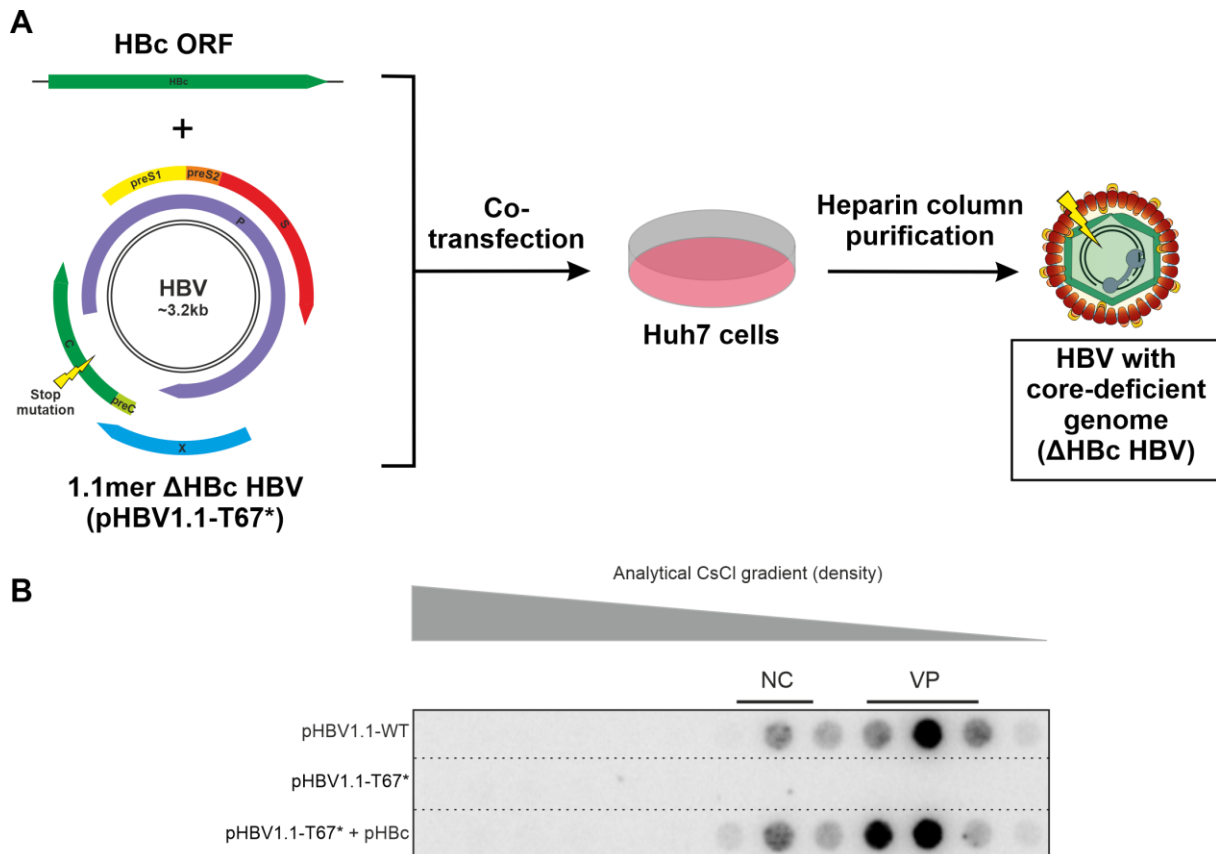


Figure 3.2. Production of Δ HBc HBV. (A) Huh7 cells were either transfected with a WT HBV overlength genomic plasmid (pHBV1.1-WT) or with a construct containing a stop mutation (lightning bolt) at position T67 of the HBc ORF (pHBV1.1-T67*). To produce Δ HBc HBV, a plasmid expressing WT HBc (pHBc) was co-transfected with pHBV1.1-T67*. Supernatant was collected every 2 days from day 1 to 9 post transfection and purified on a heparin column. (B) Collected supernatants were precipitated with PEG and 50 μ l of the precipitate was analysed by CsCl gradient centrifugation and HBV DNA dot blot. Naked capsids (NC) and virions (VP) were identified by the density of the fractions.

3.1.1.2. Δ HBc HBV is as infectious as WT HBV

To confirm whether Δ HBc HBV is comparable with WT HBV in the establishment of infection, we infected HepG2-NTCP cells with inocula at different multiplicity of viral genome equivalents (mge). Consistent with previous studies (Schulze et al. 2012), infection with WT and Δ HBc HBV displayed increasing amounts of HBsAg secretion with increasing amounts of input mge (Figure 3.3A). Remarkably, HBsAg levels upon infection with Δ HBc HBV reached

similar levels as WT HBV infection, suggesting an equal efficiency in establishment of cccDNA and transcription of subgenomic RNA. As expected, cells infected with Δ HBc HBV did not secrete HBeAg which shares the same ORF with HBc. Increasing mge of WT HBV resulted in increasing levels of HBeAg secretion as reported previously (Ni et al. 2014). Treatment with the entry inhibitor MyrB lead to a strong reduction of viral antigen levels, verifying an authentic NTCP-dependent infection pathway and showing that the measured antigens were produced from the infected cells and did not originate from residual input virus.

The analysis of intracellular viral antigens by immunofluorescence showed that Δ HBc HBV infected cells express HBsAg (red) but not HBc (green) (Figure 3.3B). Meanwhile, cells infected with WT HBV can be stained for both HBsAg and HBc. Quantification of HBsAg-positive cells showed comparable infection rates when using increasing mge of WT and Δ HBc HBV (Figure 3.3C).

HBV genome integration into the host cell chromosome occurs with the initial infection and does not depend on *de novo* produced HBc (Tu et al. 2018). Therefore, HBV genome integration serves as an additional independent marker for nuclear entry. We measured HBV DNA integration using inverse nested PCR (Tu et al. 2018; Tu and Urban 2018) from Huh7-NTCP cells infected with 200 mge of either WT or Δ HBc HBV. Integration occurred at a geometric mean frequency (\pm geometric standard deviation factor) of 4.82×10^{-5} (± 2.36) and 5.97×10^{-5} (± 1.57) integrations per cell ($p > 0.05$, two-tailed Mann-Whitney test) for WT and Δ HBc HBV, respectively (Figure 3.3D). MyrB blocks entry of HBV and therefore no integrations were detected in DNA extracted from MyrB treated cells.

Taken together, these results suggest that Δ HBc HBV enters hepatocytes via NTCP with similar efficacy to WT HBV, establishing cccDNA and HBV DNA integration, and initiating transcription and translation of HBsAg.

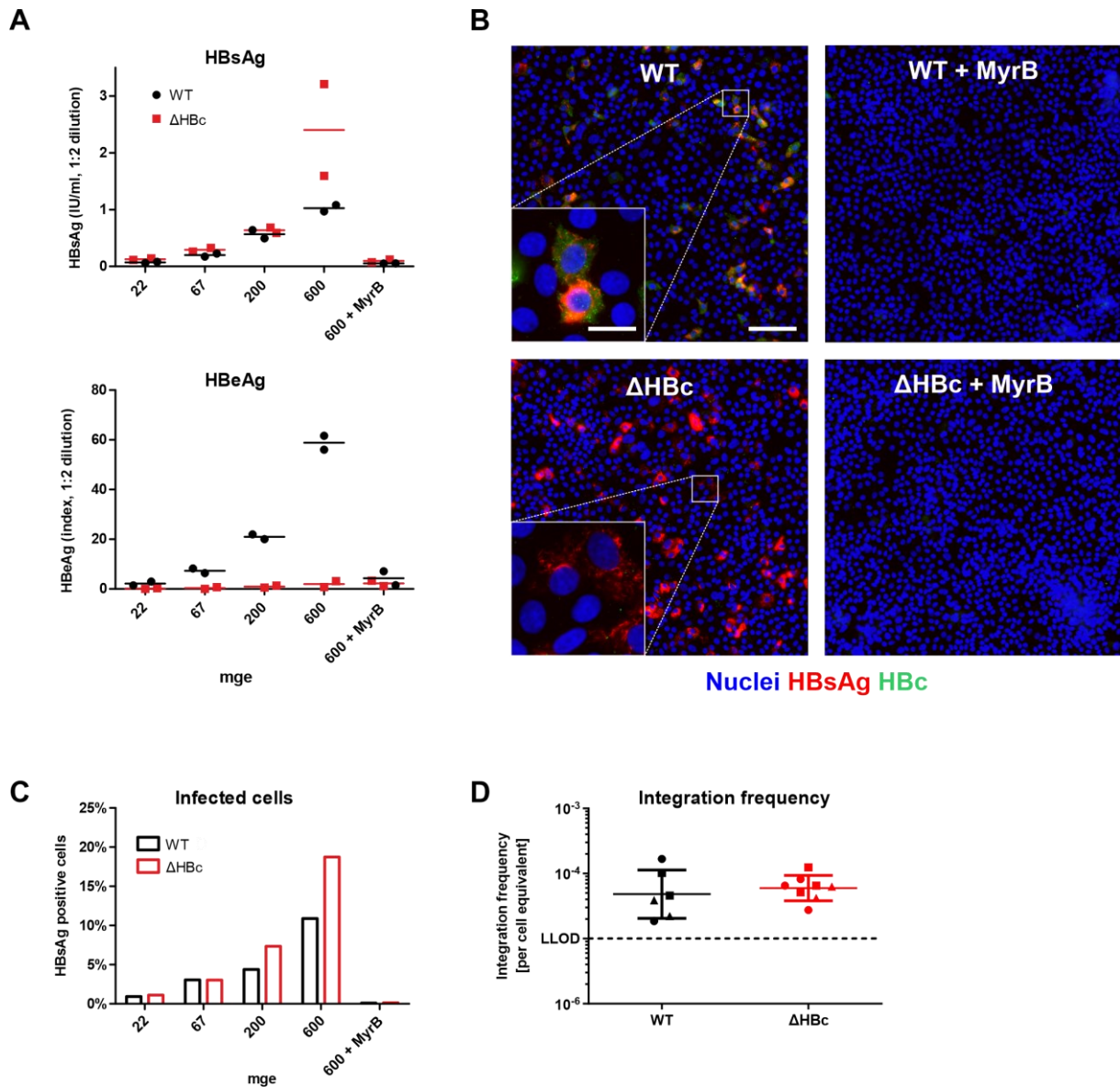


Figure 3.3. Infection with Δ HBc HBV. (A) HepG2-NTCP cells were infected with increasing viral loads of WT (black) and Δ HBc HBV (red). Cell culture supernatant was collected from day 5-7 post infection and submitted for HBsAg and HBeAg measurements. MyrB mediated inhibition of virus entry was used as control. The mean (line) of 2 independent experiments (circles/squares) is shown. (B) HepG2-NTCP cells were infected with 200 mge of WT or Δ HBc HBV. 7 dpi, the cells were fixed and immunofluorescence analysis of HBc and HBsAg was performed. MyrB was used as control for infection inhibition. Scale bars represent 100 μ m (main figure) and 20 μ m (inset). (C) HepG2-NTCP cells were infected with WT and Δ HBc HBV with increasing mge. Infection rates were determined by immunofluorescence for HBsAg and quantified using ilastik software (Berg et al. 2019). (D) Huh7-NTCP cells were infected with WT and Δ HBc HBV at mge 200. Cellular DNA was extracted 7 dpi and the rate of HBV integration was determined by inverse nested PCR and end-point titration. The results of 3 independent infections are shown (squares, circles, and triangles, line = mean \pm 95% confidence interval). Inverse nested PCR was performed by Thomas Tu.

3.1.2. Establishment of cccDNA after infection with Δ HBc HBV

The expression of HBsAg indicated successful formation of and expression from cccDNA in infected cells lacking *de novo* synthesised Hbc and HBeAg. To validate the formation of cccDNA, HepG2-NTCP cells were infected with 100 mge of WT and Δ HBc HBV and analysed for intracellular cccDNA levels 7 and 14 dpi by Southern blot. cccDNA was detectable after infection with WT HBV without an apparent increase from 7 to 14 dpi (Figure 3.4A). Formation of cccDNA was inhibited by treatment with the entry inhibitor MyrB, confirming that NTCP-dependent entry was critical for cccDNA formation. Strikingly, Δ HBc HBV infection resulted in similar amounts of cccDNA, suggesting that most of the cccDNA levels are formed by incoming virions of the initial infection but not from reimport of *de novo* synthesised capsids.

To verify this finding, we used a cccDNA specific PCR (Tu et al. 2020b) which allows the precise quantification of cccDNA numbers relative to the single-copy gene RNaseP within the same reaction tube. Comparable numbers of cccDNA copies per cell were found after infection by both viruses in HepG2-NTCP cells (Figure 3.4B). This observation was seen using multiple doses of inoculum (ranging from 22 to 600 mge), showing that the equivalence between the WT and Δ HBc HBV is not due to a cellular saturation limit of cccDNA number. cccDNA copy numbers proportionally increased with the virus load, presumably reflecting an increase in the percentage of infected cells, as previously reported (Schulze et al. 2012). cccDNA formation could be blocked by treatment with MyrB, showing that the cccDNA detected is driven by NTCP-dependent infection of the cells, rather than any HBV DNA derived from the input inoculum preparation.

We confirmed these findings in differentiated HepaRG-NTCP cells and PHH, which are more authentic *in vitro* infection systems. During the differentiation process, HepaRG-NTCP cells form hepatocyte-like colonies and represent a more authentic *in vitro* infection system (Gripon et al. 2002; Ni et al. 2014). In HepaRG-NTCP cells, cccDNA/RNaseP levels were comparable to infection in HepG2-NTCP cells (Figure 3.4C). PHH are considered to be the gold standard of cell culture systems regarding HBV infection, as they are the natural host cells of HBV and are highly susceptible to infection (Gripon et al. 1988). Similar to infection in the hepatoma cell lines, relative cccDNA levels increased with increasing mge (Figure 3.4D). However, the cccDNA/RNaseP levels detected were ~10 times higher compared to those in HepG2- and HepaRG-NTCP cells, reflecting higher infection rates in PHH due to their susceptibility to HBV infection. Furthermore, it is possible that PHH can form more cccDNA molecules per infected cell compared to hepatoma cell lines.

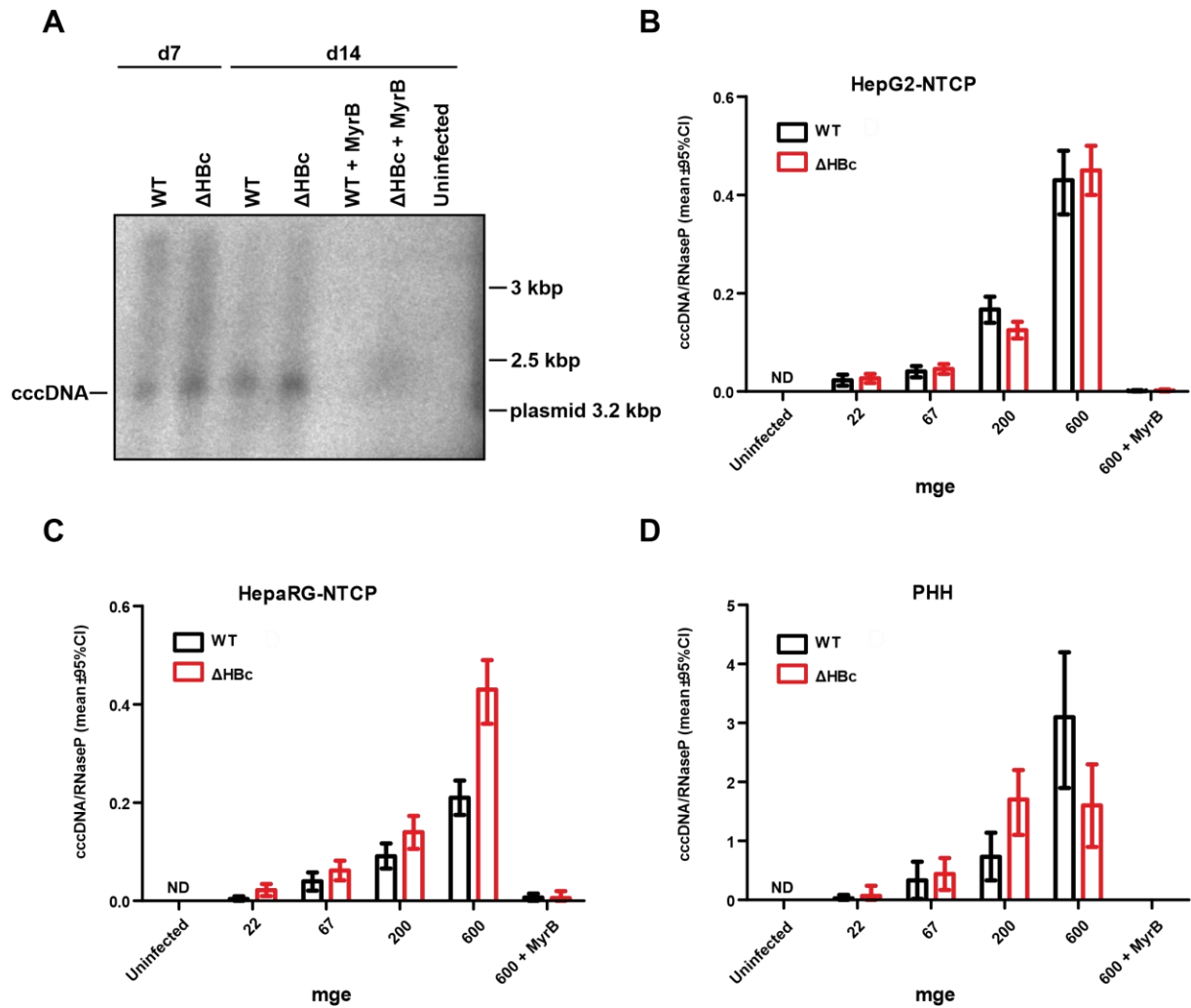


Figure 3.4. cccDNA is formed after infection with Δ HBc HBV. (A) HepG2-NTCP cells were infected with WT and Δ HBc HBV at mge 100 and DNA was extracted 7 and 14 dpi. Southern blot was performed using a 32 P-labelled HBV-specific probe. MyrB was used as control for infection inhibition. This experiment was performed by Bingqian Qu. HepG2-NTCP cells (B), HepaRG-NTCP cells (C), and PHH (D) were infected with increasing virus amounts of WT and Δ HBc HBV. 7 dpi, total cellular DNA extracts were analysed for cccDNA relative to the cellular single-copy gene RNaseP by cinqPCR. The error bars (Poisson 95% confidence interval) represent the technical error of the ddPCR assay. Results are representative of 2 independent experiments. ND, not detected. CinqPCR was performed by Thomas Tu.

3.1.3. The role of HBc in long-term maintenance and regulation of cccDNA

3.1.3.1. cccDNA is maintained during long-term infection of HepG2-NTCP cells

So far, our results have provided evidence that the incoming capsid is sufficient to establish cccDNA and *de novo* produced HBc is not needed to maintain cccDNA. However, this does not exclude a possible contribution of capsid reimport during long-term infections. We therefore took advantage of the HepG2-NTCP cell line which has been shown to support long-term infection (Ni et al. 2014). We used WT and Δ HBc HBV at mge 40 to infect HepG2-NTCP cells and investigate cccDNA replenishment over 9 weeks.

Infected cells were analysed 1, 4, and 9 weeks post infection (wpi) by immunostaining for HBc and HBsAg (Figure 3.5A). WT and Δ HBc HBV infection could be detected by HBsAg staining for all tested time points, whereas HBc positive cells were only found in WT infected cells. Quantification of HBsAg expressing cells revealed that the infection rate remained stable at 5-10% during 9 weeks of infection with either WT or Δ HBc HBV (Figure 3.5B). HepG2-NTCP cells not only remained viable during at least 9 weeks, but also supported HBV replication under the chosen culture conditions.

Each wpi, cellular DNA was extracted to quantify cccDNA by cinqPCR. cccDNA/RNaseP levels were comparable following infection with WT and Δ HBc HBV with slightly higher initial levels induced by the Δ HBc virus (Figure 3.5C). Remarkably, cccDNA levels remained very stable over 9 weeks of infection. As reported before (Ni et al. 2014), amplification of HBV infection via extracellular viral spread was not observed in this HepG2-NTCP cell clone. Additionally, a contribution of reimport of newly synthesised nucleocapsids could not be observed in WT infected cells. In contrast, total HBV DNA levels increased over time after infection with WT HBV (Figure 3.5D). Total HBV DNA levels remained low and stable in Δ HBc HBV infected cells, presumably because hepadnaviral reverse transcription occurs inside intact nucleocapsids (Beck and Nassal 2007). Treatment with MyrB inhibited cccDNA and total HBV DNA levels in both viruses.

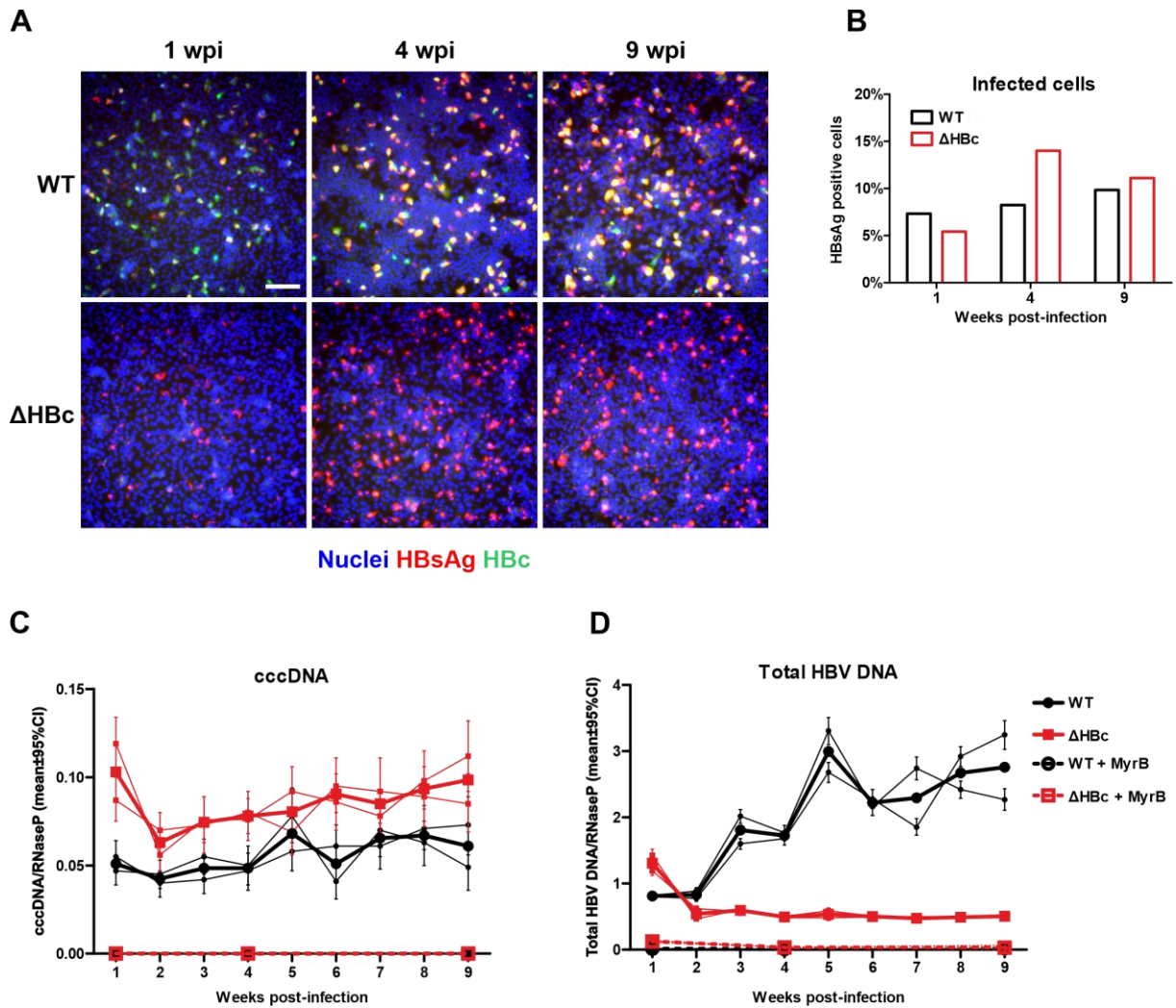


Figure 3.5. cccDNA is maintained over 9 weeks. (A) HepG2-NTCP cells were infected with WT or Δ HBc HBV at mge 40. Cells were fixed 1, 4, and 9 wpi and immunofluorescence for HBsAg (red) and HBc (green) was performed. Scale bar represents 100 μ m. (B) HBsAg positive cells were quantified using ilastik software (Berg et al. 2019). HepG2-NTCP cell were infected with WT and Δ HBc HBV and cells were harvested every week and stored at -80°C until the end of the experiment. After 9 weeks, DNA was extracted and cingPCR was performed to detect cccDNA (C) and total HBV DNA (D) levels relative to the cellular single-copy gene RNaseP. MyrB treatment was used as control for infection inhibition (1, 4, and 9 wpi). Two biological replicates (thin lines) were carried out and the error bars (Poisson 95% confidence interval) represent the technical error of the ddPCR assay. The mean value of the 2 replicates is shown as thick line. Data shown is representative of 2 independent experiments.

3.1.3.2. *De novo* expressed HBc does not affect transcription from cccDNA

HBc has been reported to bind to cccDNA and to regulate transcription thereof by epigenetic remodelling (Diab et al. 2018; Bock et al. 2001). These studies are evidenced by immunoprecipitation and electron microscopy in *in vitro* systems employing overexpression of viral factors including abundant presence of cccDNA.

To test whether *de novo* expressed HBc is functionally involved in transcription of viral RNAs, we measured intracellular HBV RNA levels (both pgRNA/precore mRNA and total HBV RNA) after infection with WT or Δ HBc HBV (Figure 3.6A). HepG2-NTCP cells were infected with both viruses at mge 40, and intracellular RNA was extracted every week for 9 weeks. We found that pgRNA/pre-core mRNA and total HBV RNA levels remain unchanged over 9 weeks of infection with either WT or Δ HBc HBV.

Additionally, we quantified HBsAg and HBeAg secretion over 9 weeks of infection (Figure 3.6B). Consistent with the results of the short-term infections, HBsAg levels followed similar courses for both infections, while HBeAg was not detected after infection with Δ HBc HBV. This also indicates that no reversion of the artificially introduced stop codon at position T67 had occurred during 9 weeks of infection. Again, MyrB treatment could block all viral markers (besides HBsAg at 7 dpi, representing input), verifying that cccDNA was established by NTCP dependent entry into the host cells.

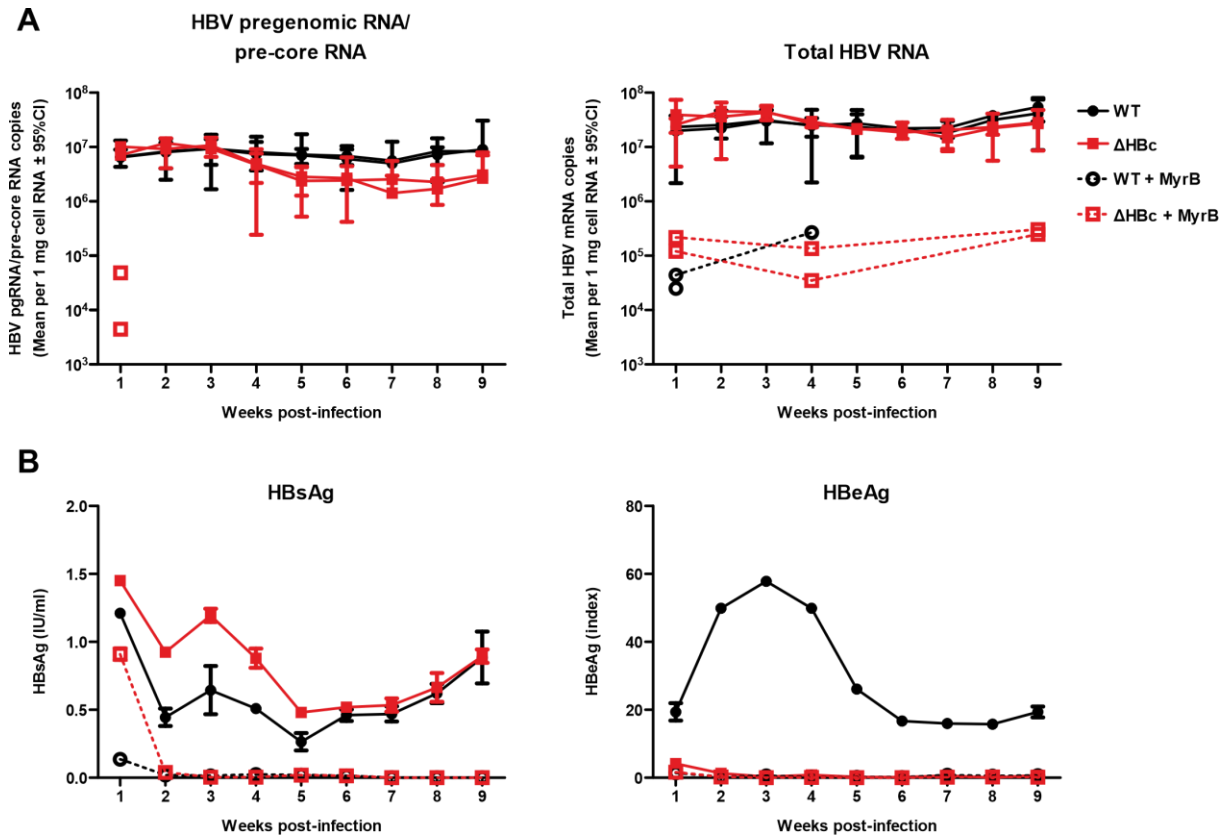


Figure 3.6. Viral RNA transcription is not affected by the absence of HBC. (A) HepG2-NTCP cells were infected with WT (black) or Δ HBc (red) HBV at mge 40. Total intracellular RNA was extracted from cells harvested each week and qPCR was performed to detect pgRNA/precore mRNA using primers targeting the precore region of the HBV genome (left) and total HBV RNA using primers targeting the HBx reading frame (right). MyrB treatment (dashed lines) was used as control for infection inhibition (1, 4, and 9 wpi). Two biological replicates were carried out (separate lines). Error bars (95% confidence interval) represent the technical error of the qPCR performed in triplicate. RNA extraction and qPCR were performed by Bingqian Qu. (B) Cell culture supernatant was harvested every week and measured for secretion of HBsAg (left) and HBeAg (right). The mean (\pm standard deviation) of two biological replicates is shown. Antigen measurements are representative of two independent experiments.

Taken together, the results shown in this chapter suggest that cccDNA maintenance behaves close to the static model in our *in vitro* infection systems. Δ HBc HBV was equally infectious as WT HBV but did not induce expression of HBC or HBeAg, as expected. Furthermore, total HBV DNA levels were reduced compared to infection with WT HBV, because pgRNA has to be encapsidated prior to reverse transcription to rcDNA (Bartenschlager et al. 1990). But cells infected with Δ HBc HBV displayed comparable levels of cccDNA, HBV RNA, and secreted HBsAg which followed the same kinetics as during a WT HBV infection. This suggests that cccDNA decay does not occur in infected cells during a steady state over long periods and *de novo* produced HBC is not needed for maintenance or transcriptional control of cccDNA. Last but not least, the finding of productive infectivity by Δ HBc HBV was important for the next chapter, where we were also using HBV with a HBC-defective genome.

3.2. Amber suppression mediated incorporation of ncAA into the HBV core protein for click chemistry labelling

Having established that Δ HBc HBV matches WT HBV in terms of infectivity and cccDNA formation, amber suppression system mediated incorporation of ncAA to rescue capsid formation instead of trans-complementing with WT HBc. The aim of this project was to fluorescently label HBc by combining genetic code expansion mediated site-specific incorporation of ncAA with click chemistry functionalised fluorophores. Amber suppression mediated engineering denotes the smallest site-specific protein tag and is therefore a promising tool to generate fluorescently labelled HBV, which has not been reported yet. First, we have optimised the incorporation rate of ncAA into HBc by improving amber suppression efficiency and by selecting multiple potential amino acid positions for ncAA incorporation. These amino acid positions were mutated to amber stop codon and the capability of the amber suppression system to rescue full-length HBc expression was investigated. Subsequently, secretion and infectivity of HBV after ncAA incorporation was tested before fluorescent labelling of HBV was performed.

Using an mCherry-GFP(TAG) fusion protein that carries an amber stop mutation in the GFP ORF, we could test the amber suppression system in Huh7 cells (Figure 3.7). Cells transfected with this mCherry-GFP(TAG) construct can be detected by their expression of mCherry. Only upon successful incorporation of a ncAA at the inserted amber stop codon within the GFP ORF, these cells will also express full-length GFP. Furthermore, specific amino acids can be directly labelled with a tetrazine-coupled dye in live cells.

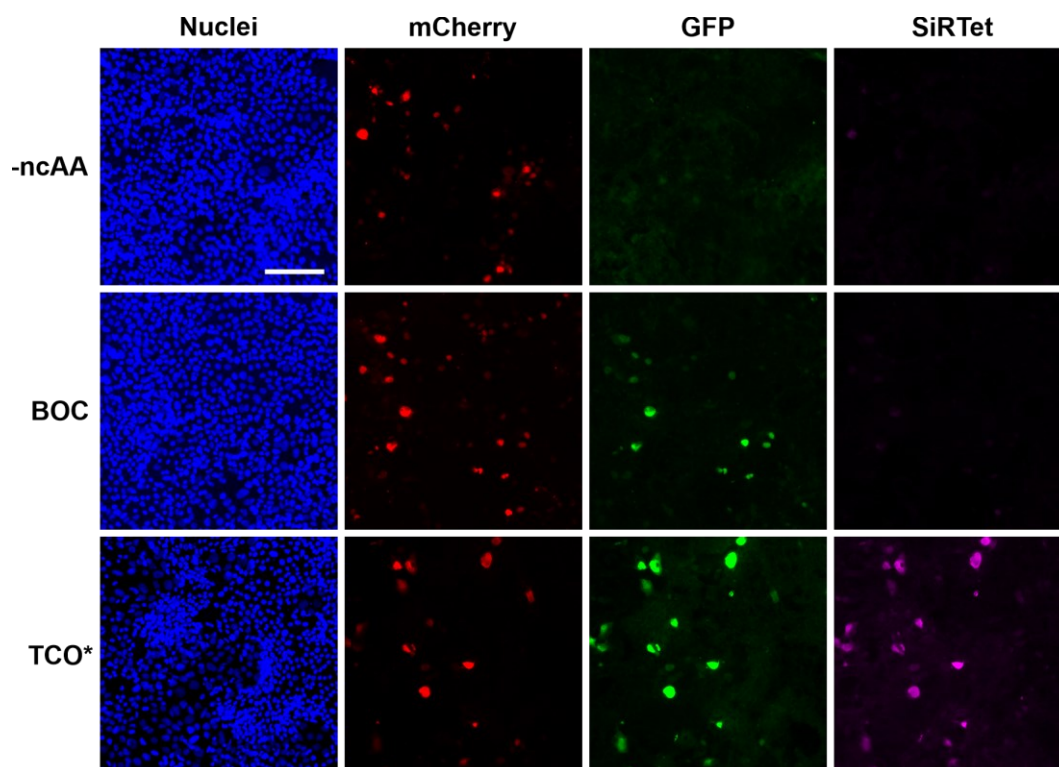


Figure 3.7. Incorporation of ncAA in Huh7 cells. Huh7 cells were co-transfected with pmCherry-GFP(TAG) and the amber suppression plasmid pNESPyIRS^{AF}/4×tRNA^{Pyl}. ncAA were added 2 days post transfection and click labelling with SiRTet was performed on day 4 post transfection. The cells were then fixed and counterstained with Hoechst. In the absence of ncAA (top row), transfected cells expressed mCherry but not GFP. Incorporation of the ncAA BOC, which is not reactive with SiRTet, results in the expression of full-length GFP (middle row). When a clickable ncAA like TCO* is incorporated in the mCherry-GFP fusion protein, it can also be fluorescently labelled with SiRTet (bottom row). Scale bar represents 100 μm .

3.2.1. Optimisation of amber suppression

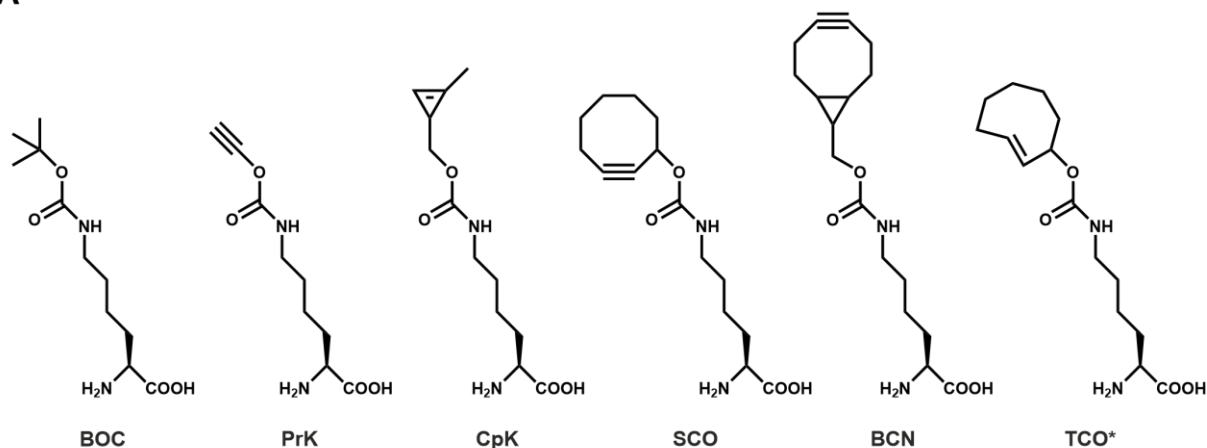
To improve the efficiency of amber suppression, we have tested plasmids which vary in tRNA^{Pyl} copy numbers and PyIRS variants. Furthermore, the incorporation efficiency and the signal intensity of the click chemistry labelling can vary based on which ncAA is used. Finally, finding a suitable position for the ncAA incorporation into the HBc is crucial. Not only does the incorporation efficiency vary between different amino acid sites, but also the amino acid exchange at a specific position might affect protein function or stability.

Finding optimal conditions for the amber suppression system is a challenging task. The efficiency of ncAA incorporation may depend on many factors including but not limited to: the protein of interest, the location of the amber stop codon within the mRNA, codons surrounding the amber stop codon, availability of ncAA, number of tRNA^{Pyl}, efficiency and cellular distribution of the PyIRS, competition for the stop codon by release factor, and supplements like ascorbic acid (Chemla et al. 2018; Jakob et al. 2019; Schmied et al. 2014; Nikic et al. 2016;

Schwartz et al. 2017). Some of these factors only affected the efficiency marginally, while changing others were not feasible. For example, the role of mRNA context effects is mostly studied in *E. coli* and still mostly uncharacterised (Chemla et al. 2018). Meanwhile, the incorporation efficiency often changed by a factor of twofold between two independent replicates. Therefore, this chapter focuses on two factors which had the highest impact on the amber suppression efficiency in our hands: the optimisation of the plasmid used for amber suppression and the selection of ncAA used to incorporate.

The amber suppression system has been used to incorporate many ncAA into proteins (Dumas et al. 2015). Within the scope of this thesis, we used ncAA (Figure 3.8A) with a click chemistry functional group except for N-epsilon-t-butyloxycarbonyl L-lysine (BOC) which was used to test most of the optimisation steps in preliminary experiments, because it is less expensive compared to the other ncAA, but it is not reactive to click chemistry dyes. PrK has an alkyne group which can be used in a CuAAC click chemistry reaction (Milles et al. 2012). Cyclooctyne-lysine (SCO) and Bicyclo [6.1.0] nonyne-lysine (BCN) can be used in SPAAC and SPIEDAC reactions (Nikic et al. 2014), whereas BCN is more reactive with tetrazine-coupled dyes. Cyclopropene L-lysine (CpK) and trans-Cyclooct-2-ene L-lysine (TCO*) can be used in SPIEDAC reactions with CpK having a smaller side chain (Schmied et al. 2014). This smaller ring structure might allow better incorporation and less interference with the protein structure and function, but the cyclopropene is also less reactive to tetrazine-coupled dyes compared to the cyclooctene.

A



B

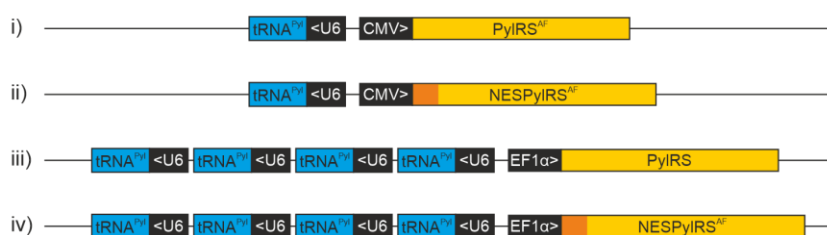


Figure 3.8. Crucial factors for the improvement of amber suppression and click labelling. (A) Chemical structure of the ncAA used in this study. **(B)** Schematic representation of the amber suppression plasmids used in this study. tRNA^{Pyl} copies (blue) are driven from RNA polymerase III U6 promoters and PylRS variants (yellow, NES in orange) are driven from CMV or EF1 α promoters.

The first experiments were performed with plasmid (i) pPylRS^{AF}/tRNA^{Pyl} (Figure 3.8B) (Plass et al. 2011). This construct expresses a PylRS variant and the correspondent tRNA^{Pyl} which are two essential components of the amber suppression system. Later, the research group of Edward Lemke noticed that the PylRS was predominantly localised to the nucleus where it would not be expected to efficiently interact with the translation machinery (Nikic et al. 2016). Therefore, they have improved this construct by introducing an NES at the N-terminus of the PylRS^{AF} protein resulting in plasmid (ii) pNESPylRS^{AF}/tRNA^{Pyl}. The plasmid (iii) pPylRS/4 \times tRNA^{Pyl} contains four copies of tRNA^{Pyl} and showed a very efficient incorporation of BOC at amber stop codons (Schmied et al. 2014). However, this construct was unable to incorporate larger amino acids like TCO* or BCN, because this PylRS variant lacks the Y306A and Y384F (AF) mutations (Yanagisawa et al. 2008; Plass et al. 2011). Therefore, we have combined two plasmids by replacing PylRS in plasmid (iii) with NESPylRS^{AF} from plasmid (ii), resulting in plasmid (iv) pNESPylRS^{AF}/4 \times tRNA^{Pyl}.

We then tested the incorporation abilities of the described amber suppression plasmids on the inserted amber stop codon at position T67 of HBc. Huh7 cells were co-transfected with plasmids expressing an overlength HBV genome with amber stop mutation in the HBc ORF

and one of the amber suppression plasmids (Figure 3.9A). In the presence of ncAA, a weak rescue of intracellular full-length HBc expression was observed with plasmid (i) for some ncAA (Figure 3.9B). Forcing the PyIRS to locate to the cytoplasm with an NES (ii) improved the incorporation rate of all ncAA. Owing to the increased tRNA^{PyI} copy numbers, plasmid (iii) could very efficiently insert BOC, PrK, and CpK but not ncAA with large ring structures. Exchanging this variant with the NESPyIRS^{AF} from plasmid (ii) finally allowed an efficient incorporation of amino acids with large ring structures (iv), but a decrease in the incorporation of small amino acids like BOC and PrK was observed. Overall, rescue of HBc expression did not reach the levels of WT HBV and showed strong variation for different amino acids.

Other means of optimising the readthrough efficiency were tested, among them a dominant negative mutant of eukaryotic release factor 1 (eRF1) and supplementation with ascorbic acid (Schmied et al. 2014; Schwartz et al. 2017). The amber suppression system competes for the amber stop codon with eukaryotic release factors which mediate termination of translation at stop codons. Overexpression of the E55D mutant of eRF1 has been described to strongly enhance ncAA incorporation at amber stop codons without increasing readthrough of stop codons in the absence of the amber suppression system (Schmied et al. 2014). Co-transfection of Huh7 cells with this eRF1 mutant did indeed increase the rescue of full-length HBc (Figure 3.9C). Finally, addition of the antioxidant ascorbic acid to the cell culture supernatant has been suggested to improve signal-to-noise ratio for amber suppression mediated click labelling (Schwartz et al. 2017) and could also increase the efficiency of ncAA incorporation in our *in vitro* system (Figure 3.9C).

Click labelling with the tetrazine-coupled click chemistry dye SiRTet was performed in live cells before the incorporated fluorescence was detected in protein gels (Figure 3.9D). BCN and TCO* were most reactive to tetrazine and the fluorescent signals were strongest after incorporation of these two amino acids. CpK and SCO on the other hand were not labelled as efficiently. As expected, no fluorescence was detected after the incorporation of BOC or PrK because these two ncAA do not react with tetrazine.

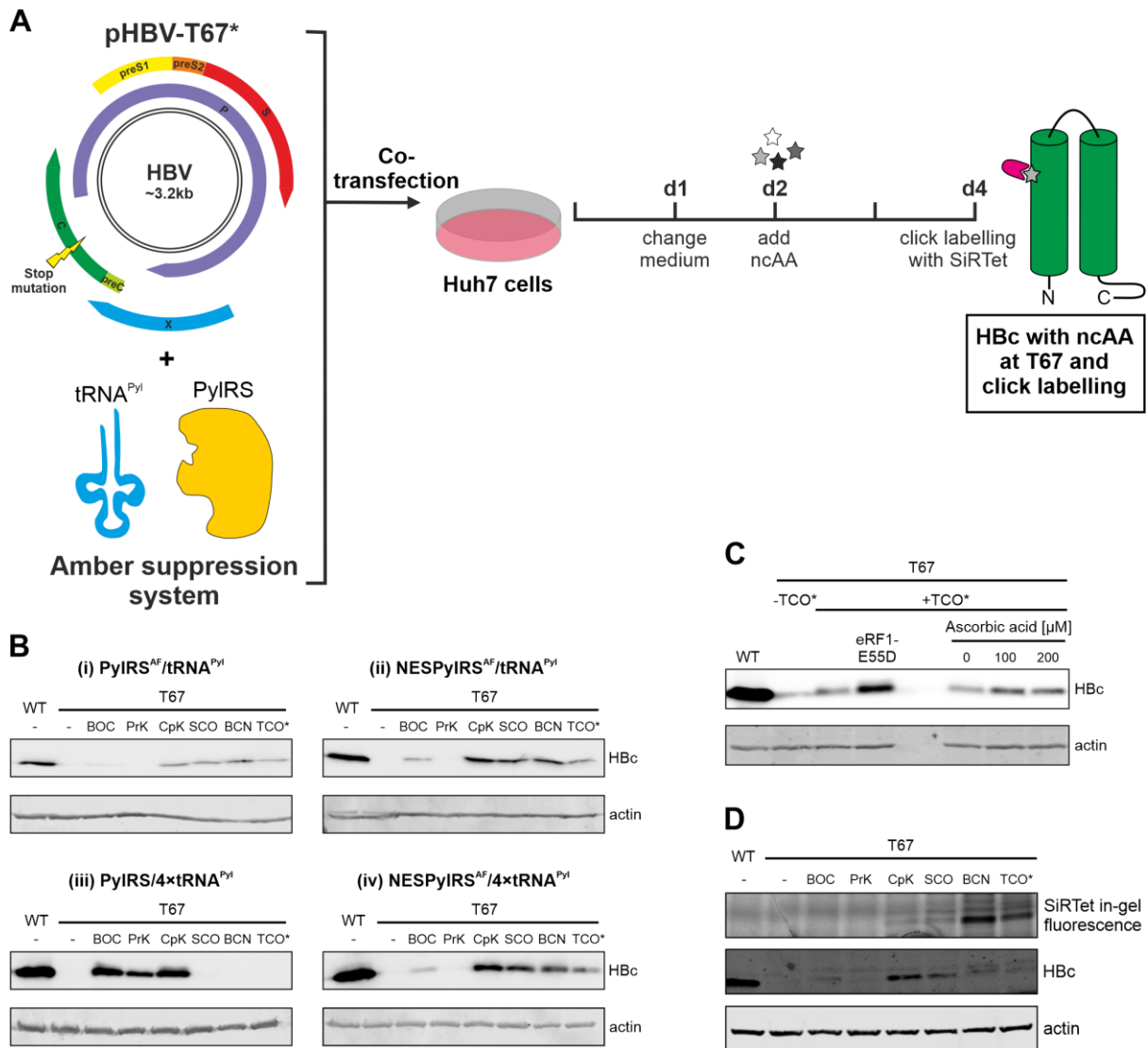


Figure 3.9. Optimisation of amber suppression efficiency at position T67 of HbC. (A) Huh7 cells were co-transfected with pHBV-T67* and one of the amber suppression constructs. Different ncAA were added two days after the transfection to the cell culture supernatants. 4 days post transfection, the incorporated ncAA were labelled with SiRTet and the cells were lysed. (B) Western blot analysis was performed to detect HbC expression after incorporation of ncAA using different amber suppression plasmids. (C) Huh7 cells were co-transfected with pHBV-T67* and (iv) pNESPyIRS^{AF}/tRNA^{Pyl} and TCO* and ascorbic acid were added 2 days post transfection. Cells were lysed 4 days post transfection and HbC levels were detected by western blot analysis. pHBV-T67*, pNESPyIRS^{AF}/tRNA^{Pyl}, and pErf1-E55D were co-transfected in 1:1:1 ratio into Huh7 cells. Cells were lysed 4 days post transfection, followed by HbC-specific western blot analysis. (D) Huh7 cells were co-transfected with pHBV-T67* and (iv) pNESPyIRS^{AF}/tRNA^{Pyl} and TCO* was added 2 days post transfection. At day 4 post transfection, cells were washed and labelled with SiRTet. After SDS-PAGE, the gels were scanned using the 700 nm channel of a LI-COR Odyssey CLx imaging system to detect incorporated fluorescence.

3.2.2. Identification of optimal amino acid sites for the introduction of ncAA into HBc

It is not possible to predict how well a specific ncAA will be incorporated into a protein of interest at a given amino acid position. Therefore, we chose several sites within the HBc ORF where a single amino acids exchange might not interfere with protein functions. HBc dimerizes and assembles into capsids with a $T = 4$ symmetry consisting of 120 HBc dimers (Bottcher et al. 1997; Wynne et al. 1999). The capsid forms very tight interactions with the envelope proteins in order to assemble into an infectious virion (Seitz et al. 2007). Altering amino acids in HBc might abrogate capsid formation, reverse transcription, or envelopment. Ponsel and Bruss have carefully analysed HBc by exchanging single amino acid positions with alanine and have shown that many single alanine exchange mutations are detrimental for virion formation (Ponsel and Bruss 2003). However, some point mutations still allowed capsid formation, envelopment, and secretion of virions. From these more flexible amino acid positions, eleven sites (S26, D32, W62, T67, V74, N75, L76, E77, L84, S87, and A131), which allowed secretion of enveloped virions after alanine mutation, were chosen for the incorporation of ncAA (Figure 3.10A). Most of these positions locate around the spike structure, hence they should not interfere with the C-terminal domain of HBc which is essential for pgRNA encapsidation and reverse transcription (Figure 3.10B) (Nassal 1992). The C-terminus of the HBc ORF overlaps with the HBV polymerase gene, however all selected sites for amber stop mutations do not overlap and should not affect the expression of polymerase. Unfortunately, no information on infectivity of these mutants was provided, as convenient HBV susceptible cell culture systems were not available when Ponsel and Bruss performed their mutational analysis. Amber stop codon point mutations at the 11 selected positions were generated within a 1.1mer overlength HBV genome expressed from a CMV promotor in a pcDNA3.1 vector.

transfected Huh7 cells was detected. This result was our first indication of successful incorporation of ncAA at an amber stop codon site of an HBV protein. Rescue of HBeAg expression by amber suppression varied between the different HBc amber stop mutants and could not be achieved for all positions, highlighting the difficulty of working with genetic code expansion. The presence of ncAA, which could potentially affect cell functions, did not have a significant effect on the secretion of HBeAg from the WT HBV plasmid.

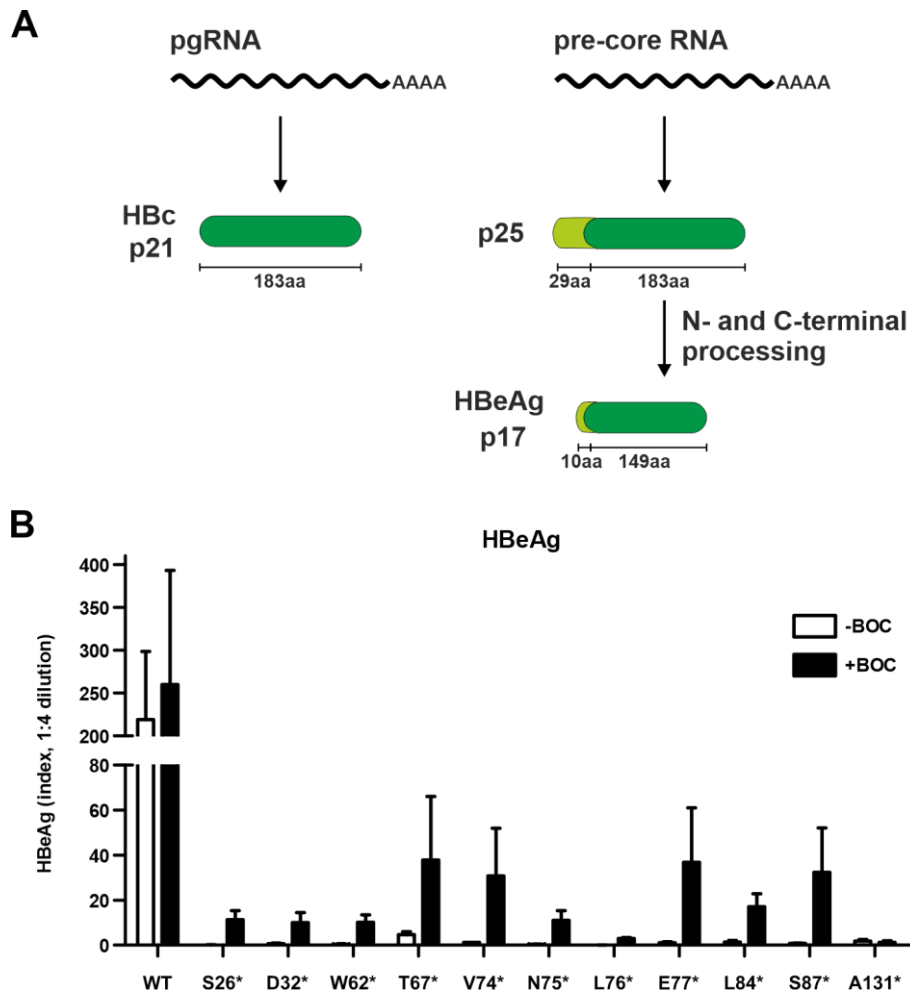


Figure 3.11. Rescue of HBeAg secretion. (A) Schematic illustration of HBeAg production. The precursor protein of HBeAg is translated from the precore mRNA. It is proteolytically processed at both ends and secreted into the cell culture supernatant where it can be detected by ELISA. (B) Huh7 cells were transfected with one of the pHBV1.1 amber mutants and the amber suppression plasmid pNESPyIRS^{AF}/tRNA^{PyI}. The ncAA BOC was added two days after transfection. Cell culture supernatant was collected from days 2-4 after transfection and secreted HBeAg levels were measured. The mean of 3 independent experiments (\pm standard deviation) is shown.

3.2.2.2. Amber suppression mediated ncAA incorporation rescues full-length HBc expression

We then investigated intracellular HBc levels after rescue of full-length HBc expression by amber suppression mediated readthrough of the inserted stop codons. Full-length HBc could not be detected in the absence of ncAA, but the incorporation of ncAA was able to rescue HBc expression (Figure 3.12A). Similar to HBeAg expression, the levels of HBc rescue varied between the different incorporation sites. On the other hand, the expression of HBc and HBeAg by the different mutants did not always correlate, for example amber suppression could efficiently rescue the HBc expression at position A131, but not the secretion of HBeAg. The position T67 was chosen for further experiments because it consistently showed the highest levels of HBeAg and HBc after incorporation of ncAA.

Consistent with the western blot results, HBc expression could also be visualised by immunofluorescence (Figure 3.12B). Only in the presence of ncAA, transfected cells expressed HBc. As expected, cells transfected with the mutant plasmid in the absence of ncAA only expressed HBsAg but not HBc. Possibly shorter fragments of the HBc protein were expressed, they were however not detected by immunostaining. The antigenic loop at the tip of the spike was missing in most of the mutants, but also for the mutant A131 we could neither detect HBeAg secretion nor truncated HBc. Therefore, it is also possible that the shorter HBc fragments are unstable and degraded rapidly.

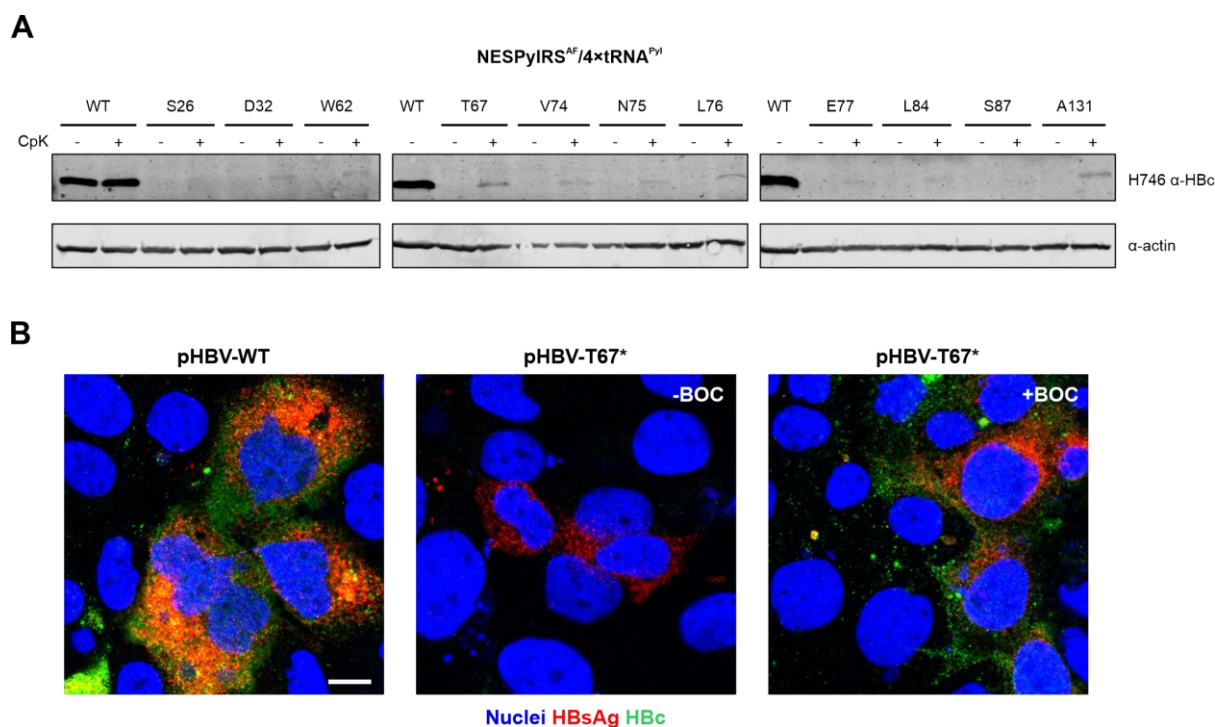


Figure 3.12. Amber suppression of HBc. (A) Huh7 cells were transfected with the different pHBV1.1 mutants and the amber suppression construct pNESPyIRS^{AF}/4×tRNA^{PyI}. CpK was added two days post transfection and the cell lysate was harvested on day 4 post transfection. SDS-PAGE was performed followed by HBc-specific western blot analysis. (B) Huh7 cells were co-transfected with pHBV1.1-T67* and pNESPyIRS^{AF}/tRNA^{PyI}. BOC was added 1 day post transfection, the cells were fixed on day 4, and analysed by immunofluorescence against HBc and HBsAg. Images were captured on a Leica SP8 confocal microscope. Scale bar represents 10 μm.

3.2.3. Click chemistry labelling of incorporated amino acids

Incorporated ncAA with cyclic alkyne or alkene groups (e.g. CpK, SCO, TCO*, and BCN) are suitable for click chemistry reaction in live cells, but extensive washes are necessary to remove excessive ncAA in the supernatant and in the cells which have not been incorporated by the amber suppression system (Schvartz et al. 2017). To be able to label intracellular HBc proteins, a membrane permeable dye was applied. Silicon rhodamine fluorophores are highly permeable and fluorogenic, thus they permit labelling and imaging of live cells (Lukinavicius et al. 2013). Tetrazine-coupled silicon rhodamine (SiRTet) can attach to incorporated ncAA and therefore fluorescently label a protein of interest site-specifically. Labelling with SiRTet is very convenient as it can be performed in live or in fixed cells. Excessive dye is removed by additional washing steps. Because of the far-red emission wavelength (674 nm) of SiRTet, its fluorescence can be detected in-gel using the 700 nm channel of a LI-COR Odyssey CLx imaging system which uses infrared detectors. After incorporation and SiRTet-labelling of TCO* at position T67 of HBc, a fluorescent signal could be detected at the molecular size of HBc (Figure 3.13A). This fluorescent band was not observed when cells were transfected with

the amber suppression reporter mCherry-GFP(TAG), in which case a fluorescent signal was detected at higher molecular weight probably corresponding to the mCherry-GFP fusion protein after amber suppression mediated rescue of full-length GFP. The in-gel fluorescence further revealed background signals of the SiRTet labelling. A strong band present in both samples at the 55 kDa marker might originate from TCO* bound to PylRS (52 kDa) and more diffuse background at all molecular sizes may be caused by suppression of amber stop codons in cellular transcripts.

Labelling with SiRTet followed by immunostaining confirmed the co-localisation of HBc with the click chemistry dye (Figure 3.13B). Confocal microscopy showed considerable background staining of SiRTet, mostly with nuclear localisation, but also displayed distinct puncta with co-localising SiRTet signal and HBc-specific immunostaining. HBsAg was present in the cytoplasm of transfected cells but did not seem to co-localise with HBc or SiRTet. As expected, the signal intensity varied depending on the incorporated ncAA. Staining of SCO resulted in relatively weak background signal and specific puncta (Figure 3.13B&C). Incorporation of BOC could be detected by the staining for full-length HBc, but labelling with SiRTet was not observed, indicating that SiRTet reacts specifically with the intended ncAA (Figure 3.13C). TCO* on the other hand is highly reactive to tetrazine-coupled dyes and its incorporation resulted in strong signal intensities, making it difficult to detect HBc-specific signals above the background. Without the introduction of an exogenously expressed amber stop mutated protein, the background staining of SiRTet was present in the entire cell and most prominent in the nucleus (Figure 3.13D). The SiRTet signal in Figure 3.13D most likely originates from ncAA still bound to PylRS or tRNA^{Pyl}, incorporated into cellular proteins with amber stop codons, or not washed out from cells. Specific puncta seem to be fewer and weaker in signal intensity.

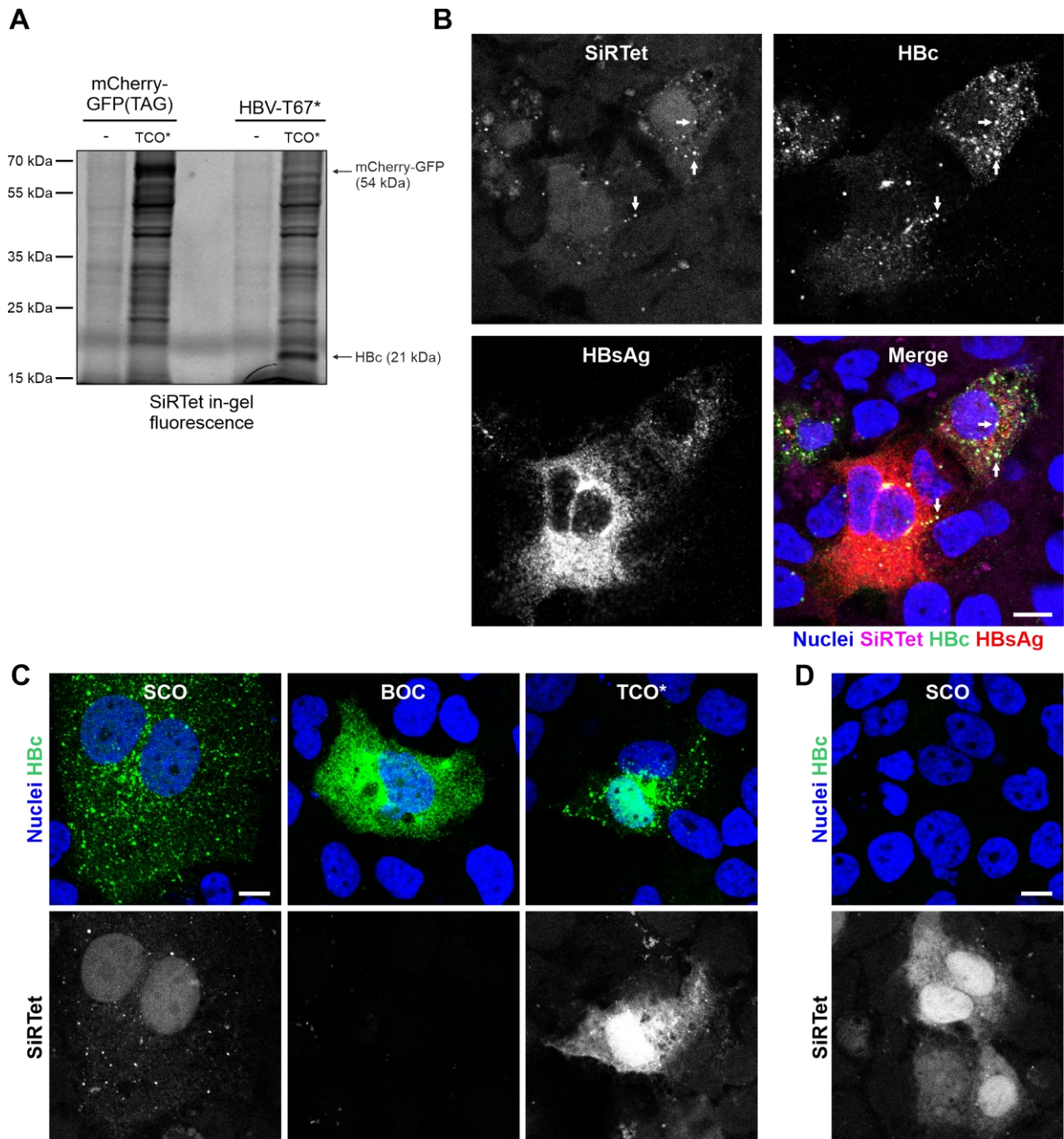


Figure 3.13. Labelling of incorporated ncAA. Huh7 cells were transfected with the T67* mutant and the amber suppression plasmid pNESPyIRS/tRNA. **(A)** TCO* was added on day 2 post transfection and on day 4, cells were washed extensively and labelled with SiRTet. After labelling, the cells were lysed and run on SDS-PAGE. The gels were scanned using the 700 nm channel of an Odyssey imaging system to detect fluorescence from incorporated SiRTet. **(B)** SCO was added from day 2 to 4 post transfection. The cells were fixed after SiRTet labelling and immunostaining for Hbc and HBsAg was performed. Examples of Hbc- and SiRTet-positive puncta are highlighted with arrows. **(C)** SCO, BOC, or TCO* were added from day 2 to 4 post transfection. After labelling with SiRTet, cells were fixed and immunostaining for Hbc was performed. **(D)** To control for labelling of unspecific incorporation of ncAA, Huh7 cells were transfected with pNESPyIRS^{AF}/tRNA^{Py1} alone. Incorporation of SCO, SiRTet labelling, and Hbc-specific immunostaining were performed as before. Images were captured on a Leica SP8 confocal microscope. Scale bars represent 10 μ m.

3.2.4. Secretion and infectivity of HBV with incorporated ncAA

3.2.4.1. HBV secretion is impaired by the incorporation of large ring structured ncAA

So far, we could detect rescue of extracellular HBeAg and intracellular HBc expression after amber suppression. We then aimed to elucidate whether incorporation of ncAA at position T67 of HBc would allow the secretion of virions. Based on the mutational analysis from Ponsel and Bruss, we knew that secretion of enveloped virions was possible after alanine substitution (Ponsel and Bruss 2003). But it remained unclear if the substitution with a ncAA might interfere with capsid assembly or envelopment and secretion of virions.

To test the secretion competence after incorporation of ncAA, Huh7 cells were transfected with the 1.1mer HBV genome with amber stop mutation at position T67 and the amber suppression plasmid pNESPyIRS^{AF}/4×tRNA^{PyI}. Different amino acids were added to the cells and the supernatants were collected and concentrated ca. 100-fold by precipitation with 6% PEG. The concentrated supernatants were then analysed by analytical CsCl density gradient centrifugation followed by HBV DNA specific dot blot. Trans-complementation with pHBc expressing the WT HBc was used as control for production and secretion of HBV DNA containing naked capsids and virions (Figure 3.14). When production of full-length HBc depended on the incorporation of ncAA, virions were only secreted at very low levels compared to the control with the supplemented WT HBc. Therefore, we applied 10 times the volume of the precipitated supernatant from the samples in which amber suppression was used to rescue HBc production. Due to the increased input, these samples showed a prominent signal in the high-density fractions, which most likely represents input plasmid DNA from the transfection. Incorporation of BOC at position T67 of HBc was able to rescue the secretion of naked capsids and virions (Figure 3.14). The background noise from the dot blot assay unfortunately did not allow for exact quantification, but the signal at the virion peak is weaker compared to the trans-complementation control. Since 10 times the volume of the BOC incorporated sample was applied to the gradient, the amount of secreted virion was presumably less than 10% of the control. Secretion of virus particles could not be detected when ncAA with large ring structures as side chain were incorporated into HBc. Even though addition of SCO, TCO*, or BCN could rescue intracellular HBc production, they had a deleterious effect on assembly or secretion of capsids. The large size of the ring structures might interfere sterically with assembly of capsids. Alternatively, even though these alkene and alkyne rings are supposedly orthogonal to cellular components, they are highly reactive and might interact with nearby amino acids when they are packed very tightly in a capsid with close interactions. CpK has a smaller ring structured side

chain and is also less reactive compared to TCO* and BCN. After incorporation of CpK into HBc, we could detect secretion of virions albeit at similar or lower levels compared to BOC (Figure 3.14).

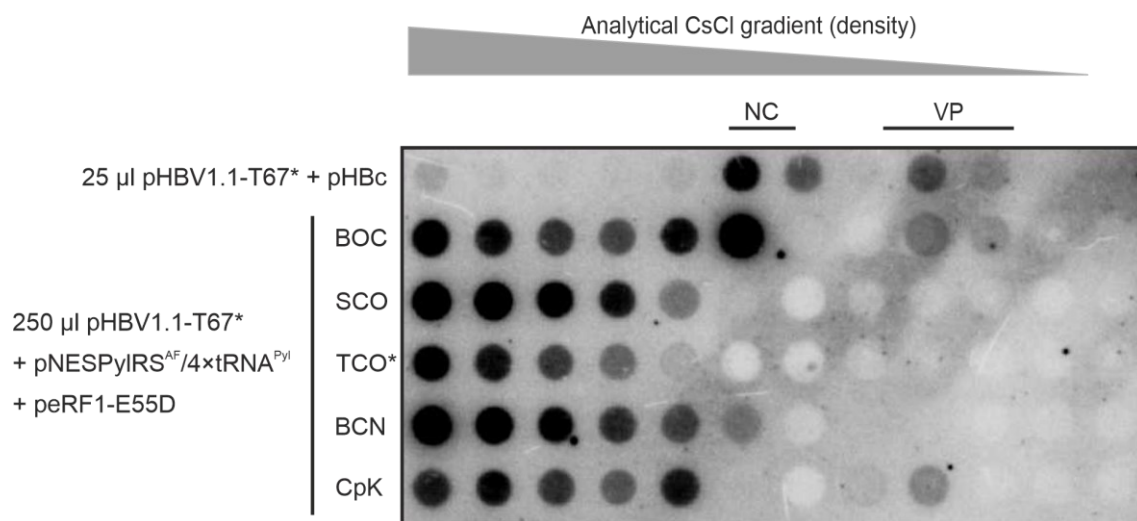


Figure 3.14. Virus production after incorporation of different ncAA at position T67. Huh7 cells were co-transfected with the T67 amber mutant, the amber suppression construct pNESPyIRS^{AF}/4×tRNA^{Pyl}, and peRF1-E55D. The different ncAA and ascorbic acid were added on day 1 post transfection and supernatant was collected every two days until 9 days post transfection. The supernatants were pooled, sterile filtrated, and concentrated by precipitation with 6% PEG. The precipitate was analysed by CsCl density gradient and subsequent HBV DNA dot blot. Naked capsids (NC) and enveloped virions (VP) were identified by the density of the fractions. Reconstitution with WT HBc was used as positive control. Virus production by incorporation of ncAA was inefficient, thus 10 times the volume of the precipitate was loaded onto the gradient compared to the control.

The position T67 of the HBc ORF was chosen after it showed the highest levels of HBeAg and HBc after amber stop codon suppression. Other amino acid positions had been less accommodative in these previous experiments regarding the rescue of HBeAg and HBc production, though some had almost equal levels compared to T67. To test if the incorporation of CpK at other sites might improve virion secretion, the virus production after amber suppression of the 11 stop mutants was investigated. After amber suppression mediated incorporation of CpK at the 11 different positions, we detected the secretion of HBV DNA containing particles (Figure 3.15). As described previously, 10 times more volume of the samples was loaded compared to the control. HBV virions were secreted after incorporation of CpK at positions S26, W62, T67, V74, L84, and S87. The T67 amber stop mutant constantly provided the strongest signal, whereas the other mutants were less capable to produce virions after amber suppression and as before, all samples showed lower levels of virus production compared to one-tenth of the control. Incorporation of CpK at other positions did not result in any virion secretion, for example HBV DNA containing particles were not detected after suppression of the amber stop codon at position A131, even though intracellular HBc

expression was rescued. Mutation at the proximity of the HBc C-terminal domain might interfere with encapsidation or reverse transcription of pgRNA. Interestingly, the D32 amber mutant could secrete naked capsids but not enveloped virions, hinting towards an envelopment defect following amino acid substitution at this position. Previously, structural analysis of HBV virions did not suggest envelope contacts with the base of the spike (Seitz et al. 2007), where D32 is located, but the functional analysis by mutational screen has revealed sites at the base of the spike to be necessary for envelopment (Ponsel and Bruss 2003).

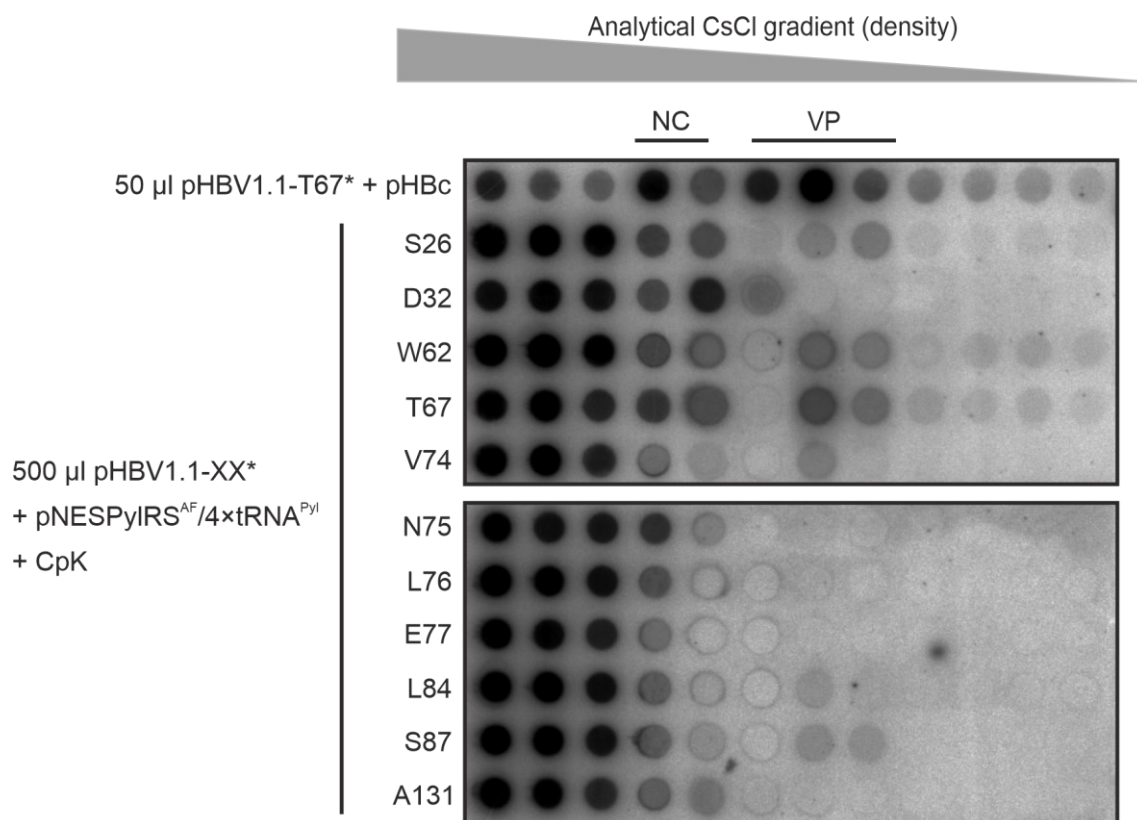


Figure 3.15. Virus production after incorporation of CpK at 11 different positions. Huh7 cells were co-transfected with the different HBV amber mutants and pNESPyIRS^{AF}/4x^tRNA^{PyI}. CpK and ascorbic acid were added on day 2 post transfection and supernatant was collected every two days until day 8. The supernatants were pooled, sterile filtrated, and precipitated with 6% PEG. The precipitate was analysed by CsCl density gradient centrifugation and subsequent HBV DNA dot blot. Naked capsids (NC) and enveloped virions (VP) were identified by the density of the fractions. Reconstitution with WT HBc was used as positive control. Virus production by incorporation of CpK was inefficient, thus 10 times the volume of the precipitate was loaded onto the gradient compared to the control.

3.2.4.2. HBV remains infectious after incorporation of ncAA in the capsid

Next, we tested whether these secreted virions remained infectious after incorporation of ncAA into HBc. HBV with BOC incorporated at position T67 of HBc (HBV-T67BOC) was used to infect HepG2-NTCP cells. WT HBV and HBV-T67BOC were produced by transfection of Huh7 cells. Supernatants from the transfected cells were analysed for secreted HBV DNA by an analytical CsCl density gradient and HBV DNA containing virion fractions were quantified

by DNA dot blot (Figure 3.16A). As expected, the stop mutated HBV genome was not able to produce HBV in the absence of ncAA. Compared to WT HBV (6.6×10^8 viral genome equivalents (vge)/ μl , after precipitation with PEG), amber suppression mediated rescue of the T67 mutant yielded a roughly 15-fold lower virus production (4.5×10^7 vge/ μl). The quantification by HBV DNA dot blot was less precise compared to the COBAS AmpliPrep/COBAS TaqMan HBV Test by the Heidelberg University Hospital Virology Diagnostics Department. Therefore, these virus stocks cannot be compared directly to the virus stocks used in chapter 3.1. Furthermore, some of the detected signals were stronger than the upper limit of the HBV DNA standard and might be oversaturated, making the quantification less reliable, but the quantification granted us an estimate of the relative virion production.

We tested the infectivity of WT HBV and HBV-T67BOC at mge 300 in HepG2-NTCP cells (Figure 3.16B). After infection, WT HBV infected cells stained positive for HBsAg (red) and HBc (green). Consistent with ΔHBc HBV infection, cells infected with HBV-T67BOC stained positive for HBsAg but not HBc. The infection of both viruses was completely blocked by MyrB indicating an authentic NTCP-dependent virus entry. Less HBsAg-positive cells could be observed after infection with HBV-T67BOC compared to WT HBV. The not very precise quantification of these virus stocks does not allow a definite conclusion, but it is possible that the amino acid substitution negatively affects infectivity.

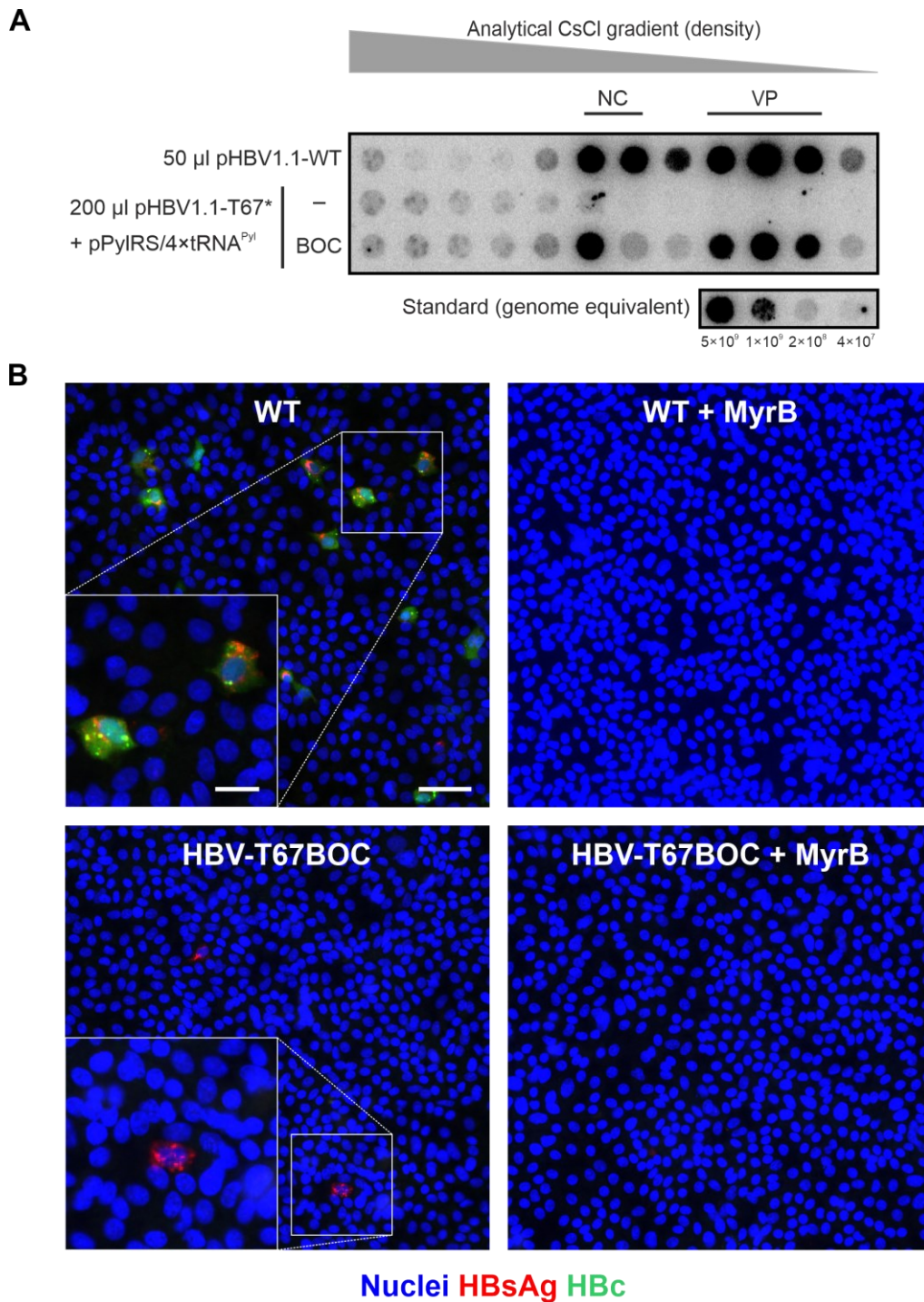


Figure 3.16. Infectivity after incorporation of BOC. (A) WT HBV and HBV-T67BOC were produced by transfection of Huh7 cells with pHBV1.1-WT or co-transfection with pHBV1.1-T67* and pPyIRS/4×tRNA^{Pyl}, respectively. BOC was added from day 3 post transfection and supernatants were collected every 2 days until day 9. The supernatants were pooled, sterile filtrated, and precipitated with 6% PEG. The precipitate was analysed by CsCl density gradient centrifugation and subsequent HBV DNA dot blot. Naked capsids (NC) and enveloped virions (VP) were identified by the density of the fractions. Titres of virions were quantified using a linear HBV fragment, excised from pHBV1.1-WT, as DNA standard and the software Quantity One. Virus production by incorporation of BOC was inefficient, thus 4 times the volume of the precipitate was loaded onto the gradient compared to the WT. (B) HepG2-NTCP cells were infected with WT HBV or HBV-T67BOC at mge 300. Cells were fixed 7 days post infection and immunofluorescence for HBs and HBc was performed. MyrB mediated blockade of HBV infection was used as control. Scale bars represent 50 µm (main figure) and 20 µm (inset).

While the incorporation of BOC could rescue the production of infectious HBV, it cannot be used in a click chemistry reaction. Since incorporation of ncAA with large ring structured side chains did not allow the secretion of virions (Figure 3.14), we examined the infectivity after incorporation of CpK. Precipitated viruses, production results of which are shown in Figure 3.15, were used to infect HepG2-NTCP cells (Figure 3.17). The analysis of intracellular HBsAg revealed that the secretion of infectious virions could be rescued by the incorporation of CpK at three positions (S26, W62, and T67). Consistent with the amount of secreted HBV DNA in virions as detected by dot blot, only very few infected cells could be detected, whereas the trans-complementation with WT HBc (Δ HBc HBV) procured high levels of infectious particles. Likewise, only infection with the virus stocks that had the strongest signals in the virions peaks resulted in the detection of HBsAg-positive cells.

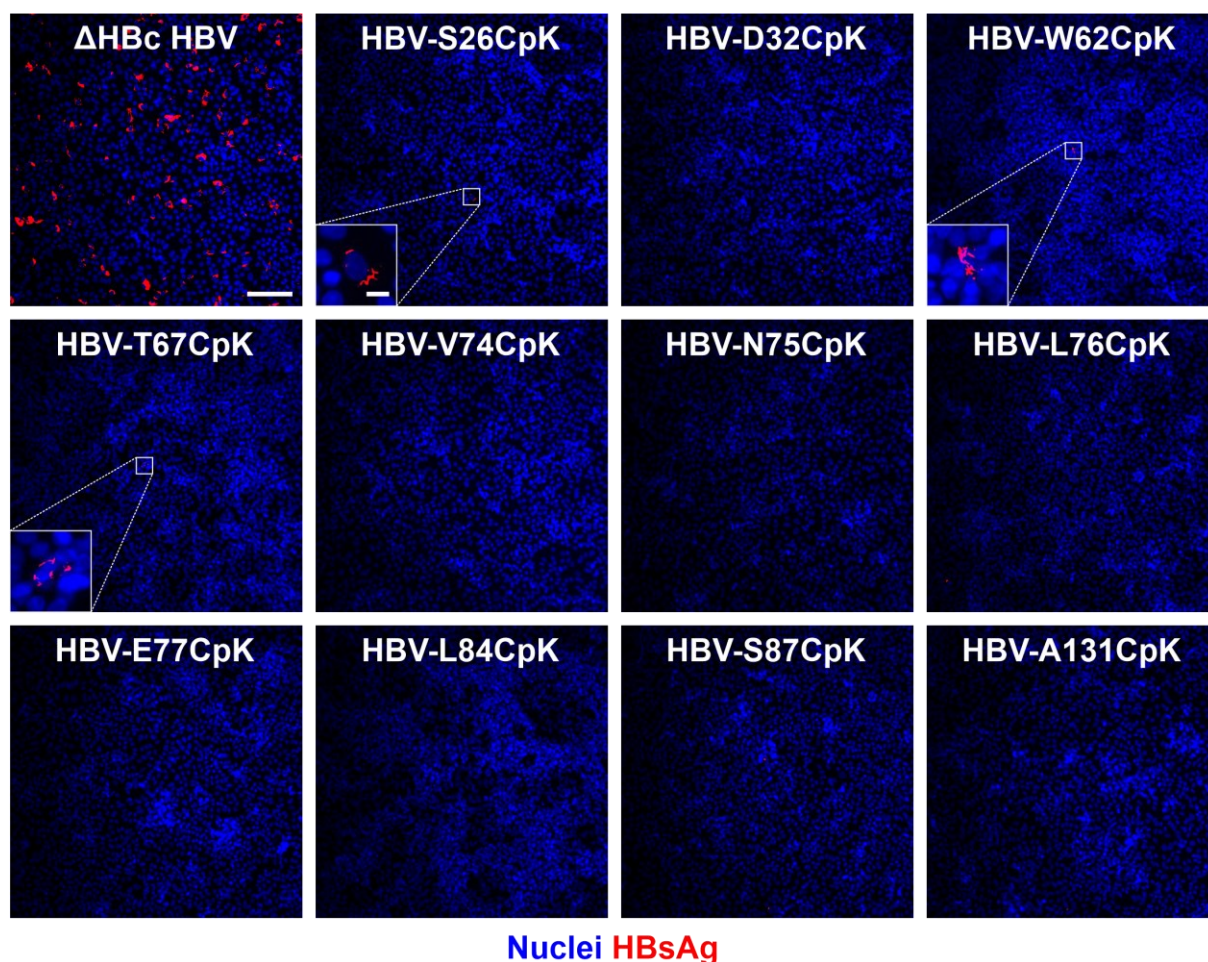


Figure 3.17. Infection after incorporation of CpK at 11 different positions of HBc. HepG2-NTCP cells were infected with the precipitated supernatants described in Figure 3.15. 5 μ l Δ HBc HBV and 25 μ l of the virus stocks with incorporated CpK were used in a 24 well format. Cells were fixed after 7 days and immunofluorescence for HBsAg was performed. Scale bars represent 100 μ m (main figure) and 10 μ m (inset).

3.2.4.3. The incorporation of PrK allows secretion of HBV without impairing infectivity

Virus production with live clickable amino acids had so far resulted in extremely low yields. Therefore, we tried to incorporate PrK which does not have a ring structured side chain and might be better incorporated into virus capsids, similar to BOC (Figure 3.8). Comparable amounts of HBV virions were detected when the T67 amber stop mutant was rescued with either BOC or PrK incorporation (Figure 3.18A). But the rescue of virion secretion by reconstitution with WT HBc was still more than 10-fold stronger. To test the infectivity of HBV after incorporation of PrK (HBV-T67PrK), we infected HepG2-NTCP cells with precipitated supernatants. Infected cells were analysed by HBsAg-specific immunofluorescence following inoculation with HBV-T67BOC or HBV-T67PrK (Figure 3.18B). Consistent with the virus secretion levels, the number of infected cells were lower compared to infection with Δ HBc HBV. As expected, the production of infectious particles was not rescued in the absence of ncAA. Unfortunately, PrK cannot be used in a live SPAAC or SPIEDAC click chemistry reaction but can undergo a copper catalysed CuAAC reaction with an azide-coupled dye. Cells must be fixed and permeabilised prior to CuAAC click labelling, however the incorporation of PrK seemed to be more promising regarding virus production and infection capabilities compared to live clickable ncAA with large ring structures.

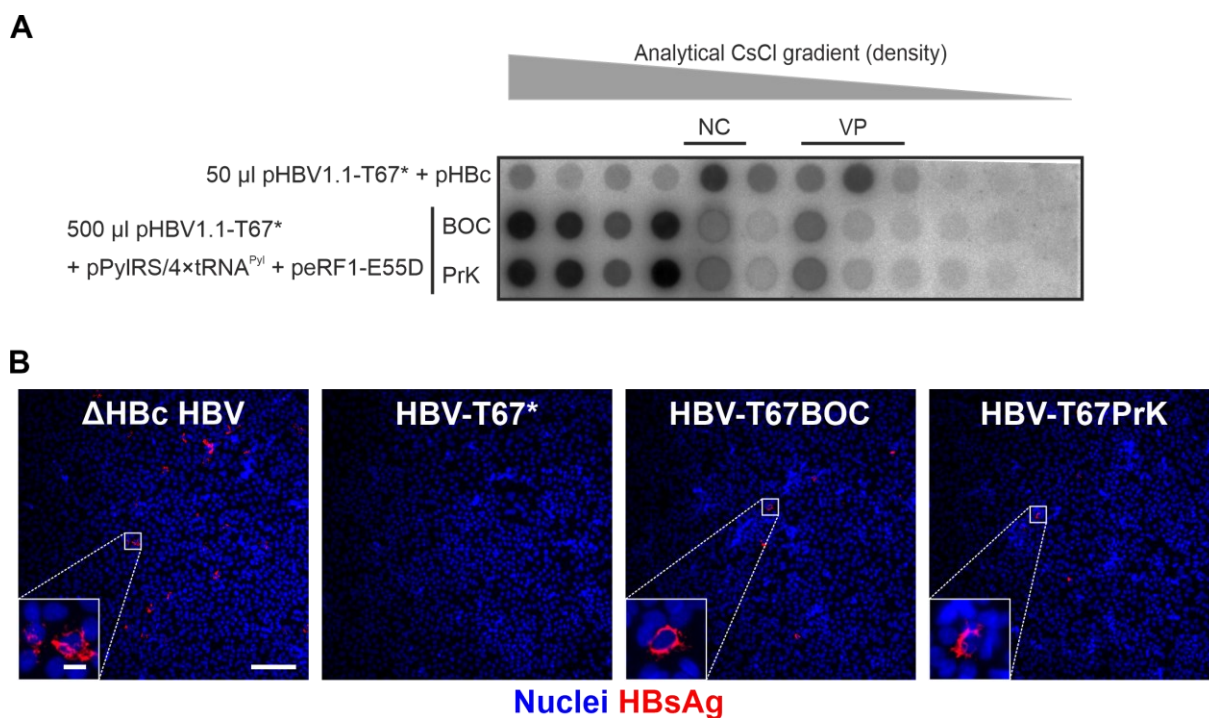


Figure 3.18. Virus production and infectivity after incorporation of PrK at position T67. (A) HBV-T67PrK was produced by co-transfection of Huh7 cells with pHBV1.1-T67*, pPyIRS/4 \times tRNA^{PyI}, and peRF1-E55D. Ascorbic acid and BOC or PrK were added to the cells 1 day post transfection and the supernatants were collected every 2 days until day 9. Cells were co-transfected with pHBV1.1-T67* and pHBc as control. The supernatants were pooled, sterile filtrated, precipitated with PEG, and analysed using CsCl gradients and HBV DNA dot blot. Virus production by incorporation of ncAA was inefficient, thus 10 times the volume of the precipitate was loaded onto the gradient compared to the control with WT HBc trans-complementation. (B) HepG2-NTCP cells were infected with precipitated Δ HBc HBV (5 μ l), HBV-T67BOC, or HBV-T67PrK (both 25 μ l). Cells were fixed after 7 days and immunofluorescence for HBsAg was performed. Scale bars represent 100 μ m (main figure) and 10 μ m (inset).

To test the suitability of PrK incorporation to obtain enough virus quantities for click labelling, we produced a large stock of virus by co-transfecting Huh7 cells with the HBV-T67 amber stop mutant and the amber suppression system in presence of PrK in the cell culture medium. The supernatants were collected, pooled, purified by heparin affinity chromatography, and concentrated on a centrifugal filter unit. The virus stocks were finally concentrated \sim 60-fold compared to the raw supernatant. The incorporation of PrK could rescue 5% of the HBV secretion relative to trans-complementation with WT HBc, as determined by qPCR (Figure 3.19A). When HepG2-NTCP cells were infected with increasing inocula of Δ HBc HBV or HBV-T67PrK virus, both viruses showed comparable numbers of HBsAg-positive cells when using identical mge of both viruses (Figure 3.19B). The similar infection rate of Δ HBc HBV and HBV-T67PrK suggested that the replacement of the threonine at position 67 of HBc with PrK did not negatively affect the infectivity of HBV. In both cases, treatment with MyrB inhibited the infection. Altogether, these results indicate that the incorporation of PrK might be

most suitable to generate HBV with clickable nucleocapsids. Still, PrK cannot be labelled in live cells, but needs to be labelled in fixed cells with a copper-catalysed click reaction.

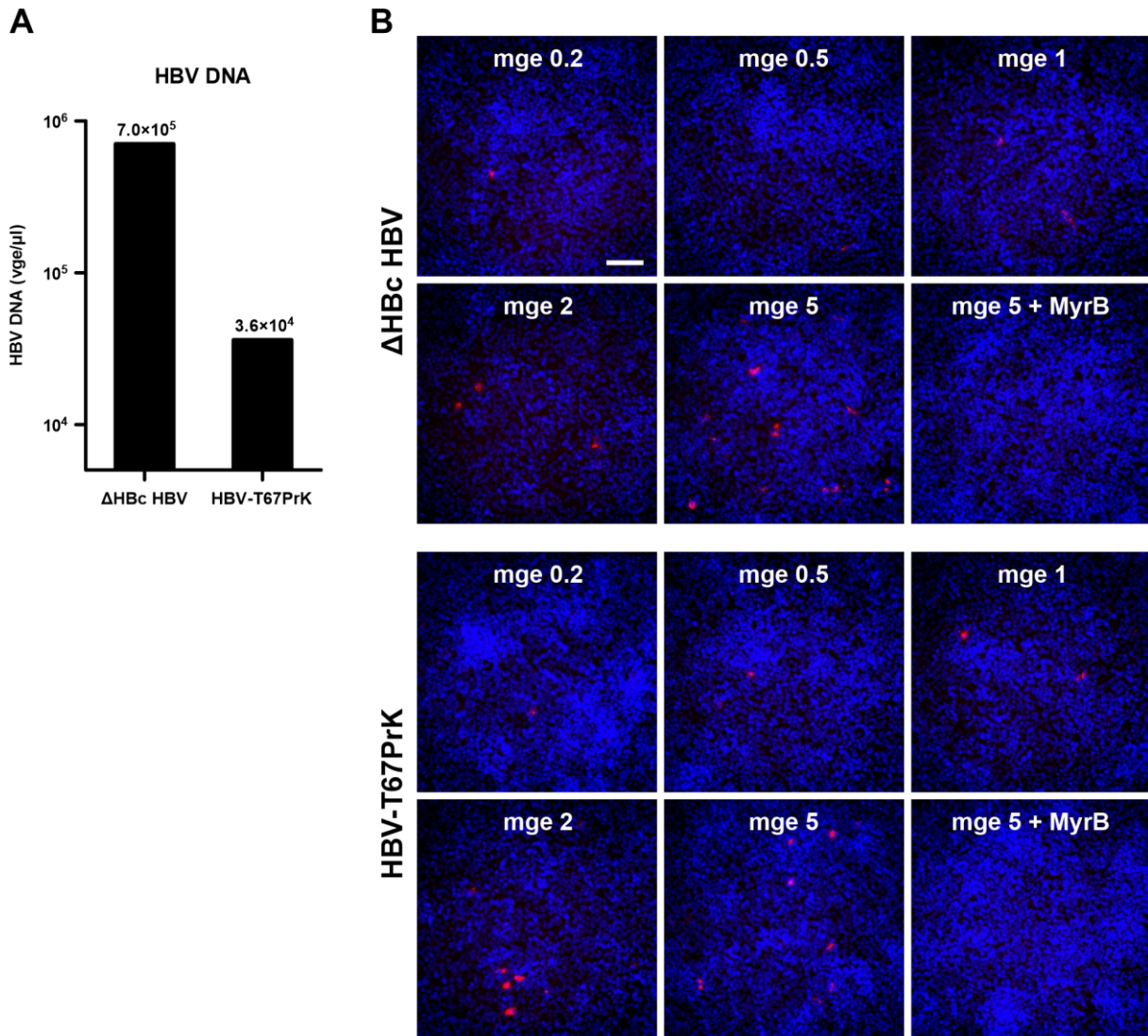


Figure 3.19. Quantification and infectivity of heparin purified HBV-T67PrK. (A) Huh7 cells were co-transfected with pHBV1.1-T67* and pHBc or pPylRS/4 \times tRNA^{Pyl} to produce Δ HBc HBV and HBV-T67PrK, respectively. PrK was added 1 day post transfection and supernatants were collected every 2 days until day 9. The supernatants were pooled, sterile filtrated, applied to heparin affinity chromatography, and concentrated on a centrifugal filter unit. HBV DNA quantification of the virus stocks was performed using the COBAS AmpliPrep/COBAS TaqMan HBV Test by the Heidelberg University Hospital Virology Diagnostics Department. (B) HepG2-NTCP cells were infected with increasing mge of Δ HBc HBV or HBV-T67PrK. Cells were fixed after 7 days and immunofluorescence for HBsAg was performed. Treatment with MyrB was used as control for infection inhibition. Scale bar represents 100 μ m.

3.2.5. Visualisation of HBV-T67PrK

3.2.5.1. Copper-catalysed click chemistry specifically labels HBV-T67PrK

To test if the incorporated PrK could be labelled, we performed CuAAC click chemistry reactions with heparin purified virions. Azide-coupled silicon rhodamine (SiR-Azide) dye was used to react with incorporated PrK. To label the capsids, HBV-T67PrK was spotted on a coverslip, CuAAC labelling, and immunostaining for viral proteins were performed. Confocal microscopy revealed co-localisation of HBc-specific immunofluorescence and the click chemistry dye suggesting successful labelling of HBc with incorporated PrK (Figure 3.20). However, the fluorescent signal was more difficult to detect and the background signal was stronger compared to immunostaining. Only very few triple positive structures (SiR-Azide, HBc, and HBsAg) indicating enveloped virions were observed. SiR-Azide and HBc double positive puncta might represent naked capsids, HBsAg positive structures on the other hand might be caused by subviral or filamentous particles.

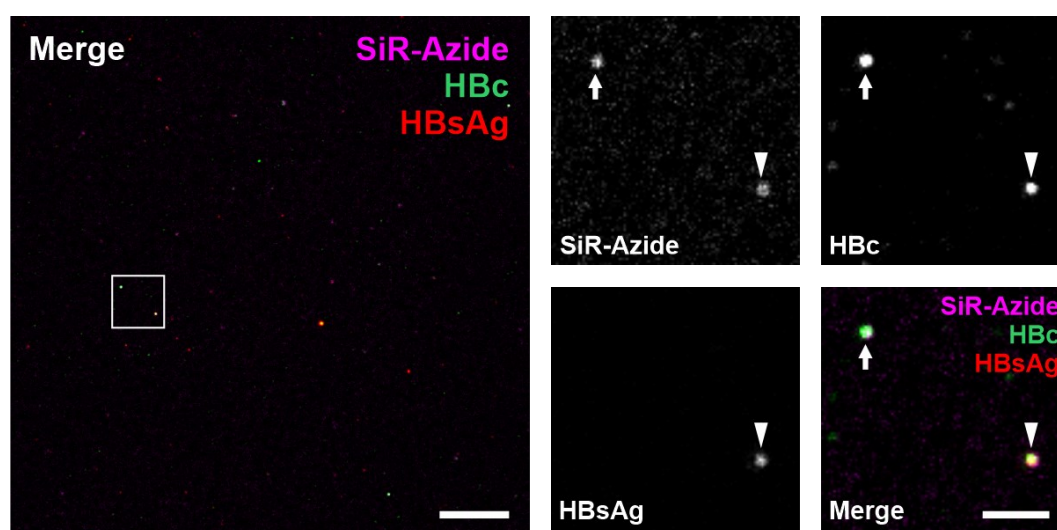


Figure 3.20. Click labelling of heparin purified HBV-T67PrK. After purification on a heparin column, 15 μ l HBV-T67PrK were spotted on a coverslip for 30 min followed by fixation for 5 min and permeabilization. Incorporated PrK was click labelled with SiR-Azide (magenta) and immunostaining for HBc (green) and HBsAg (red) was performed. Images were taken using a Leica SP8 confocal microscope. Arrowhead points to a triple positive structure, arrow denotes a naked capsid with SiR-Azide labelling. Scale bars represent 10 μ m (main figure, left) and 2 μ m (zoom-in, right).

3.2.5.2. HBV-T67PrK particles are internalised into HepG2-NTCP cells and transported to the nuclear periphery

To test if the click-labelled HBV-T67PrK could still be detected on the labelling background coming from cells, HepG2-NTCP cells were inoculated with HBV-T67PrK. Infected cells were fixed after either 30 min, 2 h, 4 h, or 8 h and subsequently HBc was labelled by immunofluorescence and CuAAC. HBV nucleocapsids could be detected in the cytoplasm of HepG2-NTCP cells after 30 min by co-staining with HBc-antibodies and click chemistry (Figure 3.21). The SiR-Azide labelling produced a strong background noise in the entire cell, while the immunostaining for HBc was more specific and showed a spotted background signal which mostly located inside the nucleus. Co-staining for an early endosome marker, early endosome antigen 1 (EEA1), revealed association of HBV with early endosomes. This finding is consistent with HBV infection being dependent on Rab5 and Rab7, markers for early and late endosomes (Macovei et al. 2013).

Starting from two hours post infection, HBV-T67PrK was detected in close proximity to the nucleus (Figure 3.21), consistent with the presumed timeline of infection establishment. At later timepoints, HBV-T67PrK particles could be found at the nuclear envelope and in the cytoplasm partially associating with early endosomes. However, click labelled nucleocapsids were not observed inside the nucleus, suggesting capsids might remain at the NPC and not efficiently enter the nucleus. Orthogonal views showed that HBV-T67PrK nucleocapsids often localise at the basolateral side of the nucleus (Figure 3.22). HBV preferentially enters hepatocytes from the basolateral membrane (Schulze et al. 2012). However, this finding is based on differentiated HepaRG cells which strongly resemble primary hepatocytes and represent a more authentic *in vitro* infection system than the HepG2-NTCP cells used in this experiment. The ectopic expression of NTCP renders HepG2 cells susceptible to HBV infection, but NTCP is most likely not expressed exclusively at the basolateral membrane in this cell line.

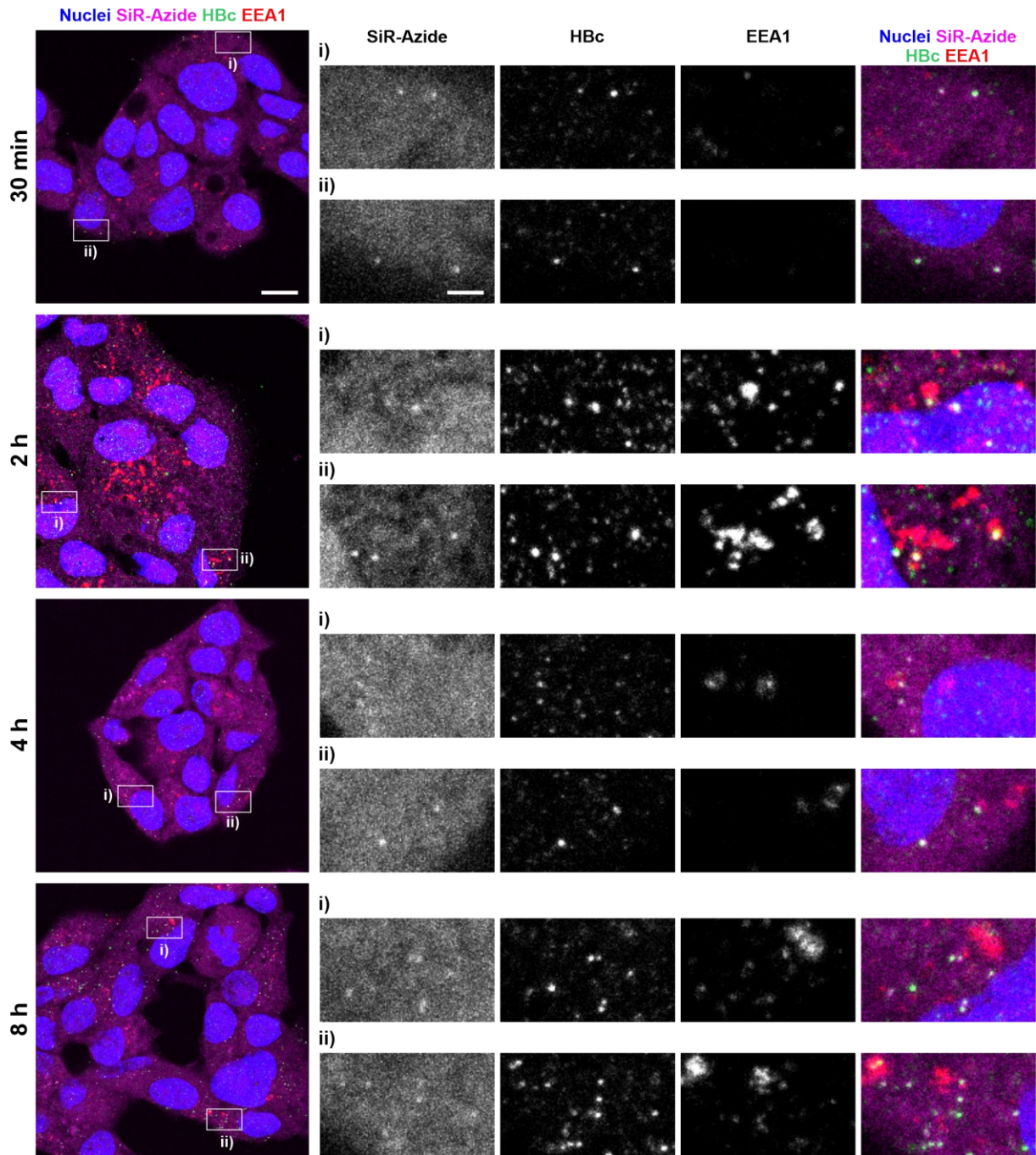


Figure 3.21. Click labelling of HBV-T67PrK on cells. HepG2-NTCP cells were infected with 15 μ l heparin column purified HBV-T67PrK and fixed at the indicated timepoints post infection. Incorporated PrK was click labelled with SiR-Azide (magenta) and immunostaining for HBc (green) and EEA1 (red) was performed. Images were taken using a Leica SP8 confocal microscope. Maximum intensity Z projection of 3 Z-steps (300 nm per step) is shown. Scale bars represent 10 μ m (main figure, left) and 2 μ m (zoom-in, right).

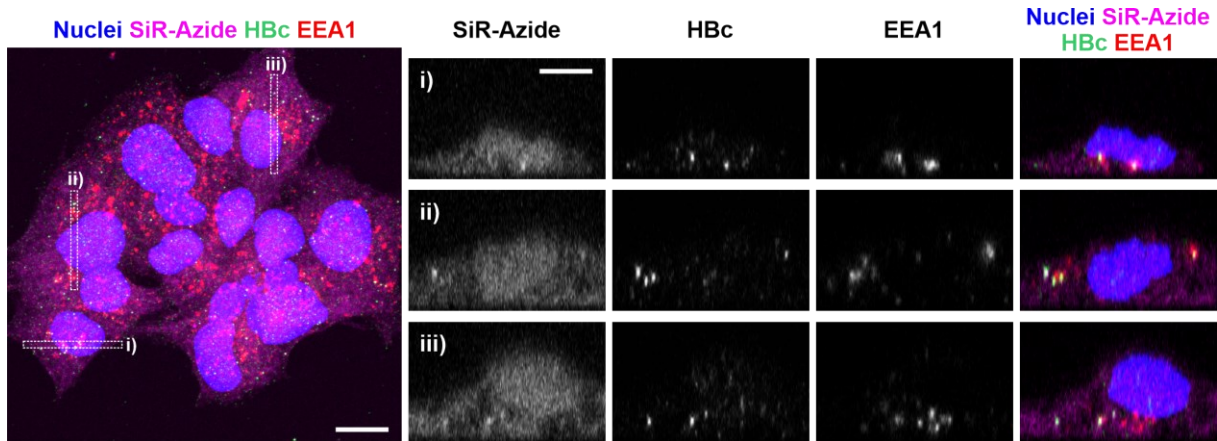


Figure 3.22. Orthogonal views of HBV-T67PrK on HepG2-NTCP cells. HepG2-NTCP cells were infected with 15 μ l heparin column purified HBV-T67PrK and fixed after 2 h. Incorporated PrK was click labelled with SiR-Azide (magenta) and immunostaining for HBc (green) and EEA1 (red) was performed. Images were taken using a Leica SP8 confocal microscope. Maximum intensity Z projection of 3 Z-steps (left) and orthogonal views (right) are shown. Scale bars represent 10 μ m (main figure, left) and 5 μ m (orthogonal views, right).

3.2.5.3. Heparin treatment inhibits internalisation of HBV-T67PrK

To verify that the labelled particles are HBV nucleocapsids derived from virions, we specifically inhibited attachment of virions to cells. Attachment of HBV to cells is mediated by affinity for HSPGs but not the specific binding to NTCP (Schulze et al. 2007). Attachment and reduced internalisation of HBV has been observed in HepG2 cells without ectopic expression of NTCP, although without inducing a productive infection (Chakraborty et al. 2020). Treatment with heparin was shown to be most efficient to inhibit attachment and internalisation of HBV. Indeed, uptake of HBV-T67PrK was markedly reduced by heparin treatment, displayed by the lower number of SiR-Azide and HBc-immunostaining double positive puncta (Figure 3.23). Although uninfected cells showed background signals for both SiR-Azide and immunofluorescence, double positive puncta were not observed, suggesting that they must originate from the virus input.

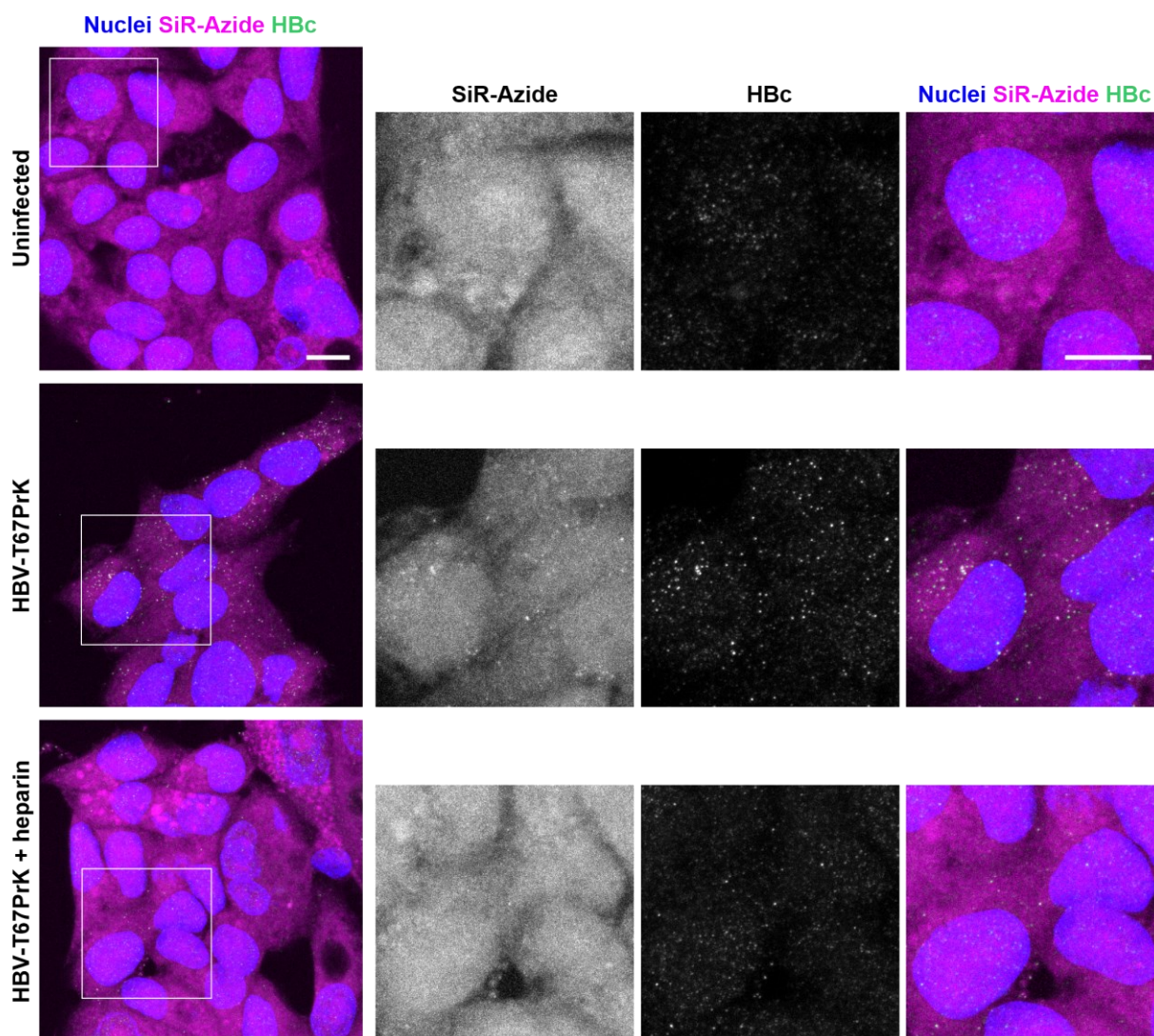


Figure 3.23. Entry inhibition of HBV-T67PrK by heparin treatment. HepG2-NTCP cells were infected with 15 μ l heparin column purified HBV-T67PrK for 8 h. For inhibition of attachment, cells were pre-treated for 30 min and co-treated during the inoculation with 500 μ g/ml heparin. Incorporated PrK was click labelled with SiR-Azide (magenta) and immunostaining for HBc (green) was performed. Images were taken using a Leica SP8 confocal microscope. Maximum intensity Z projection of is shown. Scale bars represent 10 μ m.

To summarize this chapter, we incorporated different amino acids into HBc protein at 11 pre-selected positions in context of a replication competent HBV 1.1mer. We were able to rescue full-length HBeAg and HBc expression using all tested amino acids. Unfortunately, incorporation of ncAA with large ring structured side chains did not allow virion secretion (Table 3.1). Virus production was partially rescued after incorporation of CpK, a less reactive amino acid with a smaller ring structure, and infectivity was observed after replacing amino acids S26, W62, or T67. However, the virus yield remained extremely low and only very few HBsAg-positive cells could be detected after infection. Finally, incorporation of PrK at position T67 resulted in improved virus production and secreted infectivity. We were able to use CuAAC click chemistry labelling to specifically fluorescently label HBV-T67PrK particles

inside HepG2-NTCP cells. Uptake of HBV-T67PrK was efficiently reduced by heparin treatment, indicating double positive fluorescent puncta were derived from virions.

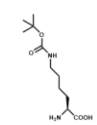
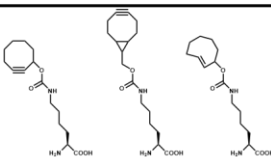
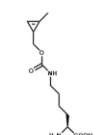
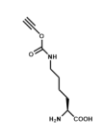
	Labelling	Incorporation into HBc	Virion secretion	Infectivity
BOC 	-	+	+++	++
SCO BCN TCO* 	+++	+	(+)	-
CpK 	+	+	++	+
PrK 	CuAAC	+	+++	++

Table 3.1. Properties of different ncAA regarding incorporation into HBV nucleocapsids.

3.3. Incorporation of TCO* at the HDV amber/W site for click chemistry labelling

HDV only has one ORF which encodes HDAg, which comes in two variants, S- and L-HDAg. The HDAg mRNA is directly transcribed from the incoming HDV genome (Figure 3.24). This mRNA encodes the S-HDAg which is conveniently terminated by an amber stop codon. During the course of viral replication, the adenosine in the stop codon position will be edited to an inosine by the cellular enzyme ADAR1. This editing event occurs in the HDV antigenome and replaces the amber stop codon (UAG) with a tryptophan codon (UGG). Translation from this ORF gives rise to L-HDAg which has a C-terminal extension of 19 amino acids. In this project, we take advantage of the natural amber stop codon of the HDAg. Hereby, we aim to apply the amber suppression system to the HDAg mRNA before editing occurs and incorporate the ncAA at the site of the amber stop codon (amber/W site). This would result in a L-HDAg in which the tryptophan (W) is replaced by the ncAA.

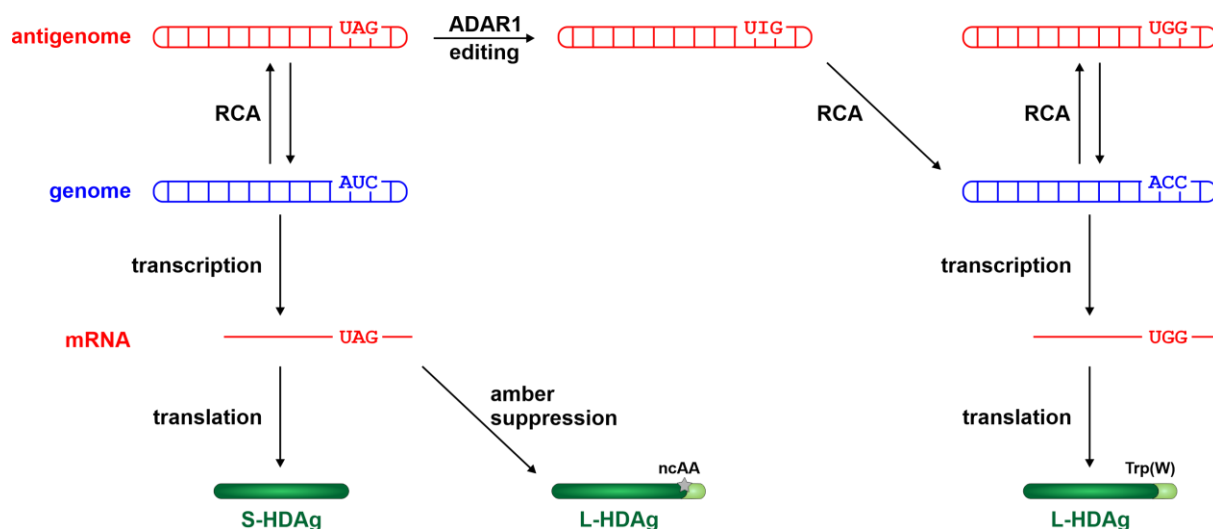


Figure 3.24. L-HDAg generation through editing or amber suppression. The incoming negative sense HDV genome (blue, left) is replicated through rolling circle amplification (RCA) with the antigenome (red) as an intermediate. HDAg mRNA is transcribed from genomic RNA and thus has the same sequence as the antigenome. At early stages of infection, HDV mRNA is terminated by an amber stop codon and translates into the S-HDAg required for replication. With ongoing replication, ADAR1 mediated editing at the amber/W occurs, giving rise to edited (anti)genomes and mRNA translating into L-HDAg. Alternatively, L-HDAg can be induced by amber suppression mediated incorporation of ncAA at the amber stop codon of unedited HDV mRNA resulting in L-HDAg with the tryptophan replaced with a ncAA.

The incorporation of ncAA into L-HDAg was examined by co-transfection of Huh7 cells. Next, TCO* containing HDV virions were produced and tested for their infectivity. To confirm that TCO* incorporation did not affect infectivity, we generated an HDV variant in which every L-HDAg contained TCO* instead of tryptophan. Finally, TCO* was click labelled with SiRTet in transfected cells and in purified virions.

3.3.1. Incorporation of TCO* at the HDV amber/W site

3.3.1.1. Amber suppression induces the expression of L-HDAg

To investigate amber suppression at the natural amber stop codon of the S-HDAg ORF, we used three plasmids that express the different forms of HDAg. The first plasmid encoded only S-HDAg without the downstream sequence of L-HDAg. The second plasmid was an imitation of HDV mRNA after ADAR1 editing and expressed the L-HDAg ORF in which the amber stop codon was changed to a tryptophan codon. The final plasmid resembled viral HDV mRNA before editing, with the amber stop codon followed by the downstream sequence that would encode the 19 amino acids of the L-HDAg. The C-terminal extension of the L-HDAg allowed us to separate S- and L-HDAg by SDS-PAGE and both proteins could be detected by antibodies specific for S-HDAg. As expected, following transfection with the first plasmid encoding the S-HDAg ORF without the downstream sequence after the amber/W site, cells only expressed S-HDAg but not L-HDAg (Figure 3.25). The L-HDAg expressing plasmid with a tryptophan codon produced two bands with greater molecular size compared to the S-HDAg. The third plasmid, which contained the original HDAg ORF without editing only expressed S-HDAg. ADAR1 mediated editing of the amber stop codon is specific for HDV antigenome and does not act on HDAg mRNA, therefore translation was terminated at the amber stop codon and only S-HDAg was expressed. But amber suppression could very efficiently read over the amber stop codon and induce the production of L-HDAg. The incorporated TCO* could furthermore be labelled with SiRTet, giving rise to two fluorescent bands at the expected molecular size of L-HDAg.

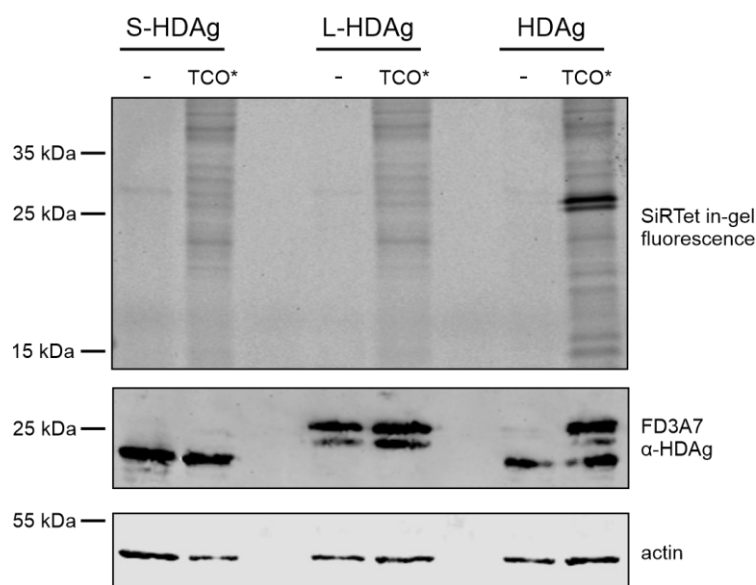


Figure 3.25. Incorporation of TCO* into the L-HDAg. Huh7 cells were co-transfected with pNESPylRS^{AF}/4×tRNA^{Py1} and either pS-HDAg, pL-HDAg, or pHDAg. TCO* was added on day 2 post transfection and on day 4 cells were washed extensively and labelled with SiRTet. After labelling the cells were lysed and run on SDS-PAGE. The gels were scanned using the 700 nm channel of an Odyssey imaging system to detect fluorescence from incorporated SiRTet. The gel was then transferred for western blot analysis with antibodies specific for HDAg and actin.

3.3.1.2. L-HDAg with incorporated TCO* can be click labelled in live cells

We then tested the ambers suppression potential in context of viral replication. The plasmid pJC126 encodes an overlength antigenome sequence of HDV genotype 1 (Gudima et al. 2002). Transfection of Huh7 cells with pJC126 resulted in expression of HDAg and replication of the HDV genome. This plasmid encodes an amber stop codon at the amber/W site, therefore it mostly expressed S-HDAg at early timepoints after transfection (Figure 3.26A). With ongoing replication, ADAR1 mediated editing of the stop codon drove the expression of L-HDAg and increasing levels of L-HDAg could be observed over time. In the presence of TCO*, the amber suppression system could act on the amber stop codon that terminated S-HDAg translation. This was particularly visible at early timepoints, when a distinct increase of intracellular L-HDAg expression levels could be observed compared to cells without TCO* (Figure 3.26A). The L-HDAg population was probably a mixture of ADAR1 and amber suppression mediated protein extension. Over time, an increasing proportion of the L-HDAg levels was derived from edited HDV RNA instead of amber suppression. Consistently, the difference in L-HDAg levels with and without TCO* incorporation diminished over time.

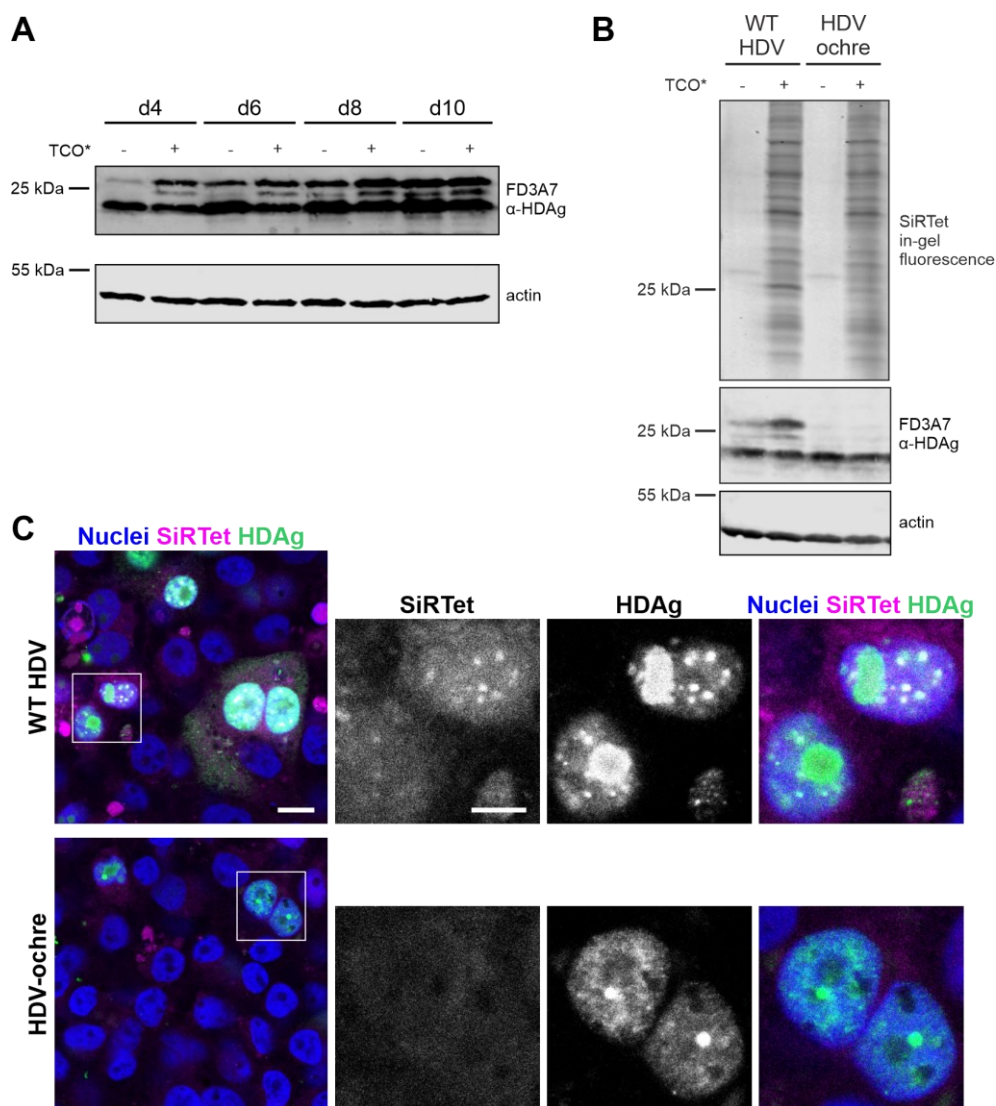


Figure 3.26. Incorporation of ncAA into the L-HDAg in context of HDV replication. Huh7 cells were co-transfected with pJC126 and pNESPylRS^{AF/4}×tRNA^{Pyl}. TCO* was added to the cell culture supernatant 2 days post transfection. **(A)** Cell lysates were collected on day 4, 6, 8, and 10 post transfection and subjected to HDAg-specific western blot analysis. **(B)** 4 days post transfection, SiRTet labelling was performed on live cells and detected as in-gel fluorescence after SDS-PAGE. Western blot analysis was performed after in-gel scanning. pJC126-ochre does not produce L-HDAg by neither ADAR1 editing nor amber suppression and was co-transfected as control. **(C)** After labelling with SiRTet (magenta) on day 4, cells were fixed and immunofluorescence for HDAg (green) was performed. Images were taken using a Leica SP8 confocal microscope. Scale bars represent 10 μm (main figure, left) and 5 μm (zoom-in, right).

The incorporated TCO* was successfully labelled with SiRTet. Visualisation of SiRTet labelled proteins in-gel revealed a fluorescent band at the size of L-HDAg (Figure 3.26B). When the amber stop codon was mutated to an ochre stop codon (HDV-ochre), neither ADAR1 nor amber suppression could induce expression of L-HDAg. Consequently, the fluorescent band at the size of L-HDAg was only observed after incorporation of TCO* at the amber stop codon, while the in-gel fluorescence analysis of HDV-ochre displayed background labelling of TCO* associated with cellular components. Co-localisation of SiRTet labelling with HDAg-specific

immunostaining was confirmed by confocal microscopy (Figure 3.26C). SiRTet-positive signals mostly localised inside the nucleus. Larger nuclear structures were positive for HDAG immunostaining but not for click labelling and might represent S-HDAG inside the nucleus. Again, co-staining was not observed when the amber/W was mutated to an ochre stop codon, which abrogates L-HDAG expression altogether.

3.3.2. Incorporation of TCO* into HDV virions

3.3.2.1. Amber suppression mediated induction of L-HDAG enhances HDV secretion

Next, we investigated whether the incorporation of TCO* into L-HDAG affects HDV virion secretion and infectivity of virions. For secretion of virions and subsequent binding to and infection of cells, HDV depends on HBV envelope proteins. Thus, a plasmid expressing the HBV envelope proteins was co-transfected with an HDV overlength antigenome and the amber suppression system (Figure 3.27A). HDV was produced in presence or absence of TCO* and cell culture supernatants were used to infect susceptible Huh7-NTCP cells. In the absence of TCO*, secretion of infectious HDV was detected over the entire time of virus production (Figure 3.27B&C). The amount of secreted infectious particles decreased over time. Addition of TCO* to cell culture supernatants resulted in a massively higher production of infectious HDV. Supernatant collected from day 4-7 was able to infect approximately 4-fold the number of cells when compared to HDV production without TCO*. The enhanced infection rate could be explained by the higher levels of L-HDAG induced by amber suppression at early timepoints of HDV replication. The abundant L-HDAG might drive the assembly of HDV RNPs and subsequent secretion thereof. After 7 days, the supernatants became less infectious and virus production decreased to the same level independent of TCO* incorporation. At these later timepoints of HDV replication, ADAR1 mediated editing at the amber/W site led to high levels of L-HDAG independent of amber suppression (Figure 3.26A). While essential for virion envelopment, L-HDAG is also a potent inhibitor of HDV replication (Chao et al. 1990), explaining the decrease in infectivity over time.

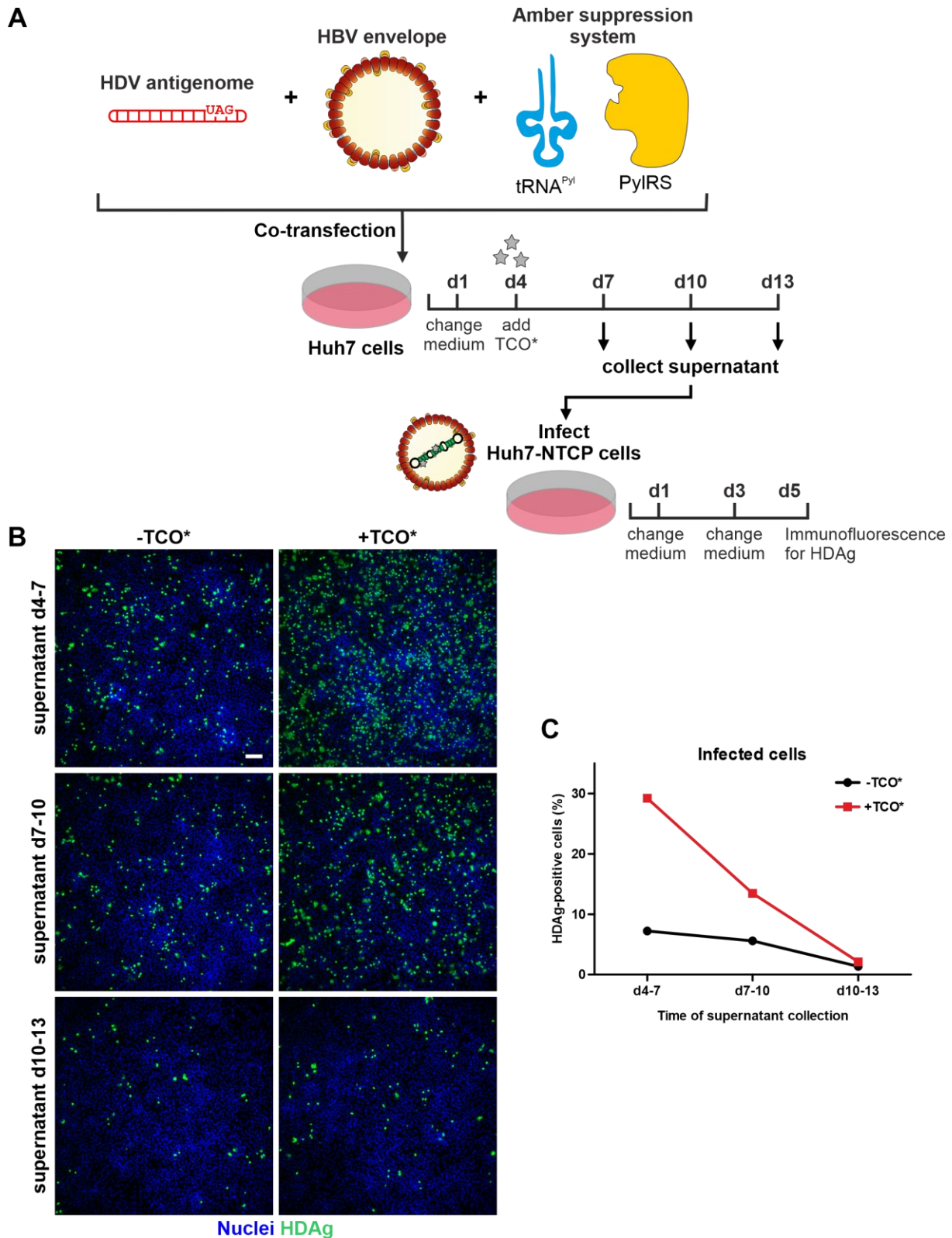


Figure 3.27. HDV secretion in presence of TCO*. (A) Huh7 cells were co-transfected with pJC126, pHB2.7-gtB, and pNESPyIRS^{AF}/4×tRNA^{Pyl}. TCO* was added from 4 days post transfection on and supernatants were collected from day 4-7, day 7-10, and day 10-13. (B) Huh7-NTCP cells were infected with collected supernatants. Cells were fixed 5 days post infection and immunofluorescence for HDAG was performed. (C) Quantification of HDAG-positive cells was performed using the software ilastik (Berg et al. 2019).

3.3.2.2. HDV remains infectious when every L-HDAg is exclusively induced by amber suppression instead of ADAR1 editing

Applying the amber suppression system to virus production with an overlength HDV antigenome expressing plasmid probably led to a mixture of L-HDAg with either TCO* or tryptophan at the amber/W site, derived from amber suppression or ADAR1 editing events, respectively. To ascertain that HDV remains infectious even when every L-HDAg contained TCO* instead of tryptophan, we replaced the amber stop codon with an ochre stop codon (UAA). With this mutant, we expected that neither the amber suppression system nor the ADAR1 editing could act on the stop codon and therefore no L-HDAg would be expressed. To our surprise, L-HDAg was still detected at late timepoints of replication albeit at much lower levels compared to WT HDV (Figure 3.28). The low levels of L-HDAg might have been induced by residual ADAR1 activity on the mutated sequence or possibly random mutation at the ochre stop codon during viral replication. Therefore, a second codon, two positions downstream of the amber/W site, was also mutated to an ochre stop codon (HDV-2×ochre) to entirely shut off L-HDAg production.

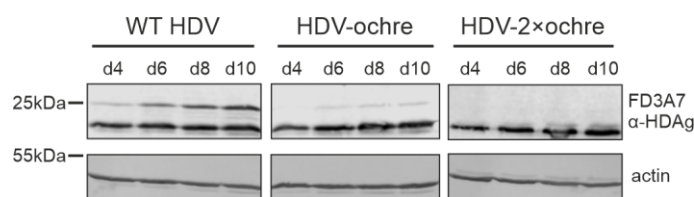


Figure 3.28. L-HDAg expression of HDV ochre mutants. Huh7 cells were transfected with pJC126 (WT HDV), pJC126-ochre (HDV-ochre), or pJC126-2×ochre (HDV-2×ochre). Cell lysates were collected at the indicated timepoints and analysed by HDAg-specific western blot.

As expected, the amber suppression did not act on the HDV ochre variants (Figure 3.29A). While incorporation of TCO* could drive L-HDAg expression during early replication of WT HDV, both ochre variants were resistant to amber suppression and did not display an increased level of L-HDAg in the presence of TCO*. When HDV ochre stop variants were trans-complemented with pHDAG, which encodes the L-HDAg ORF with the natural amber stop codon at the amber/W site, L-HDAg expression was only rescued in presence of the amber suppression system and TCO* (Figure 3.29B). Contrary to WT HDV replication, L-HDAg was mostly present during early timepoints and then levels declined. Expression of L-HDAg was only driven by initial transfection but not by HDV replication and was therefore transient. Furthermore, the early overexpression of L-HDAg might have negatively affected HDV replication. In absence of TCO*, translation of mRNA derived from pHDAG was terminated at the amber stop codon. This system allowed us to evaluate whether TCO* incorporation

impaired HDV secretion or infectivity, because every L-HDAg should have incorporated a TCO* at the amber/W site instead of a tryptophan (Figure 3.29C).

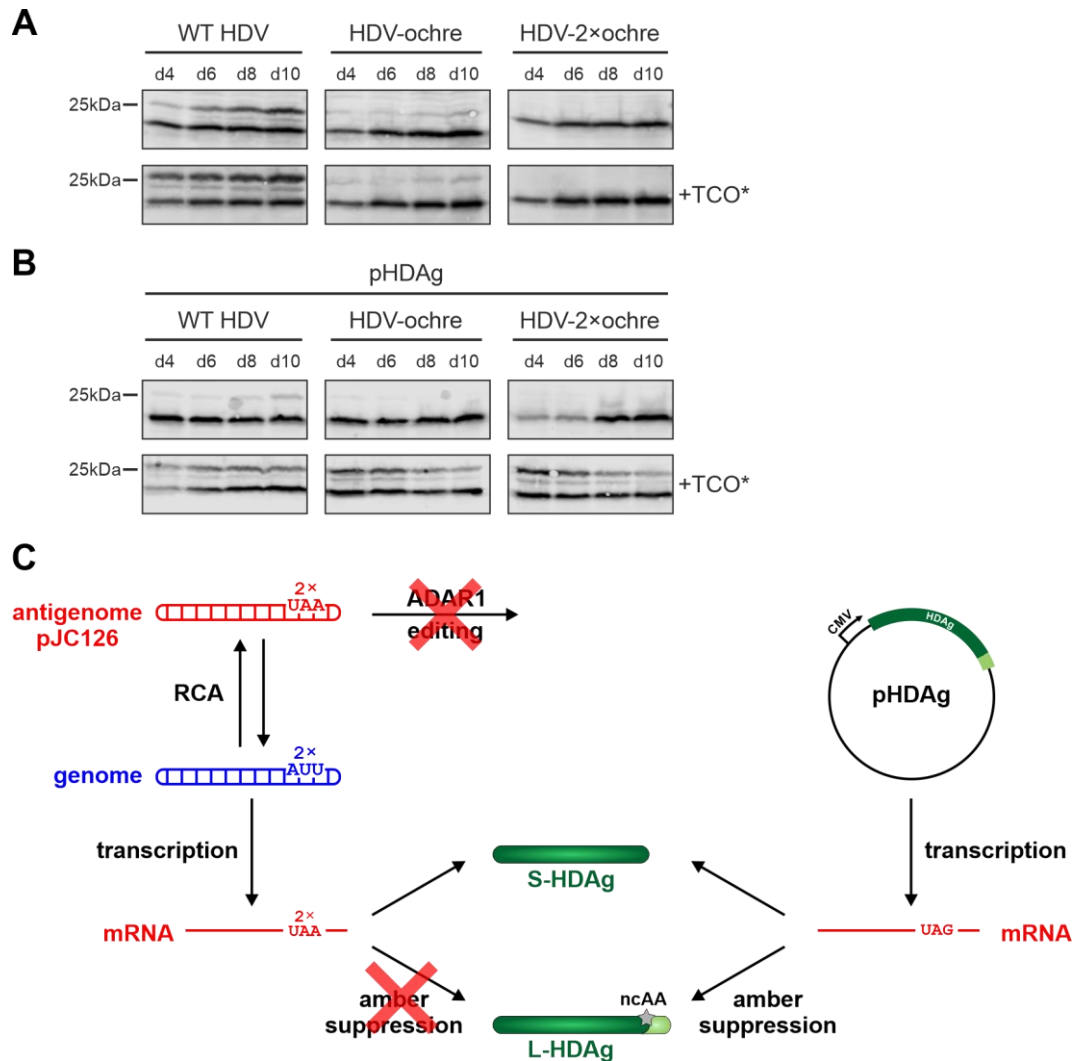


Figure 3.29. Amber suppression in HDV ochre mutants. (A) Huh7 cells were co-transfected with pNESPyIRS^{AF}/tRNA^{PyI} and pJC126 (WT HDV), pJC126-ochre (HDV-ochre), or pJC126-2×ochre (HDV-2×ochre). TCO* was added from day 2 post transfection on and cell lysates were collected at the indicated times. Western blot analysis was performed to detect the expression of S- and L-HDAg. (B) pHDAg was additionally co-transfected with the amber suppression system and the HDV variants. pHDAg encodes the entire HDAg ORF with an amber stop codon at the amber/W site. (C) HDV-2×ochre replication (left) did not result in L-HDAg expression neither by ADAR1 editing nor by amber suppression of the mRNA. Trans-complementation with pHDAg (right) allowed amber suppression mediated production of L-HDAg.

To investigate the functionality of L-HDAg with incorporated TCO*, we co-transfected Huh7 cells with 4 plasmids: pJC126-2 \times ochre to replicate HDV without L-HDAg, pHDAg for HDAg mRNA that can be subjected to amber suppression, an amber suppression vector, and a plasmid expressing the HBV envelope proteins (Figure 3.30A). Supernatant was collected from transfected cells and used to inoculate HDV-susceptible Huh7-NTCP cells. In the absence of an amber stop terminated HDAg mRNA, HDV-2 \times ochre did not produce infectious virus, as expected from the lack of L-HDAg (Figure 3.30B). Only trans-complementation with HDAg mRNA and amber suppression mediated induction of L-HDAg expression could drive the secretion of infectious HDV (Figure 3.30C). However, virus production was strongly reduced compared to WT HDV production with authentic S- and L-HDAg levels (Figure 3.30B). Overexpression of S-HDAg by co-transfection of pHDAg reduced the production of infectious particles in the WT HDV virus production (Figure 3.30C). This observation suggested that HDV remained infectious even if L-HDAg was exclusively expressed from amber suppression. The incorporation of TCO* did not obliterate virus production and tryptophan at the amber/W seemed to be negligible for HDV secretion and infectivity.

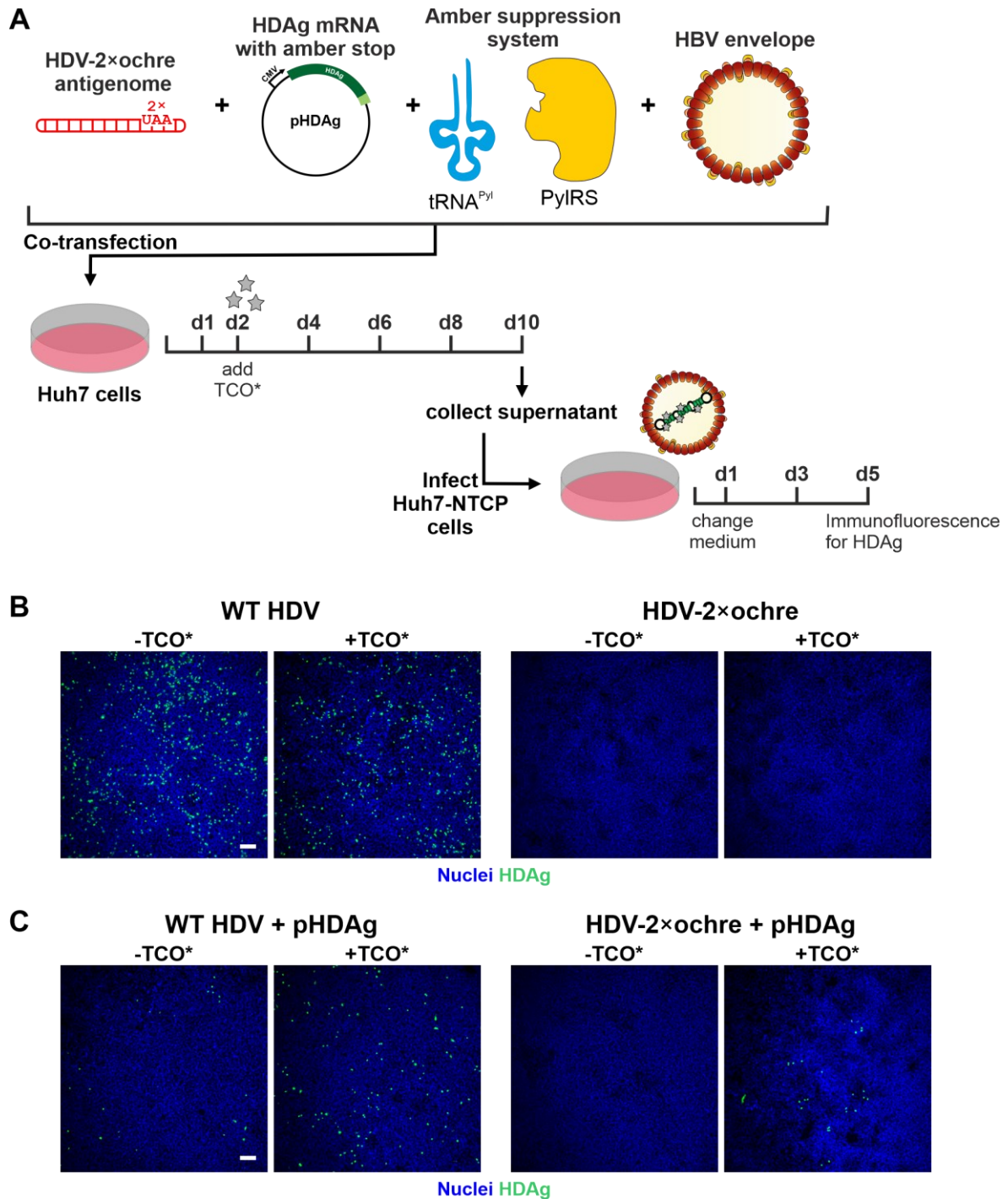


Figure 3.30. Amber suppression mediated L-HDAG expression rescued HDV-2×ochre virion secretion. (A) Huh7 cells were co-transfected with pJC126-2×ochre (or WT control), pHDAg, pNESPyIRS^{AF}/4×tRNA^{Pyl}, and pHB2.7-gtB. TCO* was added from 2 days post transfection on and HDV containing supernatants were collected from day 8-10. 20 μ l of supernatant were used to infect Huh7-NTCP cells in a 96 well format. 5 dpi, cells were fixed and analysed by HDAG-specific immunofluorescence. Cells were infected with supernatant from virus production without (B) or with pHDAg (C), together with pNESPyIRS^{AF}/4×tRNA^{Pyl}, pHB2.7-gtB, and pJC126 (left) or pJC126-2×ochre (right). Scale bars represent 100 μ m.

3.3.3. Production and infectivity of HDV-TCO*

Even though the production of infectious HDV was reduced because of the overexpression of HDAG, the observed infectivity after trans-complementation suggested that HDV was still infectious when all L-HDAG proteins in the virion contained TCO* instead of tryptophan at the amber/W site. To obtain high titres of HDV with TCO* incorporated at the amber/W site (HDV-TCO*), this system was however not well suited. Thus, we decided to collect supernatants at early timepoints of WT HDV replication (Figure 3.31A). During early phases of HDV replication, only few HDV antigenomes would be edited by ADAR1 and the amber suppression system allowed us to drive the expression of L-HDAG. Virions harvested during early timepoints were therefore expected to contain mostly L-HDAG with TCO* instead of tryptophan. The collected supernatant was purified and concentrated by heparin affinity chromatography. HDV containing fractions were eluted by increasing NaCl concentration and tested for HDAG levels. Most of the secreted HDAG was concentrated into elution fractions 2 and 3 resulting in an estimated 60-fold concentration factor compared to the raw supernatant (Figure 3.31B). Equivalent levels of S- and L-HDAG seemed to be present in enveloped and secreted HDV. When Huh7-NTCP cells were infected with fractions from the heparin affinity purification, infection rates of each fraction correlated with secreted HDAG levels (Figure 3.31C&D). After infection with raw supernatant, ~3% of the cells were positive for HDAG. Infection rates were reduced in the flow-through and wash fraction because most of the secreted infectious HDV bound to the heparin column. The first elution fraction was not infectious and probably contained the void volume of the column before elution. Infectivity was highest in elution fractions 2 and 3 with approximately half of the cells positive for HDAG and decreased with later fractions, suggesting most of the secreted infectious HDV was recovered in those two fractions. Treatment with MyrB could efficiently block infection of Huh7-NTCP cells.

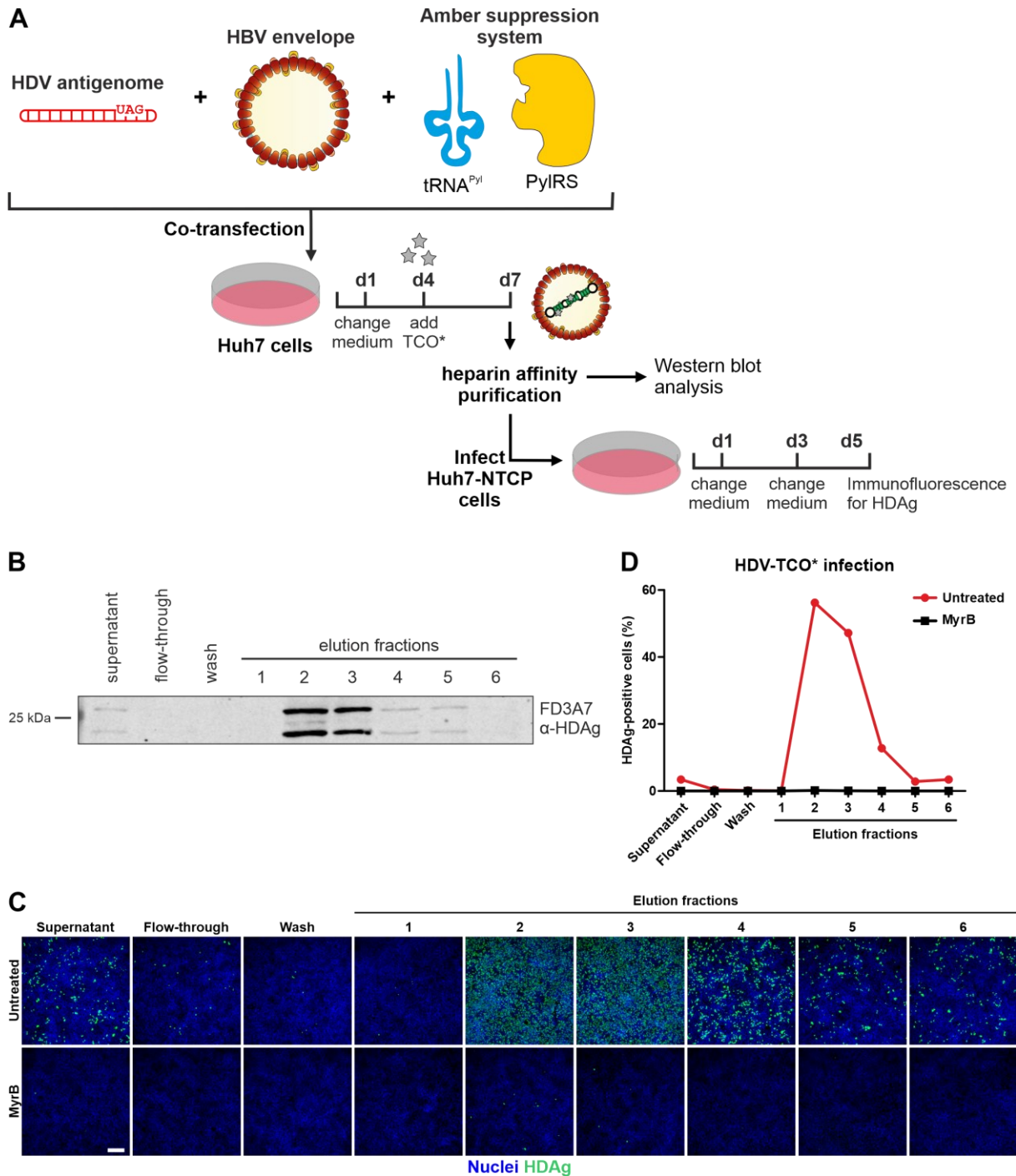


Figure 3.31. Production of HDV with incorporated TCO*. (A) Huh7 cells were co-transfected with pJC126, pHB2.7-gtB, and pNESPyIRS^{AF}/4×tRNA^{Pyl}. TCO* was added 4 days post transfection and supernatant was collected 3 days later. Supernatant was applied to heparin affinity chromatography and eluted with increasing NaCl concentration. (B) Fractions of heparin affinity purification were analysed for HDAg by SDS-PAGE and western blot. (C) Huh7-NTCP cells were infected in a 96 well format with 10 μl of supernatant or fractions. 5 dpi, cells were fixed and analysed by HDAg-specific immunofluorescence. Cells were treated with MyrB to block HDV entry. Scale bar represents 200 μm. (D) The percentage of HDAg-positive cells was quantified using ilastik (Berg et al. 2019).

3.3.4. Labelling of HDV virus particles

This high titre HDV-TCO* virus stock was used to test whether labelling could be performed on virions without affecting infectivity. Elution fractions 2 and 3 of the heparin affinity purification were pooled together and labelled with SiRTet. SiRTet labelled HDV-TCO* (HDV-TCO*-SiRTet) was washed and concentrated again on a centrifugal filter unit, resulting in a ~300-fold concentration compared to the total supernatant collect from transfected cells. A SiRTet signal could be detected as in-gel fluorescence at the size of L-HDAg, indicating that TCO* was successfully labelled inside virions (Figure 3.32A). After labelling with SiRTet, this virus was used to inoculate Huh7-NTCP cells (Figure 3.32B). Infection with this highly concentrated virus preparation resulted in ~70% HDAG-positive cells (Figure 3.32C). The high percentage of infected cells suggests that HDV remains infectious even after most of the enclosed L-HDAg contains TCO* instead of tryptophan and is coupled with a fluorescent dye.

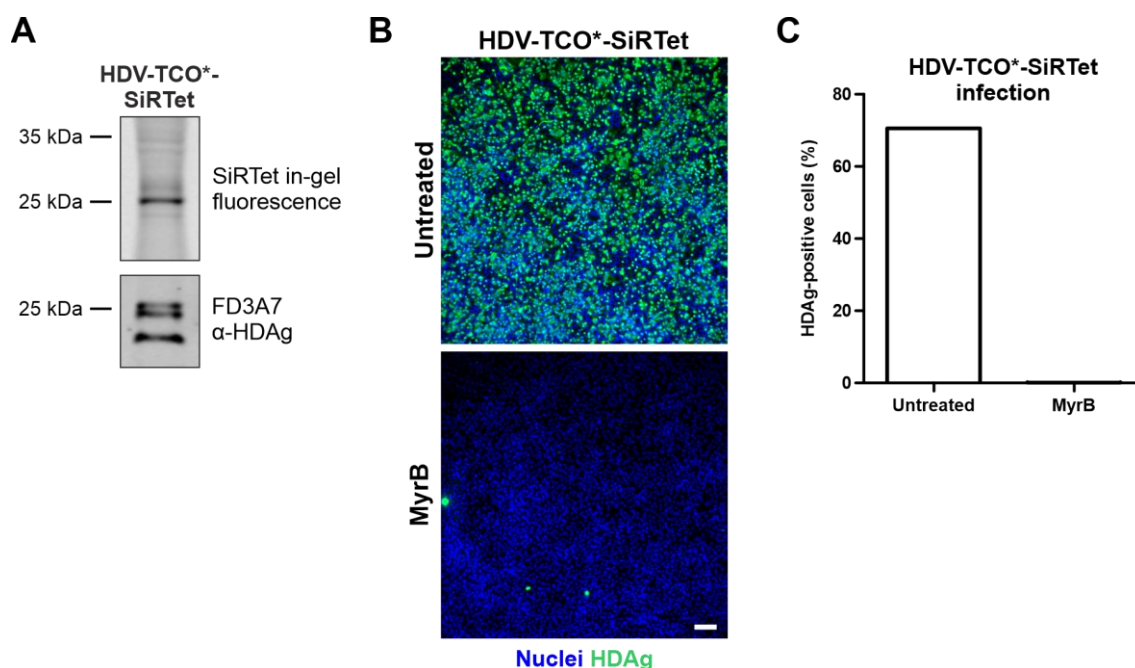


Figure 3.32. Labelling of HDV-TCO*. Elution fractions 2 and 3 of the heparin affinity purification were pooled, labelled with SiRTet, and washed and concentrated on a centrifugal filter unit. **(A)** After labelling, HDV-TCO*-SiRTet was analysed by SDS-PAGE and in-gel fluorescence. The gel was subsequently subjected to HDAG-specific western blot analysis. **(B)** Huh7-NTCP cells were infected in a 96 well format with 10 μ l of labelled and concentrated HDV-TCO*-SiRTet. Cells were fixed 5 dpi and analysed by HDAG-specific immunostaining. MyrB treatment was used to block HDV infection. Scale bar represents 100 μ m. **(C)** Percentage of HDAG-positive cells was quantified using ilastik.

3.3.5. Increased specific infectivity of HDV-TCO*

During a normal production of WT HDV, editing of the amber/W site is required for HDV assembly and secretion, but also results in packaging of edited genomes which are not expected to productively infect cells. Intrigued by the high infection rates by HDV-TCO* (Figure 3.31C) and the earlier secretion of infectious HDV (Figure 3.27C) mediated by amber suppression, we hypothesised that the early induction of L-HDAg by ncAA incorporation could mediate secretion of more unedited genomes, resulting in an increased specific infectivity. To test if HDV-TCO* was indeed more infectious, Huh7-NTCP cells were infected with HDV-TCO* and HDV2103 (a virus stock prepared by co-transfection of Huh7 cells and heparin affinity purification). Infection rates were low with low amount of virus stock HDV2103 (0.1 μ l) and increased when 5-fold higher amount of inoculum (0.5 μ l) was used (Figure 3.33). Further increase in inoculum (2.5 μ l) drastically reduced the number of HDAg-positive cells, suggesting a self-limiting infection at very high mge. This could not be observed when cells were infected with equal amounts of viral genomes of HDV-TCO*. The number of HDAg-positive cells increased with HDV-TCO* inoculum.

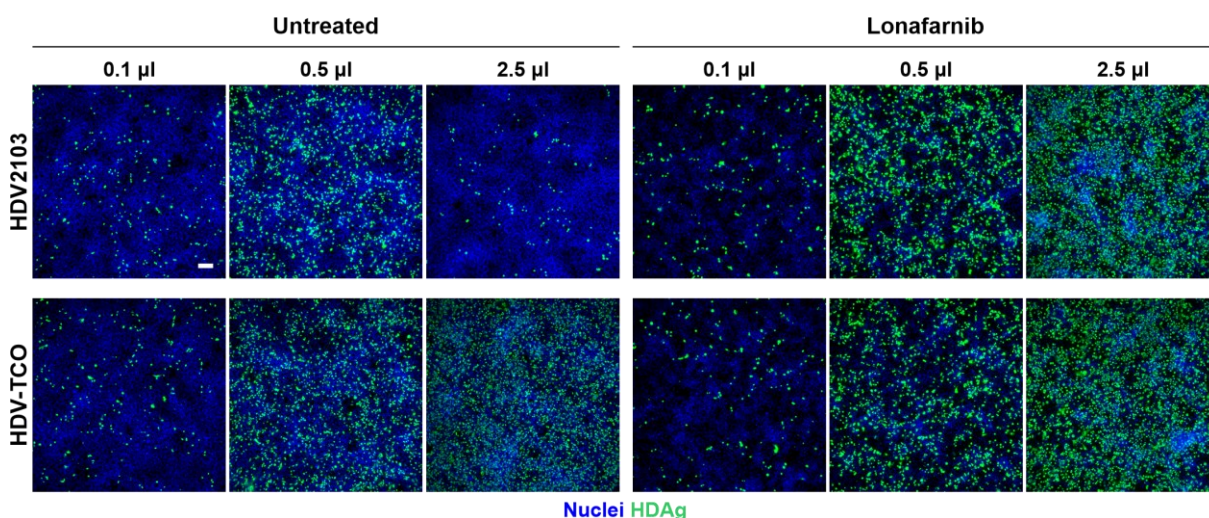


Figure 3.33. Specific infectivity of HDV-TCO*. Huh7-NTCP cells were infected with the virus stock HDV2103 or HDV-TCO* in a 48 well plate. The number of viral genomes was analysed by qPCR before equal amounts of viral genomes of both viruses were used as inocula. Cells were fixed 5 dpi and analysed by HDAg-specific immunostaining. Treatment with 2 μ M lonafarnib was maintained from 2 h before infection until 5 dpi. Scale bar represents 100 μ m.

This finding suggested that incoming edited HDV genomes, which are present in higher levels in a normal virus stock preparation compared to HDV-TCO*, might inhibit HDV replication. In addition to not being replication-competent, edited genomes might suppress replication of unedited HDV genomes by the immediate expression of L-HDAg upon infection. This effect was only observed when cells were infected with high viral inocula and consequently most cells

would be infected with multiple viruses. To test if L-HDAg was responsible for the suppression of HDV replication, cells were treated with the farnesyl transferase inhibitor lonafarnib. Farnesylation at the C-terminus of L-HDAg is required for the negative regulation of HDV replication (Hwang and Lai 1994). Indeed, the self-limiting infection at high mge was overcome with lonafarnib treatment (Figure 3.33). Inhibition of L-HDAg farnesylation resulted in increasing numbers of HDAg-positive cells with increasing inocula of HDV2103. At low inoculating doses, lonafarnib treatment could not increase the infection rate, presumably because only few cells were simultaneously infected with unedited and edited HDV genomes. The effect of lonafarnib treatment was less prominent in HDV-TCO* infected cells, as HDV-TCO* did not display a self-limiting infection in the absence of lonafarnib.

In summary, the intrinsic amber/W site of HDV provided a convenient system for incorporation of ncAA. Amber suppression mediated incorporation of ncAA induced the expression of L-HDAg and earlier secretion of HDV. The early secretion led to a higher ratio of unedited genomes, which resulted in an increased specific infectivity of HDV. Furthermore, L-HDAg with incorporated TCO* was click labelled intracellularly and in purified virions. Click labelled HDV-TCO* provides a promising tool to visualise HDV entry and RNP trafficking.

4. Discussion

4.1. Newly produced HBc does not contribute to cccDNA maintenance or expression

The contribution of *de novo* synthesised HBc to the maintenance of HBV persistence was investigated in this project. Newly formed nucleocapsid were hypothesised to be reimported into the nucleus, where they would replenish intracellular cccDNA. As cccDNA levels remain stable over long-term infections, this would implicate a continuous turnover of cccDNA.

To test the intracellular amplification of cccDNA, we generated an HBc-deficient HBV, that cannot initiate nucleocapsid production. We confirmed that an HBV genome deficient for HBc production could be rescued by trans-complementation with WT HBc (Qi et al. 2016). Trans-complementation could produce infectious but replication-deficient HBV. Moreover, we demonstrated that the incoming virus was sufficient to form and maintain cccDNA in the absence of newly synthesised HBc. *De novo* produced HBc and by extension *de novo* produced rcDNA were not required for the maintenance of cccDNA for at least nine weeks. Furthermore, the transcriptional activity of cccDNA was not affected by the absence of *de novo* HBc. Our findings suggest that cccDNA is highly stable after formation without replenishment by reimport of newly formed nucleocapsids. Therefore, cccDNA levels in *in vitro* infection closely resemble the static model of cccDNA maintenance (Figure 4.1).

Static model of cccDNA

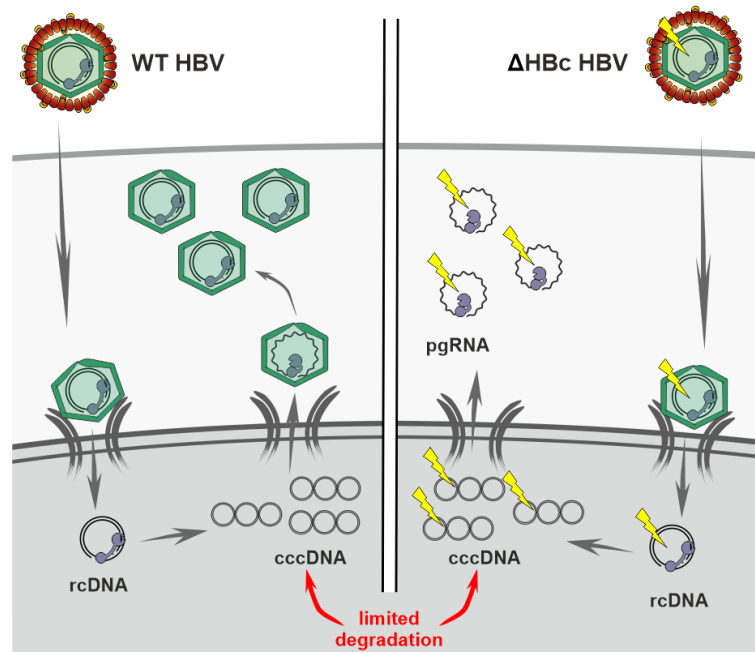


Figure 4.1. Static model of HBV cccDNA maintenance. cccDNA is formed upon the initial infection of previously uninfected cells. WT HBV infected cells (left) produce rcDNA containing capsids, whereas Δ HBc HBV infected cells (right) cannot form nucleocapsids and by extension reverse transcription from pgRNA to rcDNA does not occur. cccDNA molecules are highly stable and do not depend on replenishment.

4.1.1. cccDNA is maintained in the absence of *de novo* HBc

To examine the role of newly synthesised nucleocapsids during HBV infection, we generated and characterised Δ HBc HBV. Cells infected with Δ HBc HBV did not express HBc or secrete HBeAg, and the intracellular HBV DNA levels were reduced, because nucleocapsid formation is required for reverse transcription of pgRNA to rcDNA. WT and Δ HBc HBV infections resulted in similar levels of cccDNA, HBV DNA integration, intra- and extracellular HBsAg, and viral RNA. Long-term infections of HepG2-NTCP cells showed that *de novo* HBc (and, by extension, nucleocapsids and rcDNA) were not required to maintain HBV cccDNA copy numbers (Figure 3.5).

The static model of cccDNA maintenance is consistent with studies in a humanised mouse model in which no intracellular cccDNA amplification could be detected. Infected mice were treated with the entry inhibitor MyrB to block extracellular spread, meanwhile allowing production of nucleocapsids (Volz et al. 2013; Allweiss et al. 2018b). However, increase of cccDNA in infected cells could not be observed, suggesting that the intracellular replenishment of cccDNA may be inefficient in HBV infection. Similarly, treatment with NUCs during or

after infection did not affect cccDNA levels in cell culture experiments (Qu et al. 2018; Tu et al. 2020b).

These as well as our findings are consistent with clinical observations in patients treated with reverse transcriptase inhibitors. Substantial cccDNA reduction was only achieved after several years of treatment with NUCs (Werle-Lapostolle et al. 2004; Lai et al. 2017), emphasising the enormous stability of cccDNA. The loss of cccDNA is most likely driven by turnover of infected liver cells, while NUC treatment inhibits the spread to naïve cells. In addition, immune-tolerant HBV patients display low quasispecies variation despite high levels of HBV DNA (Homs et al. 2014), consistent with the static model that proposes a marginal role of intracellular cccDNA replenishment. Higher quasispecies complexity was found after HBeAg seroconversion, suggesting HBV variation requires hepatocyte turnover and subsequent infection of hepatocytes.

The dynamic model of intracellular cccDNA replenishment is based on observations in the related DHBV model. Reimport of nucleocapsid was reported to critically amplify cccDNA levels in DHBV-infected cells (Wu et al. 1990). In chronically infected ducks, most nuclei contain 1-17 cccDNA molecules, while 10% of the cells contain higher levels of cccDNA with fluctuation up to more than 36 cccDNA copies per cell (Zhang et al. 2003). cccDNA numbers were controlled by DHBV envelope proteins which direct viral nucleocapsids to the secretory pathway. In the absence of envelope proteins, reimport of nucleocapsids dramatically increased cccDNA levels (Summers et al. 1990). Investigation of the envelope-deficient background in HBV showed that the increase in cccDNA levels was less pronounced compared to DHBV which could generally produce more cccDNA molecules than HBV (Sprinzl et al. 2001; Kock et al. 2010). The discrepancy between avian DHBV and human HBV in terms of cccDNA amplification was driven by the virus, not the host cell (Kock et al. 2010). However, the molecular determinants of the differences remain unclear. HBV replication in an envelope-deficient background resulted in an accumulation of protein-free rcDNA instead of cccDNA, suggesting that the repair of rcDNA to cccDNA is the rate-limiting step of cccDNA amplification in humans (Gao and Hu 2007; Guo et al. 2007). HBV might have compensated for the lower cccDNA copy numbers by the acquisition of the HBx protein which is missing in DHBV. HBx protein inhibits silencing of cccDNA and therefore lower levels of cccDNA are required for sufficient expression of viral antigens (Decorsiere et al. 2016).

4.1.2. *De novo* expressed HBc does not alter HBV transcription

In addition to the neglectable role of newly produced nucleocapsids in cccDNA amplification, our long-term infection experiments showed that *de novo* synthesis of HBc was not required to maintain transcription from cccDNA. Δ HBc HBV infected cells expressed pregenomic and subgenomic HBV RNAs at comparable levels to WT HBV infection (Figure 3.6). Furthermore, HBsAg levels remained stable for more than 60 days, suggesting that abrogation of *de novo* synthesis of HBc did not considerably influence the transcriptional activity of cccDNA or the stability of viral transcripts.

Similar observations were made in transfection experiments in HepG2 cells with Δ HBc HBV genomes which indicated that HBc was not required for transcription of viral RNAs (Zhang et al. 2014). Using a similar Δ HBc HBV infection assay as reported here, Qi et al. investigated the role of HBc in cccDNA function (Qi et al. 2016). Consistent with our findings, HBsAg was expressed at similar levels after up to three weeks post infection in HepG2-NTCP cells.

This was contradictory to previous findings for HBV and in the avian DHBV model. Schultz and colleagues generated a core protein deficient virus in the DHBV model not unlike our Δ HBc HBV (Schultz et al. 1999). As Δ HBc HBV, the core deficient DHBV could form cccDNA in primary duck hepatocytes, albeit at much lower levels compared to WT DHBV, which could amplify cccDNA by intra- and extracellular replenishment. Transcription levels of viral RNAs were substantially lower after infection with the core deficient virus when compared to infection with WT virus. WT DHBV infected cells still expressed more viral RNAs when treated with a viral polymerase inhibitor to control for replenishment of cccDNA (and by extension transcription of viral RNAs from additional cccDNA). These findings suggested an important role for the DHBV core protein in transcription from cccDNA.

For human HBV, HBc was found to specifically associate with nuclear cccDNA mini-chromosomes by electron microscopy and chromatin immunoprecipitation studies and suggested to reduce the spacing between nucleosomes on cccDNA (Bock et al. 2001; Pollicino et al. 2006). In HBeAg-positive patients, nuclear distribution of HBc was associated with the first phase of HBV infection, the immune tolerant phase which exhibits high levels of viral replication (Chu and Liaw 1987). A shift to cytoplasmic accumulation of HBc was observed in the immune active phase of HBeAg-positive CHB, suggesting a replication enhancing function of nuclear HBc. In liver biopsies of CHB patients, HBc was associated with a CpG island on

cccDNA and suggested to maintain a permissive epigenetic state through hypomethylation of the CpG island (Guo et al. 2011).

The interaction between HBc and cccDNA was further described by trans-complementation assays of an HBc-deficient plasmid derived circular monomeric HBV DNA (Chong et al. 2017). Mutations in the C-terminal domain of HBc disrupted the binding to cccDNA and resulted in decreased expression from the recombinant cccDNA. The authors suggested that HBc recruits histone acetyltransferases to promote an epigenetically permissive state of cccDNA. Similar findings were obtained recently in *in vitro* infection systems and in human liver chimeric mice. Histone acetyltransferase 1 was recruited to cccDNA nucleosomes by HBc and the long non-coding RNA HULC (Yang et al. 2019). On the other hand, HBc could also assist targeting of the methyltransferase PRMT5 to cccDNA, which resulted in histone methylation and repression of viral transcription (Zhang et al. 2017), suggesting multiples roles of HBc in controlling the epigenetic state of cccDNA. Furthermore, treatment with capsid inhibitors post infection has been reported to reduce the transcriptional activity of cccDNA (Belloni et al. 2015; Lahlali et al. 2018).

Our results however suggest a neglectable function of HBc regarding transcriptional control of cccDNA. We cannot exclude that incoming HBc remains associated with cccDNA and contributes to its formation and transcription. The incoming HBc molecules might be sufficient to establish an epigenetically active state which could be further maintained by the activity of HBx. However, we and others have previously observed that hepatoma cells express HBeAg following transfection with deproteinated rcDNA extracted from HBV virions (Tu et al. 2019; Wei and Ploss 2020). Presumably, cccDNA formation is required for expression of HBeAg, which suggests that the lack of incoming HBc was not crucial for the establishment of transcriptional activity from cccDNA. To test if cccDNA can remain transcriptionally active in the total absence of HBc, it would be interesting to transfect cells with deproteinated rcDNA extracted from Δ HBc HBV.

4.1.3. Advances in molecular tools

The recently developed cinqPCR method for quantification of cccDNA was applied here to monitor cccDNA levels during long-term infection (Tu et al. 2020b). Unlike other qPCR-based methods (Luo et al. 2017; Qu et al. 2018), this method does not require exonuclease digestion of double-stranded DNA, allowing normalisation with a cellular reference gene. With the improved precision of this assay, we could detect small changes in cccDNA levels relative to

the total cell number. These findings suggest that cinqPCR is a promising tool to study novel treatments targeting cccDNA.

As second important prerequisite, the HepG2-NTCP cell line used in our group (Ni et al. 2014) was able to maintain HBV infection for at least nine weeks. Infection with Δ HBc HBV cannot spread via an extracellular pathway after the initial infection, because HBc is required to newly synthesise virions. However, extracellular spread of HBV or secretion of viral particles after infection have not been observed using this cell clone of HepG2-NTCP (Konig et al. 2019). Other HepG2-NTCP clones have been reported to facilitate extracellular spread after infection. Michailidis et al. generated a HepG2-NTCP clone that secreted infectious HBV seven days after infection and HBV spread was observed when 4% PEG was continuously maintained in the medium during the entire experiment (Michailidis et al. 2017). Spread of infection could be inhibited by MyrB and NUCs, suggesting the spread was mediated by viral replication and NTCP dependent entry of uninfected cells. König and colleagues reported a slow-proliferating HepG2-NTCP clone that efficiently secreted progeny virus leading to amplification of cccDNA levels through an extracellular route and infection of naïve cells (Konig et al. 2019). cccDNA levels were efficiently reduced by long-term treatment with NUCs and anti-HBsAg antibodies, indicating that cccDNA amplification was predominantly mediated by extracellular spread but not reimport of nucleocapsids. Similarly, Ko et al. selected a highly permissive HepG2-NTCP clone and observed extracellular spread of HBV infection (Ko et al. 2018). Interestingly, a reduction of cccDNA levels was observed following DMSO withdrawal after establishment of infection, suggesting DMSO-induced differentiation of hepatoma cells is crucial not only for expression of viral antigens but also for cccDNA stability. However, in long-term infection experiments, cccDNA was reduced when cells were treated with reverse transcriptase inhibitors, suggesting cccDNA maintenance was less stable compared to the HepG2-NTCP clone used in this study.

4.1.4. Virological and clinical implications

Our findings suggest that the total number of cccDNA molecules per infected cell might be limited and once cccDNA is established, the high stability of cccDNA does not allow nor require further formation of cccDNA. Indeed, *in vitro* infection experiments using very high multiplicities of HBV per cell could not further increase the number of cccDNA molecules per cell or the expression of viral antigens (Schulze et al. 2012; Qu et al. 2018). A precise quantification of cccDNA is difficult to achieve, however most studies reported around

1-10 cccDNA copies per infected cell. This range of cccDNA level was determined in *in vitro* infected HepaRG and HepG2-NTCP cells (Hantz et al. 2009; Qu et al. 2018; Ko et al. 2018) and in the stably transfected HepAD38 cell line (Gao and Hu 2007). The HepAD38 cells, used for HBV production in many laboratories, express many viral markers (including cccDNA) only upon induction (Ladner et al. 1997). cccDNA formation in HepAD38 cells is efficiently inhibited by treatment with capsid or reverse transcriptase inhibitors (Wu et al. 2013), suggesting cccDNA levels are established by reimport in these cells as the lack of NTCP expression does not enable extracellular spread. Nevertheless, intracellular replenishment in these cells, which express high levels of viral markers, does not result in substantially higher levels of cccDNA copy numbers. Similar copy numbers of cccDNA per cell were detected in HBeAg-positive patients and generally declined with disease progression (Bourne et al. 2007; Laras et al. 2006; Werle-Lapostolle et al. 2004; Liang et al. 2016). A study of acute HBV infection in chimpanzees also detected ~10 cccDNA copies per cell at the peak of acute infection, when almost every hepatocyte is HBV-positive (Wieland et al. 2004).

Given that reimport of nucleocapsids can form cccDNA in HBV transfected and in cell lines that stably express the HBV genome (Kock et al. 2010; Ladner et al. 1997), the possibility of intracellular cccDNA replenishment in infected hepatocytes cannot be ruled out. However, the regulation of cccDNA copy numbers and our evidence of extremely stable cccDNA suggest that reimport of nucleocapsids might only be a salvage pathway to rescue occasional degradation of cccDNA, for example by nuclease activity. A dynamic model with constant degradation and replenishment of cccDNA seems unlikely.

Like cccDNA formation, HBV DNA integration into the host genome requires nuclear entry of nucleocapsids. Consistent with our proposed model of marginal reimport, HBV DNA integration is predominantly driven by the initial infection (Tu et al. 2018). Concordantly, analysis of patient liver samples showed that HBV DNA integration occurred early during infection in chronic and acute HBV infected individuals (Mason et al. 2016; Kimbi et al. 2005).

The static model of cccDNA maintenance suggests that cccDNA is predominantly formed by infection of previously uninfected cells, but not by replenishment in the same cell. This has clinical implications on the emergence of NUC-resistant HBV variants in patients. NUC-resistant variants must infect a new hepatocyte to be established in the liver. Inhibition of virus entry could therefore efficiently prevent the emergence of variants including resistance to NUCs (Revill et al. 2020).

Long-term treatment with NUCs has resulted in reductions of cccDNA numbers in CHB patients (Werle-Lapostolle et al. 2004; Lai et al. 2017). Our data suggest that this effect was likely a result of suppression of virions production and new infection rather than inhibition of intracellular cccDNA replenishment. The reduction of cccDNA may be caused by liver turnover, as cccDNA is lost in large parts following hepatocyte proliferation (Allweiss et al. 2018b). Thus, to achieve elimination of cccDNA as prerequisite for a complete cure from CHB, a combined approach is required. First, to eliminate established cccDNA, either direct killing of infected hepatocytes or liver turnover could be achieved by an activation of immune cells. Second, the formation of new cccDNA should be inhibited by preventing hepatocyte infection with an entry inhibitor or by blocking the production of new virions using NUCs or capsid inhibitors.

4.1.5. Limitations and future work

In our *in vitro* system, we could investigate the intracellular maintenance of cccDNA, but turnover of cells as well as the extracellular spread of HBV were limited. We tested the loss of cccDNA during cell mitosis by serial splitting of infected HepG2-NTCP cells (data not shown). These experiments suggested that cccDNA was almost completely lost following cell division. This was consistent with serial transplanting of HBV-infected hepatocytes in humanised mice (Allweiss et al. 2018b). However, HBV cccDNA may survive in rare non-dividing hepatocytes. The potential role of these non-dividing cells in reactivation of occult HBV infections needs to be further investigated in the future.

The Δ HBc HBV described in this thesis could be applied to investigate the role of HBc in IFN- α mediated degradation of cccDNA. Lucifora et al. suggested that the cytidine deaminase APOBEC3A interacts with HBc to be targeted to cccDNA (Lucifora et al. 2014). Therefore, IFN- α treatment might not affect cccDNA levels in cells infected with Δ HBc HBV.

In conclusion, our findings provide evidence that *de novo* synthesised HBc plays a limited role in cccDNA maintenance. After the initial infection with WT or Δ HBc HBV, cccDNA persists in HepG2-NTCP cells and remains transcriptionally active, independent of *de novo* HBc. The static model of cccDNA maintenance suggests that therapeutic targeting of intracellular capsid reimport might not efficiently reduce cccDNA levels.

4.2. Amber suppression mediated labelling of HBc

As we had confirmed that *de novo* HBc was not necessary for the major steps in HBV replication, we continued by rescuing full-length HBc expression using the amber suppression system. The aim of this project was to incorporate ncAA into HBc for the fluorescent labelling of HBV nucleocapsids. The fluorescent labelling of HBV is particularly challenging. Due to the compact genome organisation and virion structure of HBV, genetic engineering with large fluorescent proteins or peptide tags are unlikely to succeed. Unspecific labelling with chemical dyes targets the viral envelope and requires laborious purification methods to remove excessive SVPs. Our aim was to specifically label HBV nucleocapsids, therefore we applied the amber suppression technology as minimally invasive tagging strategy. Our findings showed that incorporation of ncAA could rescue the expression of full-length HBc and secretion of infectious virions. Using CuAAC, nucleocapsids with incorporated PrK were click labelled in fixed cells. Production of HBV with labelled HBc while preserving infectivity has not been reported previously and provides a new tool to visualise entry dynamics and mechanisms of HBV.

4.2.1. Investigation of HBV entry using click labelling

The incorporation of PrK at position T67 of HBc enabled specific labelling of HBV by CuAAC. For HBV-T67PrK, infectivity was comparable to Δ HBc HBV (Figure 3.19), which we have shown before to be equally infectious as WT HBV. Unfortunately, incorporation of PrK does not allow live cell fluorescent labelling but requires a copper-catalysed click reaction in fixed cells. Nevertheless, HBV-T67PrK enabled tracking of incoming nucleocapsids on their way to the nucleus.

Nucleocapsids were co-stained by click chemistry and HBc-specific immunofluorescence, indicating reliable detection of viral particles. Nucleocapsids were found to localise at the nuclear envelope after two hours. However, at least until eight hours after infection, HBV-T67PrK particles were observed in the cytoplasm and partially still associated with an early endosome marker (Figure 3.21). This is consistent with a recent study that followed synchronised viral uptake and detected accumulation of intracellular HBV DNA over time (Chakraborty et al. 2020). Intracellular HBV DNA was first detected after one hour and peaked at 12 hours post inoculation. Subcellular fractionation showed nuclear import of HBV DNA starting from 3 hours and saturating at 12 hours after infection. At this timepoint when most

viral DNA was found in cytoplasm and nucleus, approximately 22% of the internalised HBV DNA was within the nucleus, suggesting most of the internalised HBV remained distributed in the cytoplasm. Chakraborty et al. detected nuclear cccDNA had formed after 24 hours of infection and identified the conversion of rcDNA to cccDNA as rate-limiting factor during infection, as only less than 1% of the internalised HBV DNA had been repaired to cccDNA.

Using cinqPCR, a method with higher sensitivity for cccDNA detection, we have previously shown that cccDNA formation can be detected within 12-16 h post infection, indicating virus entry and nucleocapsid trafficking towards the nucleus must occur before (Tu et al. 2020b). However, cccDNA levels increased until three days after infection, suggesting that incoming nucleocapsids might stall during different virus entry steps and contribute to cccDNA formation from 12-72 hours after inoculation. Subsequent expression from cccDNA in form of HBV pgRNA/precure RNA was detected 18 hours after infection in PHH and HepG2-NTCP cells (Khakpoor et al. 2019).

Importantly, internalisation of HBV-T67PrK was blocked by treatment with heparin. Cellular uptake of HBV was previously observed independent of NTCP (Sun et al. 2014; Chakraborty et al. 2020), suggesting unspecific internalisation of viral particles which do not productively infect cells. Blocking viral attachment to HSPGs on the other hand can inhibit binding and internalisation of HBV (Schulze et al. 2007). Heparin treatment could reduce intracellular HBV-T67PrK particles which were co-stained by click chemistry and HBc-specific immunofluorescence (Figure 3.23). This finding suggested that dual-positive puncta were indeed specific for HBV nucleocapsids derived from enveloped virions.

We could not observe entry of nucleocapsids into the nucleoplasm. This is consistent with a recent report by Paci and colleagues who have chemically labelled recombinant capsids and incubated them on HeLa cells, which have been mildly permeabilised leaving the nuclear envelope intact (Paci et al. 2020). HBV capsids accumulated at the nuclear envelope but were not observed inside the nucleus, whereas smaller bacteriophage MS2 capsids were seen to accumulate in the nucleoplasm. In contrast, similar experiments using mature HBV capsids derived from virions instead of recombinant HBc showed intranuclear accumulation of HBc (Rabe et al. 2003). When mature capsids were crosslinked by UV irradiation, they could locate to the NPC but did not enter the karyoplasm anymore, suggesting capsids disassemble at the NPC to release the viral genome, followed by translocation of capsid subunits deeper into the nucleus (Schmitz et al. 2010).

4.2.2. Amber stop codon suppression within the HBc ORF

To test if amber suppression could incorporate ncAA into HBc, eleven positions of HBc were selected as possibly suitable sites and mutated to amber stop codons. Incorporation of ncAA rescued HBsAg secretion and intracellular HBc expression at most positions. Differences of amber suppression efficiency at different positions were likely caused by mRNA context effects which are reported to affect the interaction of the stop codon with release factors and tRNAs (Chemla et al. 2018).

Virus assembly was substantially impaired after amber suppression mediated rescue of HBc expression. When using ncAA with large ring structured side chains like TCO*, virus production could not be observed. The application of the smaller CpK could rescue secretion of infectious HBV at positions S26, W62, and T67. Unfortunately, the virus yield was extremely low and not sufficient for further studies. The abrogation of virus assembly by TCO* might be caused by the larger size or the higher reactivity compared to CpK. Even though TCO* is generally orthogonal to cellular molecules, the cyclooctene has a high internal strain and might be reactive when tightly packed in a capsid. Incorporation of a non-reactive isomer of TCO* (cis-cyclooctene) needs to be tested to investigate whether the high reactivity of TCO* affected virus secretion (Nikic et al. 2014).

Genetic engineering with CpK at some other positions also displayed secretion of virions (Figure 3.15), but inoculation of HepG2-NTCP cells did not result in HBsAg-positive cells. Possibly, replacing these amino acid sites with CpK had a deleterious effect on HBV infection but more likely, the virus yield was just too low to detect infections. The HBV DNA dot blot analysis of HBV-D32CpK showed secretion of naked HBV DNA containing capsids but not enveloped virions, suggesting D32CpK inhibited envelopment. Even though alanine mutation at this position allowed secretion of virions, the same mutational screen showed that alterations at the base of the spike affected capsid envelopment (Ponsel and Bruss 2003). Hence, the larger CpK probably interfered with the interactions between envelope and capsid.

4.2.3. Limitations and future work

The incorporation of PrK only allowed CuAAC labelling in fixed cells. For live cell imaging, it would be desirable to produce HBV with ring strained ncAA like TCO* or CpK. Even though the virus yield was low, our findings suggest that CpK incorporation does not abrogate virus production or infectivity. To obtain more CpK engineered HBV, the system for virus production

needs to be optimised. Although transfection of Huh7 cells with overlength HBV genomes can produce functional virions, the virus production is transient and less efficient compared to stably transfected HepG2 cells like HepAD38. Generally, HepG2 cells have been more efficient at producing infectious HBV, but transfection efficiency of HepG2 cells is low. To optimise the yield of HBV-T67CpK, current work is focused on the generation of a stably transfected HepG2 cell line with inducible expression of the T67* HBV genome based on the HepDE19 cell line (Guo et al. 2007). After stable transfection, this cell line can express HBsAg from the endogenous promoter, while precore- and pgRNA are driven by a tetracycline-inducible promoter. When a cell line with inducible high levels of pgRNA encoding an amber stop codon in the HBc ORF is available, the amber suppression NESPylRS^{AF} and multiple copies of tRNA^{Pyl} should be introduced by transduction. AAV-mediated transduction can reach high copy numbers in infected cells and was previously shown to efficiently target hepatocytes (Lempp et al. 2017). Furthermore, AAVs containing the amber suppression PylRS/tRNA^{Pyl} pair have been reported to enable efficient ncAA incorporation (Ernst et al. 2016).

Alternatively, stable cell lines expressing amber suppression components might be better suited for virus production. Although stable amber suppression cell lines are considered to have lower ncAA incorporation efficiency compared to transient transfection, the extended time needed for virus production requires a more long-lived amber suppression. The potential of such a system was exemplified by Si et al., who produced high titres of genetically engineered IAV in stable cells as a live but replication-deficient vaccine (Si et al. 2016).

Here, we provide specific labelling of HBV-T67PrK, but visualisation of a productive infection event might be difficult to achieve. *In vitro* infections require very high mge of HBV (Schulze et al. 2012; Tu et al. 2021), usually hundreds or even thousands of viral genomes per cell. While roughly 22% of internalised HBV DNA could reach the nucleus, less than 1% is converted to cccDNA (Chakraborty et al. 2020). The fate of the excess of incoming nucleocapsids that do not contribute to cccDNA formation or even do not reach the nucleus remains unclear. Nevertheless, genetic encoding of PrK in HBV capsids for the first time enabled specific labelling of HBV while retaining full infectivity.

In conclusion, the labelling of HBV remains highly challenging. The incorporation of large ring structured ncAA was detrimental to virion assembly, whereas incorporation of the smaller CpK resulted in secretion of low amounts of infectious virions. The incorporation of PrK, an ncAA that can undergo CuAAC, at position T67 of HBc could rescue ~5% of virus secretion compared to trans-complementation with WT HBc and displayed a similar infectivity as Δ HBc HBV.

Entry dynamics were investigated with click labelled HBV-T67PrK after infection of HepG2-NTCP cells and were consistent with previously reported time frames of HBV entry. HBV-T67PrK might become a valuable tool to understand dynamics of HBV entry and molecular mechanisms involved in entry and trafficking of nucleocapsids.

4.3. Labelling of HDV ribonucleoproteins

The natural features of HDV replication seemed very advantageous for applying the amber suppression technology. Owing to the amber/W site which discriminates between the two forms of HDAg, it was not required to introduce an in-frame amber stop codon into the HDAg ORF. The incorporation of TCO* at the amber/W site was very efficient and induced the expression of L-HDAg, which in turn promoted secretion of HDV. L-HDAg could be click labelled in live cells and in purified virions, which remained infectious after fluorescent labelling. Our findings imply a self-limiting infection mediated by secreted edited genomes. Furthermore, genetic code expansion was shown to be a powerful method for the fluorescent labelling of HDV without impairment of viral infectivity.

4.3.1. Fluorescent labelling of cellular and virion L-HDAg

The efficient incorporation of TCO* at the amber/W site allowed click chemistry labelling with SiRTet in transfected cells and in purified virions. In-gel fluorescence after SDS-PAGE confirmed that SiRTet specifically labelled L-HDAg but not S-HDAg (Figure 3.26B). Combination of click labelling and HDAg-specific immunostaining in transfected cells revealed S-HDAg localisation to nucleoli, whereas SiRTet signals formed smaller nucleoplasmic sites (Figure 3.26C). Localisation of HDAg to nucleoli was observed previously (Cullen et al. 1995), but the function of nucleolar accumulation of S-HDAg remains unclear. The puncta, which were dual-positive for HDAg-immunostaining and click labelling, are consistent with reported L-HDAg localisation to nuclear speckles (Bichko and Taylor 1996). HDV RNA on the other hand could previously not be detected in nucleoli but co-localised with HDAg in nucleoplasmic foci (Cunha et al. 1998). Another study has suggested association of HDV genomes with paraspeckles which are small foci at the periphery of nuclear speckles (Beeharry et al. 2018). These studies were performed by overexpression of HDV RNA and HDAg and the replication site of HDV during authentic infection remains unknown.

Finally, labelling of HDV with incorporated TCO* was performed using the click chemistry dye SiRTet. As before, labelling was specific for L-HDAg and most importantly the dye could pass the viral envelope without affecting infectivity. After click labelling, HDV-TCO*-SiRTet retained its high specific infectivity. Quantification of HDAg and HDV RNA in sera of infected woodchucks resulted in approximately 200 HDAg molecules per HDV virion (Gudima et al. 2002). The western blot analysis of heparin affinity chromatography purified HDV suggested

that roughly half of the viral HDAG molecules are L-HDAG (Figure 3.31B). Assuming most of the L-HDAG was derived from amber suppression but not from editing events, close to 100 molecules of L-HDAG with incorporated TCO* per virion could be labelled by SiRTet.

Interestingly, Lin et al. used the amber suppression technology to genetically encode ncAA in HBV envelope proteins of HDV particles (Lin et al. 2013). However, they have missed to analyse the incorporation of ncAA at the HDV amber/W site. They have used an experimental setup where HDV was allowed to replicate for 12 days before amber codon mutated HBV envelope proteins and a PylRS/tRNA^{Pyl} pair were transfected together with ncAA addition. Presumably, ADAR1 mediated editing would have already produced large amounts of L-HDAG at this late timepoint of HDV replication, resulting in lower levels of L-HDAG with incorporated ncAA.

4.3.2. HDV secretion and infectivity are enhanced by amber suppression

Genetically encoding an ncAA at the amber/W site could efficiently induce the expression of L-HDAG without an apparent decline in virus production or infectivity. On the contrary, amber suppression mediated expression of L-HDAG was able to drive the virus secretion resulting in earlier and enhanced production of infectious HDV (Figure 3.27).

Strikingly, the early expression of L-HDAG during the production of HDV-TCO* lead to extremely high infection rates with ~70% HDAG-positive cells (Figure 3.32). This number of infected cells exceeded the previously reported saturation limit of infection with HDV produced by transfection or from a stable cell line (Ni et al. 2019). Ni et al. used increasing amounts of HDV inocula and observed a plateau of infection rate at ~20-30% HDAG-positive cells, suggesting HDV-TCO* had a higher specific infectivity compared to the original virus stock.

Usually, production of HDV requires ADAR1 mediated editing to induce the expression of L-HDAG which is required for assembly and secretion of RNPs. Editing events also lead to generation of edited genomes, which contain a CCA codon at the site complementary to the amber/W site, where unedited genomes have a CUA codon. mRNAs transcribed from edited genomes consequently carry a UGG codon at the amber/W site and directly encode L-HDAG, but not S-HDAG. Sequencing of patient sera revealed that ~32% of virions contained an edited genome (Sopena et al. 2018), suggesting edited genomes are efficiently assembled as RNPs and secreted. The role of circulating HDV containing edited genomes remains unclear, however they are not expected to replicate after infection of naïve cells, because mRNA transcribed from

edited HDV genomes cannot express S-HDAg which is required for replication (Kuo et al. 1989). L-HDAg on the other hand is not only unable to support replication but was also observed to potently inhibit HDV replication (Chao et al. 1990).

During production of HDV-TCO*, amber suppression mediated incorporation of TCO* at the amber/W site can drive the expression of L-HDAg before most of the editing can occur. Hence, HDV-TCO* most likely contains more unedited HDV genomes compared to normal virus productions or sera from HDV patients. Infection with HDV-TCO* therefore results less frequently in immediate expression of replication inhibitory L-HDAg.

Importantly, farnesylation at the C-terminus is required to elicit the replication inhibitory effect of L-HDAg (Hwang and Lai 1994). Consistently, treatment with the farnesyl transferase inhibitor lonafarnib could increase intracellular HDAg and HDV RNA levels (Lempp et al. 2019). We were able to confirm this finding by inoculating cells at high doses of HDV, at which lonafarnib treatment led to a pronounced increase in HDAg-positive cells (Figure 3.33). Our results suggest that inhibition of L-HDAg farnesylation can prevent the repression of HDV replication in a subset of cells.

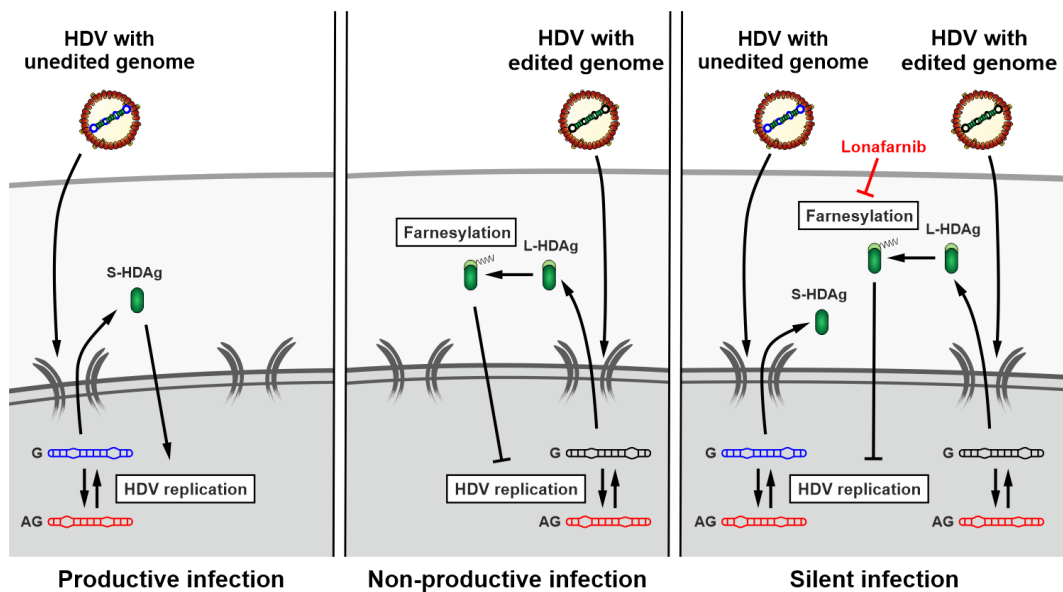


Figure 4.2. Model of self-limiting HDV infection. In cells infected with an unedited HDV genome (blue), S-HDAg is expressed and enhances viral replication, resulting in a productive infection (left). If a cell is infected with an edited HDV genome (black), L-HDAg is immediately expressed. Upon farnesylation, L-HDAg repressed HDV RNA replication, leading to a non-productive infection (middle). When a cell is simultaneously infected with unedited and edited HDV genomes, the expression of L-HDAg may completely repress viral replication, resulting in a silent infection (right). Inhibition of L-HDAg farnesylation by lonafarnib prevents the L-HDAg mediated repression of HDV replication.

Here, we propose a model of self-limiting HDV infection to explain the saturation of HDAg-positive cells when infecting with increasing doses of HDV (Figure 4.2). When cells are

infected with multiple virions which contain unedited and edited genomes, L-HDAg is rapidly expressed from edited genomes and potently inhibits replication of all HDV genomes resulting in silently infected cells. The inhibitory effect of L-HDAg depends on C-terminal farnesylation, hence treatment with lonafarnib prevents silencing of HDV replication. Increase of HDAg-positive cells after lonafarnib treatment was only seen when using high viral titres, suggesting these cells have been infected with multiple virions.

4.3.3. Reversion of ochre stop mutation

Mutation of amber to ochre stop codon at the amber/W site inhibited the induction of L-HDAg, most likely by blocking the recognition by ADAR1. The substrate specificity of ADARs is determined by sequence context, complementary nucleotides, and secondary structures of double-stranded RNA (Thomas and Beal 2017). However, low levels of L-HDAg were observed after amber to ochre stop codon mutation (Figure 3.28), suggesting residual editing activity or mutation of the ochre stop codon. ADAR1 would have to edit both adenosines of the ochre stop codon (UAA) to generate a readthrough of the stop codon. Single nucleotide mutation at the ochre stop could either revert to an amber stop, enabling editing, or produce any amino acid coding triplet in order to induce full-length L-HDAg.

A second ochre stop codon downstream of the first ochre codon could completely abolish L-HDAg expression. However, when two ochre stop codons were mutated at the amber/W site in an HDV genotype 8 expressing plasmid, L-HDAg appeared at low levels and delayed timepoints (data not shown). The HDV genotype 8 clone used in our group was shown to replicate faster than other HDV genotypes *in vitro* (Wang et al. 2021). L-HDAg expression occurred earlier compared to other genotypes resulting in earlier and stronger virus secretion. These findings suggest that the high replication rate of HDV genotype 8 could revert two ochre stop mutations and induce the expression of L-HDAg, even though there is not an apparent selection advantage of L-HDAg expression for intracellular replication.

HDV is not replicated by an RNA dependent RNA polymerase, but hijacks cellular RNA polymerases, which have lower error rates compared to viral polymerases, but produce more transcription errors when compared to cellular DNA replication (Gout et al. 2017). In sera of CHD patients, the viral quasispecies complexity was similar to that of other RNA viruses (Homs et al. 2016), suggesting the high replication activity of HDV results in a high nucleotide substitution rate.

4.3.4. Limitations and future work

Our data strongly suggests that the incorporation of TCO* did not affect HDV infectivity, as evidenced by the viral infection rates of HDV-TCO* and by the rescue of the HDV-ochre mutants. However, the trans-complementation with HDAG combined with amber suppression could only rescue low levels of secreted infectivity. As HDV requires ADAR1 mediated editing to induce L-HDAG expression, the application of ADAR1-knockout cells would be an intriguing alternative to produce HDV, in which every L-HDAG molecule contains an ncAA. Such a system would not only confirm that TCO* incorporation does not impair infectivity but might also improve the labelling intensity due to the higher number of incorporated TCO*.

Additionally, ADAR1-knockout cells could be used to produce HDV that exclusively contains unedited genomes. L-HDAG might be supplemented in the producer cells either by trans-complementation of L-HDAG or by amber suppression. According to our model of self-limiting HDV infection, such a virus should have a high specific infectivity. To further validate our model, the ratio of edited-to-unedited genomes required to silence HDV replication should be investigated. Our model also raises the question of the role of self-limiting HDV infection in natural infections. Cells infected with multiple genomes might be persistently silenced by L-HDAG or dynamically change between an active and dormant state of HDV replication. Furthermore, the effect of lonafarnib on silently infected cells should be carefully analysed. It remains unclear whether lonafarnib treatment can activate HDV replication in silently infected cells.

In summary, amber suppression mediated protein labelling and HDV seem to be a perfect match. The naturally occurring amber stop codon at the amber/W editing site allows incorporation of ncAA into L-HDAG and does not require previous insertion of an in-frame amber stop codon. Incorporation of TCO* at the amber/W site led to earlier and enhanced virus secretion and could furthermore produce virus with a higher specific infectivity. Click labelling of virions did not affect infectivity and provides a promising tool to investigate HDV entry mechanisms.

4.4. Application of genetic code expansion in HBV and HDV virology

Genetic code expansion provides a powerful tool to genetically engineer proteins. As other labelling strategies, the amber suppression technology has its drawbacks and challenges. However, due to the small sizes and genome organisations of HBV and HDV, amber suppression mediated incorporation of ncAA may be to only option to fluorescently label these viruses.

4.4.1. Challenges of the amber suppression technology

The main challenge when working with amber suppression technology is the efficiency of amber codon readthrough. Eukaryotic release factor and tRNA^{Pyl} are in constant competition for amber stop codons to terminate translation or incorporate ncAA, respectively. Among many unknown factors, efficiency of ncAA incorporation is affected by ncAA concentration, cell lines, the PylRS variant used, and expression levels of the protein of interest, tRNA^{Pyl}, and PylRS (Zhou et al. 2020; Schmied et al. 2014). The counterpart is played by the eukaryotic release factors eRF1 and eRF3, which promote termination of translation in response to stop codons. eRF1 is responsible for recognition of all three stop codons (Frolova et al. 1994; Dever and Green 2012) and reducing the activity of eRF1 can tip the scales towards ncAA incorporation. Schmied et al. found an eRF1 mutant (eRF1-E55D) which does not efficiently recognise the amber stop codon (Schmied et al. 2014). Therefore, ectopic expression of eRF1-E55D might result in inactive complexes with eRF3 and thereby improves amber suppression efficiency. While some of these factors can be partially adapted and optimised, other parameters of amber suppression efficiency such as the sequence context of the mRNA around the amber codon and of the amino acids that precede and follow the ncAA are more difficult to correct for (Chemla et al. 2018; de la Torre and Chin 2021). Many determinants of amber suppression efficiency remain unknown or have only been investigated in bacterial systems. Testing the incorporation efficiency at different positions of the protein of interest can therefore help to obtain sufficient levels of full-length protein with genetically encoded ncAA.

Premature termination of protein synthesis at introduced amber stop codons may produce large numbers of truncated proteins. Especially structural virus proteins might still interact with their truncated version which might in return interfere with assembly of fully functional viral particles. On the other side, ectopic overexpression of amber suppression components or

dominant negative eRF1 can suppress cellular amber stop codons. These undesired elongated proteins might not only impair cellular functions and viability, but the unspecific incorporation of ncAA also generates background signals when intracellular labelling is performed. After only low levels of off-target amber suppression were observed, context effects of mRNA around natural amber stop codons at the 3' end of a transcript are suggested to have evolved to be biased towards recognition by release factors in bacteria (Chemla et al. 2017). Fortunately, previous labelling experiments of cytoskeletal proteins have indicated that intracellular labelling with SiRTet is possible with low background signals when extensive washing steps are applied to remove excessive ncAA and dye (Uttamapinant et al. 2015; Schwartz et al. 2017). Additionally, studying viruses worked in our favour here because after secretion, both HBV and HDV could be purified by affinity chromatography and separated from cellular components. Fluorescently labelled and purified virions allow the investigation of virus entry events but tracking of intracellular assembly and transport of viral particles might be hampered by cellular background staining.

Finally, even though this method is minimally invasive and only exchanges one amino acid with a ncAA, it might have negative effects on virus replication, or protein stability and function. Mutational analysis of HBc by alanine point mutations of single amino acid positions has revealed severe impairment of capsid assembly and envelopment by single amino acid exchanges (Ponsel and Bruss 2003). The sensitivity of HBV capsids to single point mutations again highlights the importance of testing multiple sites for ncAA incorporation.

4.4.2. Advancements and future applications of genetic code expansion

This project has greatly benefitted from advancements made in recent years in the field of genetic code expansion. Optimisation of the plasmid system used to suppress introduced amber stop codons was crucial for the detection of rescue of full-length HBc expression (Figure 3.9). Importantly, higher copy numbers of tRNA^{Pyl} enhanced the incorporation rate of ncAA (Schmied et al. 2014; Zhou et al. 2020) and the two mutations Y306A and Y384F of PylRS were essential for incorporation of bulky ring-structured ncAA (Plass et al. 2011). Moreover, redirection of the PylRS to the cytoplasm by N-terminal addition of a NES was shown to further enhance amber suppression efficiency (Nikic et al. 2016).

The field of amber suppression and genetic code expansion is developing rapidly and further enhancement of ncAA incorporation by optimisation of the aa-RS/tRNA pairs are being pursued. Phage-assisted evolution was used to find mutants of PylRS with improved activity

and selectivity (Bryson et al. 2017; Suzuki et al. 2017), while others reported a computational approach for the discovery of new aa-RS/tRNA pairs that are orthogonal to endogenous translation components (Cervettini et al. 2020). Recent work has investigated spatial and phase separation from host translation machinery using an orthogonal translation system in an artificial, membraneless organelle (Reinkemeier et al. 2019). This organelle allowed the specific amber suppression of only the targeted mRNA and could increase specificity and efficiency of ncAA incorporation.

Once a suitable position of a protein of interest is found, the amber suppression technology enables a variety of protein modifications by site-specific engineering of proteins. Genetic code expansion has been used to incorporate more than 200 ncAA with diverse functionalities (Vargas-Rodriguez et al. 2018). In addition to click chemistry functionalised ncAA, amber suppression can be used to incorporate ncAA that mimic posttranslational modifications (Elsasser et al. 2016; Fottner et al. 2019), photocaged ncAA that enable rapid activation of protein function by light (Lemke et al. 2007), and photo-crosslinking ncAA that can identify protein interactions (Ai et al. 2011; Chin et al. 2002). Especially, incorporation of photo-crosslinking ncAA might become an important tool to discover interaction partners of viral proteins. The usefulness of photo-crosslinking amino acids has been exemplified by Yan et al. in the discovery of NTCP as functional receptor for HBV and HDV (Yan et al. 2012). They generated synthetic preS1 peptides (similar to MyrB), replaced two residues with photo-crosslinking L-photo-leucine, and conjugated a biotin tag to a C-terminal lysine residue. This modified preS1 peptide was applied to primary *Tupaia* hepatocytes, crosslinked by UV irradiation, and NTCP was discovered as interacting partner by affinity purification and mass spectrometry. Incorporation of photo-crosslinking into HBV nucleocapsids or HDV RNPs could provide a promising approach to identify host factors during replication, assembly, and virus entry.

4.5. Final conclusions

This study has investigated how HBV persists in host cells using a mutated HBV that was unable to initiate the production of HBc upon infection. Δ HBc HBV was infectious and able to form cccDNA, but reverse transcription of pgRNA to rcDNA was abrogated. Our findings provide strong evidence that a static model of cccDNA maintenance is more likely than a dynamic model that requires constant replenishment by reimport of nucleocapsids. Once formed, cccDNA molecules are highly stable and transcriptionally active independent of *de novo* synthesis HBc. Intracellular recycling of nucleocapsids might however serve as a salvage pathway to rescue occasional loss of cccDNA.

The fluorescent labelling of HBV remains highly challenging. We used the amber suppression technology which enables site-specific incorporation of click chemistry functionalised ncAAs. Combined with click chemistry dyes, this method represents the smallest fluorescent tag that can be genetically encoded into proteins. While the incorporation of ring strained amino acids did not result in sufficient rescue of virus production, incorporation of ethynyl-modified ncAAs enabled the production and labelling of fluorescent HBV. In combination with fluorescence and high-resolution microscopy, this system can provide critical insights into HBV entry dynamics and mechanisms. Further improvements in HBV production and amber suppression efficiency are required for the generation of live clickable HBV particles.

The application of amber suppression technology on HDV was facilitated by the natural amber/W site of HDV. Efficient incorporation of TCO* could be achieved. In addition, the early induction of L-HDAg expression by amber suppression resulted in earlier and stronger virus secretion and could furthermore increase the specific infectivity of HDV. Click chemistry labelling of purified HDV was achieved and provides the opportunity for investigating HDV RNP trafficking and correlative light and electron microscopy studies of HDV virions.

5. References

Abeywickrama-Samarakoon, N., Cortay, J. C., Sureau, C., Muller, S., Alfaiate, D., Guerrieri, F., Chaikuad, A., Schroder, M., Merle, P., Levrero, M., and Deny, P. 2020. 'Hepatitis Delta Virus histone mimicry drives the recruitment of chromatin remodelers for viral RNA replication', *Nat Commun*, 11: 419.

Aden, D. P., Fogel, A., Plotkin, S., Damjanov, I., and Knowles, B. B. 1979. 'Controlled synthesis of HBsAg in a differentiated human liver carcinoma-derived cell line', *Nature*, 282: 615-6.

Agard, N. J., Prescher, J. A., and Bertozzi, C. R. 2004. 'A strain-promoted [3 + 2] azide-alkyne cycloaddition for covalent modification of biomolecules in living systems', *J Am Chem Soc*, 126: 15046-7.

Ai, H. W., Shen, W., Sagi, A., Chen, P. R., and Schultz, P. G. 2011. 'Probing protein-protein interactions with a genetically encoded photo-crosslinking amino acid', *ChemBiochem*, 12: 1854-7.

Allweiss, L., Dettmer, C., Volz, T., Giersch, K., Alexandrov, A., Wedemeyer, H., Urban, S., Bockmann, J.-H., Luetgehmman, M., and Dandri, M. 2018a. 'Strong intrahepatic decline of hepatitis D virus RNA and antigen after 24 weeks of treatment with Myrcludex B in combination with Tenofovir in chronic HBV/HDV infected patients: Interim results from a multicenter, open-label phase 2b clinical trial', *Journal of Hepatology*, 68: S90.

Allweiss, L., Giersch, K., Piroso, A., Volz, T., Muench, R. C., Beran, R. K., Urban, S., Javanbakht, H., Fletcher, S. P., Lutgehetmann, M., and Dandri, M. 2021. 'Therapeutic shutdown of HBV transcripts promotes reappearance of the SMC5/6 complex and silencing of the viral genome in vivo', *Gut*.

Allweiss, L., Volz, T., Giersch, K., Kah, J., Raffa, G., Petersen, J., Lohse, A. W., Beninati, C., Pollicino, T., Urban, S., Lutgehetmann, M., and Dandri, M. 2018b. 'Proliferation of primary human hepatocytes and prevention of hepatitis B virus reinfection efficiently deplete nuclear cccDNA in vivo', *Gut*, 67: 542-52.

Alter, H. J., Holland, P. V., Morrow, A. G., Purcell, R. H., Feinstone, S. M., and Moritsugu, Y. 1975. 'Clinical and serological analysis of transfusion-associated hepatitis', *Lancet*, 2: 838-41.

Asabe, S., Wieland, S. F., Chattopadhyay, P. K., Roederer, M., Engle, R. E., Purcell, R. H., and Chisari, F. V. 2009. 'The size of the viral inoculum contributes to the outcome of hepatitis B virus infection', *J Virol*, 83: 9652-62.

Balayan, M. S., Andjaparidze, A. G., Savinskaya, S. S., Ketiladze, E. S., Braginsky, D. M., Savinov, A. P., and Poleschuk, V. F. 1983. 'Evidence for a virus in non-A, non-B hepatitis transmitted via the fecal-oral route', *Intervirology*, 20: 23-31.

- Bartenschlager, R., Junker-Niepmann, M., and Schaller, H. 1990. 'The P gene product of hepatitis B virus is required as a structural component for genomic RNA encapsidation', *J Virol*, 64: 5324-32.
- Bartenschlager, R., and Schaller, H. 1992. 'Hepadnaviral assembly is initiated by polymerase binding to the encapsidation signal in the viral RNA genome', *EMBO J*, 11: 3413-20.
- Bazinet, M., Pantea, V., Cebotarescu, V., Cojuhari, L., Jimbei, P., Anderson, M., Gersch, J., Holzmayer, V., Elsner, C., Krawczyk, A., Kuhns, M. C., Cloherty, G., Dittmer, U., and Vaillant, A. 2021. 'Persistent Control of Hepatitis B Virus and Hepatitis Delta Virus Infection Following REP 2139-Ca and Pegylated Interferon Therapy in Chronic Hepatitis B Virus/Hepatitis Delta Virus Coinfection', *Hepatol Commun*, 5: 189-202.
- Bazinet, M., Pantea, V., Placinta, G., Moscalu, I., Cebotarescu, V., Cojuhari, L., Jimbei, P., Iarovoi, L., Smesnoi, V., Musteata, T., Jucov, A., Dittmer, U., Krawczyk, A., and Vaillant, A. 2020. 'Safety and Efficacy of 48 Weeks REP 2139 or REP 2165, Tenofovir Disoproxil, and Pegylated Interferon Alfa-2a in Patients With Chronic HBV Infection Naive to Nucleos(t)ide Therapy', *Gastroenterology*, 158: 2180-94.
- Beck, J., and Nassal, M. 2007. 'Hepatitis B virus replication', *World J Gastroenterol*, 13: 48-64.
- Beeharry, Y., Goodrum, G., Imperiale, C. J., and Pelchat, M. 2018. 'The Hepatitis Delta Virus accumulation requires paraspeckle components and affects NEAT1 level and PSP1 localization', *Sci Rep*, 8: 6031.
- Belloni, L., Allweiss, L., Guerrieri, F., Pediconi, N., Volz, T., Pollicino, T., Petersen, J., Raimondo, G., Dandri, M., and Levrero, M. 2012. 'IFN-alpha inhibits HBV transcription and replication in cell culture and in humanized mice by targeting the epigenetic regulation of the nuclear cccDNA minichromosome', *J Clin Invest*, 122: 529-37.
- Belloni, L., Palumbo, G., Lupacchini, L., Li, L., Chirapu, S. R., Calvo, L., Finn, M., Lopatin, U., Zlotnick, A., and Levrero, M. 2015. 'P0529: anti capsid drugs HAP12 and AT130 target HBV core protein nuclear functions', *Journal of Hepatology*, 62: S513-S14.
- Bensch, B., Martin, B., and Thimme, R. 2014. 'Restoration of HBV-specific CD8+ T cell function by PD-1 blockade in inactive carrier patients is linked to T cell differentiation', *J Hepatol*, 61: 1212-9.
- Berg, S., Kutra, D., Kroeger, T., Straehle, C. N., Kausler, B. X., Haubold, C., Schiegg, M., Ales, J., Beier, T., Rudy, M., Eren, K., Cervantes, J. I., Xu, B., Beuttenmueller, F., Wolny, A., Zhang, C., Koethe, U., Hamprecht, F. A., and Kreshuk, A. 2019. 'ilastik: interactive machine learning for (bio)image analysis', *Nat Methods*, 16: 1226-32.
- Bergner, L. M., Orton, R. J., Broos, A., Tello, C., Becker, D. J., Carrera, J. E., Patel, A. H., Biek, R., and Streicker, D. G. 2021. 'Diversification of mammalian deltaviruses by host shifting', *Proc Natl Acad Sci U S A*, 118.

- Berke, J. M., Dehertogh, P., Vergauwen, K., Van Damme, E., Mostmans, W., Vandyck, K., and Pauwels, F. 2017. 'Capsid Assembly Modulators Have a Dual Mechanism of Action in Primary Human Hepatocytes Infected with Hepatitis B Virus', *Antimicrob Agents Chemother*, 61.
- Bichko, V. V., and Taylor, J. M. 1996. 'Redistribution of the delta antigens in cells replicating the genome of hepatitis delta virus', *J Virol*, 70: 8064-70.
- Blackman, M. L., Royzen, M., and Fox, J. M. 2008. 'Tetrazine ligation: fast bioconjugation based on inverse-electron-demand Diels-Alder reactivity', *J Am Chem Soc*, 130: 13518-9.
- Blanchet, M., and Sureau, C. 2007. 'Infectivity determinants of the hepatitis B virus pre-S domain are confined to the N-terminal 75 amino acid residues', *J Virol*, 81: 5841-9.
- Blanco-Rodriguez, G., Gazi, A., Monel, B., Frabetti, S., Scoca, V., Mueller, F., Schwartz, O., Krijnse-Locker, J., Charneau, P., and Di Nunzio, F. 2020. 'Remodeling of the Core Leads HIV-1 Preintegration Complex into the Nucleus of Human Lymphocytes', *J Virol*, 94.
- Blumberg, B. S., Alter, H. J., and Visnich, S. 1965. 'A "New" Antigen in Leukemia Sera', *JAMA*, 191: 541-6.
- Blumberg, B. S., and Millman, I. 1972. "Vaccine against viral hepatitis and process." In.: Google Patents.
- Blumberg, B. S., Sutnick, A. I., and London, W. T. 1968. 'Hepatitis and leukemia: their relation to Australia antigen', *Bull N Y Acad Med*, 44: 1566-86.
- Bock, C. T., Schranz, P., Schroder, C. H., and Zentgraf, H. 1994. 'Hepatitis B virus genome is organized into nucleosomes in the nucleus of the infected cell', *Virus Genes*, 8: 215-29.
- Bock, C. T., Schwinn, S., Locarnini, S., Fyfe, J., Manns, M. P., Trautwein, C., and Zentgraf, H. 2001. 'Structural organization of the hepatitis B virus minichromosome', *J Mol Biol*, 307: 183-96.
- Bogomolov, P., Alexandrov, A., Voronkova, N., Macievich, M., Kokina, K., Petrachenkova, M., Lehr, T., Lempp, F. A., Wedemeyer, H., Haag, M., Schwab, M., Haefeli, W. E., Blank, A., and Urban, S. 2016. 'Treatment of chronic hepatitis D with the entry inhibitor myrcludex B: First results of a phase Ib/IIa study', *J Hepatol*, 65: 490-8.
- Boni, C., Fisicaro, P., Valdatta, C., Amadei, B., Di Vincenzo, P., Giuberti, T., Laccabue, D., Zerbini, A., Cavalli, A., Missale, G., Bertoletti, A., and Ferrari, C. 2007. 'Characterization of hepatitis B virus (HBV)-specific T-cell dysfunction in chronic HBV infection', *J Virol*, 81: 4215-25.
- Borrmann, A., Milles, S., Plass, T., Dommerholt, J., Verkade, J. M., Wiessler, M., Schultz, C., van Hest, J. C., van Delft, F. L., and Lemke, E. A. 2012. 'Genetic encoding of a bicyclo[6.1.0]nonyne-charged amino acid enables fast cellular protein imaging by metal-free ligation', *Chembiochem*, 13: 2094-9.

- Bottcher, B., Wynne, S. A., and Crowther, R. A. 1997. 'Determination of the fold of the core protein of hepatitis B virus by electron cryomicroscopy', *Nature*, 386: 88-91.
- Boulon, R., Blanchet, M., Lemasson, M., Vaillant, A., and Labonte, P. 2020. 'Characterization of the antiviral effects of REP 2139 on the HBV lifecycle in vitro', *Antiviral Res*, 183: 104853.
- Bourne, E. J., Dienstag, J. L., Lopez, V. A., Sander, T. J., Longlet, J. M., Hall, J. G., Kwiatkowski, R. W., Wright, T., Lai, C. L., and Condreay, L. D. 2007. 'Quantitative analysis of HBV cccDNA from clinical specimens: correlation with clinical and virological response during antiviral therapy', *J Viral Hepat*, 14: 55-63.
- Brandenburg, B., Lee, L. Y., Lakadamyali, M., Rust, M. J., Zhuang, X., and Hogle, J. M. 2007. 'Imaging poliovirus entry in live cells', *PLoS Biol*, 5: e183.
- Bremer, B., Anastasiou, O. E., Hardtke, S., Caruntu, F. A., Curescu, M. G., Yalcin, K., Akarca, U. S., Gurel, S., Zeuzem, S., Erhardt, A., Luth, S., Papatheodoridis, G. V., Radu, M., Idilman, R., Manns, M. P., Cornberg, M., Yurdaydin, C., and Wedemeyer, H. 2021. 'Residual low HDV viraemia is associated HDV RNA relapse after PEG-IFNa-based antiviral treatment of hepatitis delta: Results from the HIDIT-II study', *Liver Int*, 41: 295-99.
- Brunetto, M. R., Moriconi, F., Bonino, F., Lau, G. K., Farci, P., Yurdaydin, C., Piratvisuth, T., Luo, K., Wang, Y., Hadziyannis, S., Wolf, E., McCloud, P., Batrla, R., and Marcellin, P. 2009. 'Hepatitis B virus surface antigen levels: a guide to sustained response to peginterferon alfa-2a in HBeAg-negative chronic hepatitis B', *Hepatology*, 49: 1141-50.
- Bruss, V. 1997. 'A short linear sequence in the pre-S domain of the large hepatitis B virus envelope protein required for virion formation', *J Virol*, 71: 9350-7.
- Bruss, V. 2007. 'Hepatitis B virus morphogenesis', *World J Gastroenterol*, 13: 65-73.
- Bruss, V., and Ganem, D. 1991. 'The role of envelope proteins in hepatitis B virus assembly', *Proc Natl Acad Sci U S A*, 88: 1059-63.
- Bruss, V., and Gerlich, W. H. 1988. 'Formation of transmembraneous hepatitis B e-antigen by cotranslational in vitro processing of the viral precore protein', *Virology*, 163: 268-75.
- Bruss, V., Hagelstein, J., Gerhardt, E., and Galle, P. R. 1996. 'Myristylation of the large surface protein is required for hepatitis B virus in vitro infectivity', *Virology*, 218: 396-9.
- Bruss, V., Lu, X., Thomssen, R., and Gerlich, W. H. 1994. 'Post-translational alterations in transmembrane topology of the hepatitis B virus large envelope protein', *EMBO J*, 13: 2273-9.
- Bryson, D. I., Fan, C., Guo, L. T., Miller, C., Soll, D., and Liu, D. R. 2017. 'Continuous directed evolution of aminoacyl-tRNA synthetases', *Nat Chem Biol*, 13: 1253-60.
- Burke, S. A., Lo, S. L., and Krzycki, J. A. 1998. 'Clustered genes encoding the methyltransferases of methanogenesis from monomethylamine', *J Bacteriol*, 180: 3432-40.

- Caredda, F., Rossi, E., d'Arminio Monforte, A., Zampini, L., Re, T., Meroni, B., and Moroni, M. 1985. 'Hepatitis B virus-associated coinfection and superinfection with delta agent: indistinguishable disease with different outcome', *J Infect Dis*, 151: 925-8.
- Cattaneo, R., Will, H., Darai, G., Pfaff, E., and Schaller, H. 1983. 'Detection of an element of the SV40 late promoter in vectors used for expression studies in COS cells', *EMBO J*, 2: 511-4.
- Cervettini, D., Tang, S., Fried, S. D., Willis, J. C. W., Funke, L. F. H., Colwell, L. J., and Chin, J. W. 2020. 'Rapid discovery and evolution of orthogonal aminoacyl-tRNA synthetase-tRNA pairs', *Nat Biotechnol*, 38: 989-99.
- Chakraborty, A., Ko, C., Henning, C., Lucko, A., Harris, J. M., Chen, F., Zhuang, X., Wettengel, J. M., Roessler, S., Protzer, U., and McKeating, J. A. 2020. 'Synchronised infection identifies early rate-limiting steps in the hepatitis B virus life cycle', *Cell Microbiol*, 22: e13250.
- Chang, F. L., Chen, P. J., Tu, S. J., Wang, C. J., and Chen, D. S. 1991. 'The large form of hepatitis delta antigen is crucial for assembly of hepatitis delta virus', *Proc Natl Acad Sci U S A*, 88: 8490-4.
- Chang, J., Nie, X., Chang, H. E., Han, Z., and Taylor, J. 2008. 'Transcription of hepatitis delta virus RNA by RNA polymerase II', *J Virol*, 82: 1118-27.
- Chang, W. S., Pettersson, J. H., Le Lay, C., Shi, M., Lo, N., Wille, M., Eden, J. S., and Holmes, E. C. 2019. 'Novel hepatitis D-like agents in vertebrates and invertebrates', *Virus Evol*, 5: vez021.
- Chao, M., Hsieh, S. Y., and Taylor, J. 1990. 'Role of two forms of hepatitis delta virus antigen: evidence for a mechanism of self-limiting genome replication', *J Virol*, 64: 5066-9.
- Chemla, Y., Friedman, M., Heltberg, M., Bakhrat, A., Nagar, E., Schwarz, R., Jensen, M. H., and Alfonta, L. 2017. 'Expanding the Genetic Code of a Photoautotrophic Organism', *Biochemistry*, 56: 2161-65.
- Chemla, Y., Ozer, E., Algov, I., and Alfonta, L. 2018. 'Context effects of genetic code expansion by stop codon suppression', *Curr Opin Chem Biol*, 46: 146-55.
- Chen, H. Y., Shen, D. T., Ji, D. Z., Han, P. C., Zhang, W. M., Ma, J. F., Chen, W. S., Goyal, H., Pan, S., and Xu, H. G. 2019. 'Prevalence and burden of hepatitis D virus infection in the global population: a systematic review and meta-analysis', *Gut*, 68: 512-21.
- Chen, P. J., Kalpana, G., Goldberg, J., Mason, W., Werner, B., Gerin, J., and Taylor, J. 1986. 'Structure and replication of the genome of the hepatitis delta virus', *Proc Natl Acad Sci U S A*, 83: 8774-8.
- Chen, P. R., Groff, D., Guo, J., Ou, W., Cellitti, S., Geierstanger, B. H., and Schultz, P. G. 2009. 'A facile system for encoding unnatural amino acids in mammalian cells', *Angew Chem Int Ed Engl*, 48: 4052-5.

- Chien, Y. C., Jan, C. F., Kuo, H. S., and Chen, C. J. 2006. 'Nationwide hepatitis B vaccination program in Taiwan: effectiveness in the 20 years after it was launched', *Epidemiol Rev*, 28: 126-35.
- Chin, J. W., Martin, A. B., King, D. S., Wang, L., and Schultz, P. G. 2002. 'Addition of a photocrosslinking amino acid to the genetic code of *Escherichiacoli*', *Proc Natl Acad Sci U S A*, 99: 11020-4.
- Chong, C. K., Cheng, C. Y. S., Tsoi, S. Y. J., Huang, F. Y., Liu, F., Seto, W. K., Lai, C. L., Yuen, M. F., and Wong, D. K. 2017. 'Role of hepatitis B core protein in HBV transcription and recruitment of histone acetyltransferases to cccDNA minichromosome', *Antiviral Res*, 144: 1-7.
- Choo, Q. L., Kuo, G., Weiner, A. J., Overby, L. R., Bradley, D. W., and Houghton, M. 1989. 'Isolation of a cDNA clone derived from a blood-borne non-A, non-B viral hepatitis genome', *Science*, 244: 359-62.
- Chou, H. C., Hsieh, T. Y., Sheu, G. T., and Lai, M. M. 1998. 'Hepatitis delta antigen mediates the nuclear import of hepatitis delta virus RNA', *J Virol*, 72: 3684-90.
- Chu, C. M., and Liaw, Y. F. 1987. 'Intrahepatic distribution of hepatitis B surface and core antigens in chronic hepatitis B virus infection. Hepatocyte with cytoplasmic/membranous hepatitis B core antigen as a possible target for immune hepatocytolysis', *Gastroenterology*, 92: 220-5.
- Coller, K. E., Berger, K. L., Heaton, N. S., Cooper, J. D., Yoon, R., and Randall, G. 2009. 'RNA interference and single particle tracking analysis of hepatitis C virus endocytosis', *PLoS Pathog*, 5: e1000702.
- Coller, K. E., Heaton, N. S., Berger, K. L., Cooper, J. D., Saunders, J. L., and Randall, G. 2012. 'Molecular determinants and dynamics of hepatitis C virus secretion', *PLoS Pathog*, 8: e1002466.
- Cullen, J. M., David, C., Wang, J. G., Becherer, P., and Lemon, S. M. 1995. 'Subcellular distribution of large and small hepatitis delta antigen in hepatocytes of hepatitis delta virus superinfected woodchucks', *Hepatology*, 22: 1090-100.
- Cunha, C., Monjardino, J., Cheng, D., Krause, S., and Carmo-Fonseca, M. 1998. 'Localization of hepatitis delta virus RNA in the nucleus of human cells', *RNA*, 4: 680-93.
- Cureton, D. K., Massol, R. H., Saffarian, S., Kirchhausen, T. L., and Whelan, S. P. 2009. 'Vesicular stomatitis virus enters cells through vesicles incompletely coated with clathrin that depend upon actin for internalization', *PLoS Pathog*, 5: e1000394.
- Dane, D. S., Cameron, C. H., and Briggs, M. 1970. 'Virus-like particles in serum of patients with Australia-antigen-associated hepatitis', *Lancet*, 1: 695-8.

- Das, D. K., Govindan, R., Nikic-Spiegel, I., Krammer, F., Lemke, E. A., and Munro, J. B. 2018. 'Direct Visualization of the Conformational Dynamics of Single Influenza Hemagglutinin Trimers', *Cell*, 174: 926-37 e12.
- Davis, L., and Chin, J. W. 2012. 'Designer proteins: applications of genetic code expansion in cell biology', *Nat Rev Mol Cell Biol*, 13: 168-82.
- de la Torre, D., and Chin, J. W. 2021. 'Reprogramming the genetic code', *Nat Rev Genet*, 22: 169-84.
- Decorsiere, A., Mueller, H., van Breugel, P. C., Abdul, F., Gerossier, L., Beran, R. K., Livingston, C. M., Niu, C., Fletcher, S. P., Hantz, O., and Strubin, M. 2016. 'Hepatitis B virus X protein identifies the Smc5/6 complex as a host restriction factor', *Nature*, 531: 386-9.
- Desai, P., and Person, S. 1998. 'Incorporation of the green fluorescent protein into the herpes simplex virus type 1 capsid', *J Virol*, 72: 7563-8.
- Dever, T. E., and Green, R. 2012. 'The elongation, termination, and recycling phases of translation in eukaryotes', *Cold Spring Harb Perspect Biol*, 4: a013706.
- Diab, A., Foca, A., Zoulim, F., Durantel, D., and Andrisani, O. 2018. 'The diverse functions of the hepatitis B core/capsid protein (HBc) in the viral life cycle: Implications for the development of HBc-targeting antivirals', *Antiviral Res*, 149: 211-20.
- Dienstag, J. L., Perrillo, R. P., Schiff, E. R., Bartholomew, M., Vicary, C., and Rubin, M. 1995. 'A preliminary trial of lamivudine for chronic hepatitis B infection', *N Engl J Med*, 333: 1657-61.
- Donkers, J. M., Zehnder, B., van Westen, G. J. P., Kwakkenbos, M. J., AP, I. J., Oude Elferink, R. P. J., Beuers, U., Urban, S., and van de Graaf, S. F. J. 2017. 'Reduced hepatitis B and D viral entry using clinically applied drugs as novel inhibitors of the bile acid transporter NTCP', *Sci Rep*, 7: 15307.
- Dryden, K. A., Wieland, S. F., Whitten-Bauer, C., Gerin, J. L., Chisari, F. V., and Yeager, M. 2006. 'Native hepatitis B virions and capsids visualized by electron cryomicroscopy', *Mol Cell*, 22: 843-50.
- Dumas, A., Lercher, L., Spicer, C. D., and Davis, B. G. 2015. 'Designing logical codon reassignment - Expanding the chemistry in biology', *Chem Sci*, 6: 50-69.
- EASL. 2017. 'EASL 2017 Clinical Practice Guidelines on the management of hepatitis B virus infection', *J Hepatol*, 67: 370-98.
- Eble, B. E., MacRae, D. R., Lingappa, V. R., and Ganem, D. 1987. 'Multiple topogenic sequences determine the transmembrane orientation of the hepatitis B surface antigen', *Mol Cell Biol*, 7: 3591-601.

- Eckhardt, M., Anders, M., Muranyi, W., Heilemann, M., Krijnse-Locker, J., and Muller, B. 2011. 'A SNAP-Tagged Derivative of HIV-1-A Versatile Tool to Study Virus-Cell Interactions', *PLoS One*, 6.
- Eckhardt, S. G., Milich, D. R., and McLachlan, A. 1991. 'Hepatitis B virus core antigen has two nuclear localization sequences in the arginine-rich carboxyl terminus', *J Virol*, 65: 575-82.
- Edmunds, W. J., Medley, G. F., Nokes, D. J., Hall, A. J., and Whittle, H. C. 1993. 'The influence of age on the development of the hepatitis B carrier state', *Proc Biol Sci*, 253: 197-201.
- Elsasser, S. J., Ernst, R. J., Walker, O. S., and Chin, J. W. 2016. 'Genetic code expansion in stable cell lines enables encoded chromatin modification', *Nat Methods*, 13: 158-64.
- Engle, R. E., De Battista, D., Danoff, E. J., Nguyen, H., Chen, Z., Lusso, P., Purcell, R. H., and Farci, P. 2020. 'Distinct Cytokine Profiles Correlate with Disease Severity and Outcome in Longitudinal Studies of Acute Hepatitis B Virus and Hepatitis D Virus Infection in Chimpanzees', *mBio*, 11.
- Ernst, R. J., Krogager, T. P., Maywood, E. S., Zanchi, R., Beranek, V., Elliott, T. S., Barry, N. P., Hastings, M. H., and Chin, J. W. 2016. 'Genetic code expansion in the mouse brain', *Nat Chem Biol*, 12: 776-78.
- Fanning, G. C., Zoulim, F., Hou, J., and Bertoletti, A. 2019. 'Therapeutic strategies for hepatitis B virus infection: towards a cure', *Nat Rev Drug Discov*, 18: 827-44.
- Farci, P., and Niro, G. A. 2012. 'Clinical features of hepatitis D', *Semin Liver Dis*, 32: 228-36.
- Fattovich, G., Giustina, G., Christensen, E., Pantalena, M., Zagni, I., Realdi, G., and Schalm, S. W. 2000. 'Influence of hepatitis delta virus infection on morbidity and mortality in compensated cirrhosis type B. The European Concerted Action on Viral Hepatitis (Eurohep)', *Gut*, 46: 420-6.
- Feinstone, S. M., Kapikian, A. Z., and Purcell, R. H. 1973. 'Hepatitis A: detection by immune electron microscopy of a viruslike antigen associated with acute illness', *Science*, 182: 1026-8.
- Ferns, R. B., Nastouli, E., and Garson, J. A. 2012. 'Quantitation of hepatitis delta virus using a single-step internally controlled real-time RT-qPCR and a full-length genomic RNA calibration standard', *J Virol Methods*, 179: 189-94.
- Findlay, G. M., and Willcox, R. R. 1945. 'Infective hepatitis; transmission by faeces and urine', *Lancet*, 2: 594-7.
- Flaum, A., Malmros, H., Persson, E., and Malmros, V. v. H. 1926. 'Eine nosocomiale Ikterus-Epidemie', *Acta Medica Scandinavica*, 64: 544-53.

- Florian, P. E., Galantou, R. N., Lazar, C., Ruta, S., Roseanu, A., and Nichita, N. 2014. 'Labeling of hepatitis B virus middle envelope protein with enhanced green fluorescent protein', *Romanian Biotechnological Letters*, 19: 9974-83.
- Fottner, M., Brunner, A. D., Bittl, V., Horn-Ghetko, D., Jussupow, A., Kaila, V. R. I., Bremm, A., and Lang, K. 2019. 'Site-specific ubiquitylation and SUMOylation using genetic-code expansion and sortase', *Nat Chem Biol*, 15: 276-84.
- Fox, J. P., Manso, C., Penna, H., and Para, M. 1942. 'Observations on the Occurrence of Icterus in Brazil following Vaccination against Yellow Fever', *American journal of Hygiene*, 36.
- Francois-Souquiere, S., Makuwa, M., Bisvigou, U., and Kazanji, M. 2016. 'Epidemiological and molecular features of hepatitis B and hepatitis delta virus transmission in a remote rural community in central Africa', *Infect Genet Evol*, 39: 12-21.
- Freitas, N., Cunha, C., Menne, S., and Gudima, S. O. 2014. 'Envelope proteins derived from naturally integrated hepatitis B virus DNA support assembly and release of infectious hepatitis delta virus particles', *J Virol*, 88: 5742-54.
- Frolova, L., Le Goff, X., Rasmussen, H. H., Cheperegin, S., Dugeon, G., Kress, M., Arman, I., Haenni, A. L., Celis, J. E., Philippe, M., and et al. 1994. 'A highly conserved eukaryotic protein family possessing properties of polypeptide chain release factor', *Nature*, 372: 701-3.
- Funk, A., Mhamdi, M., Hohenberg, H., Will, H., and Sirma, H. 2006. 'pH-independent entry and sequential endosomal sorting are major determinants of hepadnaviral infection in primary hepatocytes', *Hepatology*, 44: 685-93.
- Gane, E., Verdon, D. J., Brooks, A. E., Gaggar, A., Nguyen, A. H., Subramanian, G. M., Schwabe, C., and Dunbar, P. R. 2019. 'Anti-PD-1 blockade with nivolumab with and without therapeutic vaccination for virally suppressed chronic hepatitis B: A pilot study', *J Hepatol*, 71: 900-07.
- Gane, E. J., Kim, H. J., Visvanathan, K., Kim, Y. J., Nguyen, A. H., Wallin, J. J., Chen, D. Y., McDonald, C., Arora, P., Tan, S. K., Gaggar, A., Roberts, S. K., and Lim, Y. S. 2021. 'Safety, pharmacokinetics, and pharmacodynamics of the oral TLR8 agonist selgantolimod in chronic hepatitis B', *Hepatology*.
- Gao, W., and Hu, J. 2007. 'Formation of hepatitis B virus covalently closed circular DNA: removal of genome-linked protein', *J Virol*, 81: 6164-74.
- Garcia, P. D., Ou, J. H., Rutter, W. J., and Walter, P. 1988. 'Targeting of the hepatitis B virus precore protein to the endoplasmic reticulum membrane: after signal peptide cleavage translocation can be aborted and the product released into the cytoplasm', *J Cell Biol*, 106: 1093-104.
- Geng, M., Xin, X., Bi, L. Q., Zhou, L. T., and Liu, X. H. 2015. 'Molecular mechanism of hepatitis B virus X protein function in hepatocarcinogenesis', *World J Gastroenterol*, 21: 10732-8.

- Gerlich, W. H. 2013. 'Medical virology of hepatitis B: how it began and where we are now', *Virology*, 10: 239.
- Gerlich, W. H., and Robinson, W. S. 1980. 'Hepatitis B virus contains protein attached to the 5' terminus of its complete DNA strand', *Cell*, 21: 801-9.
- Gill, U. S., Peppas, D., Micco, L., Singh, H. D., Carey, I., Foster, G. R., Maini, M. K., and Kennedy, P. T. 2016. 'Interferon Alpha Induces Sustained Changes in NK Cell Responsiveness to Hepatitis B Viral Load Suppression In Vivo', *PLoS Pathog*, 12: e1005788.
- Gish, R. G., Given, B. D., Lai, C. L., Locarnini, S. A., Lau, J. Y., Lewis, D. L., and Schlueter, T. 2015. 'Chronic hepatitis B: Virology, natural history, current management and a glimpse at future opportunities', *Antiviral Res*, 121: 47-58.
- Glebe, D., Urban, S., Knoop, E. V., Cag, N., Krass, P., Grun, S., Bulavaite, A., Sasnauskas, K., and Gerlich, W. H. 2005. 'Mapping of the hepatitis B virus attachment site by use of infection-inhibiting preS1 lipopeptides and tupaia hepatocytes', *Gastroenterology*, 129: 234-45.
- Glenn, J. S., Watson, J. A., Havel, C. M., and White, J. M. 1992. 'Identification of a prenylation site in delta virus large antigen', *Science*, 256: 1331-3.
- Gout, J. F., Li, W., Fritsch, C., Li, A., Haroon, S., Singh, L., Hua, D., Fazelinia, H., Smith, Z., Seeholzer, S., Thomas, K., Lynch, M., and Vermulst, M. 2017. 'The landscape of transcription errors in eukaryotic cells', *Sci Adv*, 3: e1701484.
- Gray, R. D., Beerli, C., Pereira, P. M., Scherer, K. M., Samolej, J., Bleck, C. K., Mercer, J., and Henriques, R. 2016. 'VirusMapper: open-source nanoscale mapping of viral architecture through super-resolution microscopy', *Sci Rep*, 6: 29132.
- Greco-Stewart, V. S., Miron, P., Abraham, A., and Pelchat, M. 2007. 'The human RNA polymerase II interacts with the terminal stem-loop regions of the hepatitis delta virus RNA genome', *Virology*, 357: 68-78.
- Gripon, P., Cannie, I., and Urban, S. 2005. 'Efficient inhibition of hepatitis B virus infection by acylated peptides derived from the large viral surface protein', *J Virol*, 79: 1613-22.
- Gripon, P., Diot, C., Theze, N., Fourel, I., Loreal, O., Brechot, C., and Guguen-Guillouzo, C. 1988. 'Hepatitis B virus infection of adult human hepatocytes cultured in the presence of dimethyl sulfoxide', *J Virol*, 62: 4136-43.
- Gripon, P., Le Seyec, J., Rumin, S., and Guguen-Guillouzo, C. 1995. 'Myristylation of the hepatitis B virus large surface protein is essential for viral infectivity', *Virology*, 213: 292-9.
- Gripon, P., Rumin, S., Urban, S., Le Seyec, J., Glaise, D., Cannie, I., Guyomard, C., Lucas, J., Trepo, C., and Guguen-Guillouzo, C. 2002. 'Infection of a human hepatoma cell line by hepatitis B virus', *Proc Natl Acad Sci U S A*, 99: 15655-60.

- Gudima, S., Chang, J., Moraleda, G., Azvolinsky, A., and Taylor, J. 2002. 'Parameters of human hepatitis delta virus genome replication: the quantity, quality, and intracellular distribution of viral proteins and RNA', *J Virol*, 76: 3709-19.
- Guo, F., Zhao, Q., Sheraz, M., Cheng, J., Qi, Y., Su, Q., Cuconati, A., Wei, L., Du, Y., Li, W., Chang, J., and Guo, J. T. 2017. 'HBV core protein allosteric modulators differentially alter cccDNA biosynthesis from de novo infection and intracellular amplification pathways', *PLoS Pathog*, 13: e1006658.
- Guo, H., Jiang, D., Zhou, T., Cuconati, A., Block, T. M., and Guo, J. T. 2007. 'Characterization of the intracellular deproteinized relaxed circular DNA of hepatitis B virus: an intermediate of covalently closed circular DNA formation', *J Virol*, 81: 12472-84.
- Guo, Y. H., Li, Y. N., Zhao, J. R., Zhang, J., and Yan, Z. 2011. 'HBc binds to the CpG islands of HBV cccDNA and promotes an epigenetic permissive state', *Epigenetics*, 6: 720-6.
- Habib, S., and Shaikh, O. S. 2007. 'Hepatitis B immune globulin', *Drugs Today (Barc)*, 43: 379-94.
- Hantz, O., Parent, R., Durantel, D., Gripon, P., Guguen-Guillouzo, C., and Zoulim, F. 2009. 'Persistence of the hepatitis B virus covalently closed circular DNA in HepaRG human hepatocyte-like cells', *J Gen Virol*, 90: 127-35.
- Hao, B., Gong, W., Ferguson, T. K., James, C. M., Krzycki, J. A., and Chan, M. K. 2002. 'A new UAG-encoded residue in the structure of a methanogen methyltransferase', *Science*, 296: 1462-6.
- Hao, X., Shang, X., Wu, J., Shan, Y., Cai, M., Jiang, J., Huang, Z., Tang, Z., and Wang, H. 2011. 'Single-particle tracking of hepatitis B virus-like vesicle entry into cells', *Small*, 7: 1212-8.
- Heermann, K. H., Goldmann, U., Schwartz, W., Seyffarth, T., Baumgarten, H., and Gerlich, W. H. 1984. 'Large surface proteins of hepatitis B virus containing the pre-s sequence', *J Virol*, 52: 396-402.
- Heermann, K. H., Kruse, F., Seifer, M., and Gerlich, W. H. 1987. 'Immunogenicity of the gene S and Pre-S domains in hepatitis B virions and HBsAg filaments', *Intervirology*, 28: 14-25.
- Heidrich, B., Yurdaydin, C., Kabacam, G., Ratsch, B. A., Zachou, K., Bremer, B., Dalekos, G. N., Erhardt, A., Tabak, F., Yalcin, K., Gurel, S., Zeuzem, S., Cornberg, M., Bock, C. T., Manns, M. P., Wedemeyer, H., and Group, H.-S. 2014. 'Late HDV RNA relapse after peginterferon alpha-based therapy of chronic hepatitis delta', *Hepatology*, 60: 87-97.
- Herrscher, C., Pastor, F., Burlaud-Gaillard, J., Dumans, A., Seigneuret, F., Moreau, A., Patient, R., Eymieux, S., de Rocquigny, H., Hourieux, C., Roingeard, P., and Blanchard, E. 2020. 'Hepatitis B virus entry into HepG2-NTCP cells requires clathrin-mediated endocytosis', *Cell Microbiol*, 22: e13205.

- Hetzel, U., Szirovicza, L., Smura, T., Prahauer, B., Vapalahti, O., Kipar, A., and Hepojoki, J. 2019. 'Identification of a Novel Deltavirus in Boa Constrictors', *mBio*, 10.
- Homs, M., Caballero, A., Gregori, J., Taberner, D., Quer, J., Nieto, L., Esteban, R., Buti, M., and Rodriguez-Frias, F. 2014. 'Clinical application of estimating hepatitis B virus quasispecies complexity by massive sequencing: correlation between natural evolution and on-treatment evolution', *PLoS One*, 9: e112306.
- Homs, M., Rodriguez-Frias, F., Gregori, J., Ruiz, A., Reimundo, P., Casillas, R., Taberner, D., Godoy, C., Barakat, S., Quer, J., Riveiro-Barciela, M., Roggendorf, M., Esteban, R., and Buti, M. 2016. 'Evidence of an Exponential Decay Pattern of the Hepatitis Delta Virus Evolution Rate and Fluctuations in Quasispecies Complexity in Long-Term Studies of Chronic Delta Infection', *PLoS One*, 11: e0158557.
- Hong, V., Steinmetz, N. F., Manchester, M., and Finn, M. G. 2010. 'Labeling live cells by copper-catalyzed alkyne-azide click chemistry', *Bioconjug Chem*, 21: 1912-6.
- Hsieh, S. Y., Chao, M., Coates, L., and Taylor, J. 1990. 'Hepatitis delta virus genome replication: a polyadenylated mRNA for delta antigen', *J Virol*, 64: 3192-8.
- Huang, H. C., Chen, C. C., Chang, W. C., Tao, M. H., and Huang, C. 2012. 'Entry of hepatitis B virus into immortalized human primary hepatocytes by clathrin-dependent endocytosis', *J Virol*, 86: 9443-53.
- Hwang, S. B., and Lai, M. M. 1993. 'Isoprenylation mediates direct protein-protein interactions between hepatitis large delta antigen and hepatitis B virus surface antigen', *J Virol*, 67: 7659-62.
- Hwang, S. B., and Lai, M. M. 1994. 'Isoprenylation masks a conformational epitope and enhances trans-dominant inhibitory function of the large hepatitis delta antigen', *J Virol*, 68: 2958-64.
- Iwamoto, M., Saso, W., Nishioka, K., Ohashi, H., Sugiyama, R., Ryo, A., Ohki, M., Yun, J. H., Park, S. Y., Ohshima, T., Suzuki, R., Aizaki, H., Muramatsu, M., Matano, T., Iwami, S., Sureau, C., Wakita, T., and Watashi, K. 2020. 'The machinery for endocytosis of epidermal growth factor receptor coordinates the transport of incoming hepatitis B virus to the endosomal network', *J Biol Chem*, 295: 800-07.
- Iwamoto, M., Saso, W., Sugiyama, R., Ishii, K., Ohki, M., Nagamori, S., Suzuki, R., Aizaki, H., Ryo, A., Yun, J. H., Park, S. Y., Ohtani, N., Muramatsu, M., Iwami, S., Tanaka, Y., Sureau, C., Wakita, T., and Watashi, K. 2019. 'Epidermal growth factor receptor is a host-entry cofactor triggering hepatitis B virus internalization', *Proc Natl Acad Sci U S A*, 116: 8487-92.
- Jakob, L., Gust, A., and Grohmann, D. 2019. 'Evaluation and optimisation of unnatural amino acid incorporation and bioorthogonal bioconjugation for site-specific fluorescent labelling of proteins expressed in mammalian cells', *Biochem Biophys Rep*, 17: 1-9.

- Janssen, H. L. A., Brunetto, M. R., Kim, Y. J., Ferrari, C., Massetto, B., Nguyen, A. H., Joshi, A., Woo, J., Lau, A. H., Gaggar, A., Subramanian, G. M., Yoshida, E. M., Ahn, S. H., Tsai, N. C. S., Fung, S., and Gane, E. J. 2018. 'Safety, efficacy and pharmacodynamics of vesatolimod (GS-9620) in virally suppressed patients with chronic hepatitis B', *J Hepatol*, 68: 431-40.
- Jehn, J. 1885. 'Eine icterusepidemie in wahrscheinlichem Zusammenhang mit vorausgegangener revaccination', *Deutsche Medizinische Wochenschrift*, 11: 339-40.
- Jiang, B., Himmelsbach, K., Ren, H., Boller, K., and Hildt, E. 2015. 'Subviral Hepatitis B Virus Filaments, like Infectious Viral Particles, Are Released via Multivesicular Bodies', *J Virol*, 90: 3330-41.
- Kang, C., and Syed, Y. Y. 2020. 'Bulevirtide: First Approval', *Drugs*, 80: 1601-05.
- Kann, M., Sodeik, B., Vlachou, A., Gerlich, W. H., and Helenius, A. 1999. 'Phosphorylation-dependent binding of hepatitis B virus core particles to the nuclear pore complex', *J Cell Biol*, 145: 45-55.
- Kaplan, P. M., Greenman, R. L., Gerin, J. L., Purcell, R. H., and Robinson, W. S. 1973. 'DNA polymerase associated with human hepatitis B antigen', *J Virol*, 12: 995-1005.
- Karayiannis, P. 2017. 'Hepatitis B virus: virology, molecular biology, life cycle and intrahepatic spread', *Hepatol Int*, 11: 500-08.
- Kavran, J. M., Gundllapalli, S., O'Donoghue, P., Englert, M., Soll, D., and Steitz, T. A. 2007. 'Structure of pyrrolysyl-tRNA synthetase, an archaeal enzyme for genetic code innovation', *Proc Natl Acad Sci U S A*, 104: 11268-73.
- Kelemen, R. E., Mukherjee, R., Cao, X., Erickson, S. B., Zheng, Y., and Chatterjee, A. 2016. 'A Precise Chemical Strategy To Alter the Receptor Specificity of the Adeno-Associated Virus', *Angew Chem Int Ed Engl*, 55: 10645-9.
- Kennedy, D. C., McKay, C. S., Legault, M. C., Danielson, D. C., Blake, J. A., Pegoraro, A. F., Stolow, A., Mester, Z., and Pezacki, J. P. 2011. 'Cellular consequences of copper complexes used to catalyze bioorthogonal click reactions', *J Am Chem Soc*, 133: 17993-8001.
- Khakpoor, A., Ni, Y., Chen, A., Ho, Z. Z., Oei, V., Yang, N., Giri, R., Chow, J. X., Tan, A. T., Kennedy, P. T., Maini, M., Urban, S., and Bertolotti, A. 2019. 'Spatiotemporal Differences in Presentation of CD8 T Cell Epitopes during Hepatitis B Virus Infection', *J Virol*, 93.
- Kimbi, G. C., Kramvis, A., and Kew, M. C. 2005. 'Integration of hepatitis B virus DNA into chromosomal DNA during acute hepatitis B', *World J Gastroenterol*, 11: 6416-21.
- Kitamura, K., Que, L., Shimadu, M., Koura, M., Ishihara, Y., Wakae, K., Nakamura, T., Watashi, K., Wakita, T., and Muramatsu, M. 2018. 'Flap endonuclease 1 is involved in cccDNA formation in the hepatitis B virus', *PLoS Pathog*, 14: e1007124.

- Ko, C., Chakraborty, A., Chou, W. M., Hasreiter, J., Wettengel, J. M., Stadler, D., Bester, R., Asen, T., Zhang, K., Wisskirchen, K., McKeating, J. A., Ryu, W. S., and Protzer, U. 2018. 'Hepatitis B virus genome recycling and de novo secondary infection events maintain stable cccDNA levels', *J Hepatol*, 69: 1231-41.
- Koch, P., Lampe, M., Godinez, W. J., Muller, B., Rohr, K., Krausslich, H. G., and Lehmann, M. J. 2009. 'Visualizing fusion of pseudotyped HIV-1 particles in real time by live cell microscopy', *Retrovirology*, 6: 84.
- Kock, J., Rosler, C., Zhang, J. J., Blum, H. E., Nassal, M., and Thoma, C. 2010. 'Generation of covalently closed circular DNA of hepatitis B viruses via intracellular recycling is regulated in a virus specific manner', *PLoS Pathog*, 6: e1001082.
- Koh, C., Canini, L., Dahari, H., Zhao, X., Uprichard, S. L., Haynes-Williams, V., Winters, M. A., Subramanya, G., Cooper, S. L., Pinto, P., Wolff, E. F., Bishop, R., Ai Thanda Han, M., Cotler, S. J., Kleiner, D. E., Keskin, O., Idilman, R., Yurdaydin, C., Glenn, J. S., and Heller, T. 2015. 'Oral prenylation inhibition with lonafarnib in chronic hepatitis D infection: a proof-of-concept randomised, double-blind, placebo-controlled phase 2A trial', *Lancet Infect Dis*, 15: 1167-74.
- Kolb, H. C., Finn, M. G., and Sharpless, K. B. 2001. 'Click Chemistry: Diverse Chemical Function from a Few Good Reactions', *Angew Chem Int Ed Engl*, 40: 2004-21.
- Komatsu, T., Quentin-Froignant, C., Carlon-Andres, I., Lagadec, F., Rayne, F., Ragues, J., Kehlenbach, R. H., Zhang, W., Ehrhardt, A., Bystricky, K., Morin, R., Lagarde, J. M., Gallardo, F., and Wodrich, H. 2018. 'In Vivo Labelling of Adenovirus DNA Identifies Chromatin Anchoring and Biphasic Genome Replication', *J Virol*, 92.
- Konig, A., Yang, J., Jo, E., Park, K. H. P., Kim, H., Than, T. T., Song, X., Qi, X., Dai, X., Park, S., Shum, D., Ryu, W. S., Kim, J. H., Yoon, S. K., Park, J. Y., Ahn, S. H., Han, K. H., Gerlich, W. H., and Windisch, M. P. 2019. 'Efficient long-term amplification of hepatitis B virus isolates after infection of slow proliferating HepG2-NTCP cells', *J Hepatol*, 71: 289-300.
- Koniger, C., Wingert, I., Marsmann, M., Rosler, C., Beck, J., and Nassal, M. 2014. 'Involvement of the host DNA-repair enzyme TDP2 in formation of the covalently closed circular DNA persistence reservoir of hepatitis B viruses', *Proc Natl Acad Sci U S A*, 111: E4244-53.
- Kos, A., Dijkema, R., Arnberg, A. C., van der Meide, P. H., and Schellekens, H. 1986. 'The hepatitis delta (delta) virus possesses a circular RNA', *Nature*, 323: 558-60.
- Kratz, P. A., Bottcher, B., and Nassal, M. 1999. 'Native display of complete foreign protein domains on the surface of hepatitis B virus capsids', *Proc Natl Acad Sci U S A*, 96: 1915-20.
- Krugman, S., Giles, J. P., and Hammond, J. 1967. 'Infectious hepatitis. Evidence for two distinctive clinical, epidemiological, and immunological types of infection', *JAMA*, 200: 365-73.

- Kuo, M. Y., Chao, M., and Taylor, J. 1989. 'Initiation of replication of the human hepatitis delta virus genome from cloned DNA: role of delta antigen', *J Virol*, 63: 1945-50.
- Kuo, M. Y., Goldberg, J., Coates, L., Mason, W., Gerin, J., and Taylor, J. 1988a. 'Molecular cloning of hepatitis delta virus RNA from an infected woodchuck liver: sequence, structure, and applications', *J Virol*, 62: 1855-61.
- Kuo, M. Y., Sharmeen, L., Dinter-Gottlieb, G., and Taylor, J. 1988b. 'Characterization of self-cleaving RNA sequences on the genome and antigenome of human hepatitis delta virus', *J Virol*, 62: 4439-44.
- Ladner, S. K., Otto, M. J., Barker, C. S., Zaifert, K., Wang, G. H., Guo, J. T., Seeger, C., and King, R. W. 1997. 'Inducible expression of human hepatitis B virus (HBV) in stably transfected hepatoblastoma cells: a novel system for screening potential inhibitors of HBV replication', *Antimicrob Agents Chemother*, 41: 1715-20.
- Laemmli, U. K. 1970. 'Cleavage of structural proteins during the assembly of the head of bacteriophage T4', *Nature*, 227: 680-5.
- Lahlali, T., Berke, J. M., Vergauwen, K., Foca, A., Vandyck, K., Pauwels, F., Zoulim, F., and Durantel, D. 2018. 'Novel Potent Capsid Assembly Modulators Regulate Multiple Steps of the Hepatitis B Virus Life Cycle', *Antimicrob Agents Chemother*, 62.
- Lai, C. L., Wong, D., Ip, P., Kopaniszen, M., Seto, W. K., Fung, J., Huang, F. Y., Lee, B., Cullaro, G., Chong, C. K., Wu, R., Cheng, C., Yuen, J., Ngai, V., and Yuen, M. F. 2017. 'Reduction of covalently closed circular DNA with long-term nucleos(t)ide analogue treatment in chronic hepatitis B', *J Hepatol*, 66: 275-81.
- Lakadamyali, M., Rust, M. J., Babcock, H. P., and Zhuang, X. 2003. 'Visualizing infection of individual influenza viruses', *Proc Natl Acad Sci U S A*, 100: 9280-5.
- Lamas Longarela, O., Schmidt, T. T., Schoneweis, K., Romeo, R., Wedemeyer, H., Urban, S., and Schulze, A. 2013. 'Proteoglycans act as cellular hepatitis delta virus attachment receptors', *PLoS One*, 8: e58340.
- Lambert, C., Thome, N., Kluck, C. J., and Prange, R. 2004. 'Functional incorporation of green fluorescent protein into hepatitis B virus envelope particles', *Virology*, 330: 158-67.
- Laras, A., Koskinas, J., Dimou, E., Kostamena, A., and Hadziyannis, S. J. 2006. 'Intrahepatic levels and replicative activity of covalently closed circular hepatitis B virus DNA in chronically infected patients', *Hepatology*, 44: 694-702.
- Lauber, C., Seitz, S., Mattei, S., Suh, A., Beck, J., Herstein, J., Borold, J., Salzburger, W., Kaderali, L., Briggs, J. A. G., and Bartenschlager, R. 2017. 'Deciphering the Origin and Evolution of Hepatitis B Viruses by Means of a Family of Non-enveloped Fish Viruses', *Cell Host Microbe*, 22: 387-99 e6.

- Le Seyec, J., Chouteau, P., Cannie, I., Guguen-Guillouzo, C., and Gripon, P. 1999. 'Infection process of the hepatitis B virus depends on the presence of a defined sequence in the pre-S1 domain', *J Virol*, 73: 2052-7.
- Lee, Y. S., Suh, D. J., Lim, Y. S., Jung, S. W., Kim, K. M., Lee, H. C., Chung, Y. H., Lee, Y. S., Yoo, W., and Kim, S. O. 2006. 'Increased risk of adefovir resistance in patients with lamivudine-resistant chronic hepatitis B after 48 weeks of adefovir dipivoxil monotherapy', *Hepatology*, 43: 1385-91.
- Lemke, E. A., Summerer, D., Geierstanger, B. H., Brittain, S. M., and Schultz, P. G. 2007. 'Control of protein phosphorylation with a genetically encoded photocaged amino acid', *Nat Chem Biol*, 3: 769-72.
- Lempp, F. A., Ni, Y., and Urban, S. 2016. 'Hepatitis delta virus: insights into a peculiar pathogen and novel treatment options', *Nat Rev Gastroenterol Hepatol*, 13: 580-9.
- Lempp, F. A., Schlund, F., Rieble, L., Nussbaum, L., Link, C., Zhang, Z., Ni, Y., and Urban, S. 2019. 'Recapitulation of HDV infection in a fully permissive hepatoma cell line allows efficient drug evaluation', *Nat Commun*, 10: 2265.
- Lempp, F. A., Wiedtke, E., Qu, B., Roques, P., Chemin, I., Vondran, F. W. R., Le Grand, R., Grimm, D., and Urban, S. 2017. 'Sodium taurocholate cotransporting polypeptide is the limiting host factor of hepatitis B virus infection in macaque and pig hepatocytes', *Hepatology*, 66: 703-16.
- Li, L., and Zhang, Z. 2016. 'Development and Applications of the Copper-Catalyzed Azide-Alkyne Cycloaddition (CuAAC) as a Bioorthogonal Reaction', *Molecules*, 21.
- Liang, L. B., Zhu, X., Yan, L. B., Du, L. Y., Liu, C., Liao, J., and Tang, H. 2016. 'Quantitative intrahepatic HBV cccDNA correlates with histological liver inflammation in chronic hepatitis B virus infection', *Int J Infect Dis*, 52: 77-82.
- Liaw, Y. F., Sung, J. J., Chow, W. C., Farrell, G., Lee, C. Z., Yuen, H., Tanwandee, T., Tao, Q. M., Shue, K., Keene, O. N., Dixon, J. S., Gray, D. F., Sabbat, J., and Cirrhosis Asian Lamivudine Multicentre Study, G. 2004. 'Lamivudine for patients with chronic hepatitis B and advanced liver disease', *N Engl J Med*, 351: 1521-31.
- Lin, S., Yan, H., Li, L., Yang, M., Peng, B., Chen, S., Li, W., and Chen, P. R. 2013. 'Site-specific engineering of chemical functionalities on the surface of live hepatitis D virus', *Angew Chem Int Ed Engl*, 52: 13970-4.
- Liu, A. A., Zhang, Z. F., Sun, E. Z., Zheng, Z. H., Zhang, Z. L., Hu, Q. X., Wang, H. Z., and Pang, D. W. 2016. 'Simultaneous Visualization of Parental and Progeny Viruses by a Capsid-Specific HaloTag Labeling Strategy', *Acs Nano*, 10: 1147-55.
- Liu, S. L., Tian, Z. Q., Zhang, Z. L., Wu, Q. M., Zhao, H. S., Ren, B., and Pang, D. W. 2012. 'High-efficiency dual labeling of influenza virus for single-virus imaging', *Biomaterials*, 33: 7828-33.

- Loffler-Mary, H., Dumortier, J., Klentsch-Zimmer, C., and Prange, R. 2000. 'Hepatitis B virus assembly is sensitive to changes in the cytosolic S loop of the envelope proteins', *Virology*, 270: 358-67.
- Lok, A. S., Zoulim, F., Dusheiko, G., and Ghany, M. G. 2017. 'Hepatitis B cure: From discovery to regulatory approval', *J Hepatol*, 67: 847-61.
- Long, Q., Yan, R., Hu, J., Cai, D., Mitra, B., Kim, E. S., Marchetti, A., Zhang, H., Wang, S., Liu, Y., Huang, A., and Guo, H. 2017. 'The role of host DNA ligases in hepadnavirus covalently closed circular DNA formation', *PLoS Pathog*, 13: e1006784.
- Lu, M., Ma, X., Castillo-Menendez, L. R., Gorman, J., Alshahafi, N., Ermel, U., Terry, D. S., Chambers, M., Peng, D., Zhang, B., Zhou, T., Reichard, N., Wang, K., Grover, J. R., Carman, B. P., Gardner, M. R., Nikic-Spiegel, I., Sugawara, A., Arthos, J., Lemke, E. A., Smith, A. B., 3rd, Farzan, M., Abrams, C., Munro, J. B., McDermott, A. B., Finzi, A., Kwong, P. D., Blanchard, S. C., Sodroski, J. G., and Mothes, W. 2019. 'Associating HIV-1 envelope glycoprotein structures with states on the virus observed by smFRET', *Nature*, 568: 415-19.
- Lucifora, J., Xia, Y., Reisinger, F., Zhang, K., Stadler, D., Cheng, X., Sprinzl, M. F., Koppensteiner, H., Makowska, Z., Volz, T., Remouchamps, C., Chou, W. M., Thasler, W. E., Huser, N., Durantel, D., Liang, T. J., Munk, C., Heim, M. H., Browning, J. L., Dejardin, E., Dandri, M., Schindler, M., Heikenwalder, M., and Protzer, U. 2014. 'Specific and nonhepatotoxic degradation of nuclear hepatitis B virus cccDNA', *Science*, 343: 1221-8.
- Lukinavicius, G., Umezawa, K., Olivier, N., Honigsmann, A., Yang, G., Plass, T., Mueller, V., Reymond, L., Correa, I. R., Jr., Luo, Z. G., Schultz, C., Lemke, E. A., Heppenstall, P., Eggeling, C., Manley, S., and Johnsson, K. 2013. 'A near-infrared fluorophore for live-cell super-resolution microscopy of cellular proteins', *Nat Chem*, 5: 132-9.
- Luo, J., Cui, X., Gao, L., and Hu, J. 2017. 'Identification of an Intermediate in Hepatitis B Virus Covalently Closed Circular (CCC) DNA Formation and Sensitive and Selective CCC DNA Detection', *J Virol*, 91.
- Lurmann, A. 1885. 'Eine Icterusepidemie', *Berlin Klinische Wochenschrift*, 22: 20-23.
- Lutwick, L. I., and Robinson, W. S. 1977. 'DNA synthesized in the hepatitis B Dane particle DNA polymerase reaction', *J Virol*, 21: 96-104.
- Macnaughton, T. B., Shi, S. T., Modahl, L. E., and Lai, M. M. 2002. 'Rolling circle replication of hepatitis delta virus RNA is carried out by two different cellular RNA polymerases', *J Virol*, 76: 3920-7.
- Macovei, A., Petrareanu, C., Lazar, C., Florian, P., and Branza-Nichita, N. 2013. 'Regulation of hepatitis B virus infection by Rab5, Rab7, and the endolysosomal compartment', *J Virol*, 87: 6415-27.

- Macovei, A., Radulescu, C., Lazar, C., Petrescu, S., Durantel, D., Dwek, R. A., Zitzmann, N., and Nichita, N. B. 2010. 'Hepatitis B virus requires intact caveolin-1 function for productive infection in HepaRG cells', *J Virol*, 84: 243-53.
- Magnius, L., Mason, W. S., Taylor, J., Kann, M., Glebe, D., Deny, P., Sureau, C., Norder, H., and Ictv Report, C. 2020. 'ICTV Virus Taxonomy Profile: Hepadnaviridae', *J Gen Virol*, 101: 571-72.
- Marcellin, P., Wong, D. K., Sievert, W., Buggisch, P., Petersen, J., Flisiak, R., Manns, M., Kaita, K., Krastev, Z., Lee, S. S., Cathcart, A. L., Crans, G., Op den Brouw, M., Jump, B., Gaggar, A., Flaherty, J., and Buti, M. 2019. 'Ten-year efficacy and safety of tenofovir disoproxil fumarate treatment for chronic hepatitis B virus infection', *Liver Int*, 39: 1868-75.
- Marsh, M., and Helenius, A. 2006. 'Virus entry: open sesame', *Cell*, 124: 729-40.
- Mason, W. S., Gill, U. S., Litwin, S., Zhou, Y., Peri, S., Pop, O., Hong, M. L., Naik, S., Quaglia, A., Bertolotti, A., and Kennedy, P. T. 2016. 'HBV DNA Integration and Clonal Hepatocyte Expansion in Chronic Hepatitis B Patients Considered Immune Tolerant', *Gastroenterology*, 151: 986-98 e4.
- McAleer, W. J., Buynak, E. B., Maigetter, R. Z., Wampler, D. E., Miller, W. J., and Hilleman, M. R. 1984. 'Human hepatitis B vaccine from recombinant yeast', *Nature*, 307: 178-80.
- McKay, C. S., and Finn, M. G. 2014. 'Click chemistry in complex mixtures: bioorthogonal bioconjugation', *Chem Biol*, 21: 1075-101.
- Mercer, J., Schelhaas, M., and Helenius, A. 2010. 'Virus entry by endocytosis', *Annu Rev Biochem*, 79: 803-33.
- Messageot, F., Salhi, S., Eon, P., and Rossignol, J. M. 2003. 'Proteolytic processing of the hepatitis B virus e antigen precursor. Cleavage at two furin consensus sequences', *J Biol Chem*, 278: 891-5.
- Miao, Z., Zhang, S., Ou, X., Li, S., Ma, Z., Wang, W., Peppelenbosch, M. P., Liu, J., and Pan, Q. 2020. 'Estimating the Global Prevalence, Disease Progression, and Clinical Outcome of Hepatitis Delta Virus Infection', *J Infect Dis*, 221: 1677-87.
- Michailidis, E., Pabon, J., Xiang, K., Park, P., Ramanan, V., Hoffmann, H. H., Schneider, W. M., Bhatia, S. N., de Jong, Y. P., Shlomai, A., and Rice, C. M. 2017. 'A robust cell culture system supporting the complete life cycle of hepatitis B virus', *Sci Rep*, 7: 16616.
- Milich, D. R., Jones, J. E., Hughes, J. L., Price, J., Raney, A. K., and McLachlan, A. 1990. 'Is a function of the secreted hepatitis B e antigen to induce immunologic tolerance in utero?', *Proc Natl Acad Sci U S A*, 87: 6599-603.
- Milles, S., Tyagi, S., Banterle, N., Koehler, C., VanDelinder, V., Plass, T., Neal, A. P., and Lemke, E. A. 2012. 'Click strategies for single-molecule protein fluorescence', *J Am Chem Soc*, 134: 5187-95.

- Miyauchi, K., Kim, Y., Latinovic, O., Morozov, V., and Melikyan, G. B. 2009. 'HIV enters cells via endocytosis and dynamin-dependent fusion with endosomes', *Cell*, 137: 433-44.
- Mukai, T., Kobayashi, T., Hino, N., Yanagisawa, T., Sakamoto, K., and Yokoyama, S. 2008. 'Adding l-lysine derivatives to the genetic code of mammalian cells with engineered pyrrolysyl-tRNA synthetases', *Biochem Biophys Res Commun*, 371: 818-22.
- Muller, B., Daecke, J., Fackler, O. T., Dittmar, M. T., Zentgraf, H., and Krausslich, H. G. 2004. 'Construction and characterization of a fluorescently labeled infectious human immunodeficiency virus type 1 derivative', *J Virol*, 78: 10803-13.
- Müller, T. G., Zila, V., Peters, K., Schifferdecker, S., Stanic, M., Lucic, B., Laketa, V., Lusic, M., Müller, B., and Kräusslich, H.-G. 2020. 'HIV-1 uncoating by release of viral cDNA from capsid-like structures in the nucleus of infected cells', *bioRxiv*: 2020.11.13.380030.
- Nakabayashi, H., Taketa, K., Miyano, K., Yamane, T., and Sato, J. 1982. 'Growth of human hepatoma cells lines with differentiated functions in chemically defined medium', *Cancer Res*, 42: 3858-63.
- Nassal, M. 1992. 'The arginine-rich domain of the hepatitis B virus core protein is required for pregenome encapsidation and productive viral positive-strand DNA synthesis but not for virus assembly', *J Virol*, 66: 4107-16.
- Nassal, M. 2015. 'HBV cccDNA: viral persistence reservoir and key obstacle for a cure of chronic hepatitis B', *Gut*, 64: 1972-84.
- Neefe, J. R., Stokes, J., Reinhold, J. G., and Lukens, F. D. 1944. 'Hepatitis Due to the Injection of Homologous Blood Products in Human Volunteers', *J Clin Invest*, 23: 836-55.
- Neumann, H., Peak-Chew, S. Y., and Chin, J. W. 2008. 'Genetically encoding N(epsilon)-acetyllysine in recombinant proteins', *Nat Chem Biol*, 4: 232-4.
- Ni, Y., Lempp, F. A., Mehrle, S., Nkongolo, S., Kaufman, C., Falth, M., Stindt, J., Koniger, C., Nassal, M., Kubitz, R., Sultmann, H., and Urban, S. 2014. 'Hepatitis B and D viruses exploit sodium taurocholate co-transporting polypeptide for species-specific entry into hepatocytes', *Gastroenterology*, 146: 1070-83.
- Ni, Y., Sonnabend, J., Seitz, S., and Urban, S. 2010. 'The pre-s2 domain of the hepatitis B virus is dispensable for infectivity but serves a spacer function for L-protein-connected virus assembly', *J Virol*, 84: 3879-88.
- Ni, Y., Zhang, Z., Engelskircher, L., Verch, G., Tu, T., Lempp, F. A., and Urban, S. 2019. 'Generation and characterization of a stable cell line persistently replicating and secreting the human hepatitis delta virus', *Sci Rep*, 9: 10021.
- Nikic, I., Estrada Girona, G., Kang, J. H., Paci, G., Mikhaleva, S., Koehler, C., Shymanska, N. V., Ventura Santos, C., Spitz, D., and Lemke, E. A. 2016. 'Debugging Eukaryotic Genetic Code

Expansion for Site-Specific Click-PAINT Super-Resolution Microscopy', *Angew Chem Int Ed Engl*, 55: 16172-76.

Nikic, I., Kang, J. H., Girona, G. E., Aramburu, I. V., and Lemke, E. A. 2015. 'Labeling proteins on live mammalian cells using click chemistry', *Nat Protoc*, 10: 780-91.

Nikic, I., Plass, T., Schraidt, O., Szymanski, J., Briggs, J. A., Schultz, C., and Lemke, E. A. 2014. 'Minimal tags for rapid dual-color live-cell labeling and super-resolution microscopy', *Angew Chem Int Ed Engl*, 53: 2245-9.

Noren, C. J., Anthony-Cahill, S. J., Griffith, M. C., and Schultz, P. G. 1989. 'A general method for site-specific incorporation of unnatural amino acids into proteins', *Science*, 244: 182-8.

Okochi, K., and Murakami, S. 1968. 'Observations on Australia antigen in Japanese', *Vox Sang*, 15: 374-85.

Osseman, Q., Gallucci, L., Au, S., Cazenave, C., Berdance, E., Blondot, M. L., Cassany, A., Begu, D., Ragues, J., Aknin, C., Sominskaya, I., Dishlers, A., Rabe, B., Anderson, F., Pante, N., and Kann, M. 2018. 'The chaperone dynein LL1 mediates cytoplasmic transport of empty and mature hepatitis B virus capsids', *J Hepatol*, 68: 441-48.

Ostapchuk, P., Hearing, P., and Ganem, D. 1994. 'A dramatic shift in the transmembrane topology of a viral envelope glycoprotein accompanies hepatitis B viral morphogenesis', *EMBO J*, 13: 1048-57.

Otto, J. C., and Casey, P. J. 1996. 'The hepatitis delta virus large antigen is farnesylated both in vitro and in animal cells', *J Biol Chem*, 271: 4569-72.

Ou, J. H., Laub, O., and Rutter, W. J. 1986. 'Hepatitis B virus gene function: the precore region targets the core antigen to cellular membranes and causes the secretion of the e antigen', *Proc Natl Acad Sci U S A*, 83: 1578-82.

Paci, G., Zheng, T., Caria, J., Zilman, A., and Lemke, E. A. 2020. 'Molecular determinants of large cargo transport into the nucleus', *Elife*, 9.

Pante, N., and Kann, M. 2002. 'Nuclear pore complex is able to transport macromolecules with diameters of about 39 nm', *Mol Biol Cell*, 13: 425-34.

Paran, N., Geiger, B., and Shaul, Y. 2001. 'HBV infection of cell culture: evidence for multivalent and cooperative attachment', *EMBO J*, 20: 4443-53.

Paraskevopoulou, S., Pirzer, F., Goldmann, N., Schmid, J., Corman, V. M., Gottula, L. T., Schroeder, S., Rasche, A., Muth, D., Drexler, J. F., Heni, A. C., Eibner, G. J., Page, R. A., Jones, T. C., Muller, M. A., Sommer, S., Glebe, D., and Drosten, C. 2020. 'Mammalian deltavirus without hepadnavirus coinfection in the neotropical rodent *Proechimys semispinosus*', *Proc Natl Acad Sci U S A*, 117: 17977-83.

- Pasek, M., Goto, T., Gilbert, W., Zink, B., Schaller, H., MacKay, P., Leadbetter, G., and Murray, K. 1979. 'Hepatitis B virus genes and their expression in E. coli', *Nature*, 282: 575-9.
- Patient, R., Hourieux, C., Sizaret, P. Y., Trassard, S., Sureau, C., and Roingeard, P. 2007. 'Hepatitis B virus subviral envelope particle morphogenesis and intracellular trafficking', *J Virol*, 81: 3842-51.
- Peng, K., Muranyi, W., Glass, B., Laketa, V., Yant, S. R., Tsai, L., Cihlar, T., Muller, B., and Krausslich, H. G. 2014. 'Quantitative microscopy of functional HIV post-entry complexes reveals association of replication with the viral capsid', *Elife*, 3: e04114.
- Perez-Vargas, J., Amirache, F., Boson, B., Mialon, C., Freitas, N., Sureau, C., Fusil, F., and Cosset, F. L. 2019. 'Enveloped viruses distinct from HBV induce dissemination of hepatitis D virus in vivo', *Nat Commun*, 10: 2098.
- Persing, D. H., Varmus, H. E., and Ganem, D. 1987. 'The preS1 protein of hepatitis B virus is acylated at its amino terminus with myristic acid', *J Virol*, 61: 1672-7.
- Plass, T., Milles, S., Koehler, C., Schultz, C., and Lemke, E. A. 2011. 'Genetically encoded copper-free click chemistry', *Angew Chem Int Ed Engl*, 50: 3878-81.
- Plass, T., Milles, S., Koehler, C., Szymanski, J., Mueller, R., Wiessler, M., Schultz, C., and Lemke, E. A. 2012. 'Amino acids for Diels-Alder reactions in living cells', *Angew Chem Int Ed Engl*, 51: 4166-70.
- Polaris Observatory, C. 2018. 'Global prevalence, treatment, and prevention of hepatitis B virus infection in 2016: a modelling study', *Lancet Gastroenterol Hepatol*, 3: 383-403.
- Pollicino, T., Belloni, L., Raffa, G., Pediconi, N., Squadrito, G., Raimondo, G., and Levrero, M. 2006. 'Hepatitis B virus replication is regulated by the acetylation status of hepatitis B virus cccDNA-bound H3 and H4 histones', *Gastroenterology*, 130: 823-37.
- Polson, A. G., Bass, B. L., and Casey, J. L. 1996. 'RNA editing of hepatitis delta virus antigenome by dsRNA-adenosine deaminase', *Nature*, 380: 454-6.
- Polycarpo, C., Ambrogelly, A., Berube, A., Winbush, S. M., McCloskey, J. A., Crain, P. F., Wood, J. L., and Soll, D. 2004. 'An aminoacyl-tRNA synthetase that specifically activates pyrrolysine', *Proc Natl Acad Sci U S A*, 101: 12450-4.
- Polycarpo, C. R., Herring, S., Berube, A., Wood, J. L., Soll, D., and Ambrogelly, A. 2006. 'Pyrrolysine analogues as substrates for pyrrolysyl-tRNA synthetase', *FEBS Lett*, 580: 6695-700.
- Ponsel, D., and Bruss, V. 2003. 'Mapping of amino acid side chains on the surface of hepatitis B virus capsids required for envelopment and virion formation', *J Virol*, 77: 416-22.

- Prescher, J. A., and Bertozzi, C. R. 2005. 'Chemistry in living systems', *Nat Chem Biol*, 1: 13-21.
- Prince, A. M. 1968a. 'An antigen detected in the blood during the incubation period of serum hepatitis', *Proc Natl Acad Sci U S A*, 60: 814-21.
- Prince, A. M. 1968b. 'Relation of Australia and SH antigens', *Lancet*, 2: 462-3.
- Protzer, U., Nassal, M., Chiang, P. W., Kirschfink, M., and Schaller, H. 1999. 'Interferon gene transfer by a hepatitis B virus vector efficiently suppresses wild-type virus infection', *Proc Natl Acad Sci U S A*, 96: 10818-23.
- Qi, Y., Gao, Z., Xu, G., Peng, B., Liu, C., Yan, H., Yao, Q., Sun, G., Liu, Y., Tang, D., Song, Z., He, W., Sun, Y., Guo, J. T., and Li, W. 2016. 'DNA Polymerase kappa Is a Key Cellular Factor for the Formation of Covalently Closed Circular DNA of Hepatitis B Virus', *PLoS Pathog*, 12: e1005893.
- Qu, B., Ni, Y., Lempp, F. A., Vondran, F. W. R., and Urban, S. 2018. 'T5 Exonuclease Hydrolysis of Hepatitis B Virus Replicative Intermediates Allows Reliable Quantification and Fast Drug Efficacy Testing of Covalently Closed Circular DNA by PCR', *J Virol*, 92.
- Quasdorff, M., and Protzer, U. 2010. 'Control of hepatitis B virus at the level of transcription', *J Viral Hepat*, 17: 527-36.
- Rabe, B., Vlachou, A., Pante, N., Helenius, A., and Kann, M. 2003. 'Nuclear import of hepatitis B virus capsids and release of the viral genome', *Proc Natl Acad Sci U S A*, 100: 9849-54.
- Ramia, S., and Bahakim, H. 1988. 'Perinatal transmission of hepatitis B virus-associated hepatitis D virus', *Ann Inst Pasteur Virol*, 139: 285-90.
- Reinkemeier, C. D., Girona, G. E., and Lemke, E. A. 2019. 'Designer membraneless organelles enable codon reassigment of selected mRNAs in eukaryotes', *Science*, 363.
- Revell, P. A., Tu, T., Netter, H. J., Yuen, L. K. W., Locarnini, S. A., and Littlejohn, M. 2020. 'The evolution and clinical impact of hepatitis B virus genome diversity', *Nat Rev Gastroenterol Hepatol*, 17: 618-34.
- Rigg, R. J., and Schaller, H. 1992. 'Duck hepatitis B virus infection of hepatocytes is not dependent on low pH', *J Virol*, 66: 2829-36.
- Rizzetto, M., Canese, M. G., Arico, S., Crivelli, O., Trepo, C., Bonino, F., and Verme, G. 1977. 'Immunofluorescence detection of new antigen-antibody system (delta/anti-delta) associated to hepatitis B virus in liver and in serum of HBsAg carriers', *Gut*, 18: 997-1003.
- Rizzetto, M., Canese, M. G., Gerin, J. L., London, W. T., Sly, D. L., and Purcell, R. H. 1980a. 'Transmission of the hepatitis B virus-associated delta antigen to chimpanzees', *J Infect Dis*, 141: 590-602.

- Rizzetto, M., Hamid, S., and Negro, F. 2021. 'The changing scenario of hepatitis D', *J Hepatol*.
- Rizzetto, M., Hoyer, B., Canese, M. G., Shih, J. W., Purcell, R. H., and Gerin, J. L. 1980b. 'delta Agent: association of delta antigen with hepatitis B surface antigen and RNA in serum of delta-infected chimpanzees', *Proc Natl Acad Sci U S A*, 77: 6124-8.
- Rothman, D. J. 1982. 'Were Tuskegee & Willowbrook 'studies in nature'?', *Hastings Cent Rep*, 12: 5-7.
- Rudner, L., Nydegger, S., Coren, L. V., Nagashima, K., Thali, M., and Ott, D. E. 2005. 'Dynamic fluorescent imaging of human immunodeficiency virus type 1 gag in live cells by biarsenical labeling', *J Virol*, 79: 4055-65.
- Rydell, G. E., Prakash, K., Norder, H., and Lindh, M. 2017. 'Hepatitis B surface antigen on subviral particles reduces the neutralizing effect of anti-HBs antibodies on hepatitis B viral particles in vitro', *Virology*, 509: 67-70.
- Sagnelli, E., Stroffolini, T., Ascione, A., Bonino, F., Chiaramonte, M., Colombo, M., Craxi, A., Giusti, G., Manghisi, O. G., Pastore, G., and et al. 1992. 'The epidemiology of hepatitis delta infection in Italy. Promoting Group', *J Hepatol*, 15: 211-5.
- Sakin, V., Hanne, J., Dunder, J., Anders-Osswein, M., Laketa, V., Nikic, I., Krausslich, H. G., Lemke, E. A., and Muller, B. 2017. 'A Versatile Tool for Live-Cell Imaging and Super-Resolution Nanoscopy Studies of HIV-1 Env Distribution and Mobility', *Cell Chem Biol*, 24: 635-45 e5.
- Sakin, V., Paci, G., Lemke, E. A., and Muller, B. 2016. 'Labeling of virus components for advanced, quantitative imaging analyses', *Febs Letters*, 590: 1896-914.
- Schmied, W. H., Elsasser, S. J., Uttamapinant, C., and Chin, J. W. 2014. 'Efficient multisite unnatural amino acid incorporation in mammalian cells via optimized pyrrolysyl tRNA synthetase/tRNA expression and engineered eRF1', *J Am Chem Soc*, 136: 15577-83.
- Schmitz, A., Schwarz, A., Foss, M., Zhou, L., Rabe, B., Hoellenriegel, J., Stoeber, M., Pante, N., and Kann, M. 2010. 'Nucleoporin 153 arrests the nuclear import of hepatitis B virus capsids in the nuclear basket', *PLoS Pathog*, 6: e1000741.
- Schultz, U., Summers, J., Staeheli, P., and Chisari, F. V. 1999. 'Elimination of duck hepatitis B virus RNA-containing capsids in duck interferon-alpha-treated hepatocytes', *J Virol*, 73: 5459-65.
- Schulze, A., Gripon, P., and Urban, S. 2007. 'Hepatitis B virus infection initiates with a large surface protein-dependent binding to heparan sulfate proteoglycans', *Hepatology*, 46: 1759-68.
- Schulze, A., Mills, K., Weiss, T. S., and Urban, S. 2012. 'Hepatocyte polarization is essential for the productive entry of the hepatitis B virus', *Hepatology*, 55: 373-83.

- Schwartz, T., Aloush, N., Goliand, I., Segal, I., Nachmias, D., Arbely, E., and Elia, N. 2017. 'Direct fluorescent-dye labeling of alpha-tubulin in mammalian cells for live cell and superresolution imaging', *Mol Biol Cell*, 28: 2747-56.
- Seeff, L. B., Beebe, G. W., Hoofnagle, J. H., Norman, J. E., Buskell-Bales, Z., Waggoner, J. G., Kaplowitz, N., Koff, R. S., Petrini, J. L., Jr., Schiff, E. R., and et al. 1987. 'A serologic follow-up of the 1942 epidemic of post-vaccination hepatitis in the United States Army', *N Engl J Med*, 316: 965-70.
- Seitz, S., Habjanic, J., Schutz, A. K., and Bartenschlager, R. 2020. 'The Hepatitis B Virus Envelope Proteins: Molecular Gymnastics Throughout the Viral Life Cycle', *Annu Rev Virol*, 7: 263-88.
- Seitz, S., Iancu, C., Volz, T., Mier, W., Dandri, M., Urban, S., and Bartenschlager, R. 2016. 'A Slow Maturation Process Renders Hepatitis B Virus Infectious', *Cell Host Microbe*, 20: 25-35.
- Seitz, S., Urban, S., Antoni, C., and Bottcher, B. 2007. 'Cryo-electron microscopy of hepatitis B virions reveals variability in envelope capsid interactions', *EMBO J*, 26: 4160-7.
- Short, J. M., Chen, S., Roseman, A. M., Butler, P. J., and Crowther, R. A. 2009. 'Structure of hepatitis B surface antigen from subviral tubes determined by electron cryomicroscopy', *J Mol Biol*, 390: 135-41.
- Si, L., Xu, H., Zhou, X., Zhang, Z., Tian, Z., Wang, Y., Wu, Y., Zhang, B., Niu, Z., Zhang, C., Fu, G., Xiao, S., Xia, Q., Zhang, L., and Zhou, D. 2016. 'Generation of influenza A viruses as live but replication-incompetent virus vaccines', *Science*, 354: 1170-73.
- Slagle, B. L., and Bouchard, M. J. 2016. 'Hepatitis B Virus X and Regulation of Viral Gene Expression', *Cold Spring Harb Perspect Med*, 6: a021402.
- Smedile, A., Farci, P., Verme, G., Caredda, F., Cargnel, A., Caporaso, N., Dentico, P., Trepo, C., Opolon, P., Gimson, A., Vergani, D., Williams, R., and Rizzetto, M. 1982. 'Influence of delta infection on severity of hepatitis B', *Lancet*, 2: 945-7.
- Sopena, S., Godoy, C., Taberner, D., Homs, M., Gregori, J., Riveiro-Barciela, M., Ruiz, A., Esteban, R., Buti, M., and Rodriguez-Frias, F. 2018. 'Quantitative characterization of hepatitis delta virus genome edition by next-generation sequencing', *Virus Res*, 243: 52-59.
- Spearman, C. W., Dusheiko, G. M., Hellard, M., and Sonderup, M. 2019. 'Hepatitis C', *Lancet*, 394: 1451-66.
- Sprinzel, M. F., Oberwinkler, H., Schaller, H., and Protzer, U. 2001. 'Transfer of hepatitis B virus genome by adenovirus vectors into cultured cells and mice: crossing the species barrier', *J Virol*, 75: 5108-18.
- Srinivasan, G., James, C. M., and Krzycki, J. A. 2002. 'Pyrrolysine encoded by UAG in Archaea: charging of a UAG-decoding specialized tRNA', *Science*, 296: 1459-62.

- Stanaway, J. D., Flaxman, A. D., Naghavi, M., Fitzmaurice, C., Vos, T., Abubakar, I., Abu-Raddad, L. J., Assadi, R., Bhala, N., Cowie, B., Forouzanfour, M. H., Groeger, J., Hanafiah, K. M., Jacobsen, K. H., James, S. L., MacLachlan, J., Malekzadeh, R., Martin, N. K., Mokdad, A. A., Mokdad, A. H., Murray, C. J. L., Plass, D., Rana, S., Rein, D. B., Richardus, J. H., Sanabria, J., Saylan, M., Shahraz, S., So, S., Vlassov, V. V., Weiderpass, E., Wiersma, S. T., Younis, M., Yu, C., El Sayed Zaki, M., and Cooke, G. S. 2016. 'The global burden of viral hepatitis from 1990 to 2013: findings from the Global Burden of Disease Study 2013', *Lancet*, 388: 1081-88.
- Stieger, B., Hagenbuch, B., Landmann, L., Hochli, M., Schroeder, A., and Meier, P. J. 1994. 'In situ localization of the hepatocytic Na⁺/Taurocholate cotransporting polypeptide in rat liver', *Gastroenterology*, 107: 1781-7.
- Stockdale, A. J., Kreuels, B., Henrion, M. Y. R., Giorgi, E., Kyomuhangi, I., de Martel, C., Hutin, Y., and Geretti, A. M. 2020. 'The global prevalence of hepatitis D virus infection: Systematic review and meta-analysis', *J Hepatol*, 73: 523-32.
- Summers, J., Smith, P. M., and Horwich, A. L. 1990. 'Hepadnavirus envelope proteins regulate covalently closed circular DNA amplification', *J Virol*, 64: 2819-24.
- Sun, E., He, J., and Zhuang, X. 2013. 'Live cell imaging of viral entry', *Curr Opin Virol*, 3: 34-43.
- Sun, S., Yan, J., Xia, C., Lin, Y., Jiang, X., Liu, H., Ren, H., Yan, J., Lin, J., and He, X. 2014. 'Visualizing hepatitis B virus with biarsenical labelling in living cells', *Liver Int*, 34: 1532-42.
- Sureau, C., Fournier-Wirth, C., and Maurel, P. 2003. 'Role of N glycosylation of hepatitis B virus envelope proteins in morphogenesis and infectivity of hepatitis delta virus', *J Virol*, 77: 5519-23.
- Suzuki, T., Miller, C., Guo, L. T., Ho, J. M. L., Bryson, D. I., Wang, Y. S., Liu, D. R., and Soll, D. 2017. 'Crystal structures reveal an elusive functional domain of pyrrolysyl-tRNA synthetase', *Nat Chem Biol*, 13: 1261-66.
- Tahaei, S. M., Mohebbi, S. R., and Zali, M. R. 2012. 'Enteric hepatitis viruses', *Gastroenterol Hepatol Bed Bench*, 5: 7-15.
- Tang, L., Sheraz, M., McGrane, M., Chang, J., and Guo, J. T. 2019. 'DNA Polymerase alpha is essential for intracellular amplification of hepatitis B virus covalently closed circular DNA', *PLoS Pathog*, 15: e1007742.
- Tenney, D. J., Rose, R. E., Baldick, C. J., Pokornowski, K. A., Eggers, B. J., Fang, J., Wichroski, M. J., Xu, D., Yang, J., Wilber, R. B., and Colonno, R. J. 2009. 'Long-term monitoring shows hepatitis B virus resistance to entecavir in nucleoside-naive patients is rare through 5 years of therapy', *Hepatology*, 49: 1503-14.
- Thimme, R., Wieland, S., Steiger, C., Ghayeb, J., Reimann, K. A., Purcell, R. H., and Chisari, F. V. 2003. 'CD8(+) T cells mediate viral clearance and disease pathogenesis during acute hepatitis B virus infection', *J Virol*, 77: 68-76.

- Thomas, J. M., and Beal, P. A. 2017. 'How do ADARs bind RNA? New protein-RNA structures illuminate substrate recognition by the RNA editing ADARs', *Bioessays*, 39.
- Tornøe, C. W., Christensen, C., and Meldal, M. 2002. 'Peptidotriazoles on solid phase: [1,2,3]-triazoles by regiospecific copper(i)-catalyzed 1,3-dipolar cycloadditions of terminal alkynes to azides', *J Org Chem*, 67: 3057-64.
- Trepo, C. 2014. 'A brief history of hepatitis milestones', *Liver Int*, 34 Suppl 1: 29-37.
- Tu, T., Block, J. M., Wang, S., Cohen, C., and Douglas, M. W. 2020a. 'The Lived Experience of Chronic Hepatitis B: A Broader View of Its Impacts and Why We Need a Cure', *Viruses*, 12.
- Tu, T., Budzinska, M. A., Shackel, N. A., and Urban, S. 2017. 'HBV DNA Integration: Molecular Mechanisms and Clinical Implications', *Viruses*, 9.
- Tu, T., Budzinska, M. A., Vondran, F. W. R., Shackel, N. A., and Urban, S. 2018. 'Hepatitis B Virus DNA Integration Occurs Early in the Viral Life Cycle in an In Vitro Infection Model via Sodium Taurocholate Cotransporting Polypeptide-Dependent Uptake of Enveloped Virus Particles', *J Virol*, 92.
- Tu, T., and Jilbert, A. R. 2017. 'Detection of Hepatocyte Clones Containing Integrated Hepatitis B Virus DNA Using Inverse Nested PCR', *Methods Mol Biol*, 1540: 97-118.
- Tu, T., and Urban, S. 2018. 'Detection of Low Copy Number Integrated Viral DNA Formed by In Vitro Hepatitis B Infection', *J Vis Exp*.
- Tu, T., Zehnder, B., Levy, M., Micali, G., Tran, L., Dabere, O., Main, N., Shackel, N., and Urban, S. 2019. 'Hepatitis B virus (HBV) DNA integration is not driven by viral proteins', *Zeitschrift für Gastroenterologie*, 57: P5. 46.
- Tu, T., Zehnder, B., Qu, B., Ni, Y., Main, N., Allweiss, L., Dandri, M., Shackel, N., George, J., and Urban, S. 2020b. 'A novel method to precisely quantify Hepatitis B Virus covalently closed circular (ccc)DNA formation and maintenance', *Antiviral Res*: 104865.
- Tu, T., Zehnder, B., Qu, B., and Urban, S. 2021. 'De novo synthesis of hepatitis B virus nucleocapsids is dispensable for the maintenance and transcriptional regulation of cccDNA', *JHEP Rep*, 3: 100195.
- Turner, R. H., Snavelny, J. R., Grossman, E. B., Buchanan, R. N., and Foster, S. O. 1944. 'Some clinical studies of acute hepatitis occurring in soldiers after inoculation with yellow fever vaccine; with especial consideration of severe attacks', *Annals of Internal Medicine*, 20: 193-218.
- Uprichard, S. L., Wieland, S. F., Althage, A., and Chisari, F. V. 2003. 'Transcriptional and posttranscriptional control of hepatitis B virus gene expression', *Proc Natl Acad Sci U S A*, 100: 1310-5.

- Uttamapinant, C., Howe, J. D., Lang, K., Beranek, V., Davis, L., Mahesh, M., Barry, N. P., and Chin, J. W. 2015. 'Genetic code expansion enables live-cell and super-resolution imaging of site-specifically labeled cellular proteins', *J Am Chem Soc*, 137: 4602-5.
- Valenzuela, P., Medina, A., Rutter, W. J., Ammerer, G., and Hall, B. D. 1982. 'Synthesis and assembly of hepatitis B virus surface antigen particles in yeast', *Nature*, 298: 347-50.
- Vargas-Rodriguez, O., Sevostyanova, A., Soll, D., and Crnkovic, A. 2018. 'Upgrading aminoacyl-tRNA synthetases for genetic code expansion', *Curr Opin Chem Biol*, 46: 115-22.
- Volz, T., Allweiss, L., Ben, M. M., Warlich, M., Lohse, A. W., Pollok, J. M., Alexandrov, A., Urban, S., Petersen, J., Lutgehetmann, M., and Dandri, M. 2013. 'The entry inhibitor Myrcludex-B efficiently blocks intrahepatic virus spreading in humanized mice previously infected with hepatitis B virus', *J Hepatol*, 58: 861-7.
- Waldchen, S., Lehmann, J., Klein, T., van de Linde, S., and Sauer, M. 2015. 'Light-induced cell damage in live-cell super-resolution microscopy', *Sci Rep*, 5: 15348.
- Wang, I. H., Suomalainen, M., Andriasyan, V., Kilcher, S., Mercer, J., Neef, A., Luedtke, N. W., and Greber, U. F. 2013a. 'Tracking viral genomes in host cells at single-molecule resolution', *Cell Host Microbe*, 14: 468-80.
- Wang, K. S., Choo, Q. L., Weiner, A. J., Ou, J. H., Najarian, R. C., Thayer, R. M., Mullenbach, G. T., Denniston, K. J., Gerin, J. L., and Houghton, M. 1986. 'Structure, sequence and expression of the hepatitis delta (delta) viral genome', *Nature*, 323: 508-14.
- Wang, L., Brock, A., Herberich, B., and Schultz, P. G. 2001. 'Expanding the genetic code of *Escherichia coli*', *Science*, 292: 498-500.
- Wang, W., Lempp, F. A., Schlund, F., Walter, L., Decker, C., Zhang, Z., Ni, Y., and Urban, S. 2021. 'Assembly and infection efficacy of hepatitis B virus surface protein exchanges in eight hepatitis D virus genotype isolates', *J Hepatol*.
- Wang, Z., Wu, L., Cheng, X., Liu, S., Li, B., Li, H., Kang, F., Wang, J., Xia, H., Ping, C., Nassal, M., and Sun, D. 2013b. 'Replication-competent infectious hepatitis B virus vectors carrying substantially sized transgenes by redesigned viral polymerase translation', *PLoS One*, 8: e60306.
- Watanabe, T., Sorensen, E. M., Naito, A., Schott, M., Kim, S., and Ahlquist, P. 2007. 'Involvement of host cellular multivesicular body functions in hepatitis B virus budding', *Proc Natl Acad Sci U S A*, 104: 10205-10.
- Wedemeyer, H., Bogomolov, P., Blank, A., Allweiss, L., Dandri-Petersen, M., Bremer, B., Voronkova, N., Schöneweis, K., Pathil, A., and Burhenne, J. 2018. 'Final results of a multicenter, open-label phase 2b clinical trial to assess safety and efficacy of Myrcludex B in combination with Tenofovir in patients with chronic HBV/HDV co-infection', *Journal of Hepatology*, 68: S3.

- Wedemeyer, H., Schoneweis, K., Bogomolov, P., Voronkova, N., Chulanov, V., and Stepanova, T. 2019a. "Final results of a multicenter, open-label phase 2 clinical trial (MYR203) to assess safety and efficacy of myrcludex B in combination with PEG-interferon Alpha 2a in patients with chronic HBV/HDV co-infection." In *Program and abstracts of the The International Liver Congress*.
- Wedemeyer, H., Schöneweis, K., Bogomolov, P. O., Chulanov, V., Stepanova, T., Viacheslav, M., Allweiss, L., Dandri, M., Ciesek, S., and Dittmer, U. 2020. '48 weeks of high dose (10 mg) bulevirtide as monotherapy or with peginterferon alfa-2a in patients with chronic HBV/HDV co-infection', *Journal of Hepatology*, 73: S52-S53.
- Wedemeyer, H., Yurdaydin, C., Dalekos, G. N., Erhardt, A., Cakaloglu, Y., Degertekin, H., Gurel, S., Zeuzem, S., Zachou, K., Bozkaya, H., Koch, A., Bock, T., Dienes, H. P., Manns, M. P., and Group, H. S. 2011. 'Peginterferon plus adefovir versus either drug alone for hepatitis delta', *N Engl J Med*, 364: 322-31.
- Wedemeyer, H., Yurdaydin, C., Hardtke, S., Caruntu, F. A., Curescu, M. G., Yalcin, K., Akarca, U. S., Gurel, S., Zeuzem, S., Erhardt, A., Luth, S., Papatheodoridis, G. V., Keskin, O., Port, K., Radu, M., Celen, M. K., Idilman, R., Weber, K., Stift, J., Wittkop, U., Heidrich, B., Mederacke, I., von der Leyen, H., Dienes, H. P., Cornberg, M., Koch, A., Manns, M. P., and team, H.-I. s. 2019b. 'Peginterferon alfa-2a plus tenofovir disoproxil fumarate for hepatitis D (HIDIT-II): a randomised, placebo controlled, phase 2 trial', *Lancet Infect Dis*, 19: 275-86.
- Wei, L., and Ploss, A. 2020. 'Core components of DNA lagging strand synthesis machinery are essential for hepatitis B virus cccDNA formation', *Nat Microbiol*, 5: 715-26.
- Werle-Lapostolle, B., Bowden, S., Locarnini, S., Wursthorn, K., Petersen, J., Lau, G., Trepo, C., Marcellin, P., Goodman, Z., Delaney, W. E. t., Xiong, S., Brosgart, C. L., Chen, S. S., Gibbs, C. S., and Zoulim, F. 2004. 'Persistence of cccDNA during the natural history of chronic hepatitis B and decline during adefovir dipivoxil therapy', *Gastroenterology*, 126: 1750-8.
- WHO. 2016. 'Global Health Estimates 2015: Deaths by Cause, Age, Sex, by Country and by Region, 2000-2015', *Geneva, World Health Organization*.
- WHO. 2017. 'Global hepatitis report', World Health Organization. <https://www.who.int/hepatitis/publications/global-hepatitis-report2017/en/>.
- Wieland, S. F., Spangenberg, H. C., Thimme, R., Purcell, R. H., and Chisari, F. V. 2004. 'Expansion and contraction of the hepatitis B virus transcriptional template in infected chimpanzees', *Proc Natl Acad Sci U S A*, 101: 2129-34.
- Will, H., Cattaneo, R., Koch, H. G., Darai, G., Schaller, H., Schellekens, H., van Eerd, P. M., and Deinhardt, F. 1982. 'Cloned HBV DNA causes hepatitis in chimpanzees', *Nature*, 299: 740-2.
- Wille, M., Netter, H. J., Littlejohn, M., Yuen, L., Shi, M., Eden, J. S., Klaassen, M., Holmes, E. C., and Hurt, A. C. 2018. 'A Divergent Hepatitis D-Like Agent in Birds', *Viruses*, 10.

- Winer, B. Y., Shirvani-Dastgerdi, E., Bram, Y., Sellau, J., Low, B. E., Johnson, H., Huang, T., Hrebikova, G., Heller, B., Sharon, Y., Giersch, K., Gerges, S., Seneca, K., Pais, M. A., Frankel, A. S., Chiriboga, L., Cullen, J., Nahass, R. G., Lutgehetmann, M., Toettcher, J. E., Wiles, M. V., Schwartz, R. E., and Ploss, A. 2018. 'Preclinical assessment of antiviral combination therapy in a genetically humanized mouse model for hepatitis delta virus infection', *Sci Transl Med*, 10.
- Wong, S. K., and Lazinski, D. W. 2002. 'Replicating hepatitis delta virus RNA is edited in the nucleus by the small form of ADAR1', *Proc Natl Acad Sci U S A*, 99: 15118-23.
- Wu, G., Liu, B., Zhang, Y., Li, J., Arzumanyan, A., Clayton, M. M., Schinazi, R. F., Wang, Z., Goldmann, S., Ren, Q., Zhang, F., and Feitelson, M. A. 2013. 'Preclinical characterization of GLS4, an inhibitor of hepatitis B virus core particle assembly', *Antimicrob Agents Chemother*, 57: 5344-54.
- Wu, T. T., Coates, L., Aldrich, C. E., Summers, J., and Mason, W. S. 1990. 'In hepatocytes infected with duck hepatitis B virus, the template for viral RNA synthesis is amplified by an intracellular pathway', *Virology*, 175: 255-61.
- Wykes, M. N., and Lewin, S. R. 2018. 'Immune checkpoint blockade in infectious diseases', *Nat Rev Immunol*, 18: 91-104.
- Wynne, S. A., Crowther, R. A., and Leslie, A. G. 1999. 'The crystal structure of the human hepatitis B virus capsid', *Mol Cell*, 3: 771-80.
- Yan, H., Zhong, G., Xu, G., He, W., Jing, Z., Gao, Z., Huang, Y., Qi, Y., Peng, B., Wang, H., Fu, L., Song, M., Chen, P., Gao, W., Ren, B., Sun, Y., Cai, T., Feng, X., Sui, J., and Li, W. 2012. 'Sodium taurocholate cotransporting polypeptide is a functional receptor for human hepatitis B and D virus', *Elife*, 1: e00049.
- Yanagisawa, T., Ishii, R., Fukunaga, R., Kobayashi, T., Sakamoto, K., and Yokoyama, S. 2008. 'Multistep engineering of pyrrolysyl-tRNA synthetase to genetically encode N(epsilon)-(o-azidobenzyloxycarbonyl) lysine for site-specific protein modification', *Chem Biol*, 15: 1187-97.
- Yang, G., Feng, J., Liu, Y., Zhao, M., Yuan, Y., Yuan, H., Yun, H., Sun, M., Bu, Y., Liu, L., Liu, Z., Niu, J. Q., Yin, M., Song, X., Miao, Z., Lin, Z., and Zhang, X. 2019. 'HAT1 signaling confers to assembly and epigenetic regulation of HBV cccDNA minichromosome', *Theranostics*, 9: 7345-58.
- Yang, W., and Summers, J. 1999. 'Integration of hepadnavirus DNA in infected liver: evidence for a linear precursor', *J Virol*, 73: 9710-7.
- Yu, Y., Schneider, W. M., Michailidis, E., Acevedo, A., Ni, Y., Ambrose, P., Zou, C., Kabbani, M., Quirk, C., Jahan, C., Wu, X., Urban, S., Shlomai, A., de Jong, Y. P., and Rice, C. M. 2019. 'An RNA-based system to study hepatitis B virus replication and select drug-resistance mutations', *bioRxiv*.

- Yuen, M. F., Gane, E. J., Kim, D. J., Weilert, F., Yuen Chan, H. L., Lalezari, J., Hwang, S. G., Nguyen, T., Flores, O., Hartman, G., Liaw, S., Lenz, O., Kakuda, T. N., Talloen, W., Schwabe, C., Klumpp, K., and Brown, N. 2019a. 'Antiviral Activity, Safety, and Pharmacokinetics of Capsid Assembly Modulator NVR 3-778 in Patients with Chronic HBV Infection', *Gastroenterology*, 156: 1392-403 e7.
- Yuen, M. F., Locarnini, S., Lim, T. H., Strasser, S., Sievert, W., Cheng, W., Thompson, A., Given, B., Schluep, T., and Hamilton, J. 2019b. "Short term RNA interference therapy in chronic hepatitis B using JNJ-3989 brings majority of patients to HBsAg < 100 IU/ml threshold." In *International Liver Congress 2019*.
- Yuen, M. F., Schiefke, I., Yoon, J. H., Ahn, S. H., Heo, J., Kim, J. H., Lik Yuen Chan, H., Yoon, K. T., Klinker, H., Manns, M., Petersen, J., Schluep, T., Hamilton, J., Given, B. D., Ferrari, C., Lai, C. L., Locarnini, S. A., and Gish, R. G. 2020. 'RNA Interference Therapy With ARC-520 Results in Prolonged Hepatitis B Surface Antigen Response in Patients With Chronic Hepatitis B Infection', *Hepatology*, 72: 19-31.
- Yuen, R., Chen, C.-Y., Liu, C.-J., Jeng, R. W.-J., Elkhatab, M., Coffin, C., Kim, W., Greenbloom, S., Ramji, A., and Lim, Y.-S. 2019c. "Ascending dose cohort study of inarigivir-A novel RIG I agonist in chronic HBV patients: Final results of the ACHIEVE trial." In *International Liver Congress 2019*.
- Yurdaydin, C., Keskin, O., Kalkan, C., Karakaya, F., Caliskan, A., Karatayli, E., Karatayli, S., Bozdayi, A. M., Koh, C., Heller, T., Idilman, R., and Glenn, J. S. 2018. 'Optimizing lonafarnib treatment for the management of chronic delta hepatitis: The LOWR HDV-1 study', *Hepatology*, 67: 1224-36.
- Zahn, A., and Allain, J. P. 2005. 'Hepatitis C virus and hepatitis B virus bind to heparin: purification of largely IgG-free virions from infected plasma by heparin chromatography', *J Gen Virol*, 86: 677-85.
- Zanetti, A. R., Van Damme, P., and Shouval, D. 2008. 'The global impact of vaccination against hepatitis B: a historical overview', *Vaccine*, 26: 6266-73.
- Zhang, C., Zhou, X., Yao, T., Tian, Z., and Zhou, D. 2018. 'Precision Fluorescent Labeling of an Adeno-Associated Virus Vector to Monitor the Viral Infection Pathway', *Biotechnol J*, 13: e1700374.
- Zhang, W., Chen, J., Wu, M., Zhang, X., Zhang, M., Yue, L., Li, Y., Liu, J., Li, B., Shen, F., Wang, Y., Bai, L., Protzer, U., Levrero, M., and Yuan, Z. 2017. 'PRMT5 restricts hepatitis B virus replication through epigenetic repression of covalently closed circular DNA transcription and interference with pregenomic RNA encapsidation', *Hepatology*, 66: 398-415.
- Zhang, Y., Mao, R., Yan, R., Cai, D., Zhang, Y., Zhu, H., Kang, Y., Liu, H., Wang, J., Qin, Y., Huang, Y., Guo, H., and Zhang, J. 2014. 'Transcription of hepatitis B virus covalently closed circular DNA is regulated by CpG methylation during chronic infection', *PLoS One*, 9: e110442.

- Zhang, Y. Y., Zhang, B. H., Theele, D., Litwin, S., Toll, E., and Summers, J. 2003. 'Single-cell analysis of covalently closed circular DNA copy numbers in a hepadnavirus-infected liver', *Proc Natl Acad Sci U S A*, 100: 12372-7.
- Zhang, Z., and Urban, S. 2020. 'Interplay between Hepatitis D Virus and the Interferon Response', *Viruses*, 12.
- Zhang, Z., and Urban, S. 2021. 'New insights into HDV persistence: The role of interferon response and implications for upcoming novel therapies', *J Hepatol*, 74: 686-99.
- Zhang, Z., Zehnder, B., Damrau, C., and Urban, S. 2016. 'Visualization of hepatitis B virus entry - novel tools and approaches to directly follow virus entry into hepatocytes', *FEBS Lett*, 590: 1915-26.
- Zheng, Y., Yu, F., Wu, Y., Si, L., Xu, H., Zhang, C., Xia, Q., Xiao, S., Wang, Q., He, Q., Chen, P., Wang, J., Taira, K., Zhang, L., and Zhou, D. 2015. 'Broadening the versatility of lentiviral vectors as a tool in nucleic acid research via genetic code expansion', *Nucleic Acids Res*, 43: e73.
- Zhou, W., Wesalo, J. S., Liu, J., and Deiters, A. 2020. 'Genetic code expansion in mammalian cells: A plasmid system comparison', *Bioorg Med Chem*, 28: 115772.
- Zoulim, F., and Locarnini, S. 2009. 'Hepatitis B virus resistance to nucleos(t)ide analogues', *Gastroenterology*, 137: 1593-608 e1-2.

6. Publications

6.1. Peer-reviewed publications

Zehnder, B., Urban, S., Tu, T. 2021. 'A Sensitive and Specific PCR-based Assay to Quantify Hepatitis B Virus Covalently Closed Circular (ccc) DNA While Preserving Cellular DNA'. *Bio-protocol*, 11(8): e3986.

Tu, T.*, **Zehnder, B.***, Qu, B., and Urban, S. 2021. 'De novo synthesis of hepatitis B virus nucleocapsids is dispensable for the maintenance and transcriptional regulation of cccDNA'. *JHEP Reports*, 3: 100195. * co-first authors

Tu, T., **Zehnder, B.**, Qu, B., Ni, Y., Main, N., Allweiss, L., Dandri, M., Shackel, N., George, J., and Urban, S. 2020. 'A novel method to precisely quantify Hepatitis B Virus covalently closed circular (ccc)DNA formation and maintenance'. *Antiviral Res*: 104865.

Donkers, J. M., **Zehnder, B.**, van Westen, G. J. P., Kwakkenbos, M. J., AP, I. J., Oude Elferink, R. P. J., Beuers, U., Urban, S., and van de Graaf, S. F. J. 2017. 'Reduced hepatitis B and D viral entry using clinically applied drugs as novel inhibitors of the bile acid transporter NTCP'. *Scientific Reports*, 7: 15307.

Yakimovich, A., Huttunen, M., **Zehnder, B.**, Coulter, L. J., Gould, V., Schneider, C., Kopf, M., McInnes, C. J., Greber, U. F., & Mercer, J. 2017. 'Inhibition of Poxvirus Gene Expression and Genome Replication by Bisbenzimidazole Derivatives'. *Journal of Virology*, 91(18), e00838-17.

Zhang, Z., **Zehnder, B.**, Damrau, C., and Urban, S. 2016. 'Visualization of hepatitis B virus entry - novel tools and approaches to directly follow virus entry into hepatocytes'. *FEBS Letters*, 590: 1915-26.

6.2. Oral presentations

Only first author presentations are listed.

Zehnder, B., Girona, G.E., Lemke, E.A., Urban, S. 'Amber suppression mediated genetic code expansion as a novel tool for labelling and live-cell imaging of HBV core protein'. *Annual Meeting of the German Society for Virology (GfV)*, Würzburg, Germany, 16th March 2018.

Zehnder, B., Girona, G.E., Lemke, E.A., Urban, S. 'Amber suppression mediated genetic code expansion as a novel tool for labelling and live-cell imaging of HBV core protein'. *International Meeting for the Molecular Biology of Hepatitis B Viruses*, Washington DC, USA, 4th September 2017.

6.3. Poster presentations

Only first author presentations are listed.

Zehnder, B., Tu, T., Qu, B., Urban, S. 'HBV cccDNA maintenance is not affected by abrogation of *de novo* nucleocapsid synthesis in long-term *in vitro* infection models'. *International Meeting for the Molecular Biology of Hepatitis B Viruses*, Melbourne, Australia, 2nd October 2019.

Zehnder, B., Tu, T., Qu, B., Lemke, E.A., Urban, S. 'Artificial introduction of unnatural amino acids into the HBV core protein using amber suppression technology allows “click chemistry” labelling of the capsid'. *International Meeting for the Molecular Biology of Hepatitis B Viruses*, Seoul, Korea, 22nd September 2016.

7. Acknowledgments

I would like to express my sincere gratitude to Prof. Dr. Stephan Urban for giving me the opportunity to do my doctoral research in his group. I appreciate his scientific advice, support, amusing anecdotes, and his trust in me as scientist.

I would like to thank my faculty advisor Prof. Dr. Hans-Georg Kräusslich and my PhD committee members Dr. Marina Lusic and Dr. Marco Binder for their critical scientific input during my committee meeting, retreats, and seminars.

Special thanks go to all current and former members of the AG Urban for providing a stimulating working atmosphere and for many scientific and non-scientific discussions: Angga Prawira, Anja Rippert, Bingqian Qu, Christine Bekker, Christa Kuno Kuhn, Christina Kaufman, Franzi Schlund, Florian Lempp, Gnimah Eva Gnouamozi, Julius Hollnberger, Katrin Schöneweis, Lisa Walter, Martina Weiss, Mila Leuthold, Sarah Engelhardt, Shirin Nkongolo, Talisa Richardt, Thomas Tu, Volkan Sakin, Wenshi Wang, Yi Ni, Zhenfeng Zhang. It was always a pleasure working in this group. By extension, my thanks go to the HBV subgroup of the AG Bartenschlager for joining our seminars and contributing to my work. Furthermore, I appreciate the contributions of the bachelor and master's students Elisabeth Schäfer and Koleta Michalek to this work.

I would like to acknowledge all members of the Institute of Molecular Virology for their scientific advice during Friday seminars and for sharing materials and protocols. Furthermore, I am grateful to the SFB1129 programme for the funding of my position and for many interesting seminars and retreats. Special thanks are given to collaborators who are also struggling with the amber suppression technology from the research groups of apl. Prof. Dr. Barbara Müller, Prof. Dr. Hans-Georg Kräusslich, Prof. Dr. Edward A. Lemke, and Prof. Dr. Dirk Grimm.

Finally, I would like to thank Katja for her support and for accompanying me during the pandemic. My deepest thanks go to my family for their continuous support and confidence in me. Their upbringing has guided me to pursue a scientific career.